Polymerisation-induced self-assembly using industrially relevant monomers

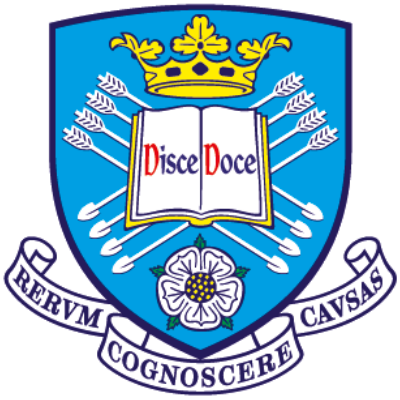

The University Of Sheffield.

Rebecca Roisin Gibson

Department of Chemistry
The University of Sheffield

Submitted to the University of Sheffield in fulfilment of the requirements for the award of Doctor of Philosophy

February 2021

Declaration

The work described in this thesis was undertaken at the University of Sheffield under the supervision of Professor Steven P. Armes between October 2016 and February 2021 and has not been submitted, either wholly or in part, for this or any other degree. All the work is the original work of the author, except where acknowledged.

Signature: _____

Rebecca Roisin Gibson

February 2021

Acknowledgements

I'd first like to thank my supervisor Prof. Steve Armes for allowing me to undertake a PhD in his group and for the opportunities to attend and speak at several conferences. I am particularly thankful for the feedback you have given which has improved my communication and built my confidence. Thank you also to his group members past and present that have helped me along the way and made Christmas meals and summer BBQs so enjoyable.

Thank you to Ashland Speciality Ingredients for partial sponsorship of my PhD, particularly to Osama and Alan for their remote supervision and allowing me to spend three months in industry working on something completely different. Thanks to Abdul, Alistair, Darren and Majda for welcoming us to the site and for keeping me going through those interesting times.

I must also thank the people who have helped with various techniques during my studies including Dr. Svetomir Tzokov and Chris Hill (TEM) and specifically during the last year under strict Covid rule: Shan for running countless NMRs, Saul for fluorescence microscopy and Tom for recording many SAXS patterns at short notice. I would also like to thank Denise and Louise in the Accounts office and Nick and Sharon in Stores for their help throughout my project.

To Drs. Fong, Beth and Duncan, our irregular meetups throughout my PhD were brilliant fun and always seemed to come at a time when I needed a break and a weekend of laughs. A particular shout out to Fong, our postal book swap and one amazing Cali road trip! Memories of sun, Mexican food, margaritas and that ridiculously brilliant night in San Fran got me though those last few months of writing up in winter.

I met some great friends during my PhD who really made my lab days enjoyable. Thanks to Naomi who was always available for a chat over a cup of tea or glass of wine, I miss the summer evenings on the balcony! To Craig and Claire, you certainly know how to wind me up (especially during badminton)! Miss you besties! To Erik for our end of the day catch ups and for all your help with SAXS, I would have been completely lost without those hours you spent helping me! I also got the chance to supervise Max for three months one summer. Thank you for refreshing my lab days and just generally being great fun. Also for the wine, best student ever award!

I am very lucky to have the encouragement from the Deane family and I am so thankful for their generosity. I would like to thank my family for supporting me over the (seemingly endless) years. In particular Mum and Dad for your encouragement to continue without ever pushing, it is a surprisingly motivational technique and removes so much pressure! I really appreciate the video calls that can last hours and the weekend breaks when I really want to forget about Chemistry. To Chris and Sylvie (and little M), thank you for your support and praise always.

Finally, a special thank you to Olly (appreciate you!). Its not a secret to say I struggled with my PhD and many times I wanted to throw in the towel. The fact that I am writing my acknowledgements to a completed Thesis is a testament to how fantastic and encouraging you are. This Thesis is dedicated to the wonderful things that have happened due to or in tandem with my PhD, one of which is you.

Abstract

This Thesis focuses on preparation of block copolymer nano-objects prepared by polymerisation-induced self-assembly (PISA) using reversible addition-fragmentation chain transfer (RAFT) polymerisation in aqueous media, alcoholic solution or various *n*-alkanes. First, a poly(*N*-(2-methacryloyloxy)ethyl pyrrolidone) (PNMEP) precursor was prepared in ethanol and used as a steric stabiliser block for the preparation of spherical nanoparticles *via* either RAFT aqueous dispersion polymerisation of 2-hydroxypropyl methacrylate (HPMA) or RAFT aqueous emulsion polymerisation of 2-ethoxyethyl methacrylate (EEMA). PNMEP homopolymer exhibits lower critical solution temperature (LCST) behaviour in water so an ionisable carboxylic acid end-group was required to ensure sufficiently hydrophilic character for its use as an electrosteric stabiliser at pH 7. However, such anionic carboxylate end-groups only enable the synthesis of kinetically-trapped spherical nanoparticles, regardless of the mean degree of polymerisation (DP) of the PNMEP block or the solids concentration. Flocculation occurred either on addition of salt to screen the electrostatic charge or by adjusting the dispersion pH below the pK_a of the carboxylic acid end-groups.

A PNMEP precursor was then used for the RAFT alcoholic dispersion polymerisation of lauryl methacrylate (LMA) to produce PNMEP-PLMA diblock copolymer nano-objects. Water was added as a co-solvent to enhance the relatively slow rate of polymerisation for such PISA formulations. The addition of 20% w/w water yielded the fastest polymerisations, which enabled the highest final LMA conversions to be achieved. Transmission electron microscopy (TEM) studies indicated the apparent formation of spherical nanoparticles for all target PLMA DPs, albeit with contamination by a minor population of lamellae. However, small-angle X-ray scattering (SAXS) studies confirmed that these diblock copolymers formed mainly vesicles rather than spheres, with thicker vesicle membranes being obtained when targeting higher PLMA DPs. The T_g of the PLMA block was around -48 °C for all target PLMA DPs, indicating that the vesicle membranes were highly deformable. Finally, the dithiobenzoate RAFT end-groups were readily removed from an aqueous dispersion of PNMEP$_{28}$-PLMA$_{87}$ vesicles at 50 °C by prolonged irradiation using visible LED light (λ = 405 nm).

Poly(*tert*-octyl acrylamide) (POAA) was used as a steric stabiliser for the RAFT dispersion polymerisation of *N*,*N*-dimethylacrylamide (DMAC) in *n*-heptane. This PISA formulation produced spherical nanoparticles but their tendency to film-form on drying meant that crosslinking was required for TEM studies. The upper critical solution temperature (UCST) behaviour of POAA$_{85}$-PDMAC$_{150}$ spherical nanoparticles in various *n*-alkanes was investigated by turbidimetry. Little or no UCST behaviour was observed for POAA$_{85}$-PDMAC$_{150}$ spheres prepared in either *n*-heptane or *n*-octane. However, progressively higher cloud points were observed for longer *n*-alkanes (2 °C for *n*-decane, 27 °C for *n*-dodecane, 35 °C for *n*-tetradecane and 55 °C for *n*-hexadecane). Dynamic light scattering (DLS) studies indicated that such nanoparticle aggregation was thermoreversible. POAA$_{85}$-PDMAC$_x$ spheres were evaluated as putative Pickering emulsifiers. Unexpectedly, these highly hydrophobic nanoparticles produced oil-in-water (o/w) rather than water-in-oil (w/o) emulsions. Further experiments suggest that these nanoparticles adsorb at the *inner surface* of the oil droplets, rather than undergoing *in situ* micellar inversion during high-shear homogenisation.

Finally, a poly(stearyl methacrylate) precursor was evaluated for the RAFT polymerisation of *N*-(2-acryloyloxy)ethyl pyrrolidone) (NAEP) in *n*-dodecane. A PSMA DP of 36 was required to ensure colloidal stability of the nano-objects, which meant that only kinetically-trapped spheres could be obtained. Owing to the immiscibility of NAEP with *n*-dodecane, elevated temperatures were required for chain extension of PSMA$_{36}$ when using this highly polar monomer. Interestingly, this formulation proved to be a rare example of a *non-aqueous* emulsion polymerisation even when the NAEP polymerisation was conducted at 90 °C. Finally, PSMA$_{36}$-PNAEP$_{70}$ spheres were briefly evaluated for their performance as a putative Pickering emulsifier to produce w/o/w double emulsions by high shear homogenisation of various *n*-dodecane/water mixtures.

Publications

Gibson, R. R.; Armes, S. P.; Musa, O. M.; Fernyhough A. End-group ionisation enables the use of poly(*N*-(2-methacryloyloxy)ethyl pyrrolidone) as an electrosteric stabiliser block for polymerisation-induced self-assembly in aqueous media. *Polymer Chemistry,* **2019**, *10*, 1312-1323.

Gibson, R. R.; Cornel, E. J.; Musa, O. M.; Fernyhough A.; Armes, S. P. RAFT dispersion polymerisation of lauryl methacrylate in ethanol–water binary mixtures: synthesis of diblock copolymer vesicles with deformable membranes. *Polymer Chemistry*, **2020**, *11*, 1785-1796.

Reproduced in part with permission from [Gibson, R. R.; Armes, S. P.; Musa, O. M.; Fernyhough A. RAFT dispersion polymerization of *N*,*N*-dimethylacrylamide in a series of *n*-alkanes using a thermoresponsive poly(*tert*-octyl acrylamide) steric stabilizer. *Polymer Chemistry,* **2021**, *12*, 2165-2174]

Gibson, R. R.; Fernyhough A; Musa, O. M.; Armes, S. P. Synthesis of well-defined diblock copolymer nano-objects by RAFT non-aqueous emulsion polymerization of *N*-(2-acryloyloxy)ethyl pyrrolidone in non-polar media. *Manuscript submitted to Polymer Chemistry*.

Patents

Authors: Deane, O. J; Musa, O. M.; Armes, S. P.; Fernyhough A.; Gibson, R. R.

Title: Methods of synthesis of homopolymers and non-homopolymers comprising repeating units derived from monomers comprising lactam and acryloyl moieties in an aqueous medium

Patent Number: US20200407470A1

Authors: Gibson, R. R.; Armes, S. P.; Musa, O. M.

Title: RAFT dispersion polymerisation of *N*,*N*-dimethylacrylamide in a series of *n*-alkanes using a poly(*tert*-octyl acrylamide) steric stabiliser.

Provisional Patent Application Number: 63/119,445

Authors: Gibson, R. R.; Armes, S. P.; Musa, O. M.

Title: Process for removal of thio-based end groups from RAFT polymers derived from monomers comprising lactam and acryloyl moieties.

Provisional Patent Application Number: 63/134,350

Conferences

Macro Group Young Researchers Meeting, Edinburgh, June 2017, **Poster Presentation**

Macro Group Young Researchers Meeting, Dublin, July 2018, **Poster Presentation**

Macro Group Young Researchers Meeting, Canterbury, July 2019, **Conference Talk**

The 258th National Meeting & Exposition of the American Chemical Society (ACS), San Diego, August 2019, **Conference Talk**

Abbreviations

ACVA	4,4'-Azobis(4-cyanopentanoic acid)
AIBN	2,2'-Azobis(2-methylpropionitrile)
ATRP	Atom transfer radical polymerisation
CMC	Critical micelle concentration
CP	Cloud point
CPDB	2-Cyano-2-propyl dithiobenzoate
CTA	Chain transfer agent
DDMAT	2-(Dodecylthiocarbonothioylthio)-2-methylpropionic acid
DLS	Dynamic light scattering
DP	Degree of polymerisation
DSC	Differential scanning calorimetry
EGDA	Ethylene glycol diacrylate
FRP	Free radical polymerisation
GC	Gas chromatography
GPC	Gel permeation chromatography
GlyMA	Glycidyl methacrylate
HBMA	4-Hydroxybutyl methacrylate
HPLC	High performance liquid chromatography
k_p	Propagation rate constant
LAM	Less activated monomer
LCST	Lower critical solution temperature
Macro-CTA	Macromolecular chain transfer agent
MAM	More activated monomer
MOEMA	2-Methoxyethyl methacrylate
M_n	Number-average molecular weight
M_p	Peak molecular weight
M_w	Weight-average molecular weight
MW	Molecular weight
MWD	Molecular weight distribution
NMP	Nitroxide-mediated polymerisation
o/w	Oil-in-water
PAA	Poly(acrylic acid)
PBA	Poly(butyl acrylate)
PBzA	Poly(benzyl acrylate)
PBzMA	Poly(benzyl methacrylate)
PDEAEMA	Poly(2-(diethylamino)ethyl methacrylate)
PDMA	Poly(2-(dimethylamino)ethyl methacrylate)
PDMAC	Poly(*N,N*-dimethyl acrylamide)
PDMS	Poly(dimethyl sulfoxide)
PEEMA	Poly(2-ethoxyethyl methacrylate)
PEG	Poly(ethylene glycol)
PEOMA	Poly((ethylene oxide) monomethyl ether metacrylate)
PETTC	4-Cyano-4-(2-phenylethanesulfanylthiocarbonyl)sulfanyl pentanoic acid
PGMA	Poly(glycerol monomethacrylate)
PHPMA	Poly(2-hydroxypropyl methacrylate)
PISA	Polymerisation-induced self-assembly
pK_a	Acid dissociation constant
PLMA	Poly(lauryl methacrylate)

PMAA	Poly(methacrylic acid)
PMMA	Poly(methyl methacrylate)
PMPC	Poly(2-(methacyloyloxy)ethylphosphorylcholine)
PNAEP	Poly(*N*-(2-acryloyloxy)ethyl pyrrolidone)
PNMEP	Poly(*N*-(2-methacryloyloxy)ethyl pyrrolidone)
PNIPAM	Poly(*N*-isopropylacrylamide)
PNVP	Poly(*N*-vinylpyrrolidone)
POAA	Poly(*tert*-octylacrylamide)
PPhA	Poly(phenyl acrylate)
PRE	Persistent radical effect
PS	Polystyrene
PSMA	Poly(stearylmethacrylate)
RAFT	Reversible addition-fragmentation chain transfer
RDRP	Reversible deactivation radical polymerisation
R_g	Radius of gyration
SAXS	Small angle X-ray scattering
TEM	Transmission electron microscopy
T_g	Glass transition temperature
T_m	Melting temperature
UCST	Upper critical solution temperature
UV-Vis	Ultraviolet-Visible
VA-044	2,2’ Azobis(2-(2-imidazolin-2-yl)propane)dihydrochloride
w/o	Water-in-oil
^{1}H NMR	^{1}H nuclear magnetic resonance

Contents

Chapter 1.

Introduction

1.1 General concepts

Polymers are intrinsic to all aspects of modern life. They are present in countless everyday objects including toothbrushes, credit cards, contact lenses, cable insulation, food packaging, garden furniture, PC monitors, printed circuit boards, car bumpers and interiors, disposable latex gloves and syringes, non-stick frying pans, cutlery, water bottles and even the clothes that we wear. In 2012, Nesvadba reported that polymer production grew at a rate of around 9% per year from 1.5 million tonnes in post-war 1950 to 230 million tonnes in 2009.[1] He predicted that globally, the growth rate would continue long term at around 4% with the fastest growth in Asia. Polymers are long chains of many monomer units that are covalently bonded together and the mean number of repeat units per chain is called the degree of polymerisation (DP).

Staudinger was the first to postulate the long-chain nature of polymers.[2] However, this revolutionary concept proved to be controversial and did not become widely accepted until Carothers provided independent experimental evidence for his hypothesis.[3,4] Carothers was also the first to recognise that polymers could be prepared *via* either condensation or addition polymerisation. The former reaction usually results in the elimination of a small molecule (or condensate). Conversely, addition polymers are prepared from either vinyl or cyclic monomers and have chemical compositions that are identical to such building blocks, *i.e.* no small molecules are eliminated during polymerisation. However, Carothers' nomenclature is no longer favoured, partly because it is now recognised that there are important examples of condensation polymerisation (*e.g.* the synthesis of polyurethanes) that do not proceed with the elimination of any small molecules. In 1953, an appreciation of differences between polymerisation mechanisms led Flory to reclassify the two main types of polymerisation as either chain or step polymerisation.[5] Thus, chain growth involves successive monomer addition to an active chain centre. In contrast, step growth involves the gradual build-up of polymer chains *via* short oligomers such as dimers and trimers, which react together to generate longer chains. Simply, the condensation-addition classification is based on polymer structure, whereas step-chain classification is based on the mechanism of polymerisation.[4] The work described in this Thesis is focused exclusively on chain polymerisations.

A homopolymer is a chain comprising just one type of monomer repeat unit, whereas a copolymer is formed by the copolymerisation of two or more types of monomers and can possess an alternating, block or statistical copolymer architecture. Examples of AB copolymers are shown below (Figure 1.1).

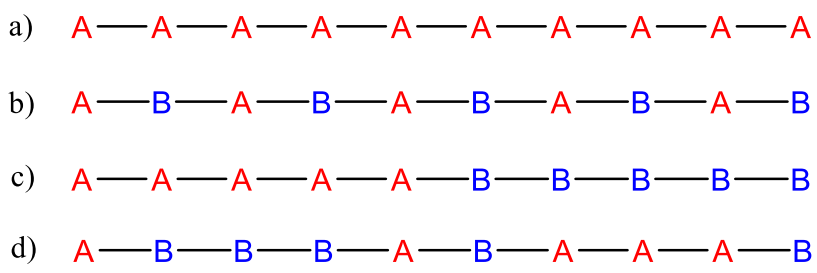

Figure 1.1. Spatial arrangements of A and B monomer repeat units in polymer chains: (a) homopolymer, (b) alternating copolymer, (c) AB diblock copolymer and (d) a statistical copolymer.

A polymer chain can also be either linear or non-linear in nature. Examples of the former are shown in Figure 1.1, whereas examples of the latter include graft copolymers, star polymers, branched copolymers or crosslinked gels. Unlike organic small molecules, polymers do not possess a discrete molecular weight. Instead, polymers exhibit a molecular weight distribution (MWD) and molecular weight moments are used to describe specific points on this curve (see Figure 1.2).

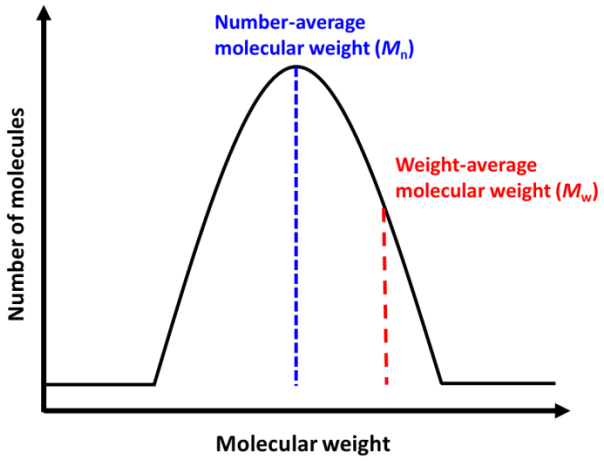

Figure 1.2. Schematic representation of a molecular weight distribution (MWD) for a polymer. The number-average molecular weight (M_n) and weight-average molecular weight (M_w) are indicated as specific moments on this curve.

The two most important moments on the MWD are the number-average molecular weight (M_n) and the weight-average molecular weight (M_w). The M_w/M_n ratio is a crude measure of the width of the MWD and is said to be the dispersity (Đ). If the dispersity is close to unity ($M_w/M_n < 1.20$), then the MWD is said to be narrow.

M_n is defined by equation 1.1:

$$M_n = \frac{\Sigma n_i M_i}{\Sigma n_i} \qquad (1.1)$$

Where M_i is the molecular weight of the i^{th} polymer chain, n is the number of chains and Σn_i is the total number of chains.

M_w is defined by equation 1.2:

$$M_w = \frac{\Sigma n_i {M_i}^2}{\Sigma n_i M_i} \qquad (1.2)$$

Unlike M_n, M_w is biased towards higher molecular weight. According to equations 1.1 and 1.2, M_w is always greater than M_n for any MWD curve of finite width. In practice, this means that all synthetic polymers exhibit dispersities greater than unity.

1.2 Free radical polymerisation

Free radical polymerisation (FRP) is a form of chain polymerisation that has a free radical active centre.[6] FRP can be applied to many functional vinyl monomers and is widely used in industry to produce high MW polymers.

FRP works well under many conditions, including polymerisations conducted in solution, emulsion, suspension, and in the bulk. It is a robust method that is relatively insensitive to impurities and can be readily performed in many solvents.

The mechanism of FRP involves initiation, propagation and termination (Figure 1.3). Initiation typically begins by thermal decomposition of an initiator that is added to the reaction mixture. Homolysis produces two radicals ($I^{\cdot}$) for each initiator molecule (I_2) and such radicals then react with the monomer (M) to produce a growing polymer radical ($P_n^{\cdot}$).

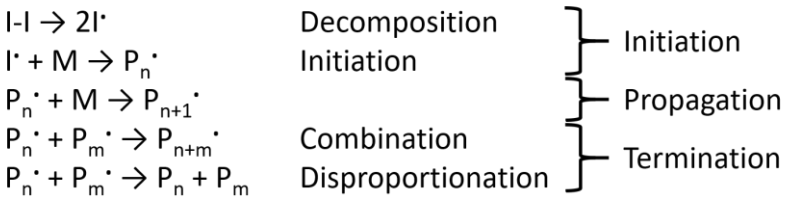

Figure 1.3. Generally accepted mechanism for free radical polymerisation (FRP).[4]

The rate of initiator decomposition (R_d) and the rate of initiation (R_i) are described by equations 1.3 and 1.4, respectively.

$$R_d = -\frac{d[I]}{dt} = k_d[I] \qquad (1.3)$$

$$R_i = -\frac{d[R\cdot]}{dt} = 2fk_d[I] \qquad (1.4)$$

Here *f* is the fraction of radicals that actually initiate chain growth (otherwise known as the initiator efficiency). Typically, *f* is less than unity because some radicals undergo side reactions instead of reacting with monomer to form polymer chains. This is known as the 'cage effect'.

The most common classes of initiator are azo and peroxides (Figure 1.4). These can be decomposed to form radicals by light irradiation, using redox chemistry, or *via* thermal decomposition. The latter approach is often used for the industrial manufacture of vinyl polymers. In this case, the half-life (the time required for the initial initiator concentration to be reduced by 50%) at a specific temperature is often used as a guide to select an appropriate initiator for a given set of reaction conditions. Such initiators undergo relatively slow thermal decomposition, which means that new radicals are generated over timescales of hours, *i.e.* throughout the duration of a polymerisation. This is one fundamental reason why vinyl polymers prepared using FRP invariably exhibit relatively broad MWDs.

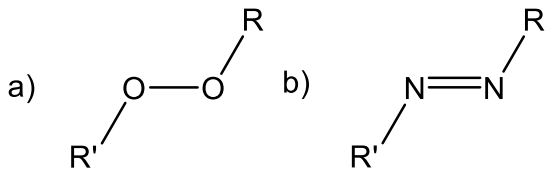

Figure 1.4. General chemical structures for (a) peroxide and (b) azo initiators.

Indeed, the rate-determining step during FRP is the rate of initiator decomposition, which dictates the overall kinetics of the polymerisation. Once radicals are formed, both initiation and propagation occur rapidly, with high MW polymer chains being formed almost immediately. The MW remains fairly constant during the course of the polymerisation while the monomer concentration decreases steadily according to first-order kinetics.

Termination of the growing polymer radicals can occur by either combination, which generates a polymer chain twice that of the kinetic chain length, or disproportionation whereby a hydrogen atom is abstracted from one growing chain to give an unsaturated and saturated species (see Scheme 1.1).

The rate equations for these two types of termination are expressed by equations 1.5 and 1.6. The overall rate of termination is given by equation 1.7 where k_t is the rate constant for termination.

$$R_{tc} = k_{tc}[M\cdot][M\cdot] \qquad (1.5)$$

$$R_{td} = k_{td}[M\cdot][M\cdot] \qquad (1.6)$$

$$R_t = -\frac{d([M\cdot])}{dt} = 2k_t[M\cdot]^2 \qquad (1.7)$$

A steady-state radical concentration of ~10^{-7} M is produced by continuous initiation and termination events. The mean lifetime of the growing polymer chains is short and, in the absence of chain transfer, high molecular weight chains are formed immediately in the early stages of polymerisation.[7]

The predominant termination mechanism depends largely on the monomer class and also the reaction temperature. For example, for the polymerisation of styrene or acrylates, polymer radicals mainly terminate by combination, whereas methacrylates favour termination by disproportionation.

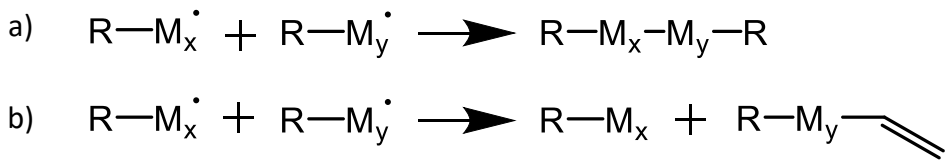

Scheme 1.1. Mechanism for free radical termination by (a) combination and (b) disproportionation.

For polymers produced by FRP, the mean number of repeat units (*i.e.* the number of monomer units consumed by each radical) is called the kinetic chain length, ν. Depending on the dominant termination mechanism, the DP of the polymer chains is equal to either ν or 2ν for disproportionation or combination, respectively if there is no chain transfer.

Chain transfer can occur to monomer, polymer, initiator or solvent, resulting in shorter polymer chains than expected. In each case, a new radical is produced which can reinitiate or truncate polymerisation. If the rate of reinitiation is sufficiently fast, the kinetics of the polymerisation will not be significantly affected.

Assuming that the radical reactivity is independent of the chain length, all propagation steps have the same rate constant (equation 1.8) where $[M\cdot]$ is the concentration of monomer, *M*, in its radical state:

$$-\frac{d[M]}{dt} = R_p = k_p[M\cdot][M] \qquad (1.8)$$

Invoking the steady-state approximation (*i.e.* $R_i = R_t$ equation 1.9) and assuming that chain transfer is negligible, it can be shown that the overall rate of polymerisation, R_p, is given by equation 1.11 where k_p is the rate constant for propagation and k_d is the rate constant for initiator decomposition.

$$R_i = R_t = 2k_t[M\cdot]^2 \qquad (1.9)$$

$$[M\cdot] = \left(\frac{R_i}{2k_t}\right)^{0.5} \qquad (1.10)$$

$$R_p = k_p[M]\left(\frac{fk_d[I]}{k_t}\right)^{0.5} \qquad (1.11)$$

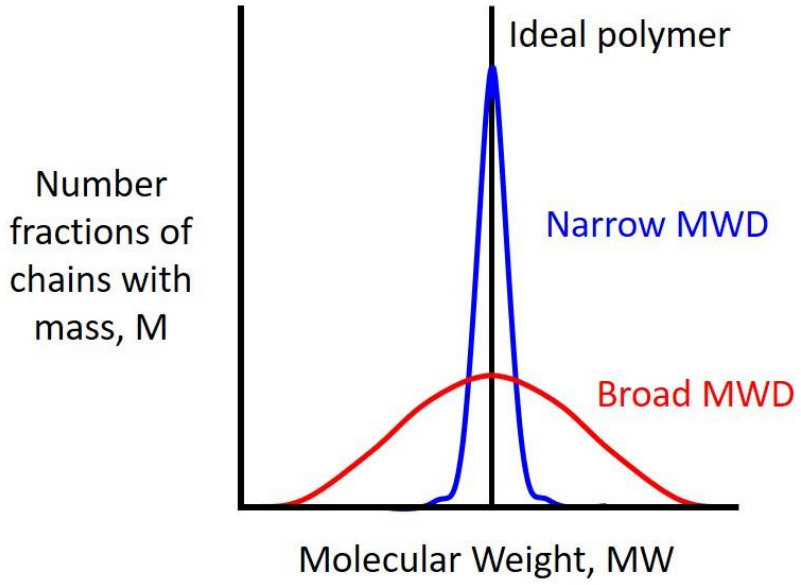

Figure 1.5. Schematic representation of molecular weight distribution curves for polymers with a relatively high dispersity (red curve), a relatively low dispersity (blue curve) or a theoretical dispersity of unity (black curve, ideal case).

FRP has exceptional tolerance for both monomer and solvent functionality and is relatively cheap and straightforward to implement. Nevertheless, alternatives to FRP have been sought for better control over the MWD (often resulting in a broad MWD, see Figure 1.5), the target MW, and the copolymer architecture.

1.3 Living anionic polymerisation

Anionic polymerisation is a type of a chain polymerisation involving an anionic active centre. Such polymerisations have so-called 'living' character because intrinsic termination of anionic chain-ends cannot occur, thus polymer chains with narrow MWDs can be produced. However, far fewer vinyl monomers are suitable for anionic polymerisation because it is intolerant of many types of protic functionality (*e.g.* hydroxyl, primary amines, secondary amines or carboxylic acid groups). Moreover, the substituent groups on the monomer must be able to stabilise the anionic active centre. Suitable vinyl monomers contain electron-withdrawing groups such as cyano, aromatic or ester groups.

The first report of living anionic polymerisation was by Szwarc in 1956.[8] He suggested that, in the absence of any termination, the polymer chains should possess narrow MWDs and remain active indefinitely. Moreover, sequential addition of a second monomer should produce well-defined diblock copolymer chains. This concept was demonstrated in a follow-up paper published in the same year by Szwarc *et al.*, who reported the synthesis of a polystyrene (PS)-polyisoprene diblock copolymer in dry tetrahydrofuran.[9] In principle, well-defined multiblock copolymers can be prepared by anionic polymerisation *via* sequential monomer addition.[10]

The rate of initiation is much faster than the rate of propagation, and propagation does not begin until initiation is complete. This allows all chains to grow uniformly and leads to a remarkably narrow MWD (typically M_w/M_n < 1.1). Moreover, the target DP is simply given by the [monomer]/[initiator] molar ratio and there is a linear evolution of MW with increasing monomer conversion (Figure 1.6). Conversely, FRP is characterised by a rapid initial increase in molecular weight before attaining a near-constant value, while poor control over the MWD is the result of (i) temporal overlap between initiation and propagation and (ii) intrinsic termination by combination and/or disproportionation.

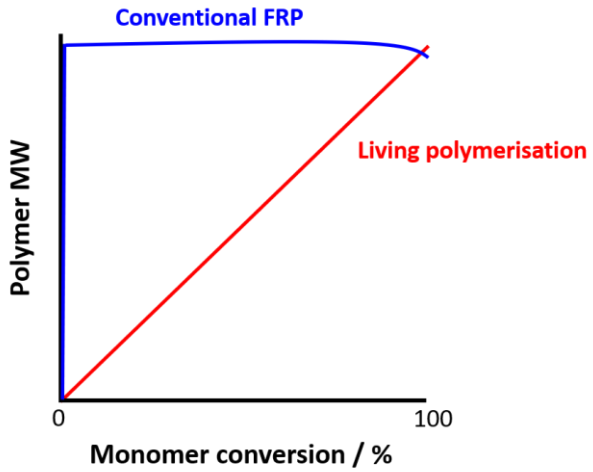

Figure 1.6. Schematic relationship between molecular weight and monomer conversion for conventional free radical polymerisation (blue curve) and living anionic polymerisation (red curve).

If the anionic polymerisation is assumed to proceed to full conversion, the desired polymer MW can be targeted using equation 1.12 where M_n is the number-average molecular weight, M is the mass of monomer and [I] is the number of moles of initiator.

$$M_n(\mathrm{g\ mol^{-1}}) = \frac{\mathrm{M\ (g)}}{\mathrm{[I]\ (mol)}} \qquad (1.12)$$

As noted earlier, the number average DP can be calculated simply by dividing [M], the number of moles of monomer by [I], see equation 1.13.

$$\mathrm{DP} = \frac{[\mathrm{M}]}{[\mathrm{I}]} \qquad (1.13)$$

Disadvantages of this method of polymerisation are that it is applicable to very few functional vinyl monomers and a rather limited range of non-protic solvents such as tetrahydrofuran, benzene, toluene or cyclohexane. This is because labile protons cause premature termination *via* rapid abstraction. In practice, water must be rigorously excluded from the monomer, solvent and all glassware. Thus, relatively few industrial processes utilise anionic polymerisation on an industrial scale. One notable exception is a US-based company, Kraton Polymers, which conducts the anionic polymerisation of monomers such as styrene, isoprene and butadiene to prepare thermoplastic elastomers (synthetic rubber) based on ABA triblock copolymers, diblock copolymers for diesel soot dispersion in engine oils and star diblock copolymers as viscosity modifiers (thickeners) for engine oils.

1.4 Pseudo-living radical polymerisation

Unlike FRP, pseudo-living radical polymerisation provides good control over the MWD and allows the synthesis of well-defined block copolymers by sequential monomer addition. This is achieved by reversible capping of the polymer radicals using a suitable reagent. This lowers the instantaneous polymer radical concentration and hence reduces premature termination by suppressing the rate of termination relative to the rate of propagation (Scheme 1.2). Rapid deactivation of the growing polymer radicals leads to an equilibrium between such species and the corresponding dormant (capped) chains. Thus, all chains have an equal probability to grow which leads to relatively narrow MWDs (M_w/M_n ~ 1.1-1.3) and a linear evolution of the molecular weight with monomer conversion.[6] Moreover, because these polymerisations involve radical species, they are relatively tolerant of monomer functionality, as well as protic sources.

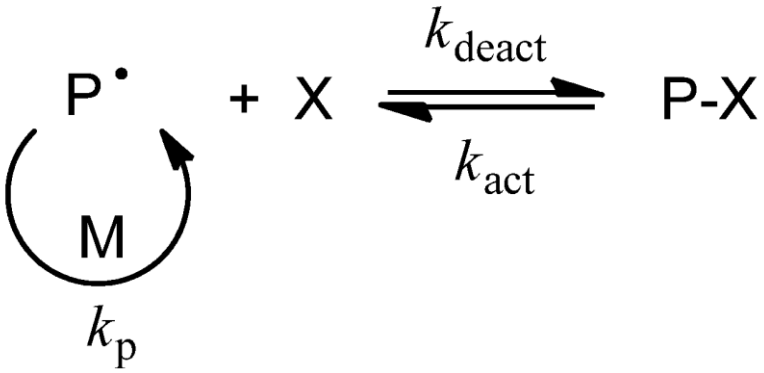

Scheme 1.2. Simplified 'Reversible Deactivation Radical Polymerisation' (RDRP) mechanism.[11]

The term 'Reversible Deactivation Radical Polymerisation' (RDRP) is often used to describe such pseudo-living radical polymerisations as some background level of termination remains prevalent.[12] Nevertheless, this general approach is highly versatile and, unlike anionic polymerisation, can be used for a wide range of functional vinyl monomers. The pseudo-living nature of the polymer chains means chain-end fidelity is maintained,[13] which enables the synthesis of well-defined block copolymers as well as other types of copolymer architectures that are not accessible by FRP (*e.g.* star polymers).

There are two main RDRP mechanisms. One involves transfer by reversible activation, which is controlled by the persistent radical effect (PRE), *e.g.* nitroxide-mediated radical polymerisation (NMP)[14–16] or atom transfer radical polymerisation (ATRP).[17,18] The alternative approach involves degenerative transfer, *e.g.* reversible addition-fragmentation chain transfer polymerisation (RAFT) polymerisation.[19]

The PRE mechanism requires a persistent radical such as a sterically hindered nitroxide. Propagating polymer radicals react with this nitroxide at a given deactivation rate constant (k_{da}). The rate constant for activation of the resulting dormant nitroxide-capped polymer chains to regenerate the propagating polymer radicals is k_a. If k_{da} exceeds k_a, then $[P_n^{\cdot}]$ is reduced and most chains are present in their dormant state at any given time. The rate of termination is lowered as the equilibrium shifts to the right, thus reducing the probability of termination.

If initiation is fast and full monomer conversion is achieved, the target DP of the polymer chains is simply given by the monomer concentration divided by the initiator concentration, equation 1.14 for ATRP and by the concentration of nitroxide for NMP, equation 1.15. [20]

$$DP = \frac{\Delta[M]}{[I]_0} \qquad (1.14)$$

$$DP = \frac{\Delta[M]}{[nitroxide]_0} \qquad (1.15)$$

1.4.1 Nitroxide-mediated polymerisation

NMP was first established by Solomon *et al.* working at the Commonwealth Scientific and Industrial Research Organisation (CSIRO).[7] NMP can be used to synthesise polymers with narrow MWDs *via* polymerisations conducted in solution, bulk, emulsion or suspension.

Historically, nitroxides have been utilised as radical traps to study radical-based reactions. This reaction is complicated by side reactions including the formation of stable alkoxyamines. It was later shown that nitroxides selectively scavenge carbon-centred radicals to produce alkoxyamines and that oxygen-centred radicals either did not react or reacted reversibly with nitroxides.[21] Moreover, some alkoxyamines undergo isomerisation, which could only be explained by reversible homolytic dissociation.[22,23] Furthermore, oligomers were obtained in some cases,[24,25] which suggested that alkoxyamines could be used to control radical polymerisations based on a reversible deactivation/activation mechanism. Nitroxide radicals reversibly cap the growing polymer chains, which allows addition of only a few monomers at a time during each chain growth event (Scheme 1.3). Control is afforded as the concentration of propagating polymer radicals is reduced and the dormant alkoxyamine-capped chain cannot be terminated prematurely.

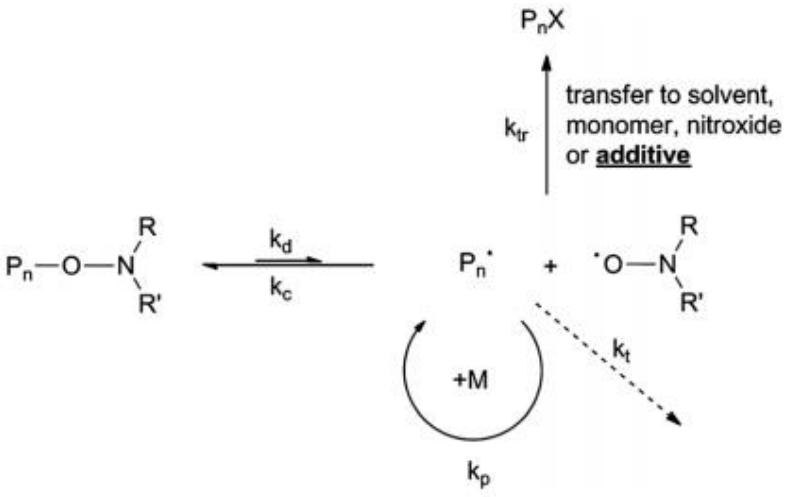

Scheme 1.3. Mechanism of nitroxide-mediated polymerisation (NMP).[26]

One advantage of NMP is its simplicity: it only requires a monomer and an alkoxyamine, as the latter acts as both the initiator and the capping agent. Monomer purification is not critical for such polymerisations. One important disadvantage of NMP is that the homopolymerisation of

methacrylates is usually problematic. This is because slow deactivation of the tertiary radical adduct increases the probability of premature termination, therefore reducing the control.[27]

High temperatures are often required owing to the relatively high bond dissociation energies of alkoxyamines.[27] After extensive research, there are now some literature examples of NMP syntheses being conducted at lower temperatures (< 100 °C).[28,29] An important example by Detrembleur and co-workers used moderate temperatures (40-50 °C) for the synthesis of methacrylic homopolymers.[30] In fact, these workers suggest that such low temperatures are important to limit the possibility of side reactions for methacrylates.

1.4.2 Atom transfer radical polymerisation

ATRP enables the polymerisation of many classes of vinyl monomers, including styrenics, (meth)acrylates and (meth)acrylamides.[6] It is considered to be a more broadly applicable polymerisation technique than NMP and consequently is much more widely studied.

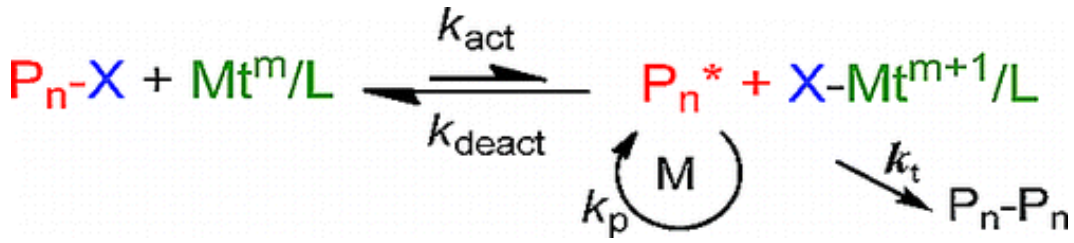

Scheme 1.4. Mechanism of metal-catalysed atom transfer radical polymerisation (ATRP).[31]

The general mechanism for ATRP is shown in Scheme 1.4. There are four essential components that are either added or produced *in situ* for ATRP to occur: a monomer (M); a (macro)initiator (P_n-X where X is usually a halogen atom); a transition metal (M^n) capable of undergoing a one-electron redox reaction; a ligand (L) that can complex to this transition metal, thus modifying the solubility and activity of this catalyst. As with all pseudo-living radical polymerisations, ATRP requires a dynamic equilibrium between activation of a dormant species and deactivation of the growing polymer radical *via* transfer of an atom (or group) from a catalyst. Activation is achieved by reaction of an alkyl halide with a transition metal-ligand complex in its lower oxidation state and deactivation occurs by reaction of the growing polymer chain with the same transition metal-ligand complex in its higher oxidation state (and containing a transferrable atom or group). Copper catalysts are the most widely used in ATRP, but various other transition metals (Ru, Fe, Ni, Mo, Re etc.) have also been shown to be suitable.[32–36]

The metal catalyst cleaves the alkyl halide bond, thus increasing the oxidation state of the metal catalyst and generating an alkyl radical. This radical then reacts with multiple monomers to

produce a polymer radical, which is reversibly capped by transfer of a halogen atom from the transition metal catalyst. ATRP provides good control over the MWD and also enables high blocking efficiencies to be achieved when preparing block copolymers.

One important disadvantage of ATRP is that most potential applications require removal of the toxic transition metal catalyst at the end of the polymerisation. Moreover, acidic monomers such as (meth)acrylic acid cannot be polymerised directly owing to side reactions such as protonation of the ligand (and hence deactivation of the catalyst). Other side reactions have also been reported that reduce the deactivation efficiency and therefore limit the control that can be achieved over the polymerisation.[37] Compared to ATRP conducted in organic solvents, ATRP catalysts are very active in polar solvents such as water, which leads to a relatively high instantaneous radical concentration and hence a reduction in MWD control.[38] However, much faster rates of polymerisation can be achieved so sometimes a small quantity of water is added to the reaction mixture to reduce the timescale required for the ATRP synthesis.[39,40]

1.4.3 Reversible addition-fragmentation chain transfer polymerisation

RAFT polymerisation was first reported in 1998 by scientists working at CSIRO.[41] It simply involves conducting FRP in the presence of an organosulfur-based chain transfer agent (CTA). The 'living' character is achieved *via* rapid, reversible chain transfer of the propagating species. RAFT polymerisation can be used to produce well-defined diblock copolymers with M_w/M_n values of less than 1.20.[42–44] It is also compatible with a range of solvents, including protic solvents such as water and lower alcohols and has been used for polymerisations in the bulk, as well as under emulsion, solution or dispersion conditions. RAFT polymerisation is highly tolerant of monomer functionality and is applicable to a wide range of vinyl monomers, including styrene, vinyl acetate, (meth)acrylates and (meth)acrylamides. The key is judicious selection of a suitable RAFT CTA for a given type of monomer, along with appropriate optimisation of the reaction conditions.[45]

Target molecular weights can be calculated using equation 1.16**:**

$$M_n(\text{theo.}) = \frac{[M]_0 - [M]_t}{[CTA]_0} M \qquad (1.16)$$

Where $[M]_0 - [M]_t$ is the amount of monomer consumed, [CTA] is the RAFT agent concentration and M is the molecular weight of the monomer. Hence the target DP of the polymer chains can be easily controlled by varying the relative [M]/[CTA] molar ratio, as shown in equation 1.17.

$$\text{DP} = \frac{[\text{M}]}{[\text{CTA}]} \qquad (1.17)$$

RAFT polymerisation and ATRP are highly versatile techniques that yield polymers with narrow MWDs. However, RAFT polymerisation is much more tolerant of carboxylic acids in the form of both acidic monomers and end-groups, whereas such species typically poison the ATRP catalyst.[46] In this Thesis, the preparation of carboxylic acid-functionalised diblock copolymers in the form of sterically-stabilised nanoparticles in either aqueous solution or aqueous alcohol mixtures has been explored. Thus, RAFT polymerisation was deemed the most suitable chemistry for such syntheses.

1.4.3.1 The RAFT mechanism

The RAFT mechanism involves five distinct steps: initiation, reversible chain transfer, reinitiation, chain equilibrium and termination (Scheme 1.5). Initiation is essentially the same as that for FRP and produces a propagating polymer radical $P_n^{\bullet}$. The addition of $P_n^{\bullet}$ to the CTA is immediately followed by fragmentation of the RAFT radical to afford a dormant species and a new radical, $R^{\bullet}$. Reinitiation then occurs, producing a new growing polymer radical, $P_m^{\bullet}$ (here the subscripts m and n denote the mean DP of each polymer radical).

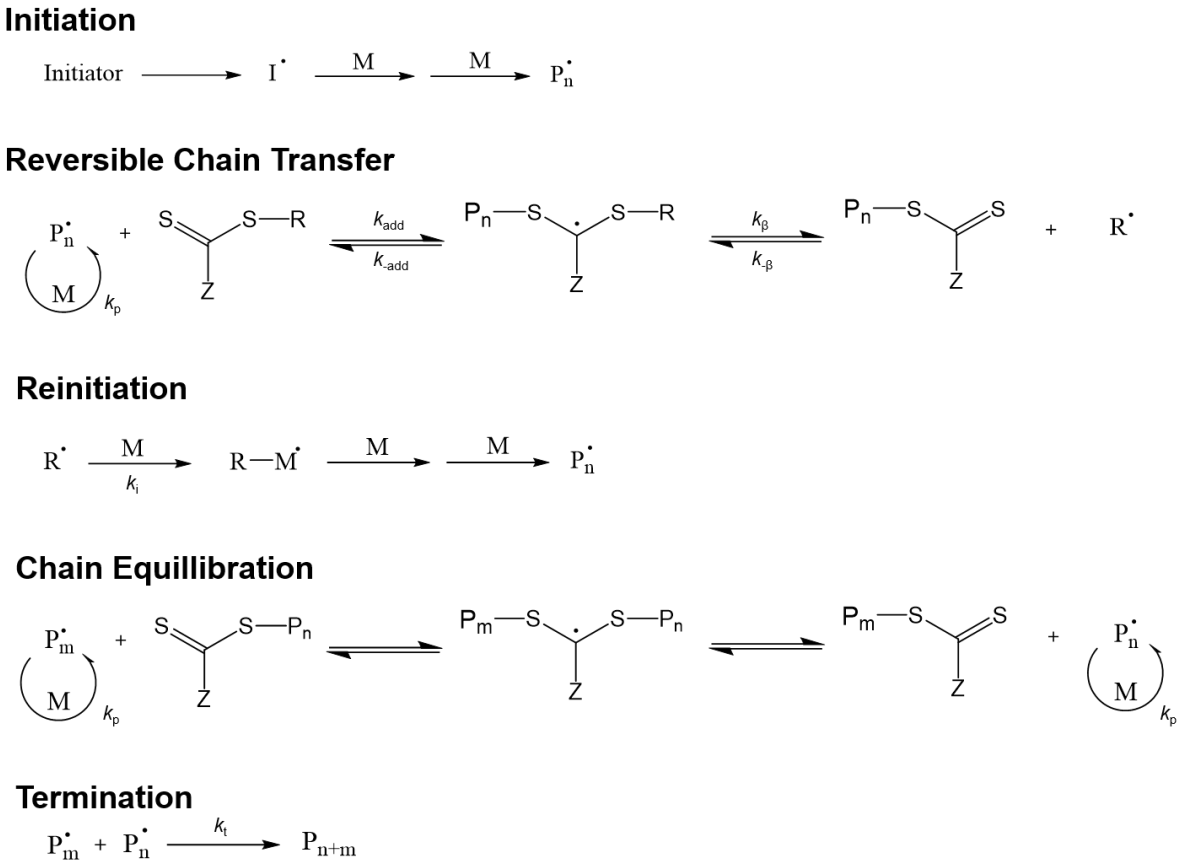

Scheme 1.5. RAFT polymerisation mechanism according to Rizzardo and co-workers.[15]

An equilibrium between the $P_n^{\bullet}$ and $P_m^{\bullet}$ radicals and their corresponding dormant species is established by rapid reversible transfer of the S=C(Z)-S group. This equilibrium maintains the pseudo-living character of RAFT polymerisation because most chains exist in their dormant, unreactive state (Figure 1.7) allowing equal opportunity for propagation. Similar chain lengths are therefore obtained for all polymer chains. RAFT polymerisation is a degenerative chain transfer process with a radical flux being required for the activation-deactivation equilibrium, hence the need for a radical initiator.

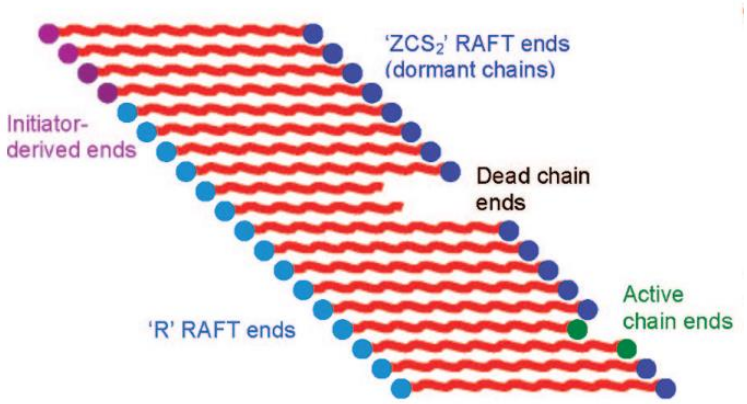

Figure 1.7. Schematic representation of the various types of polymer chains present in a RAFT polymerisation at any given time. The majority of chains exist in their dormant capped states, a small fraction have undergone premature termination and only a few chains are activated towards polymerisation.[15]

Chain termination is minimised owing to suppression of the instantaneous concentration of polymer radicals but the probability of termination increases significantly towards the end of the polymerisation, *i.e.* under monomer-starved conditions. For the formation of multiblock copolymers, RAFT polymerisations are often quenched prior to full monomer conversion to maintain chain-end fidelity, thereby minimising homopolymer contamination. However, Perrier *et al*. reported the synthesis of an icosablock (20-block) copolymer simply by sequential monomer addition, with more than 99% yield being achieved for each step.[47] Reducing the initiator in such syntheses and using highly reactive monomers proved to essential for such demanding syntheses.

There is a direct relationship between the amount of initiator used and the number of chains that undergo bimolecular termination.[45] Polymer chains are terminated with either an initiator-derived fragment or the R group from the CTA, depending on which species initiated the chain growth. Assuming that termination only occurs by disproportionation (which is likely to be a good approximation for methacrylic monomers), the number of polymer chains derived from the initiator is equal to the number of dead chains. Thus, the initiator concentration must be

minimised to maintain the 'pseudo-living' character of the polymerisation, particularly for the synthesis of such multiblock copolymers.

1.4.3.2 Choosing a RAFT agent

The Z and R substituents on the CTA play vital roles in the RAFT mechanism and therefore the CTA must be carefully selected to be suitable for a given monomer class (Figure 1.8). The Z group stabilises the transition state and the intermediate radical and hence controls the reactivity of the CTA, whereas the R group is the radical leaving group and must be capable of reinitiating the polymerisation. Moreover, the S-R bond must be relatively weak so that it can be readily cleaved.

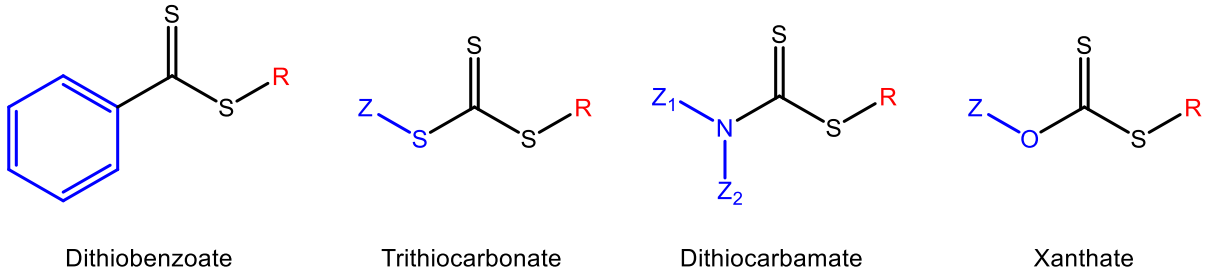

Figure 1.8. The four main classes of RAFT CTAs: dithiobenzoate, trithiocarbonate, dithiocarbamate and xanthate.

Unfortunately, the presence of the organosulfur-based RAFT end-group leads to intrinsically coloured and distinctly malodorous polymers.[44] Moreover, such end-groups (or their decomposition products) can be too toxic for certain biomedical applications.[48] Nevertheless, Z groups enable convenient end-group analysis in many cases. For example, the M_n of the polymer can be determined by gel permeation chromatography (GPC) using a UV detector and PS standards. Similarly, visible absorption spectroscopy can be used to monitor the kinetics of RAFT dispersion polymerisation [49] and the Z group can also be removed to confer desired end-group functionality.[50–52] Various methods for RAFT end-group removal have been explored, as summarised in Figure 1.9 below.

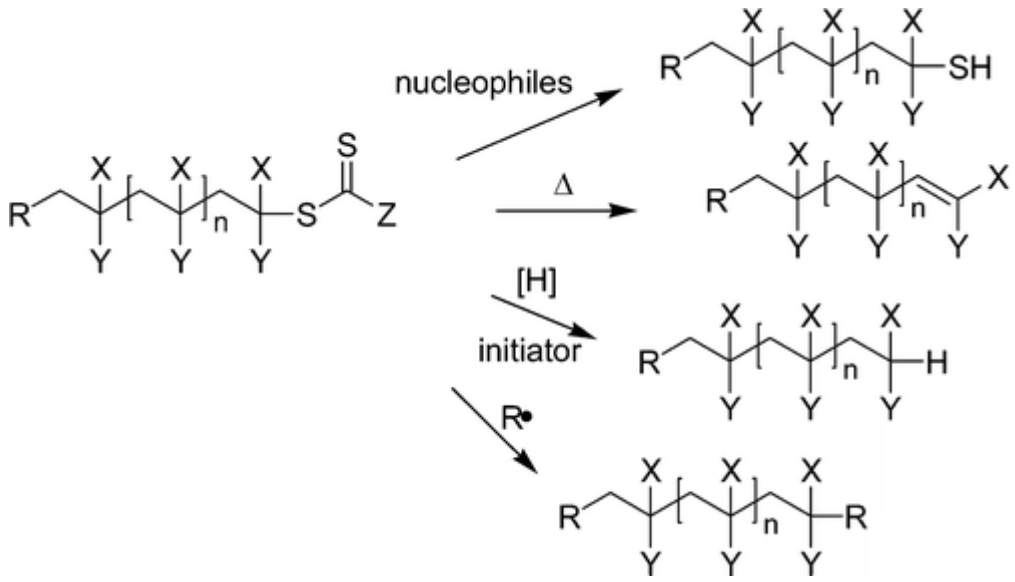

Figure 1.9. Summary of methods for Z group removal from polymers prepared by RAFT polymerisation.[50]

Most methods to remove RAFT end-groups involve thermolysis,[53] photolysis[54,55] or addition of a selective reagent[56–61] to cleave the organosulfur group from *soluble* polymer chains. In contrast, there are relatively few reports of RAFT end-group removal from block copolymer nanoparticles.[62,63]

In general, vinyl monomers can be categorised as either more activated monomers (MAMs) or less activated monomers (LAMs). MAMs are conjugated to electron-withdrawing groups and therefore possess an electron-deficient double bond; examples include methacrylates, acrylates, acrylamides and styrene. Dithiobenzoates and trithiocarbonates are well-suited for the RAFT polymerisation of MAMs: such monomers require Z groups that stabilise the intermediate radical so that radical addition to the C=S bond is favoured (Figure 1.10). The resulting propagating radical is less reactive towards polymerisation (*i.e.* it has a lower k_p and k_{add}) thus a more active RAFT agent is required to ensure good control.

In contrast, LAMs have electron-donating heteroatoms adjacent to an electron-rich double bond. They also lack an effective radical-stabilising substituent, with typical examples being *N*-vinyl pyrrolidone (NVP) and vinyl acetate (VAc). Propagating polymer radicals formed by LAMs are highly reactive (*i.e.* possess relatively high k_p and k_{add} values) and are relatively poor leaving groups. Thus, this monomer class requires either dithiocarbamates or xanthates, which make the intermediate radical less stable and favour fragmentation of the propagating polymer radical (Figure 1.10).

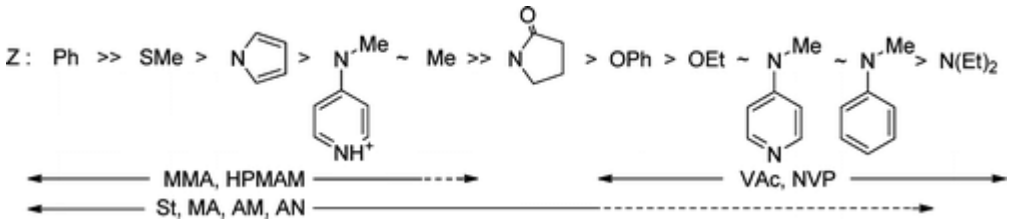

Figure 1.10. Guidelines for selection of appropriate RAFT agents (ZC(═S)SR) for various polymerisations. Addition rates decrease and fragmentation rates increase from left to right. A dashed line indicates partial control (*i.e.*, control over the target molecular weight but poor control over the MWD, or substantial retardation in the case of LAMs such as VAc or NVP).[64]

Ideally, a 'universal' RAFT CTA should enable the synthesis of well-defined block copolymers comprising both MAMs and LAMs. In principle, the reactivity of a RAFT agent can be modified by changing the external conditions. There are several reports of chain extension of a MAM-based polymer with LAMs using a so-called 'switchable' RAFT CTA based on a pyrazole.[65] However, inverting this block order is more challenging. Usually, MAMs must be polymerised first as fragmentation of the intermediate radical favours the better homolytic leaving group. Recently, Sumerlin *et al.* circumvented this problem to form a PLAM-PMAM diblock copolymer using iniferter-controlled RAFT polymerisation, as described below (Figure 1.11).[66]

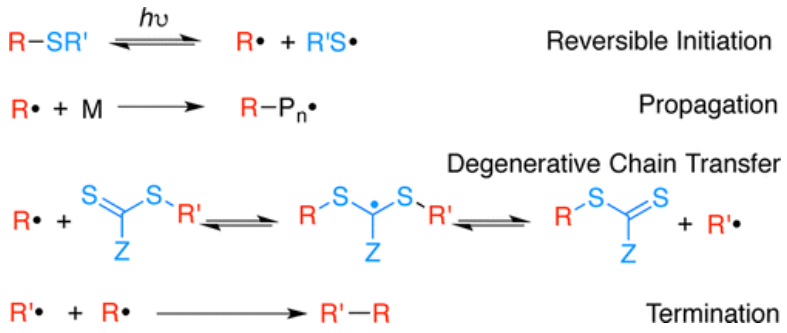

Figure 1.11. Mechanism for iniferter-controlled RAFT polymerisation as reported by Sumerlin *et al.*[67]

1.4.3.3 Initiator-free photoRAFT (iniferter-controlled RAFT)

RAFT polymerisations typically utilise a thermally activated azo or peroxide initiator. However, it is also feasible for such reactions to proceed *via* light irradiation using either a photocatalyst or a photoinitiator (Figure 1.12).

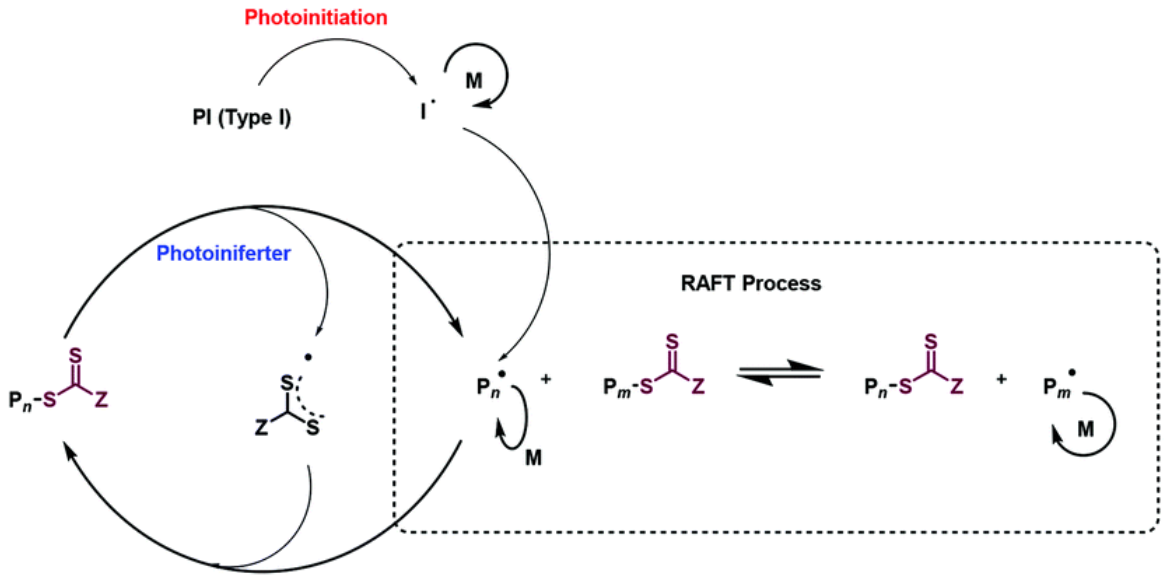

Figure 1.12. RAFT polymerisation mechanisms *via* photoinitiation and photoiniferter pathways.[68]

In fact, the RAFT CTA itself can be used as an iniferter. This approach circumvents the need to use an initiator as the carbon-sulfur bond can be cleaved by photolysis using visible light. The spin-forbidden $n \rightarrow \pi^*$ thiocarbonyl transition has an absorption energy with a λ_{max} of 400 – 500 nm, which also accounts for the distinctive colour of many RAFT agents.[69] Blue or green visible light results in β-cleavage of the carbon-sulfur bond, producing a radical that undergoes propagation and chain transfer as a conventional RAFT polymerisation.[70] Indeed, early work using iniferters to initiate polymerisations predates the RAFT polymerisation literature.[71–73]

In principle, iniferter polymerisations can continue indefinitely as radical generation is reversible. However, this is often not possible in practice because side reactions can lead to termination. Empirically, it has been found that the living character of such polymerisations depends on the irradiation time, conversion and iniferter structure.[67] Wang and co-workers were the first to identify the importance of RAFT CTA concentration for a well-controlled polymerisation. When using 2-(dodecylthiocarbonothioylthio)-2-methylpropionic acid (DDMAT), they found that photolysis was reversible at high CTA concentrations but became irreversible at low concentrations, resulting in poor control over the MWD and the production of high MW polymers (Figure 1.13).[74] Chen *et al.* suggested that light intensity may have a similar effect to CTA concentration.[67] At high levels of irradiation, most RAFT CTAs exist in their radical state so lower intensity light should confer greater control.[75]

Using blue light, McKenzie and co-workers obtained polymers with high end-group fidelity which were used for multiple chain extensions to produce hexablock copolymers in dimethyl sulfoxide

using a trithiocarbonate-based RAFT agent.[69] Each step required 24 h irradiation to achieve ≥ 92% monomer conversion for acrylate and acrylamide comonomers. Furthermore, the RAFT iniferter synthesis of homopolymers was evaluated using a series of solvents of varying polarity.

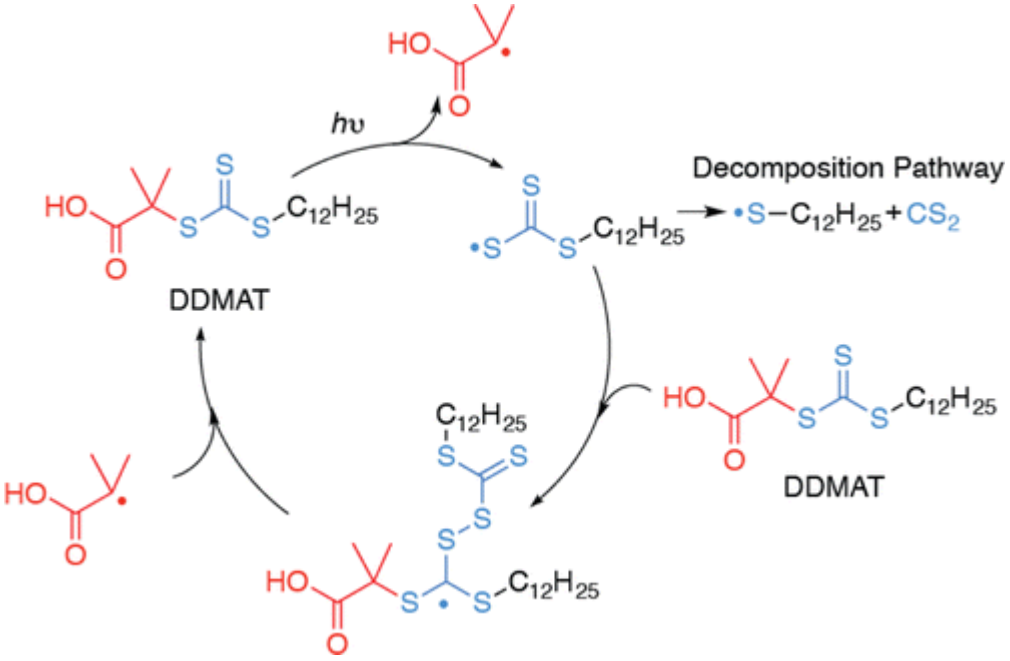

Figure 1.13. Proposed mechanism for the reversible decomposition of DDMAT by UV irradiation using high DDMAT concentrations.[67,74]

Easterling and co-workers hypothesised that photolysis of C–S bonds could generate R group macroradical intermediates normally disfavoured by the RAFT mechanism, which might allow inversion of the block sequence to produce PLAM-PMAM diblock copolymers.[66] Three poly(*N*,*N*-dimethylacrylamide) (PDMAC) precursors were synthesised using a trithiocarbonate (PDMAC-TTC), a xanthate (PDMAC-Xan) and a dithiocarbamate 'switchable' RAFT agent (PDMAC-SRA). All three precursors exhibited narrow dispersities ($M_w/M_n \leq 1.17$) and M_n values below 10 kg mol^{-1}. UV-visible spectroscopy was used to assess the $\pi \rightarrow \pi^*$ and $n \rightarrow \pi^*$ (forbidden) transitions.

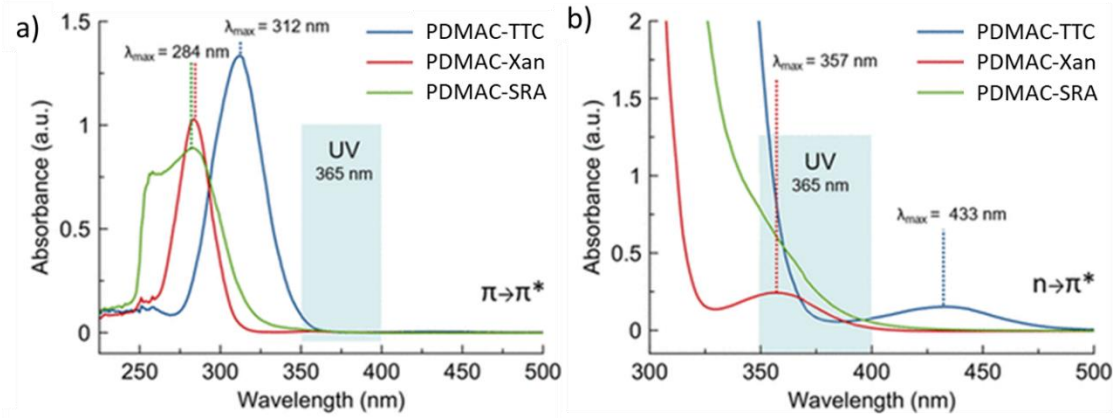

Figure 1.14. UV-visible spectra recorded for the PDMAC-TTC, PDMAC-Xan and PDMAC SRA precursors, indicating the λ_{max} values for their $\boldsymbol{\pi} \rightarrow \boldsymbol{\pi}^*$ and $\boldsymbol{n} \rightarrow \boldsymbol{\pi}^*$ transitions, respectively.[66]

For PDMAC-TTC, the $\pi \rightarrow \pi^*$ transition has a λ_{max} of 312 nm and the $n \rightarrow \pi^*$ transition has a λ_{max} of 433 nm (Figure 1.14). Using UV irradiation, pseudo first-order kinetics for the polymerisation of methyl methacrylate (MMA) was observed but slow photolysis of the PDMAC-TTC precursor resulted in higher than expected PMMA DPs.[76] Chain extension with MMA was then attempted by irradiation with blue light with the expectation that greater overlap of the forbidden TTC absorption with the blue light emission should enhance the photolysis. Unfortunately, similar results to those obtained using UV irradiation were obtained with a mixture of residual PDMAC-TTC and high MW PDMAC-PMMA diblock copolymer chains being formed after 12 h. In contrast, xanthates undergo rapid photolysis by irradiation with UV light. PDMAC-Xan had a $n \rightarrow \pi^*$ transition with a λ_{max} of 357 nm, which is close to that of the λ_{max} of 365 nm for the UV source used in these experiments. Kinetics studies indicated a pseudo first-order reaction, suggesting that a constant radical concentration was maintained throughout the polymerisation. High blocking efficiencies were achieved and markedly faster kinetics than when using PDMAC-TTC. Moreover, only mixtures of PDMAC-Xan and PMMA homopolymers could be obtained when using a thermal initiator. Finally, chain-extending PDMAC-SRA with MMA led to high blocking efficiencies – comparable to those achieved with PDMAC-Xan. This was attributed to the similarity of the $\pi \rightarrow \pi^*$ transition (for which λ_{max} = 284 nm), thus rapid cleavage of the C-S bond could be achieved.

1.5 Physical forms of polymerisation

Depending on the desired final form of the polymer, there are several physical methods of polymerisation. Such formulations include bulk, solution, precipitation, dispersion and emulsion polymerisation.

1.5.1 Bulk polymerisation

Bulk polymerisation is conducted in the absence of any solvent. A suitable initiator is one that is soluble in the pure liquid monomer. Such polymerisations can be initiated by either heating or irradiation. The reaction mixture often becomes extremely viscous as polymerisation proceeds. This can result in broad MWDs and, in the case of highly exothermic reactions, the polymerisation may become uncontrolled owing to inefficient heat transfer. Bulk polymerisation is often implemented for step polymerisations, such as the synthesis of polyesters. Small molecules can be removed under vacuum to drive the polymerisation towards the desired product, which would be problematic if a relatively volatile solvent was present. If high conversions can be achieved at acceptable viscosities, post-polymerisation purification becomes unnecessary for bulk polymerisations, which is an important advantage for industrial-scale syntheses.

1.5.2 Solution polymerisation

The monomer, initiator and resulting polymer are all soluble in the chosen solvent for a solution polymerisation. The addition of solvent to a polymerisation confers several benefits and also some disadvantages. Heat transfer and control of the mixture viscosity becomes easier but purification of the polymer, *i.e.* removal of solvent and residual unreacted monomer, becomes more difficult. The rate of polymerisation is typically also lower, partly as a result of heat transfer to solvent. Ideally, it is best to utilise a solvent that is also required in the final product, thus eliminating its removal.

1.5.3 Precipitation polymerisation

A homogeneous formulation comprising solvent, soluble monomer and soluble initiator becomes a heterogeneous system owing to the precipitation of insoluble polymer during the polymerisation. This phase separation occurs at some critical DP and/or monomer conversion and can make efficient stirring and heat dissipation somewhat problematic.

1.5.4 Dispersion polymerisation

Dispersion polymerisation differs from precipitation polymerisation as it utilises a polymeric stabiliser to produce sterically-stabilised latex particles, rather than a macroscopic precipitate. The solvent should be a good solvent for the monomer, initiator and the steric stabiliser but be a non-solvent for the growing polymer chains. Thus, as the growing polymer chains nucleate the reaction mixture becomes heterogeneous and nascent particles are formed. The steric stabiliser adsorbs onto these particles and confers colloidal stability. Unreacted monomer diffuses into these particles, which leads to further polymerisation occurring within the monomer-swollen cores. Ultimately, colloidally stable polymer latex particles are produced. Without the steric

stabiliser, the polymer would simply precipitate from the reaction medium. Dispersion polymerisation was first developed by ICI in the 1960s and is often used for the production of spherical particles between 0.1 and 10 μm.[77] It is possible to tune the particle size by varying various synthesis parameters such as the monomer concentration, polymerisation temperature and amount of steric stabiliser.[78,79] Dispersion polymerisation often utilises FRP and can be conducted in non-polar,[80] aqueous[81] or alcoholic[82,83] media.

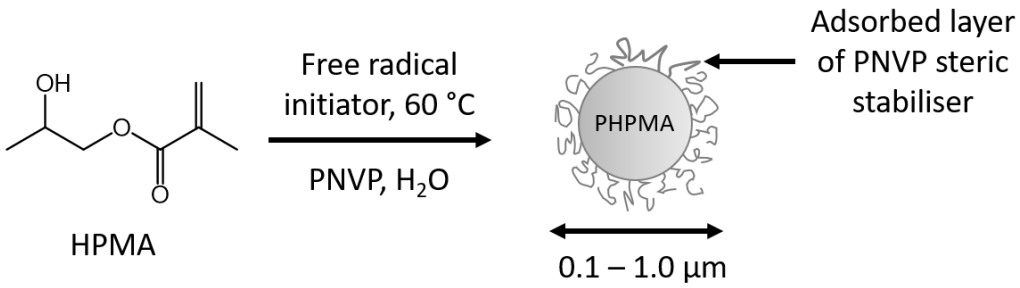

Figure 1.15. Aqueous dispersion polymerisation of 2-hydroxypropyl methacrylate (HPMA) in the presence of a suitable poly(*N*-vinyl pyrrolidone) (PNVP) steric stabiliser to produce a colloidally stable latex dispersion.[81]

For example, Ali *et al.* reported the aqueous dispersion polymerisation of 2-hydroxypropyl methacrylate (HPMA) *via* FRP.[81] As expected, macroscopic precipitation occurs in the absence of a suitable steric stabiliser. However, sterically-stabilised latex particles are produced in the presence of poly(*N*-vinyl pyrrolidone) (PNVP) and the particle size can be tuned by varying the synthetic parameters (Figure 1.15).

1.5.5 Aqueous emulsion polymerisation

Aqueous emulsion polymerisation can also be used to prepare polymer latexes.[84–87] Unlike dispersion polymerisation, it is an inherently heterogeneous formulation as the monomer is insoluble in the aqueous continuous phase. A surfactant is usually used to stabilise the monomer in the form of micron-sized droplets, although a minor fraction of monomer is also dissolved in the aqueous phase. Emulsion polymerisation enables high MW chains to be generated in a highly convenient low-viscosity (latex) form. Hence it has been widely used to manufacture solvent-borne and water-borne latexes for the paints and coatings industry. Depending on the precise formulation, the particle size can range from 50 nm up to 1000 nm.[77] Higher monomer and initiator concentrations tend to favour the formation of larger particles, whereas higher surfactant concentrations tend to produce smaller particles.

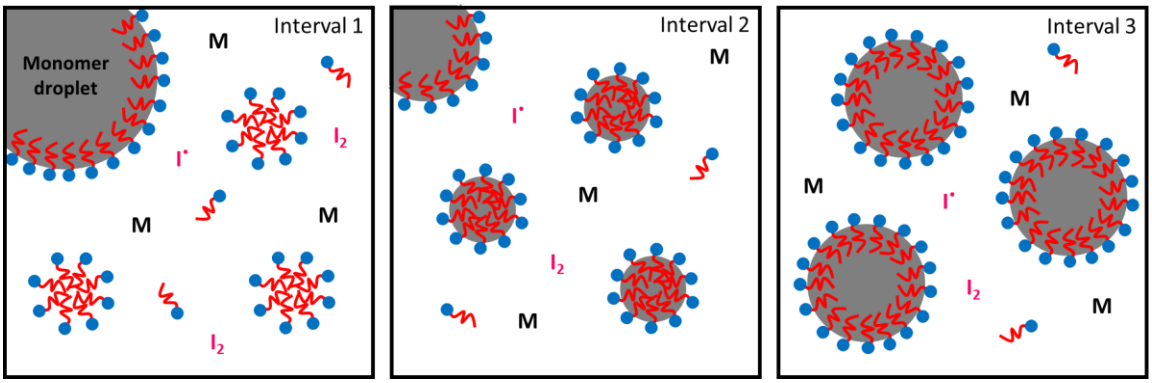

Figure 1.16. Schematic representation of the three main intervals for aqueous emulsion polymerisation conducted in the presence of a surfactant. [N.B. I_2 represents initiator molecules, $I^{\bullet}$ denotes initiator radicals and M is the monomer].[88]

Ab initio emulsion polymerisation comprises three separate intervals (Figure 1.16).[89,90] The monomer is initially present in micron-sized droplets, solubilised within much smaller (but much more numerous) surfactant micelles and a relatively small fraction is dissolved in the aqueous continuous phase. Initiator radicals can either diffuse into the micelles to initiate the polymerisation (heterogeneous nucleation) or they can react with dissolved monomer in the water (homogeneous nucleation). For the latter type of initiation, once a growing oligomeric radical reaches a critical DP it becomes insoluble and migrates into a surfactant micelle, where it continues to propagate. The number of polymer particles depends on the surfactant concentration: the more nuclei that are formed in the early stages of the polymerisation, the smaller the final latex particles. Once radicals enter the micelles, polymerisation occurs rapidly owing to the high local monomer concentration, which allows high monomer conversions to be achieved within relatively short timescales. Moreover, microcompartmentalisation reduces the probability of termination, which enables high MW polymer chains to be generated. The second interval involves diffusion of monomer from the droplet reservoirs through the aqueous solution into the micelles. This continues until all monomer is exhausted at a rate that is dictated by the aqueous solubility of the monomer. In the third and final stage, the monomer droplets are depleted and polymerisation continues within the monomer-swollen particles to produce a colloidally stable latex.

1.6 Self-assembly

Self-assembly is a thermodynamically driven process involving a molecule that contains both a solvophobic and solvophilic component.[91] Depending on the chemical structure of this

amphiphile, the self-assembled structure may involve hydrogen bonds and electrostatic interactions, as well as attractive Van der Waals interactions.

1.6.1 Self-assembly of surfactants

Surfactants are amphiphilic small molecules that reduce the interfacial tension *via* adsorption at the liquid-liquid, solid-liquid or air-liquid interface. In the case of two immiscible liquids, this enables the formation of stable emulsions.

Micelles comprise self-assembled colloidal aggregates of surfactants. Micelle formation occurs when the energy required for a single surfactant molecule to exist in its free (non-aggregated) state is higher than the entropic penalty associated with self-assembly.[92,93] At sufficiently low concentration most surfactant molecules exist as individual molecules, with self-assembly only occurring when the surfactant concentration exceeds the critical micelle concentration (CMC). According to Israelachvili,[93] the CMC is given by:

$$CMC = exp\left[-\frac{(\mu_1^0 - \mu_N^0)}{k_B T}\right] \qquad (1.18)$$

Here μ_1^0 is the chemical potential of the free amphiphile, μ_N^0 is the chemical potential of a micelle composed of *N* surfactant molecules, k_B is Boltzmann's constant and T is the absolute temperature.

There is a dynamic equilibrium between the micelles and the individual surfactant molecules; the mean residence time for a surfactant molecule within a micelle is typically below a millisecond.[94] Above the CMC, the number of micelles increases but there is always a background concentration of free surfactant. The major driving force for the self-assembly of ionic surfactants in aqueous solution is the hydrophobic effect.[93] Opposing this attractive force is the electrostatic repulsion between charged head-groups. The latter term dictates the area per molecule (α_0) that is exposed to the water. Stable micelles are formed when the repulsive and attractive forces are balanced.

According to Israelachvili and co-workers, the geometric packing parameter, *P*, (equation 1.19) can be used to predict the preferred micelle morphology, where *v* is the volume of the hydrophobic tail, a_0 is the contact area of the head-group and l_c is the length of the hydrophobic tail (Figure 1.17).[92,93]

$$P = \frac{\mathrm{v}}{a_0 l_c} \qquad (1.19)$$

The Gibbs equation ($\Delta G_{micelle} = \Delta H_{micelle} - T\Delta S_{micelle}$) can be used to explain the self-assembly of amphiphiles into micelles. A large increase in entropy drives self-assembly[95] owing to

the hydrophobic effect.[96] Water molecules form cage structures around the hydrophobic tails of individual surfactants; this local ordering increases the number of hydrogen bonds and reduces the solvent entropy.[97] On micelle formation, these clustered water molecules are released into the bulk solvent, which leads to an increase in the overall entropy of the system.

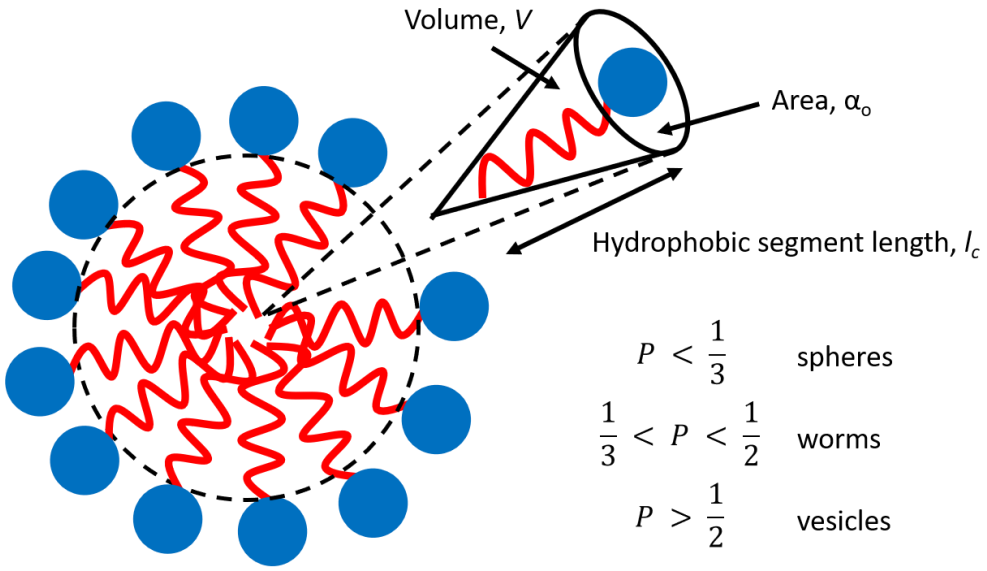

Figure 1.17. Schematic representation of the geometric packing parameter, *P*, for surfactant molecules within a micelle.

As indicated above, surfactant micelles are normally considered to be in thermodynamic equilibrium with free surfactant.[98] In contrast, diblock copolymer micelles are much more likely to be kinetically-frozen, although this depends on the nature of hydrophobic block.[95,98]

1.6.2 Self-assembly of AB diblock copolymers

AB diblock copolymers can undergo self-assembly in the bulk[99,100] owing to enthalpic incompatibility between the two blocks to produce microphase separated materials. Similarly, amphiphilic diblock copolymers undergo microphase separation in solution to produce various types of sterically-stabilised nano-objects.[101,102] Such colloidal aggregates are usually much more stable to dilution than surfactant micelles and have been widely studied over the past six decades.[103,104]

Depending on the volume fraction of each block, the overall DP and the Flory-Huggins interaction parameter (χ) between the two blocks, various copolymer morphologies can be obtained from self-assembly in the bulk.[104] The χ parameter represents the enthalpic incompatibility between the A and B blocks and varies inversely with temperature. Thus, intimate mixing between the two blocks can occur at a sufficiently high temperature. Self-consistent mean-field theory has been used to predict the phase separation of diblock copolymers in the bulk.[105,106] Such predictions are

reasonably consistent with experimental observations made for polyisoprene-*block*-PS copolymers.[104,105] Systematically increasing the volume fraction of block A induces order-order transitions from close-packed spheres (S) to cylinders (C), then gyroids (G) and finally lamellae (L), see Figure 1.18. If the volume fraction of block A then exceeds that of block B, the analogous inverse morphologies can be formed.

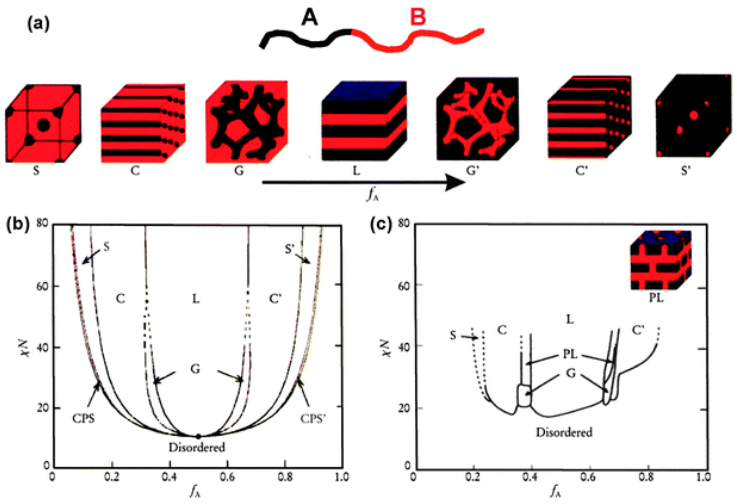

Figure 1.18. (a) AB diblock copolymer morphologies formed in the bulk where S and S' are bodied-centred cubic spheres, C and C' are hexagonally-packed cylinders, G and G' are bicontinuous gyroids and L denotes lamellae. (b) Theoretical phase diagram calculated using self-consistent mean-field theory according to the segregation parameter (χN) and the volume fraction of block A (f_A). (c) Experimental phase diagram determined for polyisoprene-polystyrene diblock copolymers where f_A is the volume fraction of the polyisoprene block and PL represents a perforated lamellae phase.[104]

It is also possible for diblock copolymers to self-assemble in a solvent that is selective for just one of the blocks. The resulting copolymer morphology depends on the diblock composition which can be linked to the geometric packing parameter originally introduced to account for surfactant self-assembly. If $P < \frac{1}{3}$, the surfactant (or diblock copolymer) forms spherical micelles, when $\frac{1}{3} < P < \frac{1}{2}$ worm-like micelles are obtained and when $P > \frac{1}{2}$ either vesicles or lamellae are obtained. If $P > 1$, inverted structures can be generated.

In reality, the copolymer morphology depends on several factors, including the nature of the monomer building blocks, the volume fraction of each block and the mean DP of each block. Often a solvent switch method is utilised where a solvent is selected that is a good solvent for one block and a bad solvent for the other. Self-assembled structures can also be generated in aqueous solution *via* a pH switch[107] or by thin film rehydration.[108] However, these protocols are typically conducted at low copolymer concentrations (≤ 1% w/w solids) and are therefore not scalable for industrial applications.

1.6.2.1 Critical solution temperatures

Polymers that become soluble at elevated temperatures exhibit upper critical solution temperature (UCST) behaviour, whereas polymers that precipitate out of solution at high temperatures exhibit lower critical solution temperature behaviour (LCST) (Figure 1.19).

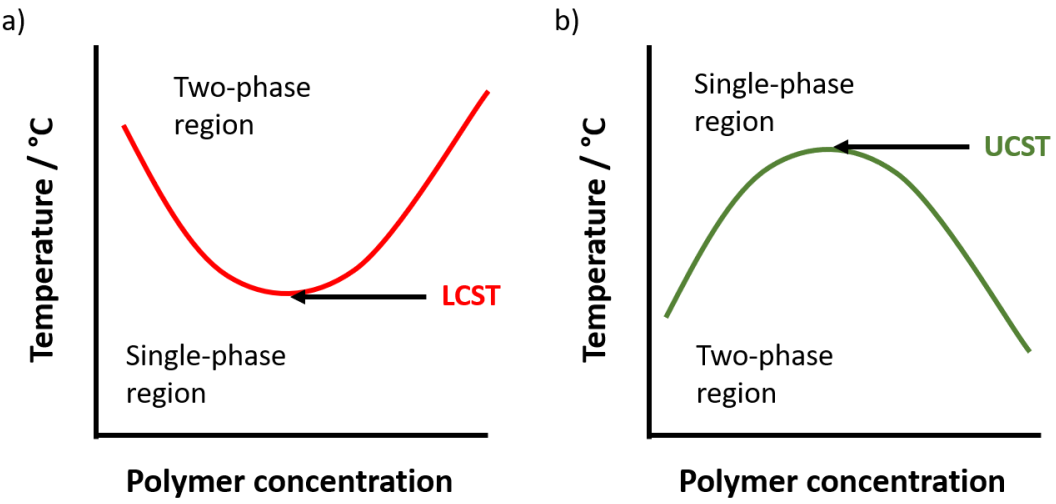

Figure 1.19. Phase diagrams illustrating (a) LCST and (b) UCST behaviour of polymers when varying the solution temperature, T, and polymer concentration. A cloud point (CP) is observed at the boundary, which is represented by a solid line.[109]

Strictly speaking, the terms UCST and LCST should only be used if a phase diagram has been constructed, otherwise only the transition temperature should be cited.[109] This is known as the cloud point (CP), because the initially transparent solution becomes turbid as the polymer chains become insoluble (Figure 1.20). A well-known example of a thermoresponsive polymer is poly(*N*-isopropylacrylamide) (PNIPAM),[110,111] which has an LCST that is almost independent of the polymer concentration or MW. At any given concentration, the CP is almost identical to the LCST so these terms are used interchangeably in this particular case.

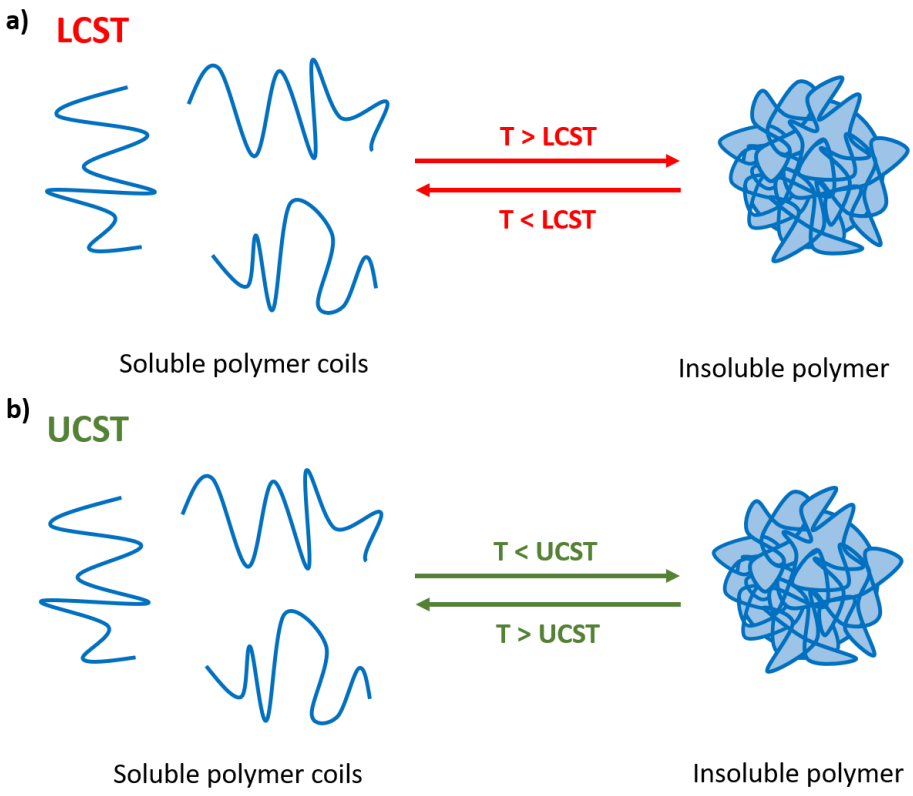

Figure 1.20. Schematic representation of a thermoresponsive polymer exhibiting (a) LCST behaviour and (b) UCST behaviour in solution**.**

The CP of PNIPAM is independent of molecular weight or concentration, as stated above. It has a CP between 32 and 33 °C and, given its biocompatibility, it is an interesting biomaterial. It is possible to cross-link PNIPAM to form hydrogels and subsequently load with drug molecules.[112,113] Inducing a coil-to-globule transition causes a reduction in gel volume, resulting in release of the entrapped drug.[114,115] It is also possible form PNIPAM microgels which have a sponge-like structure with the interstitial spaces filled with solvent, which similarly can be loaded with drugs.[116,117] These microgels combine the favourable properties of 'bulky' hydrogels (flexibility, hydrophilicity and biocompatibility)[118] with those of a colloidal dispersion (long circulation lifespan, low viscosity, high internal void fraction and diameter tuneability).[115,119] When the size of the microgel is tuned to be below 200 nm, the blood circulation time of the drug carriers is extended.[120]

Another example of a polymer that exhibits LCST behaviour is poly(*N*-(2-methacryloyloxy)ethyl pyrrolidone) (PNMEP).[121,122] PNMEP is an analogue of PNVP, which is a highly biocompatible polymer that is widely used in the health and personal care industry.[123–125] The effect of polymer structure on LCST behaviour was explored by Sun and co-workers.[121] This team compared the LCST behaviour of PNMEP (DP = 96, CP = 65.3 °C) with that of poly(*N*-(3-

acryloyloxypropyl)pyrrolidone) (PNAPP) (DP = 104, CP = 66.5 °C) and poly(*N*-(3-methacryloyloxy)propyl)pyrrolidone) (PNMPP) (DP = 100, CP = 29.5 °C). As expected, PNMEP exhibited a comparable CP to that of its isomeric acrylic analogue (PNAPP). However, addition of just one methyl group to the backbone (*i.e.* PNMPP *vs.* PNAPP) led to a 37 °C reduction in CP for polymer chains of comparable mean DP.

In contrast to LCST-type polymers, there are relatively few examples of UCST-type polymers in aqueous solution. In most cases, these literature examples are zwitterionic polymers.[126] A well-known UCST-type polymer is PS in cyclohexane; this polymer is soluble in hot cyclohexane but becomes insoluble when cooling below its CP of 35 °C.[127–129] Similarly, poly(ethylene oxide) exhibits UCST behaviour in ethanol.[130]

Several groups have synthesised doubly-thermoresponsive diblock copolymers where one block exhibits LCST-type behaviour while the other block exhibits UCST-type behaviour. Provided that the LCST is greater than the UCST, two types of diblock copolymer micelles can be formed and there is an intermediate temperature range where the copolymer chains are molecularly dissolved.

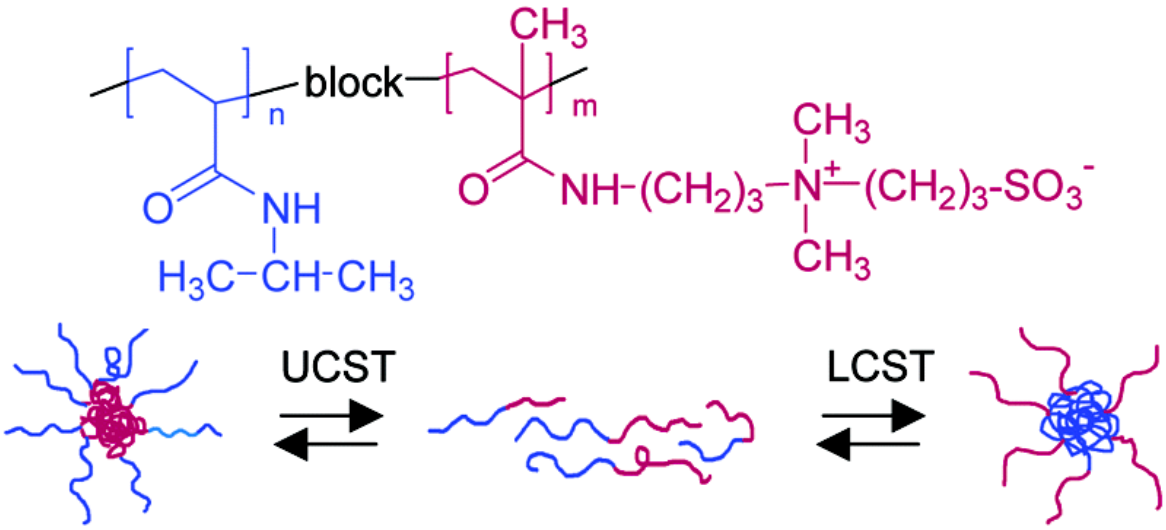

Figure 1.21. Effect of varying the solution temperature on the aggregation behaviour of PNIPAM-PSPP diblock copolymers in aqueous media.[131]

The first example of this unusual behaviour was reported by Arotçaréna *et al.* for PNIPAM-*block*-P(3-(*N*- (3-methacrylamidopropyl)-*N*,*N*-dimethyl)ammoniopropane sulfonate) (PSPP) copolymers prepared by RAFT solution polymerisation in methanol.[131] This thermoresponsive diblock copolymer can form either PNIPAM-core or PSPP-core micelles in water because PNIPAM exhibits LCST behaviour and PSPP exhibits UCST behaviour, see Figure 1.21. PSPP is a polyzwitterion and its UCST in water increases with increasing MW.[132,133]

1.7 Polymerisation-induced self-assembly

Polymerisation-induced self-assembly (PISA) is a highly versatile platform technology for the efficient synthesis of diblock copolymer nanoparticles in the form of concentrated dispersions. A soluble homopolymer precursor is chain-extended with a second monomer, whose growing chains eventually become insoluble in the chosen solvent at some critical DP. This drives *in situ* self-assembly to form sterically-stabilised nanoparticles. This approach eliminates the need for post-polymerisation processing and can be conducted at copolymer concentrations of up to 50% w/w.[134] The final diblock copolymer morphology is usually determined by the relative volume fractions of the core-forming (solvophobic) and stabiliser (solvophilic) blocks (Figure 1.22). Simply varying the target DP and the copolymer concentration often enables a range of diblock copolymer morphologies such as spheres, worms, vesicles or lamellae to be generated. In particular, the construction of pseudo-phase diagrams enables reproducible targeting of such morphologies and allows mixed phases to be avoided.[135–140] However, several other synthesis parameters can influence the copolymer morphology, including the polymerisation temperature, choice of solvent, the mean DP of each block, and the solution pH (if ionisable groups are present). This is because each of these parameters influences the effective volume of each block. In particular, kinetically-trapped spheres are often obtained if the steric stabiliser block is too long[135,141–143] or contains ionic groups.[144–147] As described previously, the geometric packing parameter used to describe the morphology of surfactant micelles can also be used to predict the final copolymer architecture of diblock copolymers.

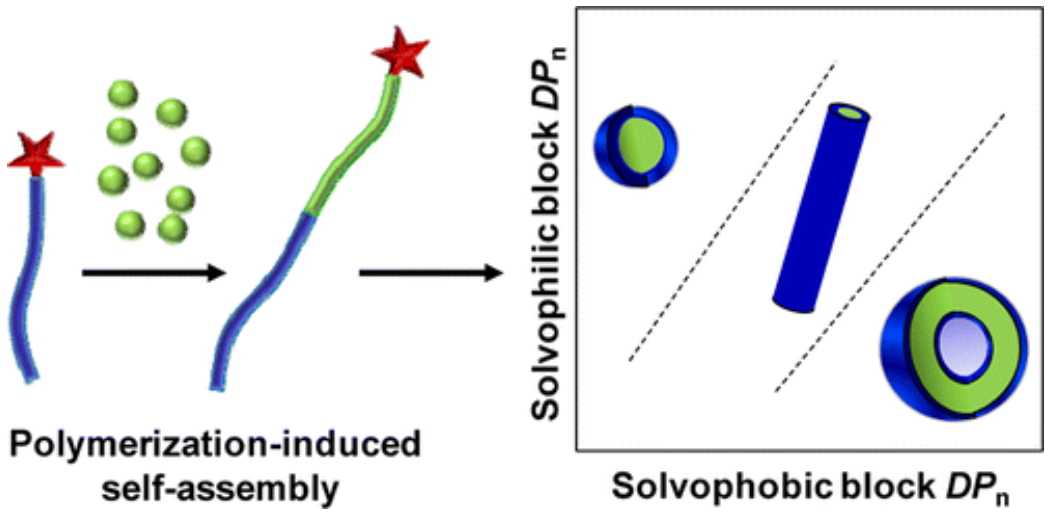

Figure 1.22. Evolution of diblock copolymer morphologies observed during PISA when varying the mean DPs of the solvophobic and solvophilic blocks.[148]

RDRP techniques are typically used for PISA syntheses of diblock copolymer nanoparticles. In this Thesis, RAFT-mediated PISA has been used exclusively for the formation of diblock copolymer

nanoparticles in various solvents. Thus, this specific topic is discussed in more detail below. Hawkett and co-workers were the first to report an efficient PISA formulation: they prepared spherical nanoparticles *via* RAFT aqueous emulsion polymerisation of methyl acrylate (MA), *n*-butyl acrylate (BA) and styrene (S).[149,150] More generally, RAFT aqueous emulsion polymerisation often leads to the formation of kinetically-trapped spheres.[150–157] However, over the past decade various strategies have been developed to produce higher order morphologies.[144,152,158–162] One particular approach recently developed by the Armes group involves selecting vinyl monomers that exhibit slightly higher solubility in aqueous solution (typically around 20 g dm^{-3}).[163–165]

Many RAFT dispersion polymerisation formulations also produce kinetically-trapped spheres, particularly when using a relatively long steric stabiliser block[135,142,143] or when working at relatively low copolymer concentration.[135,140] However, so-called higher order morphologies such as worms, vesicles or lamellae can be normally obtained by selecting appropriate conditions.[135,136,138,144,166,167] Typically, this involves using a suitably short steric stabiliser block and targeting a relatively long insoluble block at a sufficiently high copolymer concentration.[144,145,158,159] For such PISA syntheses, the evolution in copolymer morphology always appears to follow the same mechanistic pathway. If a sufficiently asymmetric diblock copolymer composition is targeted, spheres are formed initially and, as the structure-directing insoluble block grows longer, worms are formed *via* the stochastic 1D fusion of multiple spheres, followed by vesicle formation *via* transient jellyfish-like intermediates.[136,168,169] For certain types of diblock copolymers, a lamellar morphology (*i.e.* thin 2D sheets or platelets) can also be obtained.[138,170]

1.7.1 Colloidal stability

Colloids comprise particles (or droplets) that are less than 1000 nm in size dispersed within a continuous phase.[95] The colloidal stability of solid particles in a liquid medium depends on whether attractive or repulsive interactions dominate when interparticle collisions occur as a result of Brownian motion. If attractive forces dominate, the particles undergo 'sticky' collisions and become aggregated, destabilising the dispersion. However, if repulsive forces dominate, then the interparticle collisions are elastic and the dispersion remains colloidally stable. The three main mechanisms for colloidal stability are charge, steric and electrosteric stabilisation (Figure 1.23).[93,171]

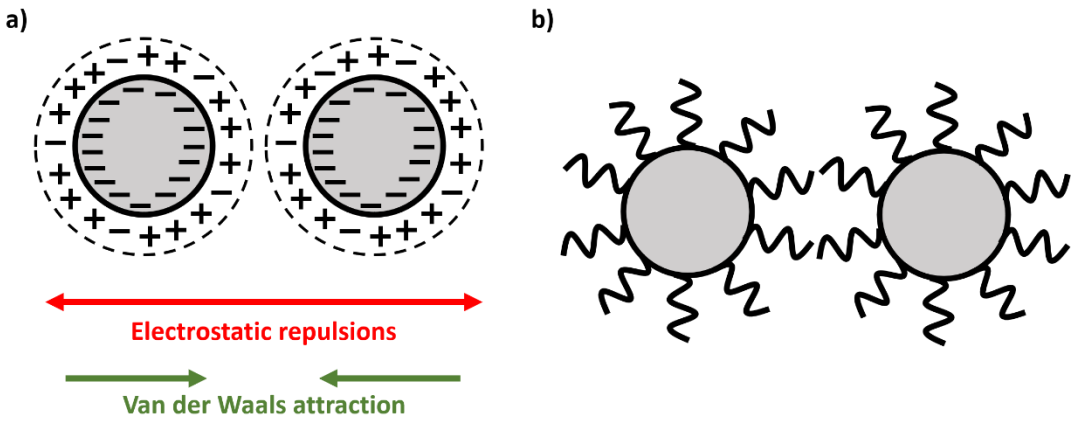

Figure 1.23. Schematic representation of (a) charge stabilisation conferred by the unfavourable interpenetration of electrical double layers surrounding anionic particles and (b) steric stabilisation conferred by unfavourable interpenetration of adsorbed layers of polymer chains at the surface of particles.

1.7.1.1 Charge stabilisation

Colloidal particles in aqueous solution can acquire surface charge by any one of four main mechanisms[95]: ion adsorption, ionisation, dissolution of ionic solids and isomorphous substitution. Each charged particle is surrounded by an electrical double layer (EDL), which contains an excess of oppositely charged ions (for example, the EDLs that surround anionic particles contain excess cations). When any two particles collide, it is the unfavourable overlap between their EDLs (rather than Coulombic repulsion) that leads to the generation of the repulsive force that accounts for their colloidal stability. Charge stabilisation is only effective in highly polar solvents such as water or lower alcohols, which are required to confer sufficient surface charge. Moreover, the addition of electrolyte causes the EDLs to shrink and weakens the repulsion force, leading to particle aggregation.

1.7.1.2 Steric stabilisation

Steric stabilisation is conferred by the physical or chemical adsorption of polymer chains onto the particle surface. Interpenetration of such 'hairy' layers is entropically unfavourable and, in a good solvent environment for the adsorbed polymer, is also enthalpically unfavourable. This generates a strong steric repulsion force that prevents neighbouring particles from getting close enough for attractive forces to dominate. The steric stabiliser must be strongly bound to the particle surface at a sufficiently high surface area coverage. Steric stabilisation offers the following advantages over charge stabilisation: (i) it enables colloidal dispersions to be prepared in either polar or non-polar media; (ii) sterically-stabilised particles are usually insensitive to added electrolyte; (iii) effective stabilisation can be achieved even for concentrated dispersions. Moreover, if aggregation of sterically-stabilised particles does occur, this is often weak and reversible. This is sometimes known as flocculation.

1.7.1.3 Electrosteric stabilisation

Electrosteric stabilisation combines aspects of both charge and steric stabilisation. In this case, the polymer adsorbed onto the particle surface may be a polyelectrolyte or perhaps contain an ionisable end-group. Alternatively, a non-ionic polymer may be adsorbed onto particles that possess substantial underlying surface charge. Thus, the repulsive forces required to offset the ever-present attractive forces can arise from both unfavourable EDL overlap and steric repulsion.

1.7.2 RAFT dispersion polymerisation

RAFT dispersion polymerisation can be used to prepare a wide range of sterically-stabilised nanoparticles in various media, ranging from water to polar solvents such as alcohols[136,143,172–174] to non-polar solvents such as *n*-alkanes,[137,175,176] mineral oil[142] or silicone oil[177]. In each case, a soluble precursor is chain-extended with a suitable miscible monomer. The soluble precursor block becomes the steric stabiliser while the growing second block becomes insoluble and structure-directing.

1.7.2.1 RAFT aqueous dispersion polymerisation

An *et al.* were the first to report RAFT aqueous dispersion polymerisation, although this terminology was not used in their study.[178] They chain-extended a PDMAC precursor with water-miscible NIPAM in aqueous solution at 70 °C. At this reaction temperature, the growing PNIPAM chains are above their LCST. Thus, micellar nucleation occurs at some critical DP and diblock copolymer spheres with PNIPAM cores and PDMAC coronas are produced. On cooling below the LCST of the PNIPAM block, these sterically-stabilised nanoparticles dissolved to form soluble chains. To prevent such dissolution, the nanoparticles were crosslinked at 70 °C using bisacrylamide so that colloidally stable water-swollen nanogels were formed on cooling instead (see Figure 1.24).

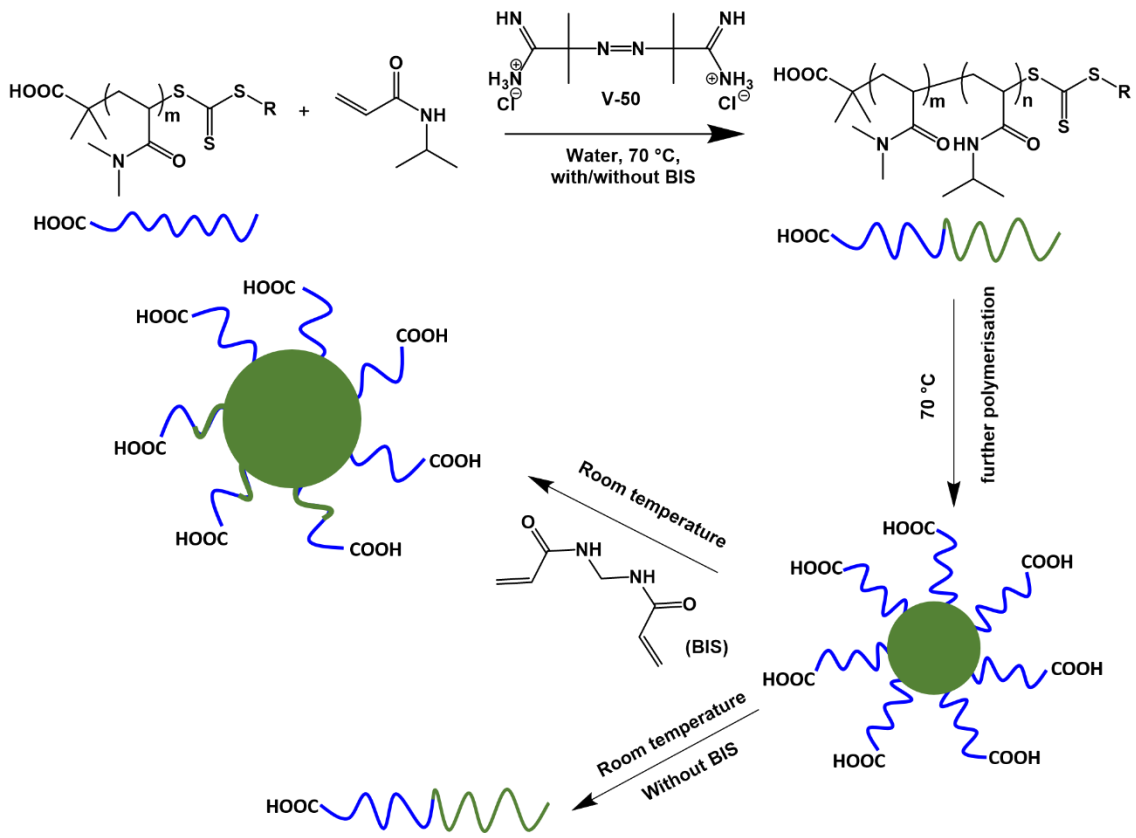

Figure 1.24. Schematic representation of the first example of RAFT aqueous dispersion polymerisation: chain extension of a PDMAC precursor with NIPAM produces spherical nanoparticles that can be subsequently cross-linked with bisacrylamide (BIS).[178]

Many research groups have used various water-soluble polymers as steric stabilisers for RAFT aqueous dispersion polymerisation in order to produce spherical, worm-like or vesicular nano-objects. A summary of some of the most common steric stabilisers and water-miscible monomers used to generate the insoluble second block are given below.

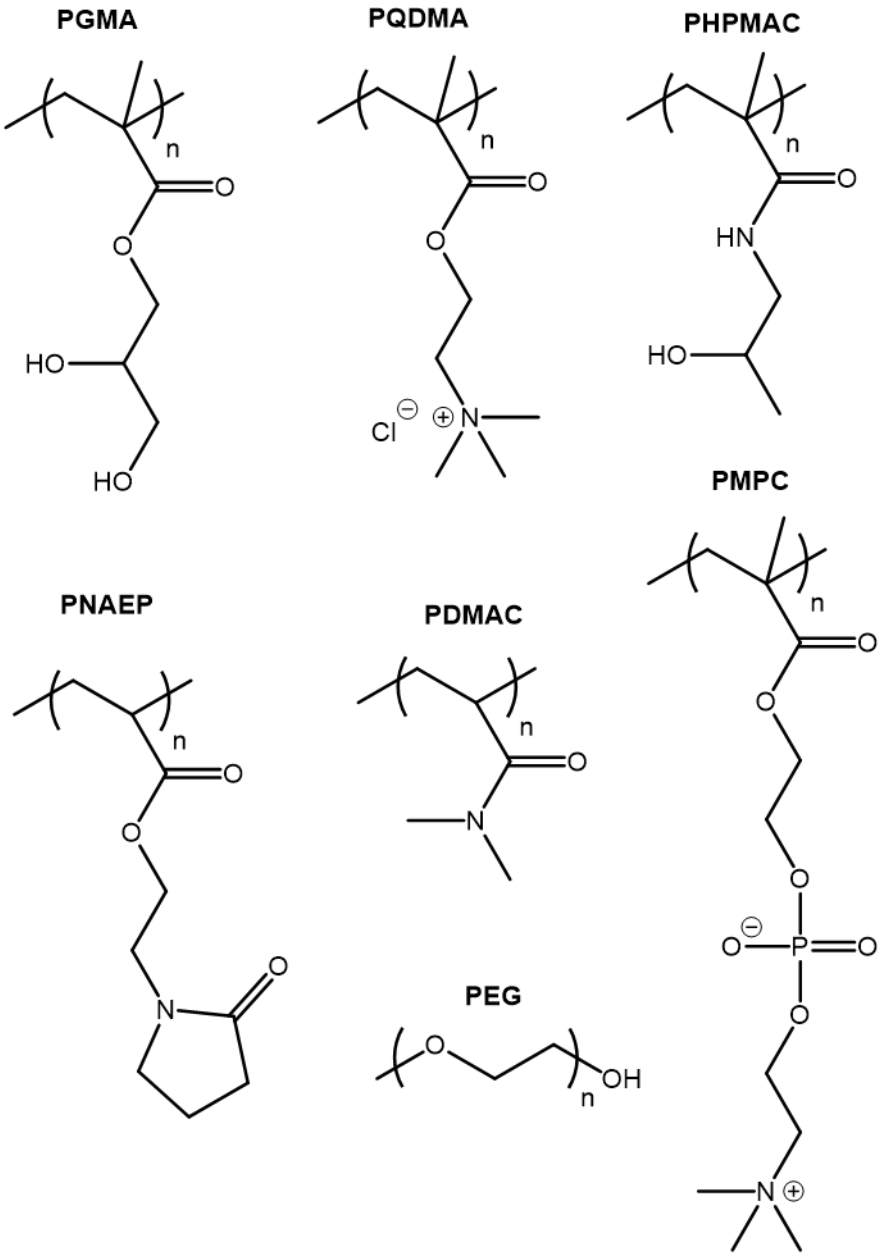

Figure 1.25. Chemical structures of seven steric stabiliser blocks commonly used in the literature for RAFT aqueous dispersion polymerisation.

Some commonly used polymers are shown in Figure 1.25, these include poly(glycerol monomethacrylate) (PGMA),[63,122,135,165,179–184] poly(2-(methacryloyloxy)ethyl trimethylammonium chloride) (PQDMA),[147] poly(2-hydroxypropyl methacrylamide) (PHPMAC),[185–188] poly(*N*-(2-acryloyloxy)ethyl pyrrolidone) (PNAEP),[189] PDMAC,[190] poly(ethylene glycol) (PEG),[139,191–193] poly(2-(methacryloyloxy)ethylphosphorylcholine) (PMPC).[194–196]

Figure 1.26 shows the chemical structures of various water-miscible monomers that have been used for RAFT aqueous dispersion polymerisation. These include HPMA,[63,135,184,197,139,146,147,179–183] NMEP,[122] 4-hydroxybutyl acrylate (HBA),[198] diacetone acrylamide (DAAM),[190] NIPAM[110,111] and

N,*N*'-diethylacrylamide (DEAM).[199,200] It should be noted that PNIPAM and PNMEP both exhibit LCST behaviour. In principle, NIPAM can be polymerised below its LCST *via* RAFT solution polymerisation prior to increasing the solution temperature to form particles.[201] However, this would not be an example of RAFT aqueous dispersion polymerisation. In contrast, Cunningham and co-workers prepared high MW PGMA-PNMEP diblock copolymers using a RAFT aqueous dispersion polymerisation formulation in order to avoid the problem of high solution viscosity.[122] Thus NMEP was polymerised above the CP of the PNMEP block to produce low-viscosity sterically-stabilised nanoparticles at 70 °C. On cooling to 20 °C, the PGMA-PNMEP diblock copolymer nanoparticles dissociated to form molecularly-dissolved copolymer chains with molecular weights approaching $1x10^6$ g mol^{-1}.

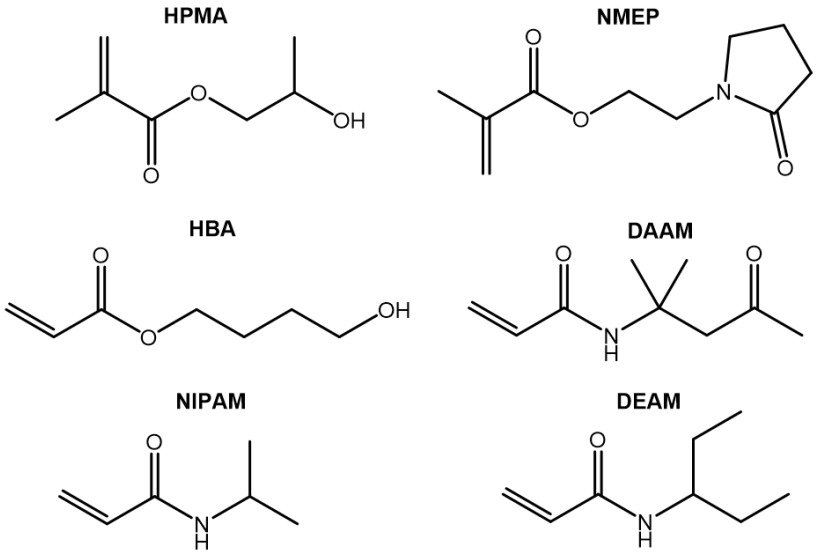

Figure 1.26. Chemical structures of six water-miscible monomers that can be used to generate the water-insoluble block required for RAFT aqueous dispersion polymerisation.

A well-studied diblock copolymer within the Armes research group is PGMA-PHPMA.[180] PGMA is a non-ionic water-soluble polymer: chain-extending this precursor with the water-miscible HPMA monomer *via* RAFT aqueous dispersion polymerisation enables the formation of well-defined PGMA-PHPMA spheres, worms or vesicles.[135,168,202,203] A master phase diagram has been recently published that enables such copolymer morphologies to be targeted with excellent reproducibility (see Figure 1.27).[203]

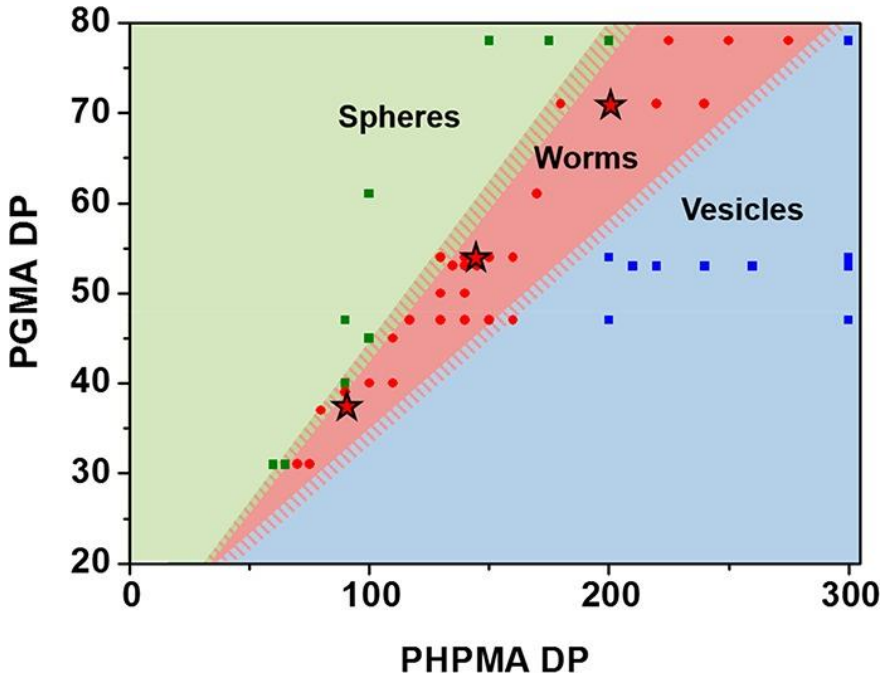

Figure 1.27. Master phase diagram constructed for PGMA-PHPMA diblock copolymer nano-objects prepared *via* RAFT aqueous dispersion polymerisation using transmission electron microscopy. This 'morphology map' enables the reproducible targeting of pure copolymer morphologies. Green squares indicate spheres, red circles represent worms and blue squares indicate vesicles. A copolymer concentration of 20% w/w was used for all syntheses except those involving PGMA DPs below 47 (since such PISA formulations are known to exhibit concentration-independent morphologies).[203]

The final copolymer morphology depends on both the copolymer concentration and also the DP of each block. Thus, it is prudent to compile a master phase diagram using steric stabiliser blocks of varying DPs. Low copolymer concentrations (*e.g.* 10% w/w) produce only kinetically-trapped spheres whose size depends on the target DP for the core-forming block. Higher copolymer concentrations (> 20% w/w) are often required to access higher order morphologies, since such conditions favour sphere-sphere fusion, which is the critical first step for the generation of worms and vesicles. Blanazs and co-workers reported the mechanism for the formation of vesicles from worms (Figure 1.28).[168] At first the worms begin to branch as there is a reduction in molecular curvature as the MW increases. An increase in the worm branching along with worm clustering causes partial coalescence to form bilayer-like structures with attached 'tentacles', a so-called 'octopi' morphology. As the core DP increases with HPMA conversion, these 'octopi' partially wrap up to form 'jellyfish', the precursor to vesicle formation. Finally, the tentacles fuse to form vesicles.

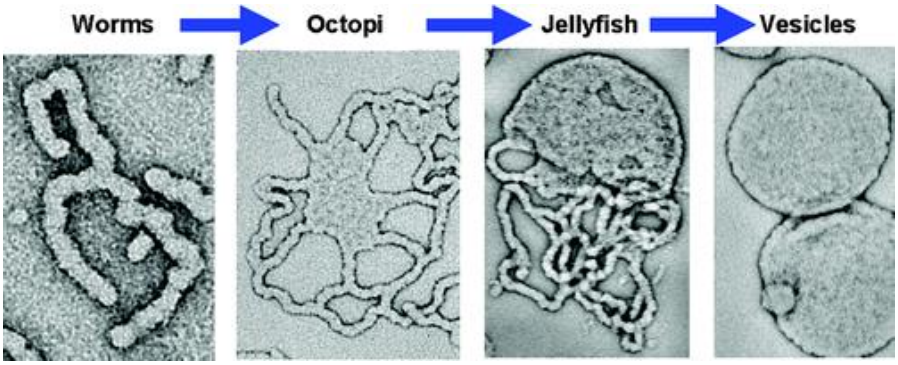

Figure 1.28. The suggested mechanism for the worm-to-vesicle transition during the PISA synthesis of $PGMA_{47}$-$PHPMA_{200}$ diblock copolymer nano-objects.[168]

Although PHPMA is always weakly hydrophobic, its degree of (partial) hydration varies with temperature. This can be sufficient to confer thermoresponsive behaviour on PGMA-PHPMA diblock copolymer nano-objects. For example, PGMA-PHPMA worms form soft free-standing gels owing to multiple inter-worm contacts.[204,205] Cooling such worm gels from 20-25 °C to 4 °C induces a reversible worm-to-sphere transition, which causes *in situ* degelation to produce a free-flowing, low-viscosity fluid.[204] Variable temperature ^{1}H NMR studies were used to demonstrate that this morphological transition is driven by the greater degree of hydration of the core-forming PHPMA block at sub-ambient temperatures. This unusual thermoresponsive behaviour was exploited by Canton and co-workers, who showed that such PGMA-PHPMA worm gels are highly biocompatible and could be used to store human stem cells for up to two weeks at 37 °C without any loss of pluripotency.[206] Interestingly, this was achieved by inducing a dormant state known as stasis.

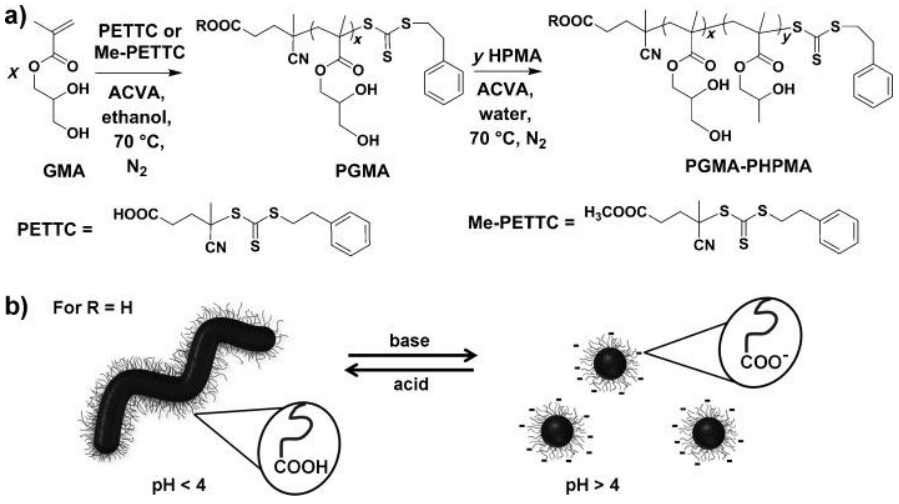

Figure 1.29. (a) Synthesis of a $PGMA_{56}$ macro-CTA *via* the RAFT solution polymerisation of GMA using a 4-cyano-4-(2-phenylethanesulfanylthiocarbonyl)sulfanylpentanoic acid (PETTC) RAFT agent and ACVA initiator, and subsequent chain extension with HPMA to form PGMA–PHPMA diblock copolymer nano-objects at pH 4. (b) The worm-to-sphere morphological transition when COOH-functionalised worms are subjected to a pH change upon addition of base.[181]

If the RAFT agent is chosen carefully PGMA-PHPMA diblock copolymers can also exhibit pH-responsive behaviour.[181–184] Lovett *et al.* reported the synthesis of HOOC-PGMA$_{56}$-PHPMA$_{155}$ diblock copolymer worms at pH 4 (Figure 1.29).[181] On increasing the pH to 6 and, thereby ionising the carboxylic acid end-group (conferred by PETTC RAFT agent), a subtle shift in the packing parameter caused a worm-to-sphere transition. Chemical decomposition of the copolymer was determined to be unlikely as the behaviour was reversible when changing the solution pH back to the original value. The pK_a of the PGMA$_{56}$ macro-CTA was determined by acid titration to be 4.7. Ionisation of this carboxylic acid end-group caused the pH responsive behaviour by increasing the degree of hydration of the PGMA stabiliser block lowering the packing parameter inducing a morphological transition. As a control experiment, a methyl derivative of the PETTC RAFT agent (Me-PETTC) was used to prepare the same diblock copolymer composition and, as expected, this copolymer exhibited no pH-response. pH responsive nano-objects offer an exciting opportunity for use as smart materials in biological applications.[207,208] Utilising ionisable end-groups to induce a morphological transition is of particular importance as small levels of base (or acid) can be added to induce such a change. This is of particular relevance if multiple cycles are required as it will minimise background salt accumulation.[209]

1.7.2.2 RAFT alcoholic dispersion polymerisation

Early work in this area was conducted by Pan *et al.*, who reported the PISA syntheses of amphiphilic diblock copolymers *via* RAFT alcoholic dispersion polymerisation of styrene.[210–213] However, rather slow polymerisation kinetics were obtained, with styrene conversions of only 30-70% being achieved after 48 h at 80 °C. This limitation makes such PISA formulations unlikely to be attractive for industrial scale-up.

As an alternative to styrene, benzyl methacrylate (BzMA) has been widely used for RAFT alcoholic dispersion polymerisation formulations.[68,141,172,214–218] In all cases, good control over the MWD was achieved but reaction times of up to 24 h were required for more than 95% BzMA conversion. This problem is well-documented for such PISA formulations. However, Zhang *et al.* reported that addition of a small amount of water to a RAFT alcoholic dispersion polymerisation significantly increased the rate of polymerisation.[214] However, adding too much water also affected the final copolymer morphology. For example, adding 5% v/v water to ethanol provided access to spheres, worms and vesicles simply by increasing the target PBzMA DP when using a poly(methacrylic acid)-*co*-poly((oligoethylene oxide) monomethyl ether methacrylate) (PMAA-*co*-PEOMA) precursor. On the other hand, using 23% v/v water merely led to kinetically-trapped spheres (see Figure 1.30).

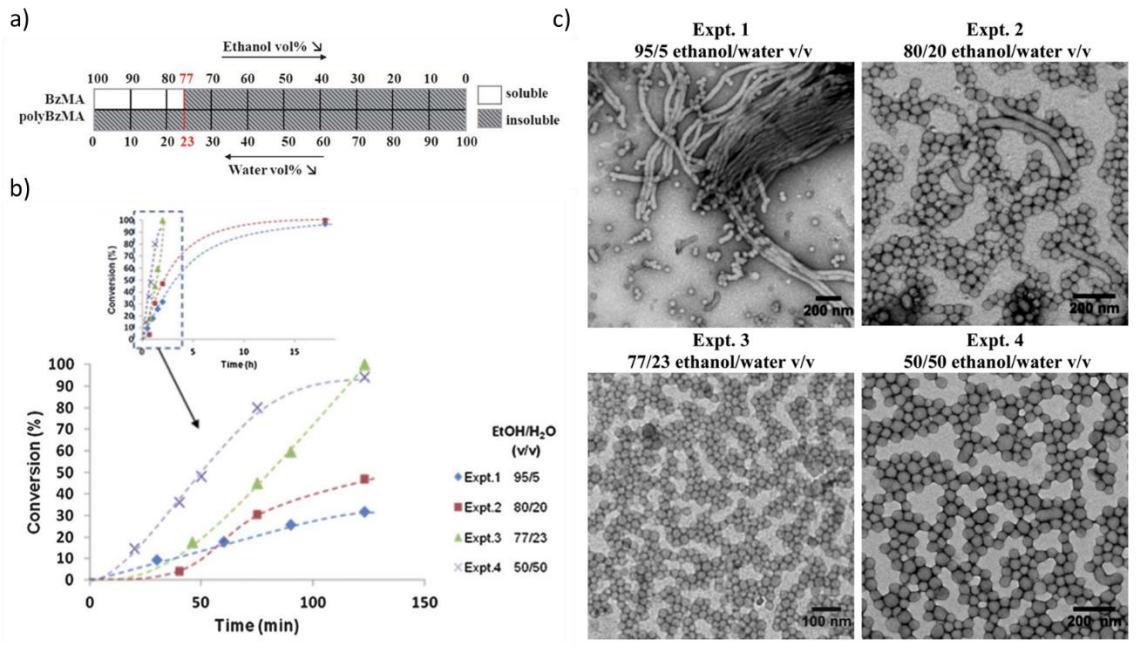

Figure 1.30. (a) Solubility test of BzMA monomer and PBzMA at 0.30 g mL^{-1} in various ethanol-water mixtures. (b) Initial conversion *vs.* time curves for the RAFT dispersion polymerisation of BzMA using a PMAA-*co*-POEMA stabiliser block in various ethanol-water mixtures. The inset indicates the final conversion *vs.* time curves obtained over longer reaction times. (c) Corresponding TEM images of the nano-objects obtained from these PISA syntheses in various ethanol-water mixtures.[214]

At around the same time, Jones and co-workers reported the chain extension of a poly(2-(dimethylamino)ethyl methacrylate) (PDMA) precursor with BzMA at 70 °C in anhydrous ethanol and also 80-20, 90-10 and 95-5% w/w ethanol-water mixtures, see Figure 1.31. Increasing the amount of water co-solvent dramatically increased the rate of BzMA polymerisation: 90% conversion was achieved within 6 h when adding 20% v/v water (as opposed to only 35% conversion when using anhydrous ethanol for the same reaction time) but limited the final copolymer morphology to kinetically-trapped spheres.[215] The much faster kinetics was attributed to stronger BzMA partitioning within the growing nascent nanoparticles, resulting in a higher local monomer concentration.

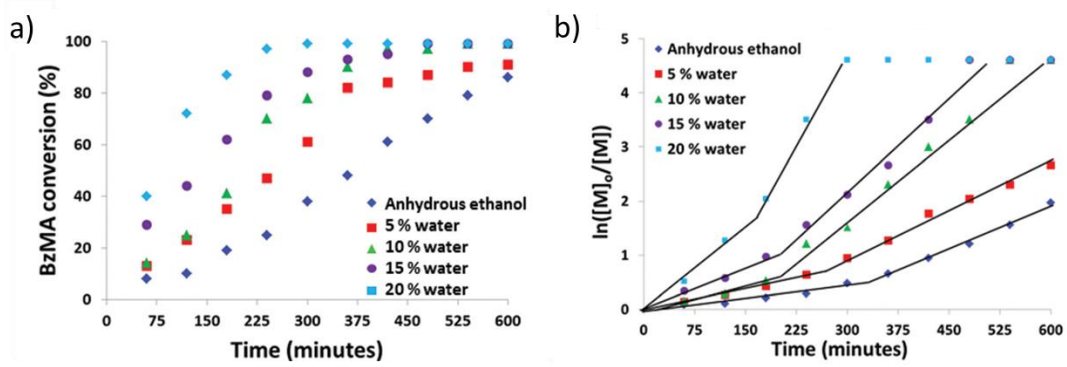

Figure 1.31. Kinetic data obtained from ^{1}H NMR spectroscopy studies for the RAFT dispersion polymerisation of BzMA at 70 °C using a $PDMA_{43}$ precursor in various ethanol-water mixtures targeting a diblock copolymer composition of $PDMA_{43}$-$PBzMA_{200}$ at 15% w/w solids: (a) conversion *vs.* time curves and (b) the corresponding semi-logarithmic plots.[215]

Increasing the amount of water as a co-solvent led to faster polymerisations (see Figure 1.31a). Inspecting the semi-logarithmic plots shown in Figure 1.31b, there is a dramatic rate enhancement after the onset of micellar nucleation. However, the reaction time (and the critical PBzMA DP) required for nucleation varied according to the solvent composition. In their prior study of the RAFT alcoholic dispersion polymerisation of BzMA, the same authors calculated that micellar nucleation occurred at a PBzMA DP of 50.[172] On addition of 0, 5, 10, 15 or 20% w/w water, micellar nucleation occurred at critical PBzMA DPs of approximately 80, 100, 100, 140 and 160, respectively. It should be noted that there was a discrepancy of approximately 30 DP when pure ethanol was used between the two reports which was expected due to the difference in DP of the PDMA stabiliser block used (31 *vs.* 43 respectively).

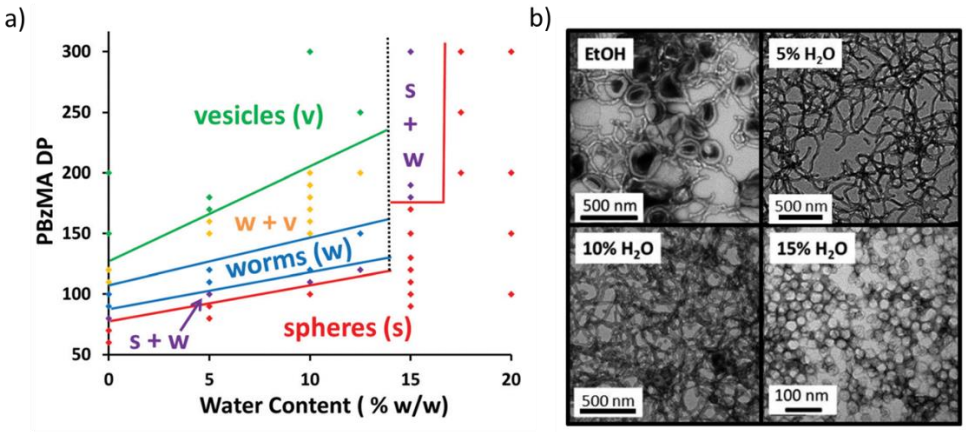

Figure 1.32. (a) Phase diagram constructed by Jones *et al.* for $PDMA_{43}$-$PBzMA_{x}$ diblock copolymers prepared *via* RAFT dispersion polymerisation of BzMA in various ethanol-water mixtures at 15% w/w solids and (b) representative TEM images of the corresponding $PDMA_{43}$-$PBzMA_{120}$ nano-objects (see image captions for the relevant water content).[215]

TEM was used to characterise the final copolymer morphology and a phase diagram was constructed for various ethanol-water mixtures when targeting a copolymer concentration of 15%

w/w for various PBzMA DPs (Figure 1.32). This phase diagram indicates that the amount of added water has a marked effect on the copolymer morphology. In particular, worms and vesicles can only be accessed when using less than 15% w/w water. Moreover, only spheres can be formed in the presence of 20% w/w water even when targeting PBzMA DPs of up to 500.

One advantage of using ethanol instead of water for PISA syntheses is that it enables weak polyelectrolytes to be used as non-ionic stabiliser blocks. In water, weak polyelectrolytes usually acquire charge *via* either ionisation or protonation, which normally limits access to worms and vesicles. Indeed, Charleux *et al.* postulated that strong inter-chain repulsion hinders access to higher order morphologies.[145] Similarly, Semsarilar *et al.* observed such restrictions when using either anionic or cationic polyelectrolytic stabiliser blocks for the RAFT aqueous dispersion polymerisation of HPMA.[146,147] Semsarilar and co-workers reported the RAFT dispersion polymerisation of BzMA in ethanol using non-ionic, zwitterionic, polyacid and polybase stabilisers (*i.e.* PGMA, PMPC, PMAA and PDMA, respectively), see Figure 1.33. In this case, using either PDMA or PMAA stabiliser blocks enabled the synthesis of spheres, worms or vesicles *via* systematic variation of the copolymer concentration and the target PBzMA DP. However, pure vesicles could not be obtained when using the PGMA stabiliser. It should also be noted that the worm and vesicle phases were contaminated with a population of spheres when utilising a PMPC stabiliser.

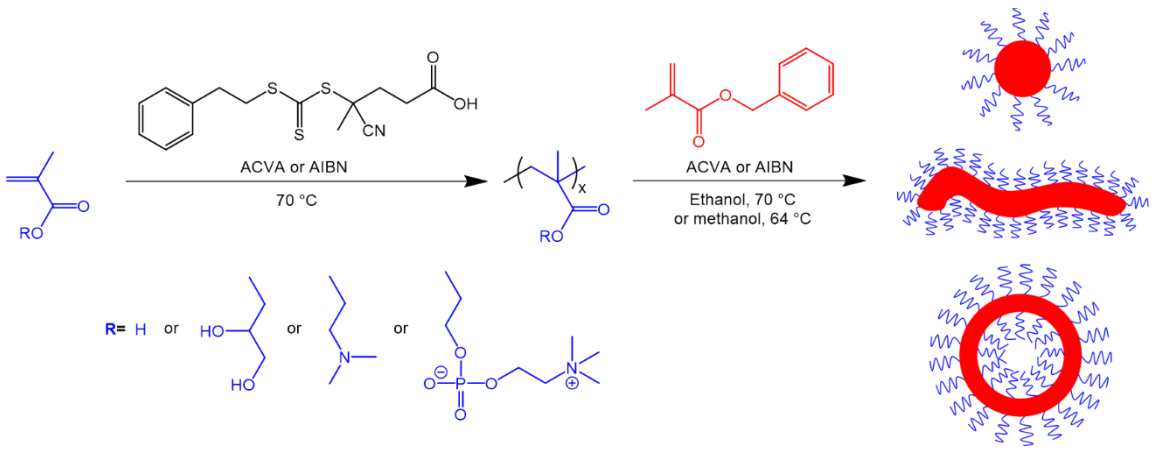

Figure 1.33. RAFT dispersion polymerisation of BzMA in ethanol using non-ionic, zwitterionic, polyacid or polybasic precursors can produce spheres, worms or vesicles.[217]

A phase diagram was constructed for $PMAA_{71}$-$PBzMA_x$ nano-objects to enable reproducible targeting of spheres, worms and vesicles (Figure 1.34).[217] A spherical morphology was obtained at low copolymer concentrations and when targeting relatively short PBzMA DPs. A pure worm phase could be obtained for almost all copolymer concentrations but only over a relatively narrow PBzMA DP range. A pure vesicle phase could be accessed when targeting a PBzMA DP of 200. As

expected, mixed phases were formed between each of the pure phases. In this case, the copolymer morphology appears to be only very weakly dependent on the copolymer concentration (mainly at 5% w/w solids).

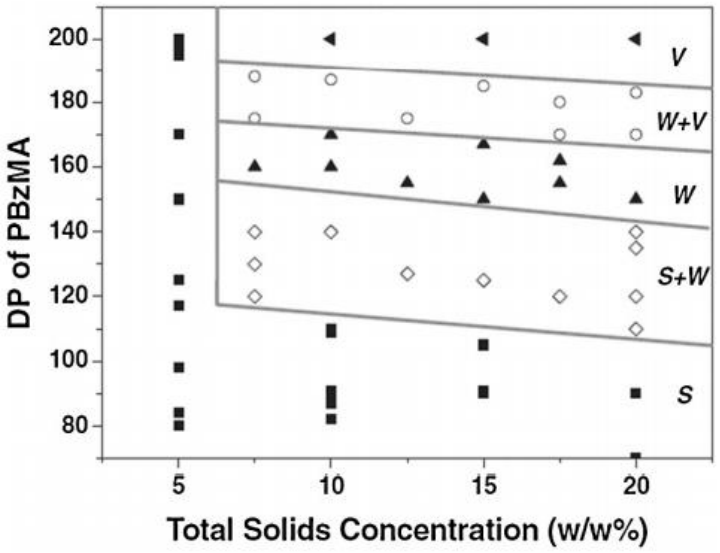

Figure 1.34. Phase diagram constructed for $PMAA_{71}$-$PBzMA_x$ diblock copolymer nano-objects prepared by RAFT dispersion polymerisation of BzMA in ethanol at 70 °C where S, W and V represent spheres, worms and vesicles, respectively.[217]

1.7.2.3 RAFT dispersion polymerisation in non-polar media

PISA in non-aqueous solvents such as lower alcohols and *n*-alkanes has also been widely reported and a 2016 review by Derry *et al.* summarises much of the important early work in this area.[169]

Charleux and co-workers reported the first examples of RAFT dispersion polymerisation in non-polar media. They used an all-acrylic formulation to produce spherical poly(2-ethylhexyl acrylate)-poly(methyl acrylate) (PEHA-PMA) diblock copolymer nanoparticles in *iso*-decane.[219–221] It was only possible to obtain spherical micelles and remarkably poor RAFT control over the MWD was achieved when using a dithiobenzoate CTA (M_w/M_n = 6.00 at the highest MA conversion of 85%) compared to a trithiocarbonate (100% conversion was achieved with a M_w/M_n of 1.21 within 4 h).[219]

Fielding *et al.* reported the first relatively well-controlled example of RAFT dispersion polymerisation in non-polar media by preparing a series of poly(lauryl methacrylate)–poly(benzyl methacrylate) (PLMA-PBzMA) nano-objects using a dithiobenzoate-based RAFT agent.[137] Spheres, worms or vesicles could be obtained in *n*-heptane when using a relatively short PLMA stabiliser block with a DP of 17 when working at sufficiently high copolymer concentrations, see Figure 1.35. Monomer conversions of more than 97% were achieved within 5 h (with a maximum M_w/M_n of 1.35 for the $PLMA_{17}$-$PBzMA_{300}$ diblock copolymers). Using a PLMA DP of 37 or above led to the

formation of kinetically-trapped spheres, which increased in size from 41 to 139 nm diameter when increasing the PBzMA DP.

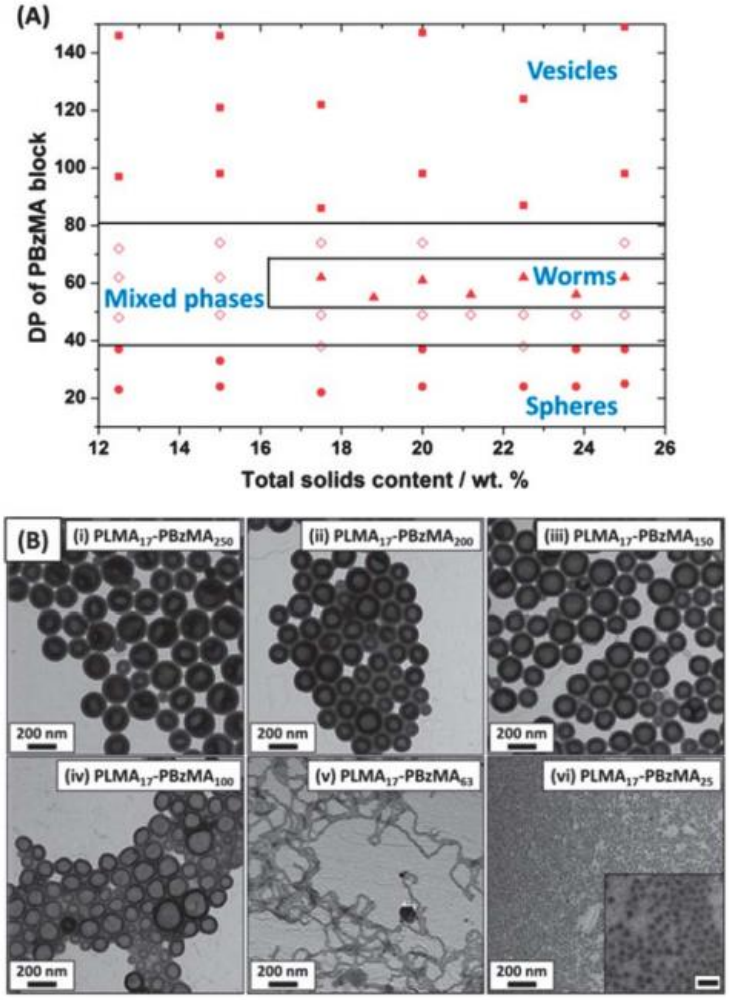

Figure 1.35. (A) Phase diagram constructed for $PLMA_{17}$-$PBzMA_x$ nano-objects prepared *via* RAFT dispersion polymerisation in *n*-heptane using cumyl dithiobenzoate RAFT agent at 90 °C (open diamond symbols indicate mixed phases). (B) Representative TEM images obtained for $PLMA_{17}$-$PBzMA_x$ nano-objects at 20% w/w solids with specific diblock compositions being indicated on each image.[137]

In a follow-up study by Fielding *et al.*, PLMA-PBzMA nano-objects were also prepared in *n*-dodecane.[175] Importantly, this higher boiling point solvent enabled the thermoresponsive behaviour of these nanoparticles to be studied. Targeting a $PLMA_{16}$-$PBzMA_{37}$ diblock copolymer afforded a soft transparent worm gel that underwent a worm-to-sphere transition on heating. This morphological transition proved to be irreversible at copolymer concentration lower than 5% w/w, presumably because the 1D fusion of multiple spheres to produce worms becomes much less efficient in dilute solution. Rheological studies indicated that the onset of degelation occurred at 47 °C. However, small angle X-ray scattering (SAXS) studies confirmed that not all worms had dissociated to form spheres at this temperature. Indeed, pure spheres were not obtained until

160 °C. Instead, a gradual reduction in the mean worm contour length was sufficient to reduce the multiple inter-worm contacts that cause gelation, since this effectively lowers the critical copolymer concentration required for a 3D percolating network.[205]

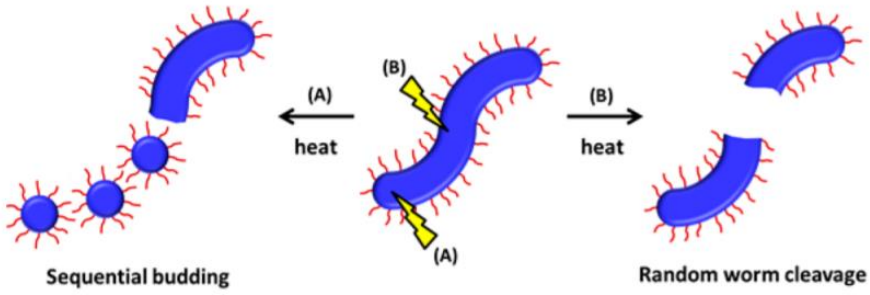

Figure 1.36. Two possible mechanisms to account for the worm-to-sphere transition that occurs on heating a dispersion of $PLMA_{16}$-$PBzMA_{37}$ worms where (A) involves sphere budding from worm ends while (B) involves random worm scission events.[175]

According to Fielding *et al.*, a worm-to-sphere transition is the result of *surface* plasticisation of the core-forming PBzMA block.[175] In this case ingress of hot solvent leads to BzMA units close to the block junction becoming partially solvated. This effectively increases the volume fraction of the stabiliser block, thereby lowering the packing parameter and hence favouring the sphere morphology. Two possible mechanisms for this worm-to-sphere transition were postulated (Figure 1.36): (A) repeated budding of spheres from worm ends or (B) random worm scission events. SAXS studies suggested that this thermal transition most likely occurs *via* sequential budding of spheres from the worm ends. It is perhaps worth emphasising here that a worm-to-vesicle transition would be expected if *uniform* plasticisation of the core-forming block had occurred at elevated temperatures. The fact that a worm-to-sphere transition actually occurs can only be rationalised in terms of *surface* plasticisation of the core-forming block. This insight can also explain thermal transitions observed for other thermoresponsive diblock copolymer nano-objects prepared *via* PISA.[204] For example, Pei *et al.* reported the use of poly(stearyl methacrylate) (PSMA) as the stabiliser block for the RAFT dispersion polymerisation of 3-phenylpropyl methacrylate (PPMA) in *n*-tetradecane[222] or *n*-octane[223] to produce spheres, worms or vesicles. These worms also formed thermoresponsive gels similar to those reported by Fielding *et al.*.[175]

For many PISA formulations, detailed phase diagrams were constructed to enable reliable targeting of pure copolymer morphologies. However, reproducing a given DP for the stabiliser block can be problematic. This is a particularly inconvenient problem if worms are required as worm phase space is notoriously narrow in many cases.[176,190,224] To address this problem, Lopez-Oliva reported the esterification of a near-monodisperse monocarbinol-functional, commercially available poly(dimethylsiloxane) (PDMS) precursor with a carboxylic acid-functionalised RAFT

agent to produce a trithiocarbonate-capped PDMS stabiliser block.[140] This precursor was subsequently chain-extended *via* RAFT dispersion polymerisation of BzMA in *n*-heptane to produce pure spheres, worms or vesicles (Figure 1.37).

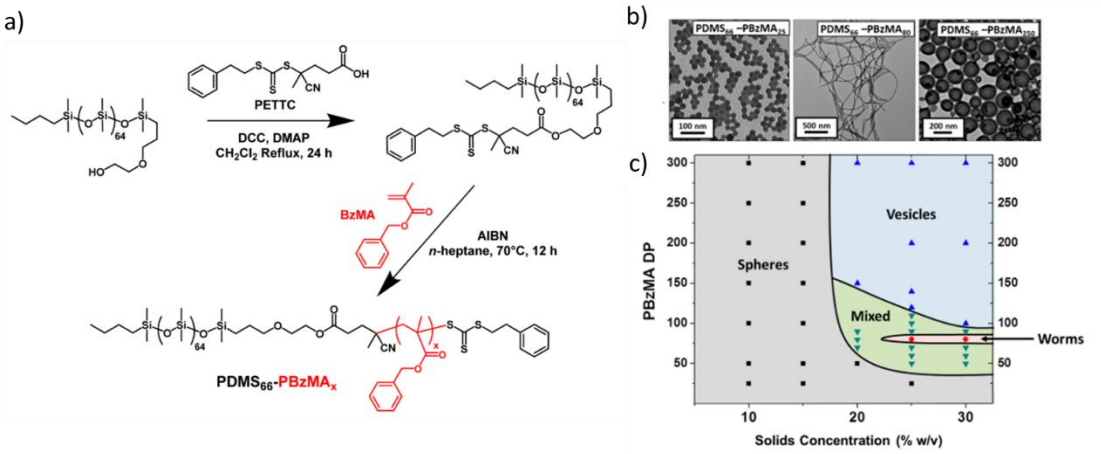

Figure 1.37. (a) Esterification of a monocarbinol-capped PDMS precursor using a carboxylic acid-functionalised RAFT agent to produce a trithiocarbonate-capped PDMS precursor that can be subsequently chain-extended *via* RAFT dispersion polymerisation of BzMA in *n*-heptane. (b) Representative TEM images of spheres, worms and vesicles produced using this PISA formulation and (c) the corresponding phase diagram constructed for this system.[140]

A similar approach has also been undertaken to produce a suitable steric stabiliser block for use in aqueous PISA. Thus, a monohydroxy-functionalised PEG_{113} precursor was esterified with a trithiocarbonate-based RAFT agent and then chain-extended *via* RAFT aqueous dispersion polymerisation of HPMA to produce well-defined spheres, worms or vesicles.[139]

1.7.2.3.1 Pickering emulsions

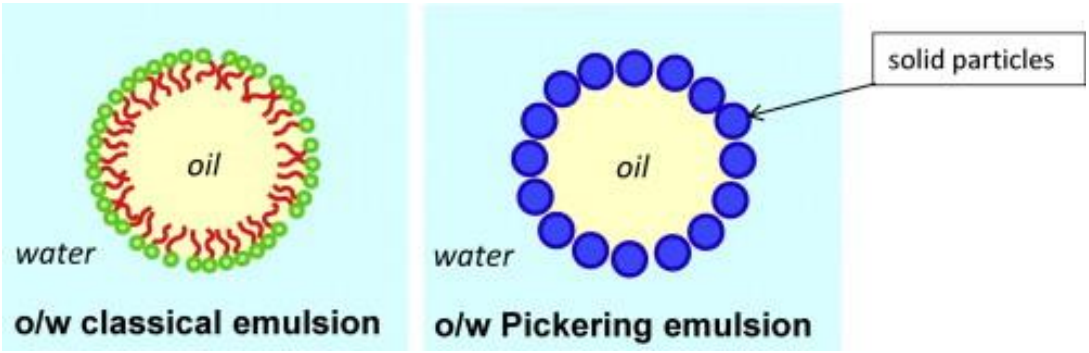

Figure 1.38. Schematic representation of (a) a surfactant-stabilised emulsion and (b) a Pickering (particle) stabilised emulsion.[225]

More than a century ago, Ramsden[226] and Pickering[227] reported that a wide range of colloidal particles can be used to stabilise emulsions instead of traditional surfactants (Figure 1.38). Suitable inorganic particles include silica,[228,229] iron oxide,[230] titanium dioxide[231] and clays[232–234] but organic polymer particles can also be utilised.[235–241] Particles adsorb irreversibly at the oil-

water interface, thus reducing the effective surface area and hence lowering the interfacial energy.[242] The particle contact angle (θ) is linked to the particle surface wettability, which dictates the type of emulsion that is formed. For θ > 90°, the particles are hydrophobic thus water-in-oil (w/o) emulsions are formed. Conversely, oil-in-water (o/w) emulsions are formed when using hydrophilic particles (for which θ < 90°). RAFT dispersion polymerisation enables the controlled synthesis of amphiphilic diblock copolymer nanoparticles that can be utilised as Pickering emulsifiers instead of traditional small molecule surfactants.[243–248]

A relevant example of using diblock copolymer nanoparticles to stabilise emulsions was reported by Cunningham and co-workers, who utilised PSMA-PNMEP spheres prepared in *n*-dodecane (Figure 1.39).[176] Using high shear homogenisation to generate the oil-water interface, these *hydrophobic* nanoparticles unexpectedly produced o/w emulsions. This surprising behaviour was attributed to *in situ* inversion of the nanoparticles during homogenisation to become *hydrophilic* spheres.

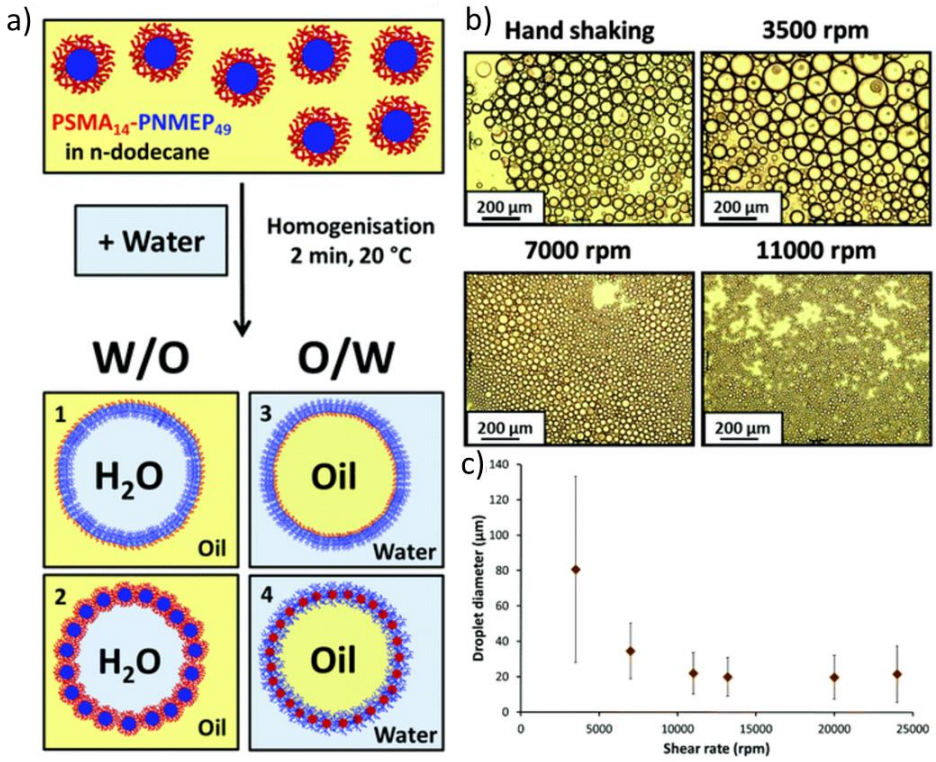

Figure 1.39. (a) Schematic representation of the four possible types of emulsions that could be formed by homogenising water using $PSMA_{14}$-$PNMEP_{49}$ spherical nanoparticles dispersed in *n*-dodecane. Scenarios 1 and 3 represent dissociation of the spherical nanoparticles into chains to provide surfactant-type stabilisation. Scenario 2 represents the $PSMA_{14}$-$PNMEP_{49}$ nanoparticles adsorbing at the interface to produce w/o Pickering emulsions, whereas scenario 4 represents inversion of these nanoparticles to form hydrophilic $PNMEP_{49}$-$PSMA_{14}$ nanoparticles that should favour the formation of o/w Pickering emulsions. (b) Optical microscopy images of the Pickering emulsions produced using 1.0% w/w $PSMA_{14}$-$PNMEP_{49}$ nanoparticles at various shear rates and (c) the effect of varying the shear rate on the mean droplet diameter as determined by laser diffraction.[176]

1.7.3 RAFT aqueous emulsion polymerisation

RAFT aqueous emulsion polymerisation combines the advantages of traditional emulsion polymerisation (high monomer conversions, fast polymerisation kinetics and low-viscosity formulations in an environmentally-friendly solvent) with much better control over the MWD.[249]

The first example of a PISA synthesis *via ab initio* RAFT aqueous emulsion polymerisation was reported by Hawkett *et al.*, who prepared poly(acrylic acid) (PAA)-PBA nanoparticles using a monomer-starved feed protocol (Figure 1.40).[149] A water-soluble PAA precursor was chain-extended with BA to form PAA-PBA oligomers. Once the PBA block reached a critical DP, *in situ* self-assembly occurred to form micelles. Under monomer-starved conditions, no monomer droplets were present in the reaction mixture, which meant that all of the RAFT agent was located within the micelles. The gradually added BA monomer diffused into the growing micelles allowing the particle to grow under reasonable RAFT control. Moderate BA conversions (65%) were achieved within 6 h with a final M_w/M_n of 1.50 being achieved. A final sphere diameter of 60 nm was determined by a particle size technique known as capillary hydrodynamic fractionation. This study was important because the authors did not use any surfactant[41,250–253] or co-solvent[254–256] which had been previously required for control. Moreover, subsequent chain extension of the PAA-PBA diblock copolymers with styrene produced ABC triblock copolymer spheres.[150]

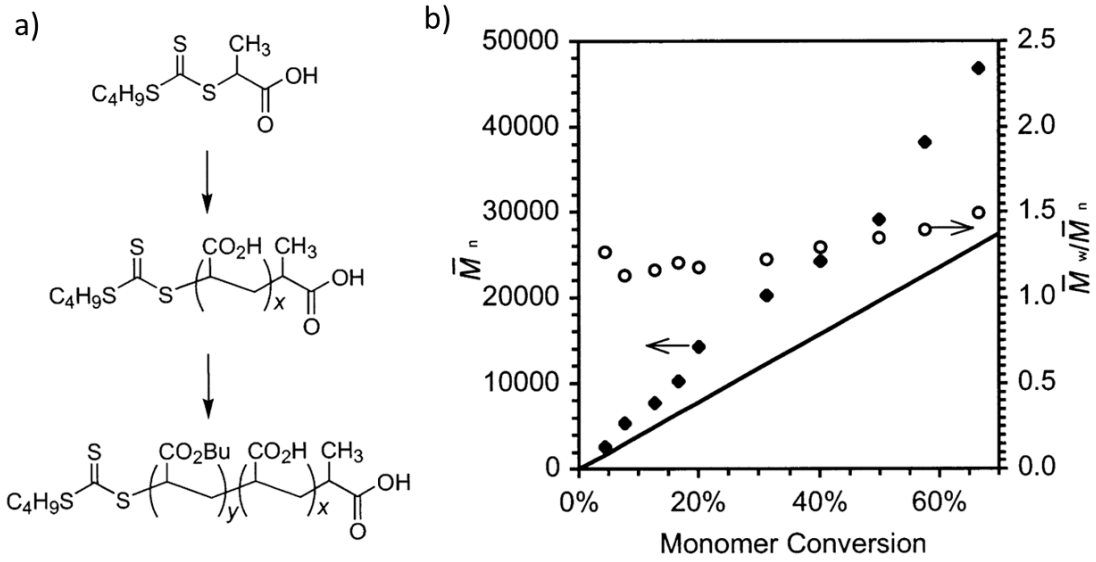

Figure 1.40. (a) Schematic representation of the synthesis of diblock copolymer spheres *via* RAFT aqueous emulsion polymerisation of BA using a PAA precursor and (b) evolution of both M_n and M_w/M_n with BA conversion, indicating reasonably good RAFT control.[149]

Since this pioneering study, RAFT aqueous emulsion polymerisation has been widely researched. The most widely-used monomer in such PISA formulations appears to be styrene.[152,154,159–161,257–260] Charleux and co-workers reported the RAFT aqueous emulsion polymerisation of styrene in

acidic solution utilising a poly(2-(diethylamino)ethyl methacrylate) (PDEA) precursor in its protonated form.[261] Well-defined spherical nanoparticles were obtained that remained stable for several months. However, these particles flocculated on raising the solution pH from 3 to above 7.3 (the pK_a of the PDEA stabiliser block).

Typically, RAFT aqueous emulsion polymerisation results in the formation of kinetically-trapped spheres.[151,153,154,257,262,263] However, higher order morphologies can be accessed by statistical copolymerisation of suitable monomers to prepare steric stabiliser blocks. For example, Charleux and co-workers reported the statistical copolymerisation of MAA and EOMA to produce P(MAA-*co*-EOMA) precursors which were subsequently chain-extended with styrene.[158] Faster kinetics, shorter induction periods and higher final styrene conversions were achieved under acidic conditions. Spheres, worms and vesicles could be produced at pH 5 by either targeting higher PS DPs or by reducing the DP of the P(MAA-*co*-EOMA) stabiliser block, which is only partially ionised at this solution pH. Subsequently, the same team showed that pH 5 was the optimum solution pH for targeting higher order morphologies and it also enabled good control over the MWD to be achieved.[159] In contrast, the stabiliser block was not sufficiently hydrophilic at pH 3.5 and only spheres could be produced under such conditions. Moreover, only poor control was achieved for polymerisations performed at pH 7. Here the highly anionic stabiliser block resulted in the formation of kinetically-trapped spheres, presumably because strong electrostatic repulsion prevented sphere-sphere fusion.

It was hypothesised that the water solubility of the vinyl monomer used to produce the insoluble structure-directing block might be important in determining whether higher order morphologies could be accessed by RAFT aqueous emulsion polymerisation. Cockram and co-workers obtained an unusual 'monkey nut' copolymer morphology *via* chain extension of a partially ionised PMAA precursor using 4-hydroxybutyl methacrylate (HBMA) at pH 5.[163] This was a somewhat surprising result, particularly given that a ionisable stabiliser block was used. Furthermore, a non-ionic PGMA precursor was used for the RAFT aqueous emulsion polymerisation of glycidyl methacrylate (GlyMA), which has a comparable aqueous solubility (24-25 g dm^{-3} at the polymerisation temperature of 50 °C) to that of HBMA (20 g dm^{-3}). A relatively short PGMA DP of 25 was required as this confers weaker steric stabilisation and hence allows stochastic 1D fusion of multiple spheres to occur, which leads to the formation of highly anisotropic worms.[164] A third example of a methacrylic monomer that exhibits sufficiently high aqueous solubility is 2-methoxyethyl methacrylate (MOEMA).[165] MOEMA has a water solubility of 19.6 g dm^{-3} at 70 °C, which is comparable to that of HBMA and GlyMA. Accordingly, spheres, worms or vesicles could be produced when utilising a relatively short PGMA precursor. The evolution in copolymer

morphology was also studied by *in situ* SAXS. This technique confirmed that the eventual formation of vesicles was preceded by intermediate sphere and worm morphologies. This progressive evolution in copolymer morphology has also been observed for various RAFT dispersion polymerisations.[136,142,168,264]

1.8 Ashland Speciality Chemicals

PNVP is used extensively in personal and home care products owing to its biocompatibility and water solubility. NVP is an example of a LAM, which it copolymerises rather poorly with many vinyl monomers (*e.g.* methacrylics and styrene). In view of this problem, Ashland has recently developed efficient syntheses of NMEP and NAEP. Unlike NVP, these two vinyl monomers can be copolymerised readily with methacrylic and acrylic comonomers. NMEP and NAEP have been prepared in-house by Ashland. This company has kindly provided such monomers for the research described in this Thesis.

In a prior University of Sheffield/Ashland collaboration, PNMEP has been used as a steric stabiliser block for RAFT alcoholic dispersion polymerisation[174] and also as a core-forming block for PISA syntheses conducted in either non-polar media[176] or water[122]. PNVP remains water-soluble at all temperatures. In contrast, PNMEP exhibits inverse temperature solubility behaviour: it is soluble at lower temperatures but precipitates from aqueous solution on heating. Moreover, its methacrylic backbone means that PNMEP exhibits a T_g of approximately 65 °C so it is a 'glassy' polymer at room temperature and does not undergo film formation (whereas PNVP is a film-forming polymer). PNAEP's acrylic backbone means that this homopolymer has a T_g of around –5 °C, enabling film formation at ambient temperature.[201] PNAEP is also significantly more hydrophilic than PNMEP: it does not exhibit inverse temperature solubility behaviour so it can act as an effective steric stabiliser for aqueous PISA formulations.

Ashland offers a range of skin, hair, oral and sun care products. In addition to their portfolio of pyrrolidone-based monomers, they also manufacture *tert*-octyl acrylamide on an industrial scale. This highly hydrophobic monomer has been incorporated into various amphiphilic copolymers for use in commercially successful hair spray formulations.

1.9 Thesis outline

This Thesis focuses on the preparation of well-defined diblock copolymer nano-objects by PISA *via* RAFT polymerisation using a wide range of formulations. Chapter 2 describes the use of a

carboxylic acid-functionalised PNMEP precursor to produce spherical nanoparticles *via* either RAFT aqueous dispersion polymerisation of HPMA or RAFT aqueous emulsion polymerisation of 2-ethoxyethyl methacrylate (EEMA), respectively. The solution pH is adjusted in such PISA syntheses to examine the effect of ionisation of the carboxylic acid end-groups on the colloidal stability of the final nanoparticles. In Chapter 3, PNMEP is utilised as a steric stabiliser for the preparation of PNMEP-PLMA vesicles *via* RAFT dispersion polymerisation of LMA in various ethanol-water mixtures. This PISA formulation was optimised with the aim of achieving relatively high LMA conversions while maintaining reasonable control over the molecular weight distribution and high blocking efficiencies. SAXS and TEM were used to characterise the copolymer morphology and RAFT end-group removal from aqueous vesicular dispersions was explored using visible light irradiation. In Chapter 4, the RAFT dispersion polymerisation of DMAC in *n*-alkanes was explored using poly(*tert*-octyl acrylamide) (POAA) as the steric stabiliser. Under certain conditions, the resulting POAA-PDMAC spheres undergo thermoreversible aggregation that is attributed to UCST behaviour for the POAA. Finally, in Chapter 5, the PISA synthesis of PSMA-PNAEP diblock copolymer nano-objects was examined *via* RAFT non-aqueous emulsion polymerisation of NAEP in non-polar media using either a conventional peroxide initiator or visible light-mediated iniferter chemistry.

1.10 References

(1) Nesvadba, P. Radical Polymerization in Industry. In *Encyclopedia of Radicals in Chemistry, Biology and Materials*; John Wiley & Sons, Ltd: Chichester, UK, 2012.

(2) Staudinger, H. Über Polymerisation. *Berichte der Dtsch. Chem. Gesellschaft (A B Ser.* **1920**, *53*, 1073–1085.

(3) Carothers, W. H.; Arvin, J. A. Studies on Polymerization and Ring Formation. II. Poly-Esters. *J. Am. Chem. Soc.* **1929**, *51*, 2560–2570.

(4) Odian, G. G. *Principles of Polymerization*; Wiley: Hoboken, 2004.

(5) Flory, P. J. *Principles of Polymer Chemistry*, First Edit.; Cornell University Press: London, 1953.

(6) Braunecker, W. A. Controlled/Living Radical Polymerization: Features, Developments, and Perspectives. *Prog. Polym. Sci.* **2007**, *32*, 93–146.

(7) Moad, G.; Rizzardo, E. Chapter 1: The History of Nitroxide-Mediated Polymerization. In *RSC Polymer Chemistry Series*; Royal Society of Chemistry, 2016; pp 1–44.

(8) Szwarc, M. “Living” Polymers. *Nature* **1956**, *178*, 1168–1169.

(9) Szwarc, M.; Levy, M.; Milkovich, R. POLYMERIZATION INITIATED BY ELECTRON TRANSFER TO MONOMER. A NEW METHOD OF FORMATION OF BLOCK POLYMERS [1]. *J. Am. Chem. Soc.* **1956**, *78*, 2656–2657.

(10) Raghunadh, V.; Baskaran, D.; Sivaram, S. Living Anionic Polymerization of Lauryl Methacrylate and Synthesis of Block Copolymers with Methyl Methacrylate. *J. Polym. Sci. Part A Polym. Chem.* **2004**, *42*, 875–882.

(11) Ghadban, A.; Albertin, L. Synthesis of Glycopolymer Architectures by Reversible-Deactivation Radical Polymerization. *Polymers* **2013**, *5*, 431–526.

(12) Jenkins, A. D.; Jones, R. G.; Moad, G. Terminology for Reversible-Deactivation Radical Polymerization Previously Called "Controlled" Radical or "Living" Radical Polymerization (IUPAC Recommendations 2010). *Pure Appl. Chem.* **2010**, *82*, 483–491.

(13) Golas, P. L.; Matyjaszewski, K. Click Chemistry and ATRP: A Beneficial Union for the Preparation of Functional Materials. *QSAR Comb. Sci.* **2007**, *26*, 1116–1134.

(14) Hawker, C. J.; Bosman, A. W.; Harth, E. New Polymer Synthesis by Nitroxide Mediated Living Radical Polymerizations. *Chemical Reviews*. 2001, pp 3661–3688.

(15) Moad, G.; Rizzardo, E.; Thang, S. H. Toward Living Radical Polymerization. *Acc. Chem. Res.* **2008**, *41*, 1133–1142.

(16) Nicolas, J.; Guillaneuf, Y.; Lefay, C.; Bertin, D.; Gigmes, D.; Charleux, B. Nitroxide-Mediated Polymerization. *Prog. Polym. Sci.* **2013**, *38*, 63–235.

(17) Fischer, H. The Persistent Radical Effect in "Living" Radical Polymerization. *Macromolecules* **1997**, *30*, 5666–5672.

(18) Balili, M. N. C.; Pintauer, T. Persistent Radical Effect in Action: Kinetic Studies of Copper-Catalyzed Atom Transfer Radical Addition in the Presence of Free-Radical Diazo Initiators as Reducing Agents. *Inorg. Chem.* **2009**, *48*, 9018–9026.

(19) Chiefari, J.; Chong, Y. K. B.; Ercole, F.; Krstina, J.; Jeffery, J.; Le, T. P. T.; Mayadunne, R. T. A.; Meijs, G. F.; Moad, C. L.; Moad, G.; Rizzardo, E.; Thang, S. H. Living Free-Radical Polymerization by Reversible Addition - Fragmentation Chain Transfer: The RAFT Process. *Macromolecules* **1998**, *31*, 5559–5562.

(20) Greszta, D.; Mardare, D.; Matyjaszewski, K. "Living" Radical Polymerization. 1. Possibilities and Limitations. *Macromolecules* **1994**, *27*, 638–644.

(21) Rizzardo, E.; Solomon, D. H. A New Method for Investigating the Mechanism of Initiation of Radical Polymerization. *Polym. Bull.* **1979**, *1*, 529–534.

(22) Moad, G.; Rizzardo, E.; Solomon, D. H. A Product Study of the Nitroxide Inhibited Thermal Polymerization of Styrene. *Polym. Bull.* **1982**, *6*, 589–593.

(23) Cuthbertson, M. J.; Rizzardo, E.; Solomon, D. H. The Reactions of T-Butoxyl with Unsaturated Hydrocarbons: Structure and Reactivity of Allylic Radicals. *Aust. J. Chem.* **1983**, *36*, 1957–1973.

(24) Moad, G.; Rizzardo, E.; Solomon, D. H. The Reaction of Benzoyloxy Radicals with Styrene Implications Concerning the Structure of Polystyrene. *J. Macromol. Sci. Part A - Chem.* **1982**, *17*, 51–59.

(25) Moad, G.; Rizzardo, E.; Solomon, D. H. Selectivity of the Reaction of Free Radicals with Styrene. *Macromolecules* **1982**, *15*, 909–914.

(26) Petton, L.; Ciolino, A. E.; Dervaux, B.; Du Prez, F. E. From One-Pot Stabilisation to in Situ Functionalisation in Nitroxide Mediated Polymerisation: An Efficient Extension towards Atom Transfer Radical Polymerisation. *Polym. Chem.* **2012**, *3*, 1867–1878.

(27) Grubbs, R. B. Nitroxide-Mediated Radical Polymerization: Limitations and Versatility. *Polym. Rev.* **2011**, *51*, 104–137.

(28) Abreu, C. M. R.; Mendonça, P. V.; Serra, A. C.; Noble, B. B.; Guliashvili, T.; Nicolas, J.; Coote, M. L.; Coelho, J. F. J. Nitroxide-Mediated Polymerization of Vinyl Chloride at Low Temperature: Kinetic and Computational Studies. *Macromolecules* **2016**, *49*, 490–498.

(29) Cunningham, M. F.; Ng, D. C. T.; Milton, S. G.; Keoshkerian, B. Low Temperature TEMPO-Mediated Styrene Polymerization in Miniemulsion. *J. Polym. Sci. Part A Polym. Chem.* **2006**, *44*, 232–242.

(30) Detrembleur, C.; Jérôme, C.; De Winter, J.; Gerbaux, P.; Clément, J.-L.; Guillaneuf, Y.; Gigmes, D. Nitroxide Mediated Polymerization of Methacrylates at Moderate Temperature. *Polym. Chem.* **2014**, *5*, 335–340.

(31) Matyjaszewski, K. Atom Transfer Radical Polymerization (ATRP): Current Status and Future Perspectives. *Macromolecules* **2012**, *45*, 4015–4039.

(32) Kotani, Y.; Kamigaito, M.; Sawamoto, M. FeCp(CO)2I: A Phosphine-Free Half-Metallocene-Type Iron(II) Catalyst for Living Radical Polymerization of Styrène. *Macromolecules* **1999**, *32*, 6877–6880.

(33) Teodorescu, M.; Gaynor, S. G.; Matyjaszewski, K. Halide Anions as Ligands in Iron-Mediated Atom Transfer Radical Polymerization. *Macromolecules* **2000**, *33*, 2335–2339.

(34) Le Grognec, E.; Claverie, J.; Poli, R. Radical Polymerization of Styrene Controlled by Half-Sandwich Mo(III)/Mo(IV) Couples: All Basic Mechanisms Are Possible. *J. Am. Chem. Soc.* **2001**, *123*, 9513–9524.

(35) Maria, S.; Stoffelbach, F.; Mata, J.; Daran, J. C.; Richard, P.; Poli, R. The Radical Trap in Atom Transfer Radical Polymerization Need Not Be Thermodynamically Stable. A Study of the MoX3(PMe3) 3 Catalysts. *J. Am. Chem. Soc.* **2005**, *127*, 5946–5956.

(36) Kotani, Y.; Kamigaito, M.; Sawamoto, M. Living Radical Polymerization of Para-Substituted Styrenes and Synthesis of Styrene-Based Copolymers with Rhenium and Iron Complex Catalysts. *Macromolecules* **2000**, *33*, 6746–6751.

(37) Tsarevsky, N. V.; Pintauer, T.; Matyjaszewski, K. Deactivation Efficiency and Degree of Control over Polymerization in ATRP in Protic Solvents. *Macromolecules* **2004**, *37*, 9768–9778.

(38) Qiu, J.; Charleux, B.; Matyjaszewski, K. Controlled/Living Radical Polymerization in Aqueous Media: Homogeneous and Heterogeneous Systems. *Prog. Polym. Sci.* **2001**, *26*, 2083–2134.

(39) Costa, J. R. C.; Mendonça, P. V.; Maximiano, P.; Serra, A. C.; Guliashvili, T.; Coelho, J. F. J. Ambient Temperature “Flash” SARA ATRP of Methyl Acrylate in Water/Ionic Liquid/Glycol Mixtures. *Macromolecules* **2015**, *48*, 6810–6815.

(40) Mendes, J. P.; Mendonça, P. V.; Maximiano, P.; Abreu, C. M. R.; Guliashvili, T.; Serra, A. C.; Coelho, J. F. J. Getting Faster: Low Temperature Copper-Mediated SARA ATRP of Methacrylates, Acrylates, Styrene and Vinyl Chloride in Polar Media Using Sulfolane/Water Mixtures. *RSC Adv.* **2016**, *6*, 9598–9603.

(41) Chiefari, J.; Chong, Y. K. B.; Ercole, F.; Krstina, J.; Jeffery, J.; Le, T. P. T.; Mayadunne, R. T. A.; Meijs, G. F.; Moad, C. L.; Moad, G.; Rizzardo, E.; Thang, S. H. Living Free-Radical Polymerization by Reversible Addition - Fragmentation Chain Transfer : The RAFT

Process. *Macromolecules* **1998**, *31*, 5559–5562.

(42) Moad, G.; Rizzardo, E.; Thang, S. H. Living Radical Polymerization by the RAFT Process—A First Update. *Aust. J. Chem* **2006**, *59*, 669–692.

(43) Moad, G.; Rizzardo, E.; Thang, S. H. Living Radical Polymerization by the RAFT Process A Second Update. *Aust. J. Chem.* **2009**, *62*, 1402–1472.

(44) Moad, G.; Rizzardo, E.; Thang, S. H. Living Radical Polymerization by the RAFT Process a Third Update. *Aust. J. Chem.* **2012**, *65*, 985–1076.

(45) Perrier, S. 50th Anniversary Perspective: RAFT Polymerization A User Guide. *Macromolecules* **2017**, *50*, 7433–7447.

(46) Fu, L.; Simakova, A.; Fantin, M.; Wang, Y.; Matyjaszewski, K. Direct ATRP of Methacrylic Acid with Iron-Porphyrin Based Catalysts. **2018**, *7*, 30.

(47) Gody, G.; Maschmeyer, T.; Zetterlund, P. B.; Perrier, S. Rapid and Quantitative One-Pot Synthesis of Sequence-Controlled Polymers by Radical Polymerization. *Nat. Commun.* **2013**, *4*, 2505.

(48) Pissuwan, D.; Boyer, C.; Gunasekaran, K.; Davis, T. P.; Bulmus, V. In Vitro Cytotoxicity of RAFT Polymers. *Biomacromolecules* **2010**, *11*, 412–420.

(49) Cornel, E. J.; van Meurs, S.; Smith, T.; O'Hora, P. S.; Armes, S. P. In Situ Spectroscopic Studies of Highly Transparent Nanoparticle Dispersions Enable Assessment of Trithiocarbonate Chain-End Fidelity during RAFT Dispersion Polymerization in Nonpolar Media. *J. Am. Chem. Soc.* **2018**, *140*, 12980–12988.

(50) Chong, Y. K.; Moad, G.; Rizzardo, E.; Thang, S. H. Thiocarbonylthio End Group Removal from RAFT-Synthesized Polymers by Radical-Induced Reduction. *Macromolecules* **2007**, *40*, 4446–4455.

(51) Moad, G.; Rizzardo, E.; Thang, S. H. End-Functional Polymers, Thiocarbonylthio Group Removal/Transformation and Reversible Addition-Fragmentation-Chain Transfer (RAFT) Polymerization. *Polym. Int.* **2011**, *60*, 9–25.

(52) Willcock, H.; O'Reilly, R. K. End Group Removal and Modification of RAFT Polymers. *Polym. Chem.* **2010**, *1*, 149–157.

(53) Chong, B.; Moad, G.; Rizzardo, E.; Skidmore, M.; Thang, S. H. Thermolysis of RAFT-Synthesized Poly(Methyl Methacrylate). *Aust. J. Chem.* **2006**, *59*, 755–762.

(54) Carmean, R. N.; Figg, C. A.; Scheutz, G. M.; Kubo, T.; Sumerlin, B. S. Catalyst-Free Photoinduced End-Group Removal of Thiocarbonylthio Functionality. *ACS Macro Lett.* **2017**, *6*, 185–189.

(55) Mattson, K. M.; Pester, C. W.; Gutekunst, W. R.; Hsueh, A. T.; Discekici, E. H.; Luo, Y.; Schmidt, B. V. K. J.; McGrath, A. J.; Clark, P. G.; Hawker, C. J. Metal-Free Removal of Polymer Chain Ends Using Light. *Macromolecules* **2016**, *49*, 8162–8166.

(56) Patton, D. L.; Mullings, M.; Fulghum, T.; Advincula, R. C. A Facile Synthesis Route to Thiol-Functionalized α,ω-Telechelic Polymers via Reversible Addition Fragmentation Chain Transfer Polymerization. *Macromolecules* **2005**, *38*, 8597–8602.

(57) Qiu, X. P.; Winnik, F. M. Facile and Efficient One-Pot Transformation of RAFT Polymer End Groups via a Mild Aminolysis/Michael Addition Sequence. *Macromol. Rapid Commun.* **2006**, *27*, 1648–1653.

(58) Boyer, C.; Davis, T. P. One- Pot Synthesis and Biofunctionalization of Glycopolymers via RAFT Polymerization and Thiol-Ene Reactions. *Chem. Commun.* **2009**, No. 40, 6029–6031.

(59) Boyer, C.; Bulmus, V.; Davis, T. P. Efficient Usage of Thiocarbonates for Both the Production and the Biofunctionalization of Polymers. *Macromol. Rapid Commun.* **2009**, *30*, 493–497.

(60) Zhou, K.; Cao, H.; Gao, P.; Cui, Z.; Ding, Y.; Cai, Y. Autocatalytic Self-Sorting in Biomimetic Polymer. *Macromolecules* **2016**, *49*, 2189–2196.

(61) Alagi, P.; Hadjichristidis, N.; Gnanou, Y.; Feng, X. Fast and Complete Neutralization of Thiocarbonylthio Compounds Using Trialkylborane and Oxygen: Application to Their Removal from RAFT-Synthesized Polymers. *ACS Macro Lett.* **2019**, *8*, 664–669.

(62) Matioszek, D.; Dufils, P. E.; Vinas, J.; Destarac, M. Selective and Quantitative Oxidation of Xanthate End-Groups of RAFT Poly(n-Butyl Acrylate) Latexes by Ozonolysis. *Macromol. Rapid Commun.* **2015**, *36*, 1354–1361.

(63) Jesson, C. P.; Pearce, C. M.; Simon, H.; Werner, A.; Cunningham, V. J.; Lovett, J. R.; Smallridge, M. J.; Warren, N. J.; Armes, S. P. H2O2 Enables Convenient Removal of RAFT End-Groups from Block Copolymer Nano-Objects Prepared via Polymerization-Induced Self- Assembly in Water. *Macromolecules* **2017**, *50*, 182–191.

(64) Keddie, D. J.; Moad, G.; Rizzardo, E.; Thang, S. H. RAFT Agent Design and Synthesis. *Macromolecules* **2012**, *45*, 5321–5342.

(65) Benaglia, M.; Chiefari, J.; Chong, Y. K.; Moad, G.; Rizzardo, E.; Thang, S. H. Universal (Switchable) RAFT Agents. *J. Am. Chem. Soc.* **2009**, *131*, 6914–6915.

(66) Easterling, C. P.; Xia, Y.; Zhao, J.; Fanucci, G. E.; Sumerlin, B. S. Block Copolymer Sequence Inversion through Photoiniferter Polymerization. *ACS Macro Lett.* **2019**, *8*, 1461–1466.

(67) Chen, M.; Zhong, M.; Johnson, J. A. Light-Controlled Radical Polymerization: Mechanisms, Methods, and Applications. *Chem. Rev.* **2016**, *116*, 10167–10211.

(68) Zaquen, N.; Azizi, W. A. A. W.; Yeow, J.; Kuchel, R. P.; Junkers, T.; Zetterlund, P. B.; Boyer, C. Alcohol-Based PISA in Batch and Flow: Exploring the Role of Photoinitiators. *Polym. Chem.* **2019**, *10*, 2406–2414.

(69) McKenzie, T. G.; Fu, Q.; Wong, E. H. H.; Dunstan, D. E.; Qiao, G. G. Visible Light Mediated Controlled Radical Polymerization in the Absence of Exogenous Radical Sources or Catalysts. *Macromolecules* **2015**, *48*, 3864–3872.

(70) Jung, K.; Boyer, C.; Zetterlund, P. B. RAFT Iniferter Polymerization in Miniemulsion Using Visible Light. *Polym. Chem.* **2017**, *8*, 3965–3970.

(71) Otsu, T.; Yoshida, M. Role of Initiator-transfer Agent-terminator (Iniferter) in Radical Polymerizations: Polymer Design by Organic Disulfides as Iniferters. *Macromol. Rapid Commun.* **1982**, *3*, 127–132.

(72) Otsu, T.; Kuriyama, A. Living Mono- and Biradical Polymerizations in Homogeneous System Synthesis of AB and ABA Type Block Copolymers. *Polym. Bull.* **1984**, *11*, 135–142.

(73) Otsu, T. Iniferter Concept and Living Radical Polymerization. *J. Polym. Sci. Part A Polym. Chem.* **2000**, *38*, 2121–2136.

(74) Wang, H.; Li, Q.; Dai, J.; Du, F.; Zheng, H.; Bai, R. Real-Time and in Situ Investigation of "Living"/Controlled Photopolymerization in the Presence of a Trithiocarbonate.

Macromolecules **2013**, *46*, 2576–2582.

(75) Zhou, H.; Johnson, J. A. Photo-Controlled Growth of Telechelic Polymers and End-Linked Polymer Gels. *Angew. Chemie Int. Ed.* **2013**, *52*, 2235–2238.

(76) Carmean, R. N.; Becker, T. E.; Sims, M. B.; Sumerlin, B. S. Ultra-High Molecular Weights via Aqueous Reversible-Deactivation Radical Polymerization. *Chem* **2017**, *2*, 93–101.

(77) Arshady, R. Suspension, Emulsion, and Dispersion Polymerization: A Methodological Survey. *Colloid Polym. Sci.* **1992**, *270*, 717–732.

(78) Paine, A. J. Dispersion Polymerization of Styrene in Polar Solvents. 7. A Simple Mechanistic Model to Predict Particle Size. *Macromolecules* **1990**, *23*, 3109–3117.

(79) Lok, K. P.; Ober, C. K. Particle Size Control in Dispersion Polymerization of Polystyrene. *Can. J. Chem.* **1985**, *63*, 209–216.

(80) Barrett, K. E. J. Dispersion Polymerisation in Organic Media. *Br. Polym. J.* **1973**, *5*, 259–271.

(81) Ali, A. M. I.; Pareek, P.; Sewell, L.; Schmid, A.; Fujii, S.; Armes, S. P.; Shirley, I. M. Synthesis of Poly(2-Hydroxypropyl Methacrylate) Latex Particles via Aqueous Dispersion Polymerization. *Soft Matter* **2007**, *3*, 1003–1013.

(82) Almog, Y.; Reich, S.; Levy, M. Monodisperse Polymeric Spheres in the Micron Size Range by a Single Step Process. *Br. Polym. J.* **1982**, *14*, 131–136.

(83) Baines, F. L.; Dionisio, S.; Billingham, N. C.; Armes, S. P. Use of Block Copolymer Stabilizers for the Dispersion Polymerization of Styrene in Alcoholic Media. *Macromolecules* **1996**, *29*, 3096–3102.

(84) Qun Wang; Shoukuan Fu; Tongyin Yu. Emulsion Polymerization. *Prog. Polym. Sci.* **1994**, *19*, 703–753.

(85) Asua, J. M. Emulsion Polymerization: From Fundamental Mechanisms to Process Developments. *J. Polym. Sci. Part A Polym. Chem.* **2004**, *42*, 1025–1041.

(86) Ugelstad, J.; El-Aasser, M. S.; Vanderhoff, J. W. Emulsion Polymerization: Initiation of Polymerization in Monomer Droplets. *J. Polym. Sci. Polym. Lett. Ed.* **1973**, *11*, 503–513.

(87) Ugelstad, J.; Mörk, P. C.; Aasen, J. O. Kinetics of Emulsion Polymerization. *J. Polym. Sci. Part A-1 Polym. Chem.* **1967**, *5*, 2281–2288.

(88) Thickett, S. C.; Gilbert, R. G. Emulsion Polymerization: State of the Art in Kinetics and Mechanisms. *Polymer* **2007**, *48*, 6965–6991.

(89) Chern, C. S. Emulsion Polymerization Mechanisms and Kinetics. *Prog. Polym. Sci.* **2006**, *31*, 443–486.

(90) Asua, J. M. Emulsion Polymerization: From Fundamental Mechanisms to Process Developments. *J. Polym. Sci. Part A Polym. Chem.* **2004**, *42*, 1025–1041.

(91) Raffa, P.; Wever, D. A. Z.; Picchioni, F.; Broekhuis, A. A. Polymeric Surfactants: Synthesis, Properties, and Links to Applications. *Chem. Rev.* **2015**, *115*, 8504–8563.

(92) Israelachvili, J. N.; Mitchell, D. J.; Ninham, B. W. Theory of Self-Assembly of Hydrocarbon Amphiphiles into Micelles and Bilayers. *J. Chem. Soc. Faraday Trans. 2 Mol. Chem. Phys.* **1976**, *72*, 1525–1568.

(93) Israelachvili, J. *Intermolecular and Surface Forces*; Elsevier: Santa Barbara, 2011.

(94) Kronberg, B.; Holmberg, K.; Lindman, B. *Surface Chemistry of Surfactants and Polymers*; John Wiley & Sons, Ltd: Chichester, UK, 2014.

(95) Cosgrove, T. *Colloid Science*; Cosgrove, T., Ed.; Blackwell Publishing Ltd.: Oxford, UK, 2005.

(96) Tanford, C. The Hydrophobic Effect and the Organization of Living Matter. *Science* **1978**, *200*, 1012–1018.

(97) Frank, H. S.; Evans, M. W. Free Volume and Entropy in Condensed Systems III. Entropy in Binary Liquid Mixtures; Partial Molal Entropy in Dilute Solutions; Structure and Thermodynamics in Aqueous Electrolytes. *J. Chem. Phys.* **1945**, *13*, 507–532.

(98) Matyjaszewski, K.; Gnanou, Y.; Leibler, L. *Macromolecular Engineering : Precise Synthesis, Materials Properties, Applications*; Wiley-VCH: Hoboken, USA, 2007.

(99) Bates, F. S.; Fredrickson, G. H. Block Copolymer Thermodynamics: Theory and Experiment. *Annu. Rev. Phys. Chem.* **1990**, *41*, 525–557.

(100) Thomas, E. L.; Anderson, D. M.; Henkee, C. S.; Hoffman, D. Periodic Area-Minimizing Surfaces in Block Copolymers. *Nature* **1988**, *334*, 598–601.

(101) Discher, D. E.; Eisenberg, A. Polymer Vesicles. *Science* **2002**, *297*, 967–973.

(102) Zhang, L.; Eisenberg, A. Multiple Morphologies of "Crew-Cut" Aggregates of Polystyrene-b-Poly(Acrylic Acid) Block Copolymers. *Science* **1995**, *268*, 1728–1731.

(103) Riess, G. Micellization of Block Copolymers. *Prog. Polym. Sci.* **2003**, *28*, 1107–1170.

(104) Mai, Y.; Eisenberg, A. Self-Assembly of Block Copolymers. *Chem. Soc. Rev.* **2012**, *41*, 5969–5985.

(105) Bates, F. S.; Fredrickson, G. H. Block Copolymers—Designer Soft Materials. *Phys. Today* **1999**, *52*, 32–38.

(106) Matsen, M. W.; Bates, F. S. Unifying Weak- and Strong-Segregation Block Copolymer Theories. *Macromolecules* **1996**, *29*, 1091–1098.

(107) Bütün, V.; Armes, S. P.; Billingham, N. C. Synthesis and Aqueous Solution Properties of Near-Monodisperse Tertiary Amine Methacrylate Homopolymers and Diblock Copolymers. *Polymer* **2001**, *42*, 5993–6008.

(108) Howse, J. R.; Jones, R. A. L.; Battaglia, G.; Ducker, R. E.; Leggett, G. J.; Ryan, A. J. Templated Formation of Giant Polymer Vesicles with Controlled Size Distributions. *Nat. Mater.* **2009**, *8*, 507–511.

(109) Gandhi, A.; Paul, A.; Sen, S. O.; Sen, K. K. Studies on Thermoresponsive Polymers: Phase Behaviour, Drug Delivery and Biomedical Applications. *Asian J. Pharm. Sci.* **2015**, *10*, 99–107.

(110) Heskins, M.; Guillet, J. E. Solution Properties of Poly(N-Isopropylacrylamide). *J. Macromol. Sci. Part A - Chem.* **1968**, *2*, 1441–1455.

(111) Schild, H. G. Poly(N-Isopropylacrylamide): Experiment, Theory and Application. *Prog. Polym. Sci.* **1992**, *17*, 163–249.

(112) Chen, Y.; Gao, Y.; Da Silva, L. P.; Pirraco, R. P.; Ma, M.; Yang, L.; Reis, R. L.; Chen, J. A

Thermo-/PH-Responsive Hydrogel (PNIPAM-PDMA-PAA) with Diverse Nanostructures and Gel Behaviors as a General Drug Carrier for Drug Release. *Polym. Chem.* **2018**, *9*, 4063–4072.

(113) Ma, C.; Shi, Y.; Pena, D. A.; Peng, L.; Yu, G. Thermally Responsive Hydrogel Blends: A General Drug Carrier Model for Controlled Drug Release. *Angew. Chemie* **2015**, *127*, 7484–7488.

(114) Raju, R.; Bandyopadhyay, S.; Sharma, A.; Gonzalez, S.; Carlsen, P.; Gautun, O.; Glomm, W. Synthesis, Characterization and Drug Loading of Multiresponsive p[NIPAm-Co-PEGMA] (Core)/p[NIPAm-Co-AAc] (Shell) Nanogels with Monodisperse Size Distributions. *Polymers* **2018**, *10*, 309.

(115) Smeets, N. M. B.; Hoare, T. Designing Responsive Microgels for Drug Delivery Applications. *J. Polym. Sci. Part A Polym. Chem.* **2013**, *51*, 3027–3043.

(116) Hoare, T.; Pelton, R. Impact of Microgel Morphology on Functionalized Microgel-Drug Interactions. *Langmuir* **2008**, *24*, 1005–1012.

(117) Kim, Y. K.; Kim, E. J.; Lim, J. H.; Cho, H. K.; Hong, W. J.; Jeon, H. H.; Chung, B. G. Dual Stimuli-Triggered Nanogels in Response to Temperature and PH Changes for Controlled Drug Release. *Nanoscale Res. Lett.* **2019**, *14*, 77.

(118) Cao, M.; Wang, Y.; Hu, X.; Gong, H.; Li, R.; Cox, H.; Zhang, J.; Waigh, T. A.; Xu, H.; Lu, J. R. Reversible Thermoresponsive Peptide-PNIPAM Hydrogels for Controlled Drug Delivery. *Biomacromolecules* **2019**, *20*, 3601–3610.

(119) Guan, Y.; Zhang, Y. PNIPAM Microgels for Biomedical Applications: From Dispersed Particles to 3D Assemblies. *Soft Matter* **2011**, *7*, 6375–6384.

(120) Alexis, F.; Pridgen, E.; Molnar, L. K.; Farokhzad, O. C. Factors Affecting the Clearance and Biodistribution of Polymeric Nanoparticles. *Mol. Pharm.* **2008**, *5*, 505–515.

(121) Sun, J.; Peng, Y.; Chen, Y.; Liu, Y.; Deng, J.; Lu, L.; Cai, Y. Effect of Molecular Structure on Thermoresponsive Behaviors of Pyrrolidone-Based Water-Soluble Polymers. *Macromolecules* **2010**, *43*, 4041–4049.

(122) Cunningham, V. J.; Derry, M. J.; Fielding, L. A.; Musa, O. M.; Armes, S. P. RAFT Aqueous Dispersion Polymerization of N -(2-(Methacryloyloxy)Ethyl)Pyrrolidone: A Convenient Low Viscosity Route to High Molecular Weight Water-Soluble Copolymers. *Macromolecules* **2016**, *49*, 4520–4533.

(123) Teodorescu, M.; Bercea, M. Poly(Vinylpyrrolidone) – A Versatile Polymer for Biomedical and Beyond Medical Applications. *Polym. Plast. Technol. Eng.* **2015**, *54*, 923–943.

(124) Sun, X.; Cao, Z.; Yeh, C. K.; Sun, Y. Antifungal Activity, Biofilm-Controlling Effect, and Biocompatibility of Poly(N-Vinyl-2-Pyrrolidinone)-Grafted Denture Materials. *Colloids Surfaces B Biointerfaces* **2013**, *110*, 96–104.

(125) Haaf, F.; Sanner, A.; Straub, F. Polymers of N-Vinylpyrrolidone: Synthesis, Characterization and Uses. *Polym. J.* **1985**, *17*, 143–152.

(126) Seuring, J.; Agarwal, S. Polymers with Upper Critical Solution Temperature in Aqueous Solution. *Macromol. Rapid Commun.* **2012**, *33*, 1898–1920.

(127) Saeki, S.; Kuwahara, N.; Konno, S.; Kaneko, M. Upper and Lower Critical Solution Temperatures in Polystyrene Solutions. II. *Macromolecules* **1973**, *6*, 589–593.

(128) Vshivkov, S. A.; Safronov, A. P. The Conformational Coil-Globule Transition of Polystyrene in Cyclohexane Solution. *Macromol. Chem. Phys.* **1997**, *198*, 3015–3023.

(129) Siporska, A.; Szydlowski, J.; Rebelo, L. P. N. Solvent H/D Isotope Effects on Miscibility and θ-Temperature in the Polystyrene-Cyclohexane System. *Phys. Chem. Chem. Phys.* **2003**, *5*, 2996–3002.

(130) Ho, D. L.; Hammouda, B.; Kline, S. R.; Chen, W. R. Unusual Phase Behavior in Mixtures of Poly(Ethylene Oxide) and Ethyl Alcohol. *J. Polym. Sci. Part B Polym. Phys.* **2006**, *44*, 557–564.

(131) Arotçaréna, M.; Heise, B.; Ishaya, S.; Laschewsky, A. Switching the inside and the Outside of Aggregates of Water-Soluble Block Copolymers with Double Thermoresponsivity. *J. Am. Chem. Soc.* **2002**, *124*, 3787–3793.

(132) Huglin, M. B.; Radwan, M. A. Unperturbed Dimensions of a Zwitterionic Polymethacrylate. *Polym. Int.* **1991**, *26*, 97–104.

(133) Köberle, P.; Laschewsky, A.; Lomax, T. D. Interactions of a Zwitterionic Polysoap and Its Cationic Analog with Inorganic Salts. *Die Makromol. Chemie, Rapid Commun.* **1991**, *12*, 427–433.

(134) D'Agosto, F.; Rieger, J.; Lansalot, M. RAFT-Mediated Polymerization-Induced Self-Assembly. *Angew. Chemie - Int. Ed.* **2020**, *59*, 8368–8392.

(135) Blanazs, A.; Ryan, A. J.; Armes, S. P. Predictive Phase Diagrams for RAFT Aqueous Dispersion Polymerization: Effect of Block Copolymer Composition, Molecular Weight, and Copolymer Concentration. *Macromolecules* **2012**, *45*, 5099–5107.

(136) Zehm, D.; Ratcliffe, L. P. D.; Armes, S. P. Synthesis of Diblock Copolymer Nanoparticles via RAFT Alcoholic Dispersion Polymerization: Effect of Block Copolymer Composition, Molecular Weight, Copolymer Concentration, and Solvent Type on the Final Particle Morphology. *Macromolecules* **2013**, *46*, 128–139.

(137) Fielding, L. A.; Derry, M. J.; Ladmiral, V.; Rosselgong, J.; Rodrigues, A. M.; Ratcliffe, L. P. D.; Sugihara, S.; Armes, S. P. RAFT Dispersion Polymerization in Non-Polar Solvents: Facile Production of Block Copolymer Spheres, Worms and Vesicles in n-Alkanes. *Chem. Sci.* **2013**, *4*, 2081–2087.

(138) Yang, P.; Ratcliffe, L. P. D.; Armes, S. P. Efficient Synthesis of Poly(Methacrylic Acid)-*Block* -Poly(Styrene- *Alt* - *N* -Phenylmaleimide) Diblock Copolymer Lamellae Using RAFT Dispersion Polymerization. *Macromolecules* **2013**, *46*, 8545–8556.

(139) Warren, N. J.; Mykhaylyk, O. O.; Mahmood, D.; Ryan, A. J.; Armes, S. P. RAFT Aqueous Dispersion Polymerization Yields Poly(Ethylene Glycol)-Based Diblock Copolymer Nano-Objects with Predictable Single Phase Morphologies. *J. Am. Chem. Soc.* **2014**, *136*, 1023–1033.

(140) Lopez-Oliva, A. P.; Warren, N. J.; Rajkumar, A.; Mykhaylyk, O. O.; Derry, M. J.; Doncom, K. E. B.; Rymaruk, M. J.; Armes, S. P. Polydimethylsiloxane-Based Diblock Copolymer Nano-Objects Prepared in Nonpolar Media via RAFT-Mediated Polymerization-Induced Self-Assembly. *Macromolecules* **2015**, *48*, 3547–3555.

(141) Rubio, A.; Desnos, G.; Semsarilar, M. Nanostructured Membranes from Soft and Hard Nanoparticles Prepared via RAFT-Mediated PISA. *Macromol. Chem. Phys.* **2018**, *219*, 1800351.

(142) Derry, M. J.; Fielding, L. A.; Warren, N. J.; Mable, C. J.; Smith, A. J.; Mykhaylyk, O. O.; Armes, S. P. In Situ Small-Angle X-Ray Scattering Studies of Sterically-Stabilized Diblock Copolymer Nanoparticles Formed during Polymerization-Induced Self-Assembly in Non-Polar Media. *Chem. Sci.* **2016**, *7*, 5078–5090.

(143) Jones, E. R.; Mykhaylyk, O. O.; Semsarilar, M.; Boerakker, M.; Wyman, P.; Armes, S. P. How Do Spherical Diblock Copolymer Nanoparticles Grow during RAFT Alcoholic Dispersion Polymerization? *Macromolecules* **2016**, *49*, 172–181.

(144) Boissé, S.; Rieger, J.; Belal, K.; Di-Cicco, A.; Beaunier, P.; Li, M. H.; Charleux, B. Amphiphilic Block Copolymer Nano-Fibers via RAFT-Mediated Polymerization in Aqueous Dispersed System. *Chem. Commun.* **2010**, *46*, 1950–1952.

(145) Boissé, S.; Rieger, J.; Pembouong, G.; Beaunier, P.; Charleux, B. Influence of the Stirring Speed and CaCl2 Concentration on the Nano-Object Morphologies Obtained via RAFT-Mediated Aqueous Emulsion Polymerization in the Presence of a Water-Soluble MacroRAFT Agent. *J. Polym. Sci. Part A Polym. Chem.* **2011**, *49*, 3346–3354.

(146) Semsarilar, M.; Ladmiral, V.; Blanazs, A.; Armes, S. P. Anionic Polyelectrolyte-Stabilized Nanoparticles via RAFT Aqueous Dispersion Polymerization. *Langmuir* **2012**, *28*, 914–922.

(147) Semsarilar, M.; Ladmiral, V.; Blanazs, A.; Armes, S. P. Cationic Polyelectrolyte-Stabilized Nanoparticles via RAFT Aqueous Dispersion Polymerization. *Langmuir* **2013**, *29*, 7416–7424.

(148) Charleux, B.; Delaittre, G.; Rieger, J.; D'Agosto, F. Polymerization-Induced Self-Assembly: From Soluble Macromolecules to Block Copolymer Nano-Objects in One Step. *Macromolecules* **2012**, *45*, 6753–6765.

(149) Ferguson, C. J.; Hughes, R. J.; Pham, B. T. T.; Hawkett, B. S.; Gilbert, R. G.; Serelis, A. K.; Such, C. H. Effective Ab Initio Emulsion Polymerization under RAFT Control. *Macromolecules* **2002**, *35*, 9243–9245.

(150) Ferguson, C. J.; Hughes, R. J.; Nguyen, D.; Pham, B. T. T.; Gilbert, R. G.; Serelis, A. K.; Such, C. H.; Hawkett, B. S. Ab Initio Emulsion Polymerization by RAFT-Controlled Self-Assembly. *Macromolecules* **2005**, *38*, 2191–2204.

(151) Rieger, J.; Zhang, W.; Stoffelbach, F.; Charleux, B. Surfactant-Free RAFT Emulsion Polymerization Using Poly(N,N -Dimethylacrylamide) Trithiocarbonate Macromolecular Chain Transfer Agents. *Macromolecules* **2010**, *43*, 6302–6310.

(152) Chaduc, I.; Crepet, A.; Boyron, O.; Charleux, B.; D'Agosto, F.; Lansalot, M. Effect of the PH on the RAFT Polymerization of Acrylic Acid in Water. Application to the Synthesis of Poly(Acrylic Acid)-Stabilized Polystyrene Particles by RAFT Emulsion Polymerization. *Macromolecules* **2013**, *46*, 6013–6023.

(153) Cunningham, V. J.; Alswieleh, A. M.; Thompson, K. L.; Williams, M.; Leggett, G. J.; Armes, S. P.; Musa, O. M. Poly(Glycerol Monomethacrylate)–Poly(Benzyl Methacrylate) Diblock Copolymer Nanoparticles via RAFT Emulsion Polymerization: Synthesis, Characterization, and Interfacial Activity. *Macromolecules* **2014**, *47*, 5613–5623.

(154) Truong, N. P.; Dussert, M. V.; Whittaker, M. R.; Quinn, J. F.; Davis, T. P. Rapid Synthesis of Ultrahigh Molecular Weight and Low Polydispersity Polystyrene Diblock Copolymers by RAFT-Mediated Emulsion Polymerization. *Polym. Chem.* **2015**, *6*, 3865–3874.

(155) Akpinar, B.; Fielding, L. A.; Cunningham, V. J.; Ning, Y.; Mykhaylyk, O. O.; Fowler, P. W.;

Armes, S. P. Determining the Effective Density and Stabilizer Layer Thickness of Sterically Stabilized Nanoparticles. *Macromolecules* **2016**, *49*, 5160–5171.

(156) Cockram, A. A.; Bradley, R. D.; Lynch, S. A.; Fleming, P. C. D.; Williams, N. S. J.; Murray, M. W.; Emmett, S. N.; Armes, S. P. Optimization of the High-Throughput Synthesis of Multiblock Copolymer Nanoparticles in Aqueous Media *via* Polymerization-Induced Self-Assembly. *React. Chem. Eng.* **2018**, *3*, 645–657.

(157) Jesson, C. P.; Cunningham, V. J.; Smallridge, M. J.; Armes, S. P. Synthesis of High Molecular Weight Poly(Glycerol Monomethacrylate) via RAFT Emulsion Polymerization of Isopropylideneglycerol Methacrylate. *Macromolecules* **2018**, *51*, 3221–3232.

(158) Zhang, X.; Boissé, S.; Zhang, W.; Beaunier, P.; D'Agosto, F.; Rieger, J.; Charleux, B. Well-Defined Amphiphilic Block Copolymers and Nano-Objects Formed *in Situ* via RAFT-Mediated Aqueous Emulsion Polymerization. *Macromolecules* **2011**, *44*, 4149–4158.

(159) Zhang, W.; D'Agosto, F.; Boyron, O.; Rieger, J.; Charleux, B. Toward a Better Understanding of the Parameters That Lead to the Formation of Nonspherical Polystyrene Particles via RAFT-Mediated One-Pot Aqueous Emulsion Polymerization. *Macromolecules* **2012**, *45*, 4075–4084.

(160) Khor, S. Y.; Truong, N. P.; Quinn, J. F.; Whittaker, M. R.; Davis, T. P. Polymerization-Induced Self-Assembly: The Effect of End Group and Initiator Concentration on Morphology of Nanoparticles Prepared via RAFT Aqueous Emulsion Polymerization. *ACS Macro Lett.* **2017**, *6*, 1013–1019.

(161) Truong, N. P.; Quinn, J. F.; Anastasaki, A.; Rolland, M.; Vu, M. N.; Haddleton, D. M.; Whittaker, M. R.; Davis, T. P. Surfactant-Free RAFT Emulsion Polymerization Using a Novel Biocompatible Thermoresponsive Polymer. *Polym. Chem.* **2017**, *8*, 1353–1363.

(162) Truong, N. P.; Quinn, J. F.; Anastasaki, A.; Haddleton, D. M.; Whittaker, M. R.; Davis, T. P. Facile Access to Thermoresponsive Filomicelles with Tuneable Cores. *Chem. Commun.* **2016**, *52*, 4497–4500.

(163) Cockram, A. A.; Neal, T. J.; Derry, M. J.; Mykhaylyk, O. O.; Williams, N. S. J.; Murray, M. W.; Emmett, S. N.; Armes, S. P. Effect of Monomer Solubility on the Evolution of Copolymer Morphology during Polymerization-Induced Self-Assembly in Aqueous Solution. *Macromolecules* **2017**, *50*, 796–802.

(164) Hatton, F. L.; Park, A. M.; Zhang, Y.; Fuchs, G. D.; Ober, C. K.; Armes, S. P. Aqueous One-Pot Synthesis of Epoxy-Functional Diblock Copolymer Worms from a Single Monomer: New Anisotropic Scaffolds for Potential Charge Storage Applications. *Polym. Chem.* **2019**, *10*, 194–200.

(165) Brotherton, E. E.; Hatton, F. L.; Cockram, A. A.; Derry, M. J.; Czajka, A.; Cornel, E. J.; Topham, P. D.; Mykhaylyk, O. O.; Armes, S. P. In Situ Small-Angle X-Ray Scattering Studies during Reversible Addition-Fragmentation Chain Transfer Aqueous Emulsion Polymerization. *J. Am. Chem. Soc.* **2019**, *141*, 13664–13675.

(166) He, W. D.; Sun, X. L.; Wan, W. M.; Pan, C. Y. Multiple Morphologies of PAA-b-PSt Assemblies throughout RAFT Dispersion Polymerization of Styrene with PAA Macro-CTA. *Macromolecules* **2011**, *44*, 3358–3365.

(167) Wan, W. M.; Sun, X. L.; Pan, C. Y. Morphology Transition in RAFT Polymerization for Formation of Vesicular Morphologies in One Pot. *Macromolecules* **2009**, *42*, 4950–4952.

(168) Blanazs, A.; Madsen, J.; Battaglia, G.; Ryan, A. J.; Armes, S. P. Mechanistic Insights for

Block Copolymer Morphologies: How Do Worms Form Vesicles? *J. Am. Chem. Soc.* **2011**, *133*, 16581–16587.

(169) Derry, M. J.; Fielding, L. A.; Armes, S. P. Polymerization-Induced Self-Assembly of Block Copolymer Nanoparticles via RAFT Non-Aqueous Dispersion Polymerization. *Prog. Polym. Sci.* **2016**, *52*, 1–18.

(170) Yang, P.; Mykhaylyk, O. O.; Jones, E. R.; Armes, S. P. RAFT Dispersion Alternating Copolymerization of Styrene with *N* -Phenylmaleimide: Morphology Control and Application as an Aqueous Foam Stabilizer. *Macromolecules* **2016**, *49*, 6731–6742.

(171) Birdi, K. S. *Surface and Colloid Chemistry : Principles and Applications*; CRC Press: Boca Raton, USA, 2009.

(172) Jones, E. R.; Semsarilar, M.; Blanazs, A.; Armes, S. P. Efficient Synthesis of Amine-Functional Diblock Copolymer Nanoparticles via RAFT Dispersion Polymerization of Benzyl Methacrylate in Alcoholic Media. *Macromolecules* **2012**, *45*, 5091–5098.

(173) Semsarilar, M.; Penfold, N. J. W.; Jones, E. R.; Armes, S. P. Semi-Crystalline Diblock Copolymer Nano-Objects Prepared via RAFT Alcoholic Dispersion Polymerization of Stearyl Methacrylate. *Polym. Chem.* **2015**, *6*, 1751–1757.

(174) Cunningham, V. J.; Ning, Y.; Armes, S. P.; Musa, O. M. Poly(N-2-(Methacryloyloxy)Ethyl Pyrrolidone)-Poly(Benzyl Methacrylate) Diblock Copolymer Nano-Objects via RAFT Alcoholic Dispersion Polymerisation in Ethanol. *Polymer* **2016**, *106*, 189–199.

(175) Fielding, L. A.; Lane, J. A.; Derry, M. J.; Mykhaylyk, O. O.; Armes, S. P. Thermo-Responsive Diblock Copolymer Worm Gels in Non-Polar Solvents. *J. Am. Chem. Soc.* **2014**, *136*, 5790–5798.

(176) Cunningham, V. J.; Armes, S. P.; Musa, O. M. Synthesis, Characterisation and Pickering Emulsifier Performance of Poly(Stearyl Methacrylate)–Poly(N-2-(Methacryloyloxy)Ethyl Pyrrolidone) Diblock Copolymer Nano-Objects via RAFT Dispersion Polymerisation in n-Dodecane. *Polym. Chem.* **2016**, *7*, 1882–1891.

(177) Rymaruk, M. J.; Hunter, S. J.; O'Brien, C. T.; Brown, S. L.; Williams, C. N.; Armes, S. P. RAFT Dispersion Polymerization in Silicone Oil. *Macromolecules* **2019**, *52*, 2822–2832.

(178) An, Z.; Shi, Q.; Tang, W.; Tsung, C.-K.; Hawker, C. J.; Stucky, G. D. Facile RAFT Precipitation Polymerization for the Microwave-Assisted Synthesis of Well-Defined, Double Hydrophilic Block Copolymers and Nanostructured Hydrogels. *J. Am. Chem. Soc.* **2007**, *129*, 14493–14499.

(179) Ratcliffe, L. P. D.; Ryan, A. J.; Armes, S. P. From a Water-Immiscible Monomer to Block Copolymer Nano-Objects via a One-Pot RAFT Aqueous Dispersion Polymerization Formulation. *Macromolecules* **2013**, *46*, 769–777.

(180) Warren, N. J.; Armes, S. P. Polymerization-Induced Self-Assembly of Block Copolymer Nano-Objects via RAFT Aqueous Dispersion Polymerization. *J. Am. Chem. Soc.* **2014**, *136*, 10174–10185.

(181) Lovett, J. R.; Warren, N. J.; Ratcliffe, L. P. D.; Kocik, M. K.; Armes, S. P. PH-Responsive Non-Ionic Diblock Copolymers: Ionization of Carboxylic Acid End-Groups Induces an Order-Order Morphological Transition. *Angew. Chemie Int. Ed.* **2015**, *54*, 1279–1283.

(182) Lovett, J. R.; Warren, N. J.; Armes, S. P.; Smallridge, M. J.; Cracknell, R. B. Order–Order Morphological Transitions for Dual Stimulus Responsive Diblock Copolymer Vesicles.

Macromolecules **2016**, *49*, 1016–1025.

(183) Penfold, N. J. W.; Lovett, J. R.; Warren, N. J.; Verstraete, P.; Smets, J.; Armes, S. P. PH-Responsive Non-Ionic Diblock Copolymers: Protonation of a Morpholine End-Group Induces an Order-Order Transition. *Polym. Chem.* **2016**, *7*, 79–88.

(184) Penfold, N. J. W.; Lovett, J. R.; Verstraete, P.; Smets, J.; Armes, S. P. Stimulus-Responsive Non-Ionic Diblock Copolymers: Protonation of a Tertiary Amine End-Group Induces Vesicle-to-Worm or Vesicle-to-Sphere Transitions. *Polym. Chem.* **2017**, *8*, 272–282.

(185) Jäger, A.; Jäger, E.; Surman, F.; Höcherl, A.; Angelov, B.; Ulbrich, K.; Drechsler, M.; Garamus, V. M.; Rodriguez-Emmenegger, C.; Nallet, F.; Štěpánek, P. Nanoparticles of the Poly([N-(2-Hydroxypropyl)]Methacrylamide)-b-Poly[2-(Diisopropylamino)Ethyl Methacrylate] Diblock Copolymer for PH-Triggered Release of Paclitaxel. *Polym. Chem.* **2015**, *6*, 4946–4954.

(186) Koziolová, E.; Kostka, L.; Kotrchová, L.; Šubr, V.; Konefal, R.; Nottelet, B.; Etrych, T. N-(2-Hydroxypropyl)Methacrylamide-Based Linear, Diblock, and Starlike Polymer Drug Carriers: Advanced Process for Their Simple Production. *Biomacromolecules* **2018**, *19*, 4003–4013.

(187) Tucker, B. S.; Sumerlin, B. S. Poly(N-(2-Hydroxypropyl) Methacrylamide)-Based Nanotherapeutics. *Polym. Chem.* **2014**, *5*, 1566–1572.

(188) Alfurhood, J. A.; Sun, H.; Kabb, C. P.; Tucker, B. S.; Matthews, J. H.; Luesch, H.; Sumerlin, B. S. Poly(: N -(2-Hydroxypropyl)Methacrylamide)-Valproic Acid Conjugates as Block Copolymer Nanocarriers. *Polym. Chem.* **2017**, *8*, 4983–4987.

(189) Deane, O. J.; Musa, O. M.; Fernyhough, A.; Armes, S. P. Synthesis and Characterization of Waterborne Pyrrolidone-Functional Diblock Copolymer Nanoparticles Prepared via Surfactant-Free RAFT Emulsion Polymerization. *Macromolecules* **2020**, *53*, 1422–1434.

(190) Byard, S. J.; Williams, M.; McKenzie, B. E.; Blanazs, A.; Armes, S. P. Preparation and Cross-Linking of All-Acrylamide Diblock Copolymer Nano-Objects via Polymerization-Induced Self-Assembly in Aqueous Solution. *Macromolecules* **2017**, *50*, 1482–1493.

(191) Rieger, J.; Grazon, C.; Charleux, B.; Alaimo, D.; Jérôme, C. Pegylated Thermally Responsive Block Copolymer Micelles and Nanogels via in Situ RAFT Aqueous Dispersion Polymerization. *J. Polym. Sci. Part A Polym. Chem.* **2009**, *47*, 2373–2390.

(192) Pound, G.; Aguesse, F.; McLeary, J. B.; Lange, R. F. M.; Klumperman, B. Xanthate-Mediated Copolymerization of Vinyl Monomers for Amphiphilic and Double-Hydrophilic Block Copolymers with Poly(Ethylene Glycol). *Macromolecules* **2007**, *40*, 8861–8871.

(193) Sponchioni, M.; O'Brien, C. T.; Borchers, C.; Wang, E.; Rivolta, M. N.; Penfold, N. J. W.; Canton, I.; Armes, S. P. Probing the Mechanism for Hydrogel-Based Stasis Induction in Human Pluripotent Stem Cells: Is the Chemical Functionality of the Hydrogel Important? *Chem. Sci.* **2020**, *11*, 232–240.

(194) Gaitzsch, J.; Messager, L.; Morecroft, E.; Meier, W. Vesicles in Multiple Shapes: Fine-Tuning Polymersomes' Shape and Stability by Setting Membrane Hydrophobicity. *Polymers* **2017**, *9*, 483.

(195) Sugihara, S.; Armes, S. P.; Blanazs, A.; Lewis, A. L. Non-Spherical Morphologies from Cross-Linked Biomimetic Diblock Copolymers Using RAFT Aqueous Dispersion Polymerization. *Soft Matter* **2011**, *7*, 10787–10793.

(196) Lomas, H.; Massignani, M.; Abdullah, K. A.; Canton, I.; Lo Presti, C.; MacNeil, S.; Du, J.; Blanazs, A.; Madsen, J.; Armes, S. P.; Lewis, A. L.; Battaglia, G. Non-Cytotoxic Polymer Vesicles for Rapid and Efficient Intracellular Delivery. *Faraday Discuss.* **2008**, *139*, 143–159.

(197) Gibson, R. R.; Armes, S. P.; Musa, O. M.; Fernyhough, A. End-Group Ionisation Enables the Use of Poly(N -(2-Methacryloyloxy)Ethyl Pyrrolidone) as an Electrosteric Stabiliser Block for Polymerisation-Induced Self-Assembly in Aqueous Media. *Polym. Chem.* **2019**, *10*, 1312–1323.

(198) Byard, S. J.; O'Brien, C. T.; Derry, M. J.; Williams, M.; Mykhaylyk, O. O.; Blanazs, A.; Armes, S. P. Unique Aqueous Self-Assembly Behavior of a Thermoresponsive Diblock Copolymer. *Chem. Sci.* **2020**, *11*, 396–402.

(199) Grazon, C.; Rieger, J.; Sanson, N.; Charleux, B. Study of Poly(N,N-Diethylacrylamide) Nanogel Formation by Aqueous Dispersion Polymerization of N,N-Diethylacrylamide in the Presence of Poly(Ethylene Oxide)-b-Poly(N,N-Dimethylacrylamide) Amphiphilic Macromolecular RAFT Agents. *Soft Matter* **2011**, *7*, 3482–3490.

(200) Rieger, J.; Grazon, C.; Charleux, B.; Alaimo, D.; Jérôme, C. Pegylated Thermally Responsive Block Copolymer Micelles and Nanogels via in Situ RAFT Aqueous Dispersion Polymerization. *J. Polym. Sci. Part A Polym. Chem.* **2009**, *47*, 2373–2390.

(201) Deane, O. J.; Lovett, J. R.; Musa, O. M.; Fernyhough, A.; Armes, S. P. Synthesis of Well-Defined Pyrrolidone-Based Homopolymers and Stimulus-Responsive Diblock Copolymers via RAFT Aqueous Solution Polymerization of 2-(N-Acryloyloxy)Ethylpyrrolidone. *Macromolecules* **2018**, *51*, 7756–7766.

(202) Li, Y.; Armes, S. P. RAFT Synthesis of Sterically Stabilized Methacrylic Nanolatexes and Vesicles by Aqueous Dispersion Polymerization. *Angew. Chemie - Int. Ed.* **2010**, *49*, 4042–4046.

(203) Warren, N. J.; Derry, M. J.; Mykhaylyk, O. O.; Lovett, J. R.; Ratcliffe, L. P. D.; Ladmiral, V.; Blanazs, A.; Fielding, L. A.; Armes, S. P. Critical Dependence of Molecular Weight on Thermoresponsive Behavior of Diblock Copolymer Worm Gels in Aqueous Solution. *Macromolecules* **2018**, *51*, 8357–8371.

(204) Blanazs, A.; Verber, R.; Mykhaylyk, O. O.; Ryan, A. J.; Heath, J. Z.; Douglas, C. W. I.; Armes, S. P. Sterilizable Gels from Thermoresponsive Block Copolymer Worms. *J. Am. Chem. Soc.* **2012**, *134*, 9741–9748.

(205) Lovett, J. R.; Derry, M. J.; Yang, P.; Hatton, F. L.; Warren, N. J.; Fowler, P. W.; Armes, S. P. Can Percolation Theory Explain the Gelation Behavior of Diblock Copolymer Worms? *Chem. Sci.* **2018**, *9*, 7138–7144.

(206) Canton, I.; Warren, N. J.; Chahal, A.; Amps, K.; Wood, A.; Weightman, R.; Wang, E.; Moore, H.; Armes, S. P. Mucin-Inspired Thermoresponsive Synthetic Hydrogels Induce Stasis in Human Pluripotent Stem Cells and Human Embryos. *ACS Cent. Sci.* **2016**, *2*, 65–74.

(207) Bae, Y.; Fukushima, S.; Harada, A.; Kataoka, K. Design of Environment-Sensitive Supramolecular Assemblies for Intracellular Drug Delivery: Polymeric Micelles That Are Responsive to Intracellular PH Change. *Angew. Chemie - Int. Ed.* **2003**, *42*, 4640–4643.

(208) Dai, S.; Ravi, P.; Tam, K. C. PH-Responsive Polymers: Synthesis, Properties and Applications. *Soft Matter* **2008**, *4*, 435–449.

(209) Morse, A. J.; Armes, S. P.; Thompson, K. L.; Dupin, D.; Fielding, L. A.; Mills, P.; Swart, R. Novel Pickering Emulsifiers Based on PH-Responsive Poly(2- (Diethylamino)Ethyl Methacrylate) Latexes. *Langmuir* **2013**, *29*, 5446–5475.

(210) Wan, W.-M.; Sun, X.-L.; Pan, C.-Y. Formation of Vesicular Morphologies via Polymerization Induced Self-Assembly and Re-Organization. *Macromol. Rapid Commun.* **2010**, *31*, 399–404.

(211) Wan, W. M.; Pan, C. Y. One-Pot Synthesis of Polymeric Nanomaterials via RAFT Dispersion Polymerization Induced Self-Assembly and Re-Organization. *Polym. Chem.* **2010**, *1*, 1475–1484.

(212) Huang, C. Q.; Pan, C. Y. Direct Preparation of Vesicles from One-Pot RAFT Dispersion Polymerization. *Polymer* **2010**, *51*, 5115–5121.

(213) Cai, W.; Wan, W.; Hong, C.; Huang, C.; Pan, C. Morphology Transitions in RAFT Polymerization. *Soft Matter* **2010**, *6*, 5554–5561.

(214) Zhang, X.; Rieger, J.; Charleux, B. Effect of the Solvent Composition on the Morphology of Nano-Objects Synthesized via RAFT Polymerization of Benzyl Methacrylate in Dispersed Systems. *Polym. Chem.* **2012**, *3*, 1502.

(215) Jones, E. R.; Semsarilar, M.; Wyman, P.; Boerakker, M.; Armes, S. P. Addition of Water to an Alcoholic RAFT PISA Formulation Leads to Faster Kinetics but Limits the Evolution of Copolymer Morphology. *Polym. Chem.* **2016**, *7*, 851–859.

(216) North, S. M.; Jones, E. R.; Smith, G. N.; Mykhaylyk, O. O.; Annable, T.; Armes, S. P. Adsorption of Small Cationic Nanoparticles onto Large Anionic Particles from Aqueous Solution: A Model System for Understanding Pigment Dispersion and the Problem of Effective Particle Density. *Langmuir* **2017**, *33*, 1275–1284.

(217) Semsarilar, M.; Jones, E. R.; Blanazs, A.; Armes, S. P. Efficient Synthesis of Sterically-Stabilized Nano-Objects via RAFT Dispersion Polymerization of Benzyl Methacrylate in Alcoholic Media. *Adv. Mater.* **2012**, *24*, 3378–3382.

(218) Semsarilar, M.; Ladmiral, V.; Blanazs, A.; Armes, S. P. Poly(Methacrylic Acid)-Based AB and ABC Block Copolymer Nano-Objects Prepared via RAFT Alcoholic Dispersion Polymerization. *Polym. Chem.* **2014**, *5*, 3466–3475.

(219) Houillot, L.; Bui, C.; Save, M.; Charleux, B.; Farcet, C.; Moire, C.; Raust, J.-A.; Rodriguez, I. Synthesis of Well-Defined Polyacrylate Particle Dispersions in Organic Medium Using Simultaneous RAFT Polymerization and Self-Assembly of Block Copolymers. A Strong Influence of the Selected Thiocarbonylthio Chain Transfer Agent. *Macromolecules* **2007**, *40*, 6500–6509.

(220) Houillot, L.; Bui, C.; Farcet, C.; Moire, C.; Raust, J. A.; Pasch, H.; Save, M.; Charleux, B. Dispersion Polymerization of Methyl Acrylate in Nonpolar Solvent Stabilized by Block Copolymers Formed in Situ via the RAFT Process. *ACS Appl. Mater. Interfaces* **2010**, *2*, 434–442.

(221) Raust, J. A.; Houillot, L.; Save, M.; Charleux, B.; Moire, C.; Farcet, C.; Pasch, H. Two Dimensional Chromatographic Characterization of Block Copolymers of 2-Ethylhexyl Acrylate and Methyl Acrylate, P2EHA-b-PMA, Produced via RAFT-Mediated Polymerization in Organic Dispersion. *Macromolecules* **2010**, *43*, 8755–8765.

(222) Pei, Y.; Thurairajah, L.; Sugita, O. R.; Lowe, A. B. RAFT Dispersion Polymerization in Nonpolar Media: Polymerization of 3-Phenylpropyl Methacrylate in n -Tetradecane with

Poly(Stearyl Methacrylate) Homopolymers as Macro Chain Transfer Agents. *Macromolecules* **2015**, *48*, 236–244.

(223) Pei, Y.; Sugita, O. R.; Thurairajah, L.; Lowe, A. B. Synthesis of Poly(Stearyl Methacrylate-b-3-Phenylpropyl Methacrylate) Nanoparticles in n-Octane and Associated Thermoreversible Polymorphism. *RSC Adv.* **2015**, *5*, 17636–17646.

(224) Williams, M.; Penfold, N. J. W.; Lovett, J. R.; Warren, N. J.; Douglas, C. W. I.; Doroshenko, N.; Verstraete, P.; Smets, J.; Armes, S. P. Bespoke Cationic Nano-Objects: Via RAFT Aqueous Dispersion Polymerisation. *Polym. Chem.* **2016**, *7*, 3864–3873.

(225) Chevalier, Y.; Bolzinger, M. A. Emulsions Stabilized with Solid Nanoparticles: Pickering Emulsions. *Colloids Surfaces A Physicochem. Eng. Asp.* **2013**, *439*, 23–34.

(226) Ramsden, W. Separation of Solids in the Surface-Layers of Solutions and 'Suspensions' (Observations on Surface-Membranes, Bubbles, Emulsions, and Mechanical Coagulation).—Preliminary Account. *Proc. R. Soc. London* **1903**, *72*, 156–164.

(227) Pickering, S. U. CXCVI. - Emulsions. *J. Chem. Soc. Trans.* **1907**, *91*, 2001–2021.

(228) Binks, B. P.; Lumsdon, S. O. Effects of Oil Type and Aqueous Phase Composition on Oil-Water Mixtures Containing Particles of Intermediate Hydrophobicity. *Phys. Chem. Chem. Phys.* **2000**, *2*, 2959–2967.

(229) Binks, B. P.; Lumsdon, S. O. Catastrophic Phase Inversion of Water-in-Oil Emulsions Stabilized by Hydrophobie Silica. *Langmuir* **2000**, *16*, 2539–2547.

(230) Madivala, B.; Vandebril, S.; Fransaer, J.; Vermant, J. Exploiting Particle Shape in Solid Stabilized Emulsions. *Soft Matter* **2009**, *5*, 1717–1727.

(231) Chen, T.; Colver, P. J.; Bon, S. A. F. Organic–Inorganic Hybrid Hollow Spheres Prepared from TiO2-Stabilized Pickering Emulsion Polymerization. *Adv. Mater.* **2007**, *19*, 2286–2289.

(232) Williams, M.; Armes, S. P.; York, D. W. Clay-Based Colloidosomes. *Langmuir* **2012**, *28*, 1142–1148.

(233) Cauvin, S.; Colver, P. J.; Bon, S. A. F. Pickering Stabilized Miniemulsion Polymerization: Preparation of Clay Armored Latexes. *Macromolecules* **2005**, *38*, 7887–7889.

(234) Bon, S. A. F.; Colver, P. J. Pickering Miniemulsion Polymerization Using Laponite Clay as a Stabilizer. *Langmuir* **2007**, *23*, 8316–8322.

(235) Velev, O. D.; Furusawa, K.; Nagayama, K. Assembly of Latex Particles by Using Emulsion Droplets as Templates. 1. Microstructured Hollow Spheres. *Langmuir* **1996**, *12*, 2374–2384.

(236) Velev, O. D.; Nagayama, K. Assembly of Latex Particles by Using Emulsion Droplets. 3. Reverse (Water in Oil) System. *Langmuir* **1997**, *13*, 1856–1859.

(237) Binks, B. P.; Lumsdon, S. O. Pickering Emulsions Stabilized by Monodisperse Latex Particles: Effects of Particle Size. *Langmuir* **2001**, *17*, 4540–4547.

(238) Aveyard, R.; Binks, B. P.; Clint, J. H.; Fletcher, P. D.; Horozov, T. S.; Neumann, B.; Paunov, V. N.; Annesley, J.; Botchway, S. W.; Nees, D.; Parker, A. W.; Ward, A. D.; Burgess, A. N. Measurement of Long-Range Repulsive Forces between Charged Particles at an Oil-Water Interface. *Phys. Rev. Lett.* **2002**, *88*, 2461021–2461024.

(239) Binks, B. P.; Murakami, R.; Armes, S. P.; Fujii, S. Temperature-Induced Inversion of Nanoparticle-Stabilized Emulsions. *Angew. Chemie* **2005**, *117*, 4873–4876.

(240) Fujii, S.; Cai, Y.; Weaver, J. V. M.; Armes, S. P. Syntheses of Shell Cross-Linked Micelles Using Acidic ABC Triblock Copolymers and Their Application as PH-Responsive Particulate Emulsifiers. *J. Am. Chem. Soc.* **2005**, *127*, 7304–7305.

(241) Reynaert, S.; Moldenaers, P.; Vermant, J. Control over Colloidal Aggregation in Monolayers of Latex Particles at the Oil-Water Interface. *Langmuir* **2006**, *22*, 4936–4945.

(242) Binks, B. P. Particles as Surfactants—Similarities and Differences. *Curr. Opin. Colloid Interface Sci.* **2002**, *7*, 21–41.

(243) Thompson, K. L.; Chambon, P.; Verber, R.; Armes, S. P. Can Polymersomes Form Colloidosomes? *J. Am. Chem. Soc.* **2012**, *134*, 12450–12453.

(244) Thompson, K. L.; Mable, C. J.; Cockram, A.; Warren, N. J.; Cunningham, V. J.; Jones, E. R.; Verber, R.; Armes, S. P. Are Block Copolymer Worms More Effective Pickering Emulsifiers than Block Copolymer Spheres? *Soft Matter* **2014**, *10*, 8615–8626.

(245) Thompson, K. L.; Lane, J. A.; Derry, M. J.; Armes, S. P. Non-Aqueous Isorefractive Pickering Emulsions. *Langmuir* **2015**, *31*, 4373–4376.

(246) Thompson, K. L.; Mable, C. J.; Lane, J. A.; Derry, M. J.; Fielding, L. A.; Armes, S. P. Preparation of Pickering Double Emulsions Using Block Copolymer Worms. *Langmuir* **2015**, *31*, 4137–4144.

(247) Mable, C. J.; Warren, N. J.; Thompson, K. L.; Mykhaylyk, O. O.; Armes, S. P. Framboidal ABC Triblock Copolymer Vesicles: A New Class of Efficient Pickering Emulsifier. *Chem. Sci.* **2015**, *6*, 6179–6188.

(248) Thompson, K. L.; Fielding, L. A.; Mykhaylyk, O. O.; Lane, J. A.; Derry, M. J.; Armes, S. P. Vermicious Thermo-Responsive Pickering Emulsifiers. *Chem. Sci.* **2015**, *6*, 4207–4214.

(249) Zhou, J.; Yao, H.; Ma, J. Recent Advances in RAFT-Mediated Surfactant-Free Emulsion Polymerization. *Polym. Chem.* **2018**, *9*, 2532–2561.

(250) Uzulina, I.; Kanagasabapathy, S.; Claverie, J. Reversible Addition Fragmentation Transfer (RAFT) Polymerization in Emulsion. *Macromol. Symp.* **2000**, *150*, 33–38.

(251) Monteiro, M. J.; Sjöberg, M.; Vlist, J. van der; Göttgens, C. M. Synthesis of Butyl Acrylate–Styrene Block Copolymers in Emulsion by Reversible Addition-fragmentation Chain Transfer: Effect of Surfactant Migration upon Film Formation. *J. Polym. Sci. Part A Polym. Chem.* **2000**, *38*, 4206–4217.

(252) Monteiro, M. J.; De Barbeyrac, J. Free-Radical Polymerization of Styrene in Emulsion Using a Reversible Addition - Fragmentation Chain Transfer Agent with a Low Transfer Constant: Effect on Rate, Particle Size, and Molecular Weight. *Macromolecules* **2001**, *34*, 4416–4423.

(253) Prescott, S. W.; Ballard, M. J.; Rizzardo, E.; Gilbert, R. G. RAFT in Emulsion Polymerization: What Makes It Different? *Aust. J. Chem.* **2002**, *55*, 415–424.

(254) Prescott, S. W.; Ballard, M. J.; Rizzardo, E.; Gilbert, R. G. Successful Use of RAFT Techniques in Seeded Emulsion Polymerization of Styrene: Living Character, RAFT Agent Transport, and Rate of Polymerization. *Macromolecules* **2002**, *35*, 5417–5425.

(255) Szkurhan, A. R.; Georges, M. K. Stable Free-Radical Emulsion Polymerization.

Macromolecules **2004**, *37*, 4776–4782.

(256) Szkurhan, A. R.; Kasahara, T.; Georges, M. K. Reversible-Addition Fragmentation Chain Transfer Radical Emulsion Polymerization by a Nanoprecipitation Process. *J. Polym. Sci. Part A Polym. Chem.* **2006**, *44*, 5708–5718.

(257) Chaduc, I.; Girod, M.; Antoine, R.; Charleux, B.; D'Agosto, F.; Lansalot, M. Batch Emulsion Polymerization Mediated by Poly(Methacrylic Acid) MacroRAFT Agents: One-Pot Synthesis of Self-Stabilized Particles. *Macromolecules* **2012**, *45*, 5881–5893.

(258) Zhang, W.; D'Agosto, F.; Dugas, P. Y.; Rieger, J.; Charleux, B. RAFT-Mediated One-Pot Aqueous Emulsion Polymerization of Methyl Methacrylate in Presence of Poly(Methacrylic Acid-Co-Poly(Ethylene Oxide) Methacrylate) Trithiocarbonate Macromolecular Chain Transfer Agent. *Polymer* **2013**, *54*, 2011–2019.

(259) Pham, B. T. T.; Nguyen, D.; Huynh, V. T.; Pan, E. H.; Shirodkar-Robinson, B.; Carey, M.; Serelis, A. K.; Warr, G. G.; Davey, T.; Such, C. H.; Hawkett, B. S. Aqueous Polymeric Hollow Particles as an Opacifier by Emulsion Polymerization Using Macro-RAFT Amphiphiles. *Langmuir* **2018**, *34*, 4255–4263.

(260) Zhang, W. J.; Hong, C. Y.; Pan, C. Y. Fabrication and Characterization of Silica Nanotubes with Controlled Dimensions. *J. Mater. Chem. A* **2014**, *2*, 7819–7828.

(261) Manguian, M.; Save, M.; Charleux, B. Batch Emulsion Polymerization of Styrene Stabilized by a Hydrophilic Macro-RAFT Agent. *Macromol. Rapid Commun.* **2006**, *27*, 399–404.

(262) Rieger, J.; Stoffelbach, F.; Bui, C.; Alaimo, D.; Jérôme, C.; Charleux, B. Amphiphilic Poly(Ethylene Oxide) Macromolecular RAFT Agent as a Stabilizer and Control Agent in Ab Initio Batch Emulsion Polymerization. *Macromolecules* **2008**, *41*, 4065–4068.

(263) Rieger, J.; Osterwinter, G.; Bui, C.; Stoffelbnach, F.; Charleux, B. Surfactant-Free Controlled/Living Radical Emulsion (Co)Polymerization of n-Butyl Acrylate and Methyl Methacrylate via RAFT Using Amphiphilic Polyethylene Oxide-Based Trithiocarbonate Chain Transfer Agents. *Macromolecules* **2009**, *42*, 5518–5525.

(264) Zhu, Y.; Yang, B.; Chen, S.; Du, J. Polymer Vesicles: Mechanism, Preparation, Application, and Responsive Behavior. *Prog. Polym. Sci.* **2017**, *64*, 1–22.

Chapter 2.

The use of an anionic RAFT end-group to enable poly(*N*-(2-methacryloyloxy)ethyl pyrrolidone) as an electrosteric stabiliser for aqueous RAFT PISA

Reproduced in part with permission from [Gibson, R. R.; Armes, S. P.; Musa, O. M.; Fernyhough A. End-group ionisation enables the use of poly(*N*-(2-methacryloyloxy)ethyl pyrrolidone) as an electrosteric stabiliser block for polymerisation-induced self-assembly in aqueous media. *Polymer Chemistry,* **2019**, *10*, 1312-1323]

2.1 Introduction

Thermoresponsive polymers exhibiting LCST behaviour have received substantial interest, particularly in the context of drug delivery.[1–7] Undoubtedly, the most studied example is PNIPAM, which exhibits a CP at around 32 °C.[8,9] This critical temperature can be raised *via* statistical copolymerisation of NIPAM with various hydrophilic monomers[10,11] or by employing hydrophilic end-groups.[12,13] Pyrrolidone-functional polymers are usually biocompatible and therefore offer an alternative to PNIPAM for potential bioapplications. In particular, PNMEP exhibits inverse solubility behaviour, see Figure 2.1.[14–16] At around ambient temperature, the pyrrolidone ring forms hydrogen bonds with water that confer aqueous solubility, despite the relatively hydrophobic methacrylic backbone. However, such hydrogen bonding is disrupted on heating to a sufficiently high temperature, causing PNMEP to precipitate from aqueous solution.

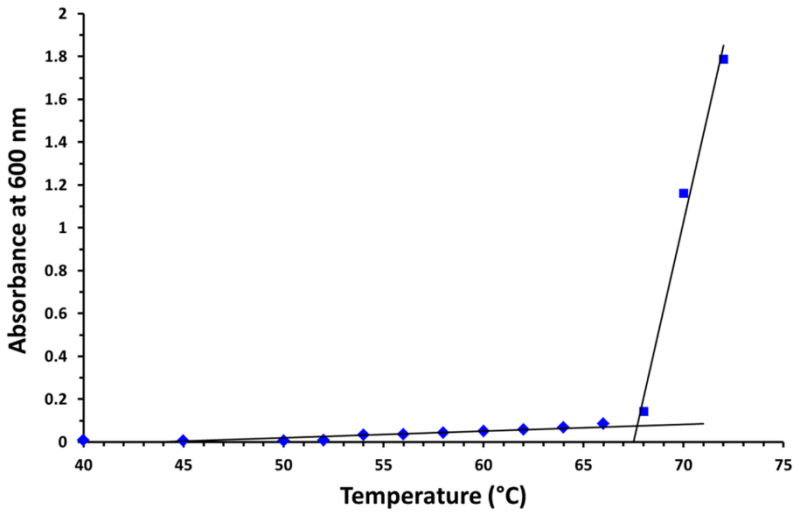

Figure 2.1. An absorbance (at 600 nm) *vs.* temperature plot for a $PNMEP_{172}$ homopolymer prepared *via* RAFT solution polymerisation in ethanol to determine its LCST by turbidimetry.[16]

PISA enables the rational design of block copolymer nanoparticles, including spheres, worms and vesicles.[17–20] For example, Cunningham and co-workers reported the RAFT dispersion polymerisation of BzMA in ethanol using PNMEP as a steric stabiliser block.[21] Alternatively, PNMEP can be utilised as a core-forming block for RAFT dispersion polymerisation formulations conducted in *n*-dodecane.[22] Importantly, each of these literature examples utilise PNMEP in non-aqueous solvents in which it does not exhibit thermoresponsive behaviour. In aqueous solution, such behaviour has been used to prepare sterically-stabilised block copolymer particles with weakly hydrophobic PNMEP cores in water at 70 °C that subsequently dissolve to afford molecularly-dissolved copolymer chains on cooling to ambient temperature (Figure 2.2). This strategy has enabled the synthesis of relatively high molecular weight PNMEP *via* RAFT aqueous

dispersion polymerisation.[16] However, it also suggests that PNMEP does not have sufficient hydrophilic character to be used as a steric stabiliser block for PISA formulations conducted in aqueous media. In the present study, we show that this apparent limitation can be overcome by the judicious use of an appropriate RAFT agent.

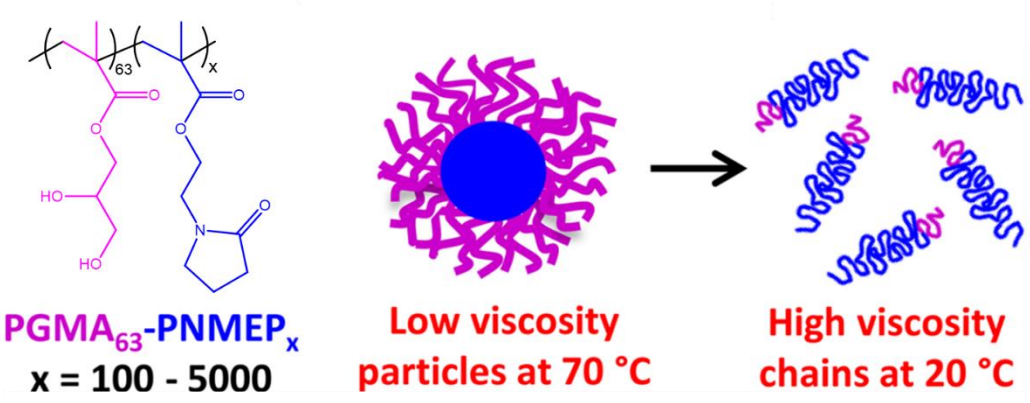

Figure 2.2. High molecular weight water-soluble polymers produced by an aqueous dispersion PISA formulation conducted at 70 °C which is above the CP of the PNMEP 'core' forming block.[16]

PHEMA had been classified as water-insoluble.[23,24] However, Weaver *et al.* reported that for relatively short poly(2-hydroxyethyl methacrylate) (PHEMA) chains (DP < 45), LCST behaviour was observed at pH 6.5, while no LCST behaviour occurred under the same conditions for PHEMA oligomers (*e.g.* DP = 20).[3] By reducing the solution pH to 2.2, the terminal morpholine end-groups became protonated, thus increasing the hydrophilic character of the PHEMA chains and ensuring their aqueous solubility at all temperatures for DPs of up to 50.

In principle, higher molecular weight should reduce the CP as the entropy of mixing becomes less favourable.[25,26] However, such molecular weight-dependent LCST behaviour is not necessarily characteristic of all water-soluble polymers. In particular, end-group effects can play an important role: hydrophilic end-groups typically increase the CP, whereas hydrophobic end-groups usually reduce it.[27,28,29] For example, Luan *et al.* removed the hydrophobic dithiobenzoate group from a series of PNIPAM-poly(*N*-(2-hydroxypropyl) methacrylamide) diblock copolymers by aminolysis to produce thiol-capped chains.[30] This derivatisation raised the CP of the thiol-functional copolymers by up to 23 °C relative to the precursor copolymer. Moreover, the increase in CP observed for lower molecular weight copolymers suggested that end-group effects are particularly strong in this regime.[30]

Summers *et al.* investigated the effect of converting a pyridyl disulfide end-group into a thioglycerol group.[12] Higher CPs were observed for both a di(ethylene glycol) methyl ether

methacrylate / oligo(ethylene glycol) methyl ether methacrylate statistical copolymer and also for a PNIPAM homopolymer. No CP was observed for relatively short PNIPAM chains, which again suggests that end-groups can have a substantial influence in the lower molecular weight limit.

Herein we demonstrate that ionisation of a single terminal carboxylic acid group (derived from a RAFT CTA) renders PNMEP sufficiently hydrophilic to serve as a suitable stabiliser block for PISA syntheses conducted in aqueous media. This is demonstrated for both the RAFT aqueous dispersion polymerisation of 2-hydroxypropyl methacrylate (HPMA) and the RAFT aqueous emulsion polymerisation of 2-ethoxyethyl methacrylate (EEMA).

2.2 Experimental

2.2.1 Materials

N-(2-(Methacryloyloxy)ethyl pyrrolidone (NMEP; 98% purity) was kindly provided by Ashland Inc. (Delaware, USA) and was used without further purification. 2-Hydroxypropyl methacrylate (HPMA) was provided by GEO Specialty Chemicals (Hythe, UK). 2-Ethoxyethyl methacrylate (EEMA), ethanol (≥99.8%) and NaOH were purchased from Sigma Aldrich UK. 4,4'-Azobis(4-cyanopentanoic acid) (ACVA; 99%) was purchased from Alfa Aesar (Heysham, UK). 2,2'-Azobis(2-(2-imidazolin-2-yl)propane)dihydrochloride (VA-044) was purchased from Wako Pure Chemical Industries (Japan). d_4-Methanol and d_6-dimethyl sulfoxide were purchased from Goss Scientific Instruments Ltd. (Cheshire, UK), while 4-cyano-4-(2-phenylethanesulfanylthiocarbonyl)sulfanyl pentanoic acid (PETTC) RAFT agent was synthesised as previously reported.[31] Deionised water was used for all experiments.

2.2.2 Synthesis of a $PNMEP_x$ macro-CTA by RAFT solution polymerisation at 70 °C.

A typical protocol for a $PNMEP_{53}$ macro-CTA is described below. Macro-CTAs with other mean DPs (19 – 89) were also synthesised by varying the NMEP/PETTC molar ratio.

NMEP (10.99 g, 55.7 mmol), PETTC RAFT agent (0.27 g, 0.80 mmol; target DP = 70), ACVA (44.6 mg, 0.59 mmol; PETTC/ACVA molar ratio = 5.0) and ethanol (16.96 g, 40% w/w solids) were weighed into a 50 mL round-bottom flask and degassed with stirring in ice for 30 min. The reaction was allowed to proceed for 210 min in an oil bath set to 70 °C resulting in a monomer conversion of 69% judged by ^{1}H NMR spectroscopy. The crude polymer was precipitated into diethyl ether to remove residual monomer before freeze-drying from water to afford a dry yellow powder. The

mean DP was judged to be 53 by comparing the integrals of the aromatic signals associated with the trithiocarbonate end group at 7-8 ppm to the methylene carbonyl proton signal at 2.5 ppm. Gel permeation chromatography (GPC) analysis using dimethyl formamide (DMF) eluent indicated an M_n of 7 700 g mol^{-1} and M_w/M_n of 1.26 against a series of ten near-monodisperse poly(methyl methacrylate) (PMMA) calibrants.

2.2.3 PISA synthesis of PNMEP$_{42}$-PHPMA$_x$ diblock copolymer nanoparticles *via* RAFT aqueous dispersion polymerisation of HPMA at 44 °C.

A typical protocol for the synthesis of PNMEP$_{42}$-PHPMA$_{300}$ is described as follows: PNMEP$_{42}$ macro-CTA (0.06 g, 6.96 µmol), HPMA (0.30 g, 2.09 mmol), VA-044 (0.40 mg, 1.39 µmol added as a 10 mg/g VA-044 in water stock solution: PNMEP$_{42}$ macro-CTA/VA-044 molar ratio = 5.0) and water (1.45 g) were added to a 14 mL vial and the solution pH was adjusted from 3.8 to pH 7 with NaOH. The reaction vial was sealed and degassed under N_2 for 30 min before placing in a pre-heated oil bath set at 44 °C for 16 h. The polymerisation was quenched by exposing to air. The polymer nanoparticles were characterised by ^{1}H NMR spectroscopy in d$_4$-methanol, dynamic light scattering (DLS) and transmission electron microscopy (TEM) with 0.1% w/w aqueous dispersions prepared using deionised water. DMF GPC analysis indicated M_n = 46 300 g mol^{-1} and M_w/M_n = 1.44. ^{1}H NMR analysis indicated >99% HPMA monomer conversion in all cases. Other diblock compositions were prepared by adjusting the amount of HPMA monomer to target PHPMA DPs of 150 – 400.

2.2.4 PISA synthesis of PNMEP$_{53}$-PEEMA$_x$ diblock copolymer nanoparticles *via* RAFT aqueous emulsion polymerisation of EEMA at 44 °C.

The pH of the reaction mixture was adjusted prior to addition of EEMA monomer. A typical protocol for the synthesis of PNMEP$_{53}$-PEEMA$_{100}$ nanoparticles is described: PNMEP$_{53}$ macro-CTA (0.12 g, 11.10 µmol), VA-044 (0.07 mg, 2.22 µmol added as a 10 mg/g VA-044 in water stock solution: PNMEP$_{53}$ macro-CTA/VA-044 molar ratio = 5.0) and water (1.19 g) were added to a 14 mL vial and the pH was adjusted to 7 using NaOH. EEMA (0.18 g, 1.11 mmol) was then added to the vial which was then sealed and degassed using N_2 for 30 min. The reaction was placed into a pre-heated oil bath set to 44 °C for 5 h. After quenching the polymerisation by exposure to air, portions of the resulting copolymer nanoparticles were freeze-dried prior to GPC and ^{1}H NMR analysis in chloroform and DMSO respectively. 0.1 %w/w dispersions for DLS and TEM analysis were prepared using deionised water. Chloroform GPC analysis indicated M_n = 13 800 g mol^{-1} and M_w/M_n = 1.31. ^{1}H NMR analysis indicated >99% monomer conversion in all cases. Other diblock compositions were prepared by adjusting the amount of EEMA monomer to target PEEMA DP of 100 – 600.

2.2.5 Copolymer characterisation

2.2.5.1 *^{1}H NMR spectroscopy.* d_4-Methanol was used to record the ^{1}H NMR spectra of the PNMEP$_x$ macro-CTAs and the PNMEP$_{42}$-PHPMA$_x$ diblock copolymers. The PNMEP$_{53}$-PEEMA$_x$ diblock copolymers were freeze-dried prior to recording the ^{1}H NMR spectra in d_6-DMSO. The spectrometer used was a 400 MHz Bruker Avance 400 spectrometer.

2.2.5.2 *Gel permeation chromatography (GPC).* The molecular weights of both the PNMEP homopolymers and PNMEP$_{42}$-PHPMA$_x$ copolymers were obtained using DMF GPC at 60 °C. The eluent contained 10 mmol LiBr at a flow rate of 1.0 mL min^{-1}. For PNMEP$_{53}$-PEEMA$_x$ copolymers, the M_n was obtained using chloroform GPC containing 0.25% v/v triethylamine at 35 °C. Two Polymer Laboratories PL gel 5 µm Mixed C columns were connected in series to a Varian 390 multidetector suite (refractive index detector) and a Varian 290 LC pump injection module. For PNMEP homopolymers, a Polymer Laboratories PL gel 5 µm Mixed C column was connected in series to a Polymer Laboratories PL gel 5 µm Mixed E column to aid resolution of the lower molecular weight chains. Ten near-monodisperse PMMA standards (M_n = 625 – 618 000 g mol^{-1}) were used for calibration and the data were analysed using Varian Cirrus GPC software.

2.2.5.3 *Dynamic light scattering (DLS).* A Malvern Zetasizer NanoZS instrument was used to determine the intensity-average hydrodynamic diameter of the copolymer nanoparticles at 20 °C at a scattering angle of 173 °. 0.1% w/w copolymer dispersions were analysed at pH 7 using 1 cm disposable plastic cuvettes. The data was averaged over three consecutive runs for each sample. Aqueous electrophoresis measurements were also conducted at 20 °C but were diluted to 0.1% w/w using 1 mM KCl. The pH was adjusted using either HCl or KOH as required.

2.2.5.4 *Transmission electron microscopy (TEM).* Copper/palladium grids were surface-coated in-house to produce a thin film of amorphous carbon before plasma glow-discharged for 40 s producing a hydrophilic surface. 15 µL of 0.1% w/w aqueous copolymer dispersions at pH 7 were deposited onto the grids for 60 s, blotted to remove the excess solution before being negatively stained using 15 µL uranyl formate solution (0.75% w/v) for 20 s. The excess stain was removed by blotting and the grid was further dried using a vacuum hose. A FEI Tecnai Spirit microscope operating at 80 kV fitted with a Gatan 1kMS600CW CCD camera was used to image the grids.

2.2.5.5 *Cloud point (CP) determination.* Spectra were recorded for 1.0 w/w aqueous solutions of PNMEP$_x$ homopolymers of varying DPs using a Varian Cary 300 Bio UV-visible spectrometer. Samples were heated at 1.0 °C min^{-1} with spectra recorded at 1.0 °C intervals between 25 and 90 °C. The solution pH was adjusted using NaOH and HCl. The point of inflection on a plot of

transmittance (recorded at an arbitrary wavelength of 600 nm) *vs.* temperature was used to determine the CP.[32]

2.2.5.6 UV absorption spectroscopy. UV spectra were recorded between 200 and 400 nm using a PC-controlled UV-1800 spectrophotometer at 25 °C using a 1 cm path length quartz cell. A Beer–Lambert curve was constructed using a series of 18 PETTC solutions in chloroform. The absorption maximum at 298 nm assigned to the trithiocarbonate group was used for this calibration plot, and PETTC concentrations were selected such that the absorbance always remained below unity. Subsequently, the mean DP for each of the seven PNMEP homopolymers was determined using the molar extinction coefficient of 11 909 ± 120 mol^{-1} dm^3 cm^{-1} determined for PETTC.

2.3 Results and discussion

There are a large number of reports of aqueous PISA syntheses involving polyelectrolytic steric stabilisers.[33–41] However, there are far fewer studies of the effect of charged end-groups on otherwise non-ionic steric stabiliser chains. For example, end-group ionisation effects have been recently reported for various aqueous PISA formulations by Lovett and co-workers[42,43] and Penfold *et al.*[44,45] In each case, ionisation (or protonation) of a terminal carboxylic acid (or tertiary amine) group led to a change in the diblock copolymer morphology owing to greater solvation of the non-ionic steric stabiliser block, which leads to a subtle shift in the fractional packing parameter. In contrast, we show herein that end-group ionisation is *an essential prerequisite to ensure colloidal stability* when using PNMEP as a moderately hydrophilic stabiliser block.

2.3.1 Synthesis of PNMEP homopolymers *via* RAFT solution polymerisation in ethanol

A series of PNMEP homopolymers were prepared by RAFT solution polymerisation of NMEP in ethanol using a PETTC RAFT agent at 70 °C, see Scheme 2.1. Depending on the target DP, these polymerisations were allowed to proceed for between 100 min and 4 h prior to being quenched by cooling to 20 °C followed by exposure to air.

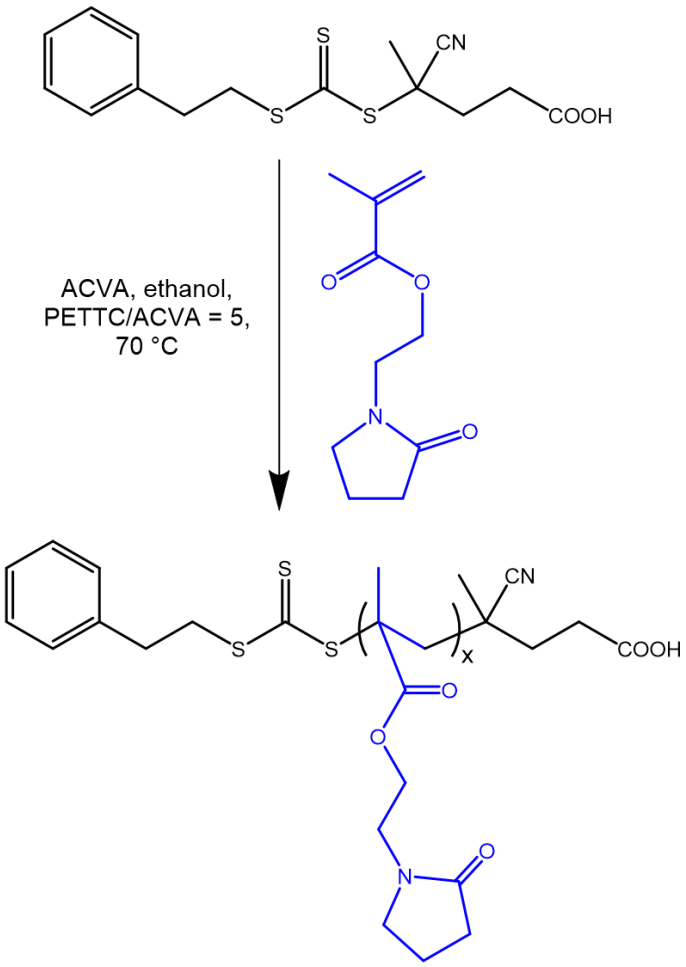

Scheme 2.1. Synthesis of PNMEP$_x$ homopolymer precursors by RAFT solution polymerisation of NMEP in ethanol using PETTC at 70 °C.

To assess the living character of the RAFT solution polymerisation of NMEP, aliquots were extracted over 390 min when targeting a DP of 70. The RAFT solution polymerisation kinetics for the synthesis of a PNMEP macro-CTA (target DP = 70) using PETTC RAFT agent (PETTC/ACVA ratio = 5.0) at 70 °C in ethanol (40% w/w solids) are shown in Figure 2.3. Monomer conversion was monitored by ^{1}H NMR spectroscopy; full NMEP conversion was achieved within 6 h. DMF GPC curves indicated a linear increase in molecular weight with NMEP conversion, as expected. The final homopolymer had a M_n of 11 600 g mol^{-1} and an M_w/M_n of 1.15, indicating good control.

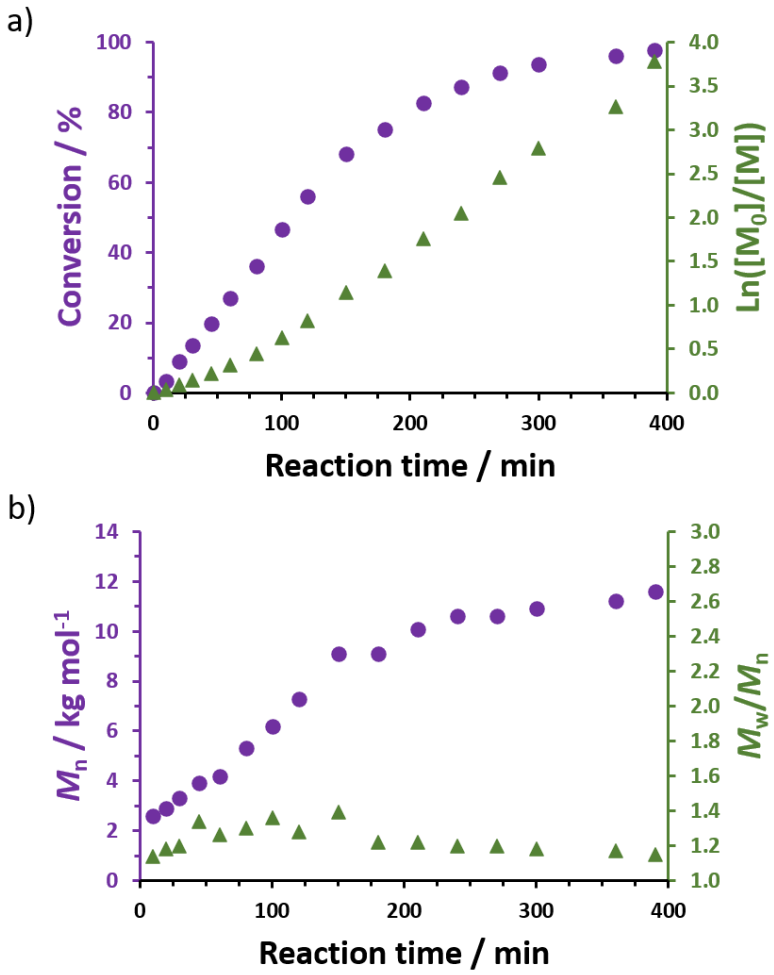

Figure 2.3. (a) Conversion *vs.* time plots and corresponding semi-logarithmic data for the synthesis of a PNMEP macro-CTA (target DP = 70) using PETTC RAFT agent in ethanol at 70 °C at 20% w/w solids concentration and (b) the corresponding molecular weight (M_n) and polydispersity (M_w/M_n) *vs.* NMEP conversion determined by DMF GPC against PMMA calibration standards.

^{1}H NMR spectroscopy studies of the seven PNMEP macro-CTAs synthesised for this Chapter indicated 70-90% conversion and, after purification by precipitation, mean DPs ranging between 19 and 89. DMF GPC analysis confirmed the expected linear increase in molecular weight with PNMEP DP (see Figure 2.3b and Table 2.1). The mean DP for each of the seven PNMEP homopolymers was also determined using UV spectroscopy; these data are reasonably consistent with that determined by end-group analysis using ^{1}H NMR spectroscopy. The relationship between GPC molecular weight and the mean DP as determined by UV spectroscopy is shown in Figure 2.4.

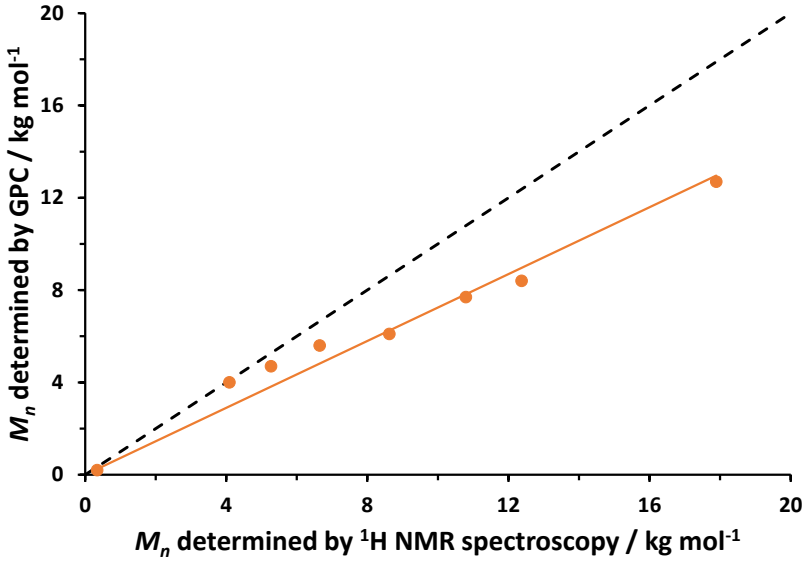

Figure 2.4. Relationship between number-average molecular weight (M_n) as determined by DMF GPC (refractive index detector) and M_n determined by end-group using ^{1}H NMR spectroscopy for a series of seven PNMEP homopolymers prepared by RAFT solution polymerisation of NMEP in ethanol at 70 °C (R^2 = 0.97). Ideal behaviour (*i.e.* no GPC calibration error) is indicated by the dotted line. The solid line is a line of best fit, which indicates that an error of approximately 28% is incurred when using PMMA calibration standards to analyse PNMEP homopolymers when using DMF eluent.

2.3.2 Aqueous solution properties of PNMEP homopolymers

Using PETTC confers a terminal carboxylic acid group on each PNMEP chain (see Scheme 2.1). The pK_a for this end-group was determined for each homopolymer by acid titration of a 20% w/w solution in water at 20 °C (Figure 2.5). The pK_a increased from 5.07 to 5.44 for mean PNMEP DPs of between 19 and 89. There is a possibility that the terminal acid group may be 'buried' inside PNMEP coils (potentially due to complexes formed with the pyrrolidone ring) thereby screening them from deprotonation on the addition of base. It is feasible to assume that this behaviour would have a greater chance of occurring on increasing the DP of the polymer which may account for the unexpected trend that is shown in Figure 2.5.

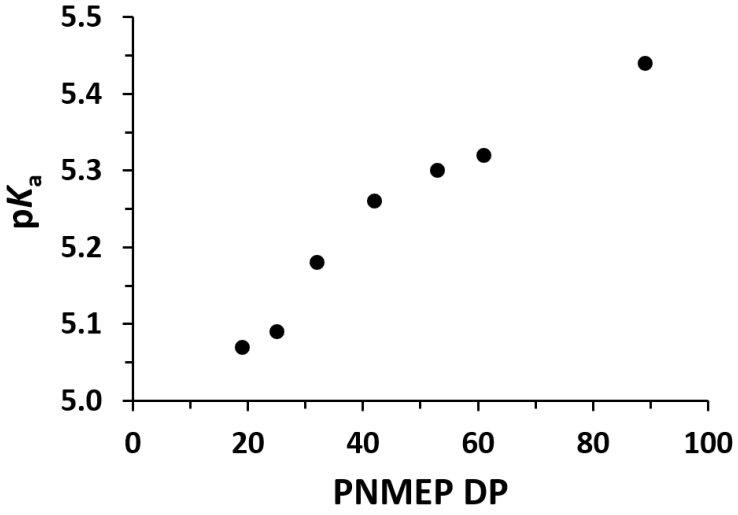

Figure 2.5. Effect of varying the mean DP on the pK_a of the carboxylic acid end-group as determined by acid titration for a series of near-monodisperse $PNMEP_x$ homopolymers prepared by RAFT solution polymerisation of NMEP in ethanol at 70 °C using the PETTC RAFT agent (see Scheme 2.1).

CPs were determined for 1.0% w/w aqueous solutions of a series of seven PNMEP homopolymers at either pH 3 or pH 7 by turbidimetry at an arbitrary fixed wavelength of 600 nm. CPs observed at pH 7 were always significantly higher compared to those determined at pH 3. This thermal transition occurred over a broader temperature range for relatively short PNMEP chains (DP < 50) at pH 7. Moreover, no CP was observed for PNMEP DPs above 50 on heating up to 90 °C at this pH, which corresponds to the upper limit temperature for our instrument set-up. 1.0% w/w aqueous solutions of $PNMEP_x$ were placed in an oil bath and heated up to 100 °C. Each solution remained transparent, indicating that LCST behaviour was eliminated for DPs greater than 50 at a solution pH of 7. At pH 3, a solution of $PNMEP_{53}$ homopolymer exhibited a CP of 64 °C, so ionisation of the terminal carboxylic acid group raises the CP of $PNMEP_{53}$ chains by 26 °C in this particular case (Figure 2.6).

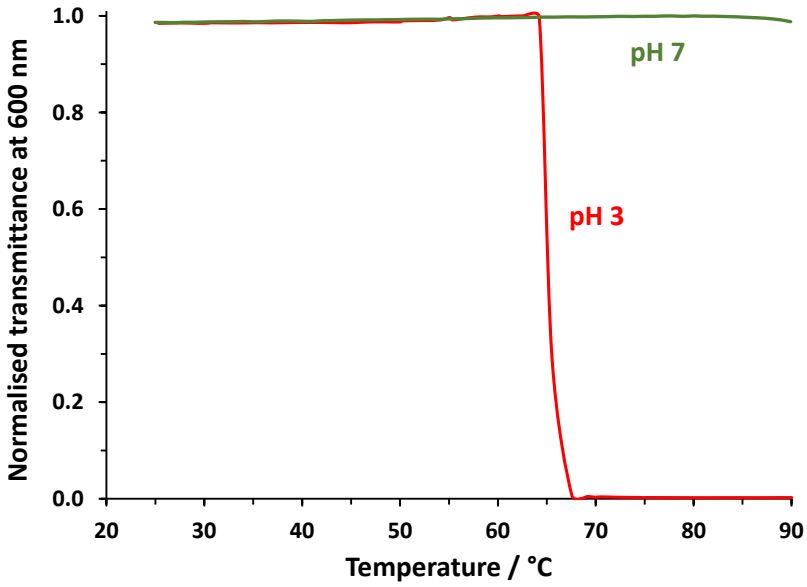

Figure 2.6. Normalised transmittance at 600 nm against temperature for 1.0% w/w aqueous solutions of a $PNMEP_{53}$ homopolymer at either pH 3 or pH 7. A CP of approximately 64 °C was obtained at pH 3 (red curve) but no CP was observed for the same homopolymer at pH 7.

Interestingly, higher CP values were observed for increasing PNMEP DP, contrary to normal behaviour.[16,25,26] However, Miasnikova *et al.* observed a similar trend when examining end-group effects on the LCST behaviour of methoxy-capped poly(diethylene glycol acrylate) (PDEGA) homopolymers.[46] More specifically, a series of PDEGA homopolymers were synthesised using a bistrithiocarbonate RAFT agent that conferred tert-butyl benzoate groups on both chain-ends. These hydrophobic *tert*-butyl groups were selectively removed in a post-polymerisation step to generate hydrophilic benzoic acid end-groups. Higher CPs were observed with increasing DP for both the precursor and the benzoic acid-terminated PDEGA homopolymers.[46] Thus, for the *tert*-butyl-terminated homopolymers, the CPs increased monotonically from 9.0 °C (DP = 28) to 41.2 °C (DP = 513), while the corresponding CPs for the benzoic acid-terminated PDEGA homopolymers ranged from 16.8 °C to 42.0 °C. Furthermore, Miasnikova *et al.* observed an *increase* in CP when using a more hydrophilic end-group for PDEGA homopolymers of the same DP.[46] This effect is analogous to that obtained when adjusting the solution pH for an aqueous solution of a given PNMEP homopolymer from pH 3 to 7 (see Figure 2.7a). Miasnikova *et al.* tentatively suggested that their unexpected observations might be due to conformational effects of the hydrophobic acrylic backbone.[46] In the context of the present study, it is perhaps worth emphasising that the same remarkable phenomenon is observed for a water-soluble *methacrylic* polymer, which has significantly lower chain mobility (the glass transition temperature of PNMEP is above ambient

temperature). However, it is noteworthy that normal LCST behaviour (*i.e.* a systematic *reduction* in CP with increasing DP) was observed by Cunningham and co-workers for a series of PNMEP hompolymers prepared using a non-ionic dithiobenzoate RAFT agent, which suggests that end-groups play an important role in determining CP.[16]

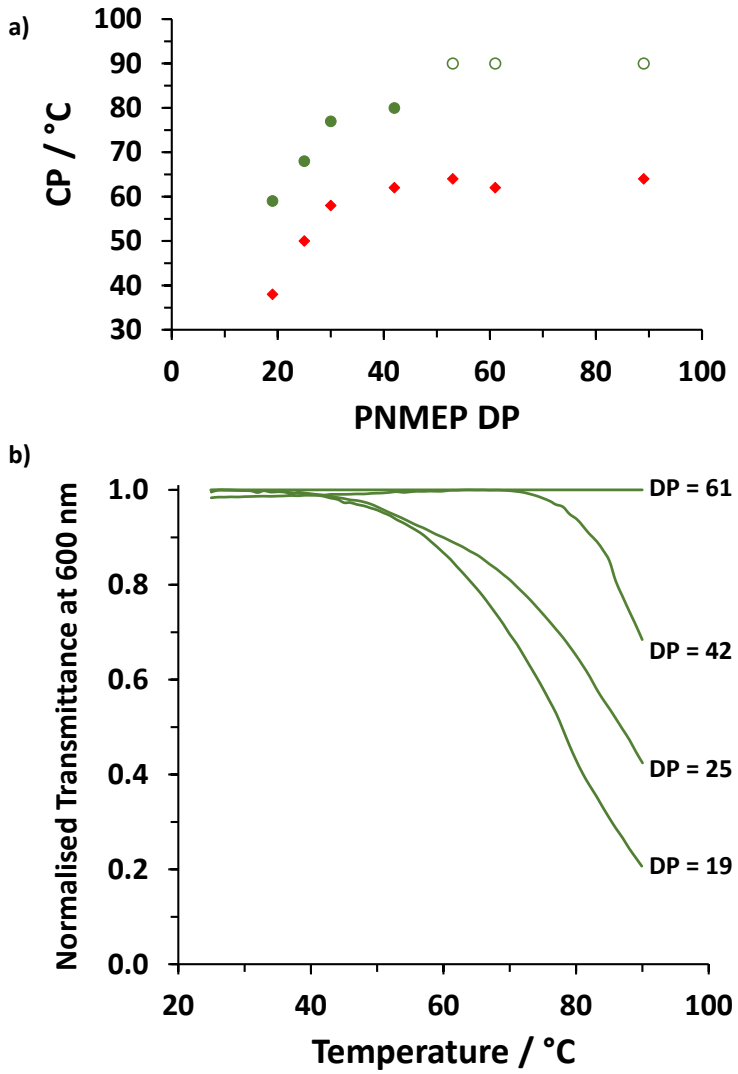

Figure 2.7. (a) Relationship between CP (°C) determined for 1.0% w/w aqueous solution and PNMEP homopolymer DP at pH 3 (◆) and pH 7 (●). The (○) symbol indicates that no CP was observed using turbidimetry on heating up to 90 °C (which corresponds to the upper limit temperature for the instrument set-up). (b) Normalised transmittance at 600 nm for a series of seven PNMEP homopolymers with mean DPs of 19 to 89 at pH 7.

At pH 7, thermal transitions were relatively broad for shorter PNMEPs (DP < 32), whereas homopolymers with higher DPs exhibited relatively sharp CP values. Similar effects were also observed by Miasnikova *et al.,*[46] who suggested that dispersity effects (expected to be stronger

for lower molecular weights) might lead to broader transitions for lower DPs. Alternatively, the sharper transitions observed for higher DPs might be the result of cooperative collapse.[46] As discussed above, lower molecular weight polymers are usually more sensitive to end-group effects. Given that the RAFT agent used to prepare these PNMEP homopolymers contains a hydrophobic aromatic ring, this could lead to lower CP values in this case. Relatively sharp thermal transitions were observed at pH 3 (Figure 2.6) while broader less well-defined transitions were only observed at pH 7 (Figure 2.7b).

When determining CP values, non-zero final transmittances were observed for all $PNMEP_x$ homopolymers at pH 7 (see Figure 2.7b). Thus, the data obtained at pH 7 are best regarded as estimates. In contrast, these 1.0% w/w aqueous solutions became completely opaque (zero transmittance) above their CP for turbidity studies conducted at pH 3. It is clear from these turbidimetry studies that ionisation of the terminal carboxylic acid group raises the CP of PNMEP homopolymers. In principle, this significant increase in hydrophilic character should enable RAFT aqueous dispersion (or emulsion) polymerisation syntheses to be conducted, provided that the polymerisation temperature remains well below the CP of the stabiliser block.

Table 2.1. Summary of molecular weight and CP data for a series of PNMEP homopolymers prepared by RAFT ethanolic solution polymerisation as determined by DMF GPC and turbidimetry, respectively. The pK_a of each homopolymer was determined by acid titration and is an average of three measurements.

Reaction time / min	Target DP	PNMEP DP[a]	Theoretical DP	Conversion[b] / %	M_n[c] / g mol^{-1}	M_w/M_n[c]	CP / °C		pK_a
							pH 3	pH 7	
100	22	19	17	77	3 300	1.13	38	59	5.07
210	30	25	22	73	4 200	1.14	50	68	5.09
200	40	32	9	72	5 500	1.15	61	81	5.18
210	50	42	37	74	6 400	1.15	62	80	5.26
210	70	53	48	69	8 200	1.19	64	>90	5.30
195	60	61	54	90	9 200	1.20	62	>90	5.32
240	100	89	81	81	12 600	1.21	64	>90	5.44

[a]Determined by end-group analysis using ^{1}H NMR spectroscopy. [b]Determined by ^{1}H NMR analysis in d_4-methanol. [c]Determined by DMF GPC (relative to PMMA calibration standards).

2.3.3 Synthesis of $PNMEP_{42}$-$PHPMA_x$ diblock copolymer nanoparticles *via* RAFT aqueous dispersion polymerisation of HPMA

A $PNMEP_{42}$ homopolymer was prepared by RAFT solution polymerisation of NMEP in ethanol using PETTC at 70 °C prior to purification by precipitation into excess diethyl ether. ^{1}H NMR analysis indicated 74% NMEP conversion and a mean DP of 42 after purification (based on end-group analysis of the aromatic groups). DMF GPC analysis indicated an M_n of 6 100 g mol^{-1} and an M_w/M_n of 1.22, which suggests good RAFT control. This water-soluble precursor was subsequently chain-extended at pH 7 *via* RAFT aqueous dispersion polymerisation of HPMA at 44 °C targeting a copolymer concentration of 20% w/w, see Scheme 2.2. A series of $PNMEP_{42}$-$PHPMA_x$ diblock copolymer nanoparticles were prepared by varying the target DP of PHPMA from 150 to 400.

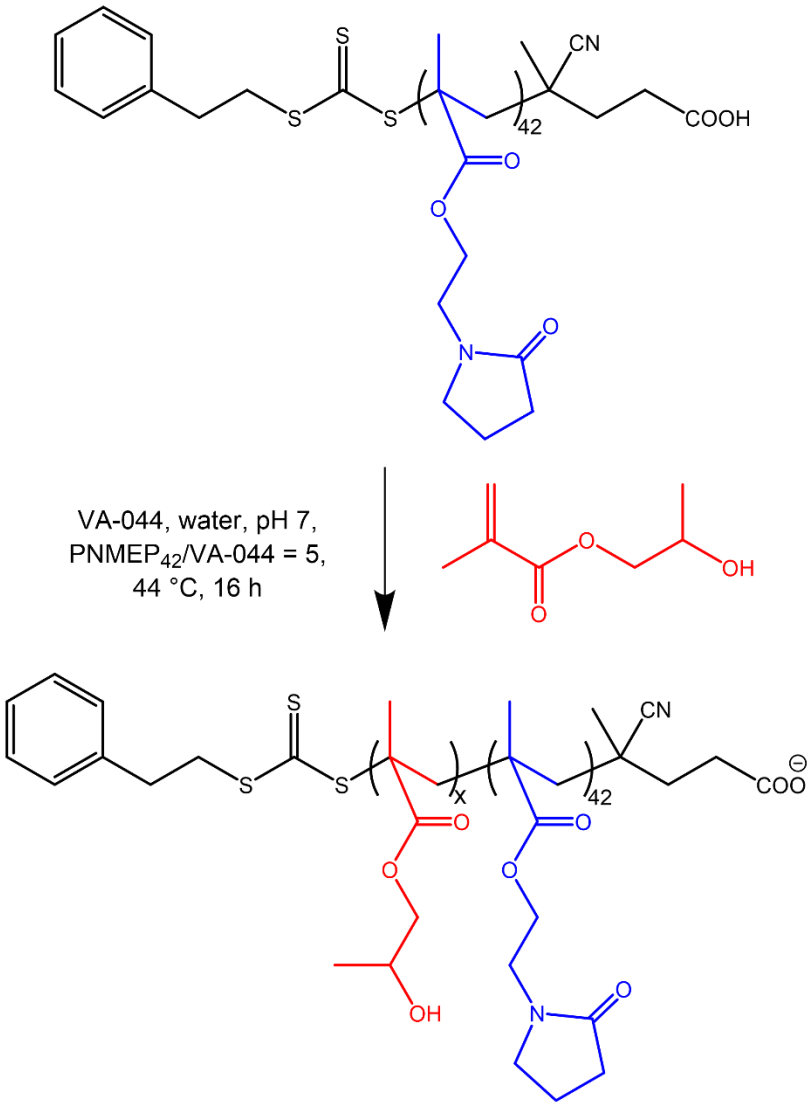

Scheme 2.2. Synthesis of $PNMEP_{42}$-$PHPMA_x$ diblock copolymer nanoparticles at pH 7 by RAFT aqueous dispersion polymerisation of HPMA at 44 °C.

It is well-known that RAFT polymerisation becomes problematic above pH 7 because this leads to loss of RAFT end-groups *via* hydrolysis.[47,48] Thus, in each case the reaction solution was adjusted to pH 7.0 ± 0.1 before the HPMA polymerisation was allowed to proceed overnight. More than 99% conversion was achieved for all syntheses as judged by ^{1}H NMR spectroscopy (see Figure 2.8).

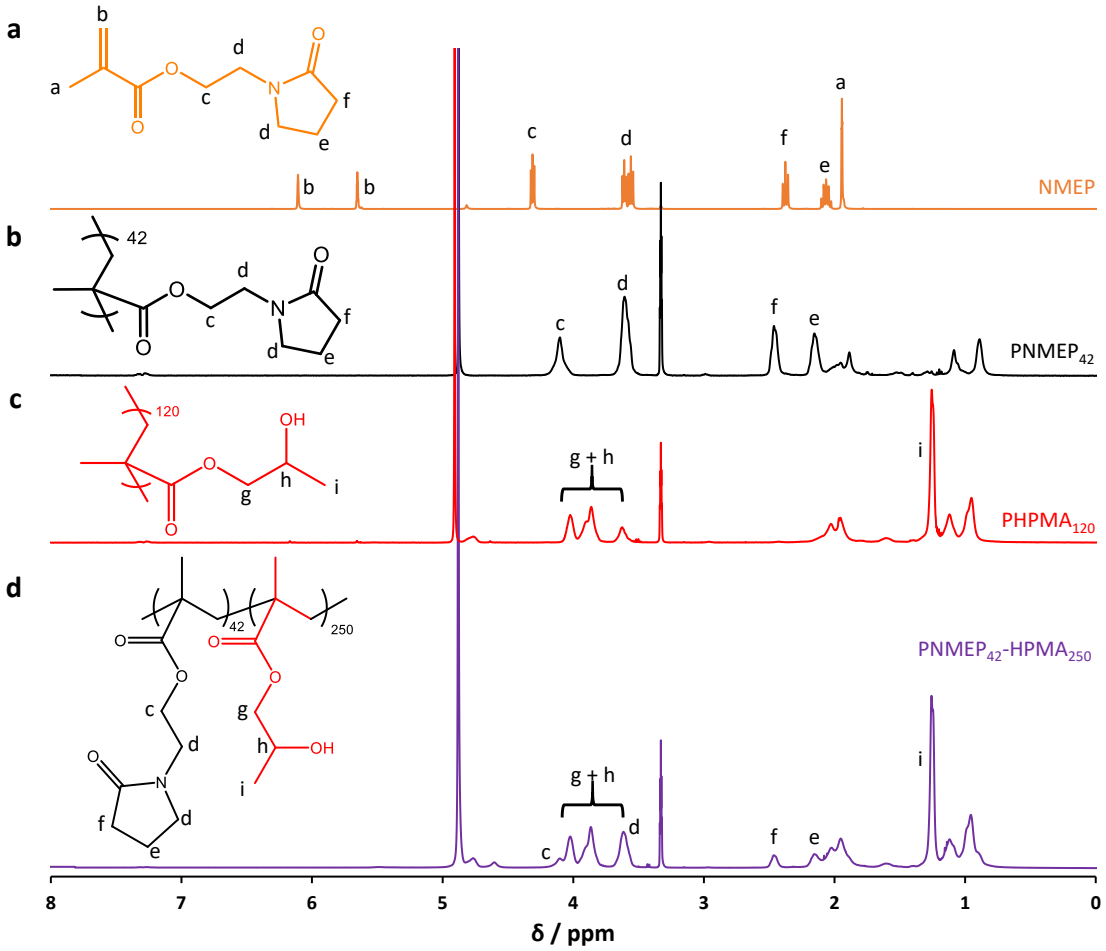

Figure 2.8. ^{1}H NMR spectra recorded in d_4-methanol for (a) NMEP monomer, (b) $PNMEP_{42}$ macro-CTA, (c) $PHPMA_{120}$ homopolymer and (d) $PNMEP_{42}$-$PHPMA_{250}$ diblock copolymer. Comparison of the integrated PNMEP signals at 2.5 ppm with those assigned to the PHPMA at 1.3 ppm enables a diblock copolymer composition of $PNMEP_{42}$-$PHPMA_{245}$ to be calculated, which is in good agreement with that expected based on the target composition (see spectrum d).

DMF GPC was used to analyse this series of diblock copolymers (see Figure 2.9). Increasing the target DP of the PHPMA core-forming block led to progressively broader MWDs (higher M_w/M_n values) as RAFT control was gradually lost although the GPC traces remained unimodal. Relatively high blocking efficiencies were achieved but a minor fraction of the $PNMEP_{42}$ precursor chains could not be chain-extended. Nevertheless, the M_n increased linearly with the mean PHPMA DPs determined from ^{1}H NMR analysis.

Table 2.2. Summary of target diblock copolymer compositions, HPMA conversions determined by ^{1}H NMR spectroscopy, number-average molecular weights (M_n) and dispersities (M_w/M_n) determined by DMF GPC analysis, and z-average particle diameter and polydispersities (PDI) determined by DLS analysis of dilute aqueous dispersions at pH 7.

Target copolymer composition	Conversion[a] / %	GPC[b]		DLS[c]	
		M_n / g mol^{-1}	M_w/M_n	Z-average diameter / nm	PDI
$PNMEP_{42}$ precursor	74	6 100	1.22	/	/
$PNMEP_{42}$-$PHPMA_{150}$	>99	26 600	1.30	25	0.32
$PNMEP_{42}$-$PHPMA_{200}$	>99	33 300	1.32	35	0.15
$PNMEP_{42}$-$PHPMA_{250}$	>99	39 300	1.43	53	0.07
$PNMEP_{42}$-$PHPMA_{300}$	>99	46 300	1.44	59	0.06
$PNMEP_{42}$-$PHPMA_{350}$	>99	53 100	1.44	64	0.08
$PNMEP_{42}$-$PHPMA_{400}$	>99	56 600	1.59	81	0.23

[a]Determined by ^{1}H NMR spectroscopy in d_4-methanol. [b]DMF eluent, refractive index detector (relative to PMMA calibration standards. [c]Nanoparticle dispersions were diluted to 0.1% w/w using deionised water.

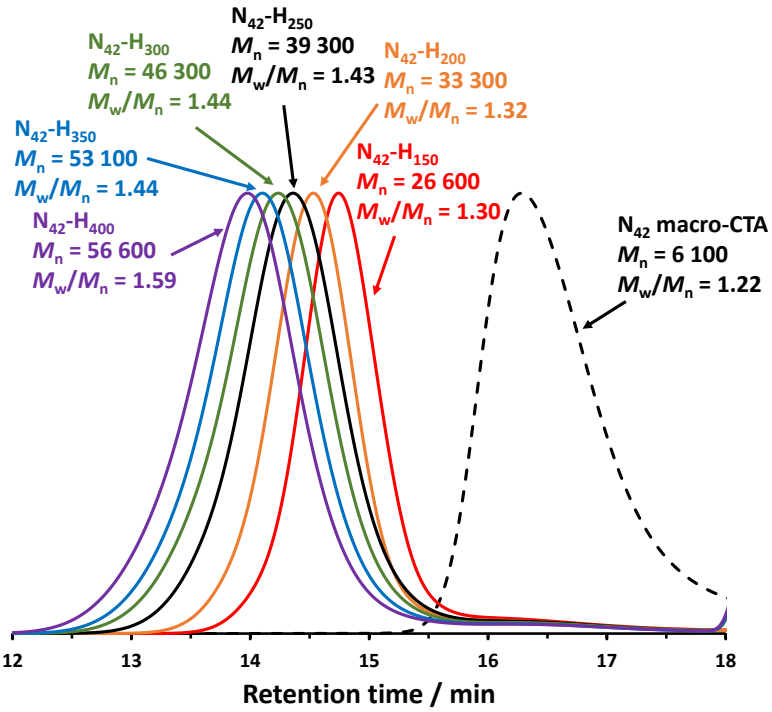

Figure 2.9. DMF GPC curves recorded for a series of $PNMEP_{42}$-$PHPMA_x$ diblock copolymers and the corresponding $PNMEP_{42}$ precursor (refractive index detector; calibration using a series of near-monodisperse PMMA standards). (For brevity, 'N' denotes PNMEP and 'H' denotes PHPMA).

TEM was used in conjunction with DLS to analyse the $PNMEP_{42}$–$PHPMA_x$ diblock copolymer nanoparticles. DLS indicated the formation of relatively small nanoparticles, with narrow, monomodal size distributions being obtained in some cases, see Table 2.2. TEM studies of the dried nanoparticles confirmed that for $PNMEP_{42}$–$PHPMA_{150}$ and $PNMEP_{42}$–$PHPMA_{200}$ exhibit ill-defined morphologies, while spherical morphologies are obtained when targeting higher DPs, see Figure 2.10. Presumably, the anionic surface charge prevents the formation of so-called higher order morphologies such as worms or vesicles. Davis *et al.* reported a similar finding when investigating the effect of the RAFT end-groups hydrophobicity on the final diblock copolymer morphology.[49]

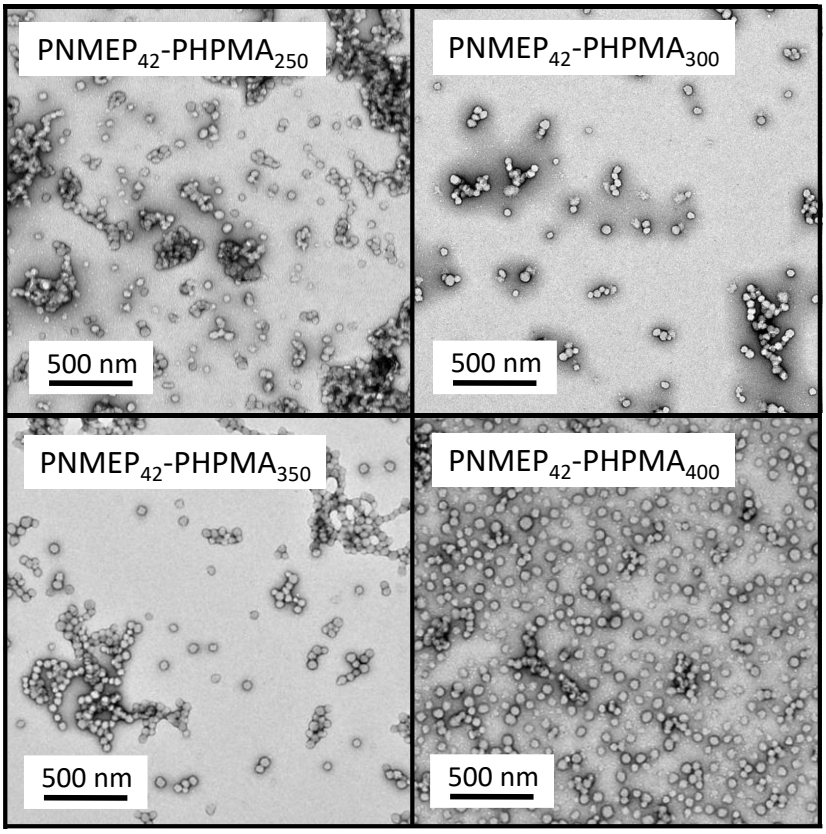

Figure 2.10. Representative TEM images recorded for dried dilute aqueous dispersions of $PNMEP_{42}$-$PHPMA_x$ diblock copolymer nanoparticles prepared at pH 7 showing spherical nanoparticles regardless of the DP of the PHPMA core-forming block.

As a control experiment, the synthesis of $PNMEP_{42}$-$PHPMA_{200}$ diblock copolymers *via* RAFT aqueous dispersion polymerisation was attempted using the conditions stated above but at a solution pH of 3. The pK_a of $PNMEP_{42}$ is 5.26, hence the degree of ionisation of the carboxylic acid end-group was relatively low. Macroscopic phase separation was observed with a white upper layer of PHPMA homopolymer and a yellow layer of $PNMEP_{42}$-$PHPMA_x$ (see Figure 2.11a). Another

control experiment was also undertaken using a $PNMEP_{40}$ macro-CTA prepared with the non-ionic RAFT agent, CPDB. As expected, macroscopic precipitation was observed (Figure 2.11b).

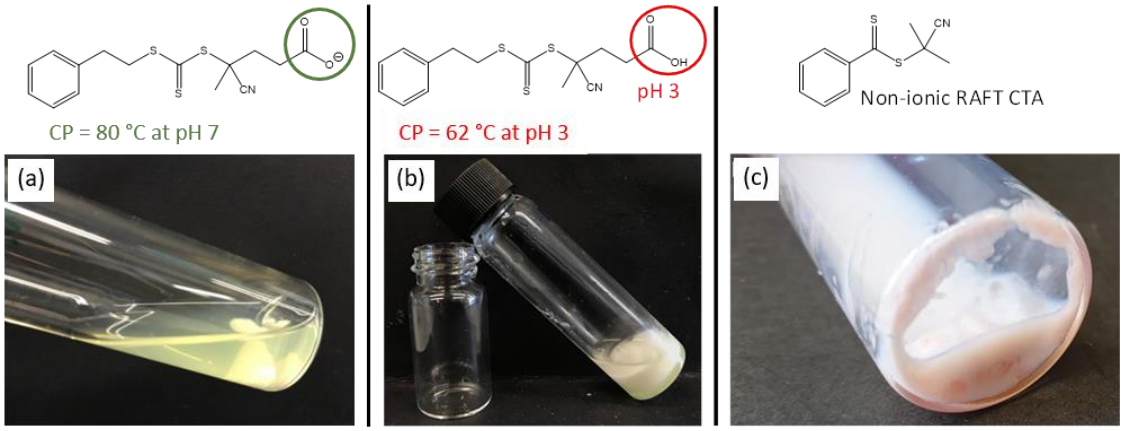

Figure 2.11. (a) Digital image of successful PISA synthesis of $PNMEP_{42}$-$PHPMA_{200}$ conducted at pH 7. (b) Digital image of an unsuccessful PISA synthesis conducted at pH 3. The target diblock copolymer composition was $PNMEP_{42}$-$PHPMA_{200}$. Macroscopic precipitation is evident for this PISA formulation. (c) Digital image of the unsuccessful PISA synthesis of $PNMEP_{40}$-$PHPMA_{200}$ nanoparticles prepared in water with a non-ionic RAFT agent, CPDB.

In view of these unsuccessful PISA syntheses conducted at pH 3 or with a non-ionic RAFT agent, the anionic carboxylate end-groups on the PNMEP stabiliser chains were considered likely to play an important role in conferring colloidal stability at pH 7. This hypothesis was examined by systematically lowering the pH of a 0.1% w/w aqueous dispersion of $PNMEP_{42}$-$PHPMA_{300}$ nanoparticles while conducting DLS and electrophoresis studies at 20 °C to examine the extent of nanoparticle aggregation, see Figure 2.12a. The z-average particle diameter remained constant at approximately 58 nm from pH 8 to pH 5, with corresponding zeta potentials of -30 to -20 mV over this range. However, the apparent particle diameter increased significantly to 260 nm at pH 4.5, which is below the pK_a of the $PNMEP_{42}$ macro-CTA (pK_a = 5.26). This indicates that incipient flocculation of these nanoparticles occurs as the degree of ionisation of their end-groups falls below 50%. Zeta potentials became progressively less negative at lower pH, stabilising at approximately -3.0 mV below pH 4. Moreover, the flocculated nanoparticles could not be redispersed on adjusting the solution pH back to pH 7. This is in contrast to the reversible aggregation-redispersion behaviour reported by Lovett and co-workers[42,43] and Penfold *et al.*[44,45] for closely related nanoparticles. Clearly, anionic surface charge makes an important contribution to the colloidal stability of these $PNMEP_{42}$-$PHPMA_{300}$ nanoparticles. Similar observations have been recently reported by Biais and co-workers for the synthesis of 'loop-stabilised' BAB triblock

copolymer nanoparticles prepared *via* RAFT aqueous dispersion polymerisation of diacetone acrylamide using a bifunctional benzoic acid-functionalised RAFT agent.[50]

As further proof that the colloidal stability of these nanoparticles is at least partly governed by their anionic end-groups, the effect of addition of an electrolyte was explored. It is well known that charge-stabilised nanoparticles are readily flocculated on addition of salt, whereas sterically-stabilised nanoparticles usually remain colloidally stable under such conditions.[51]

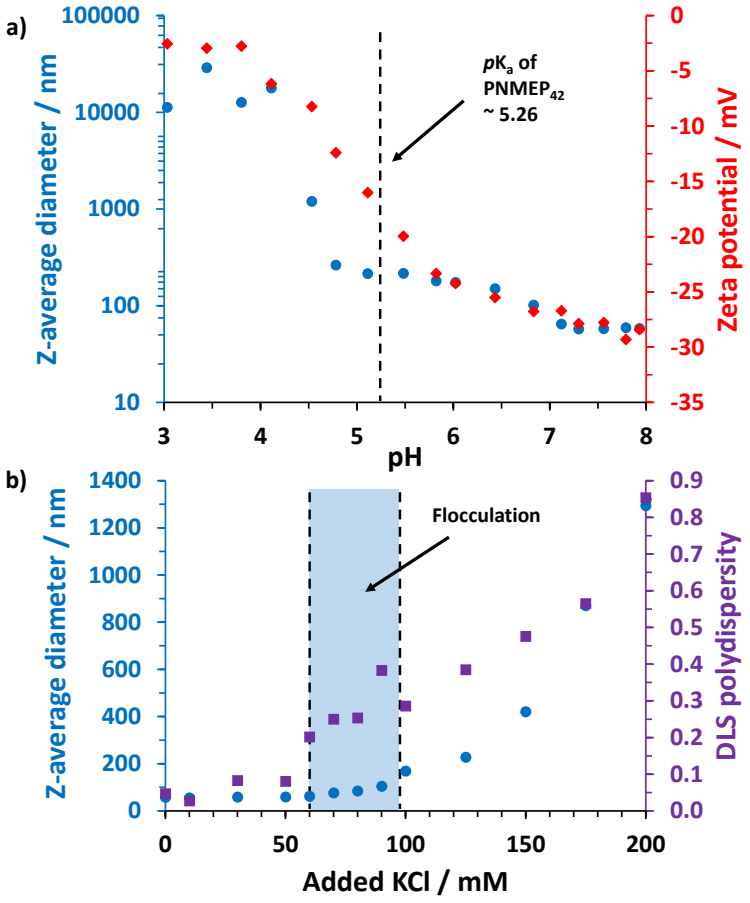

Figure 2.12. (a) Zeta potential (♦) and z-average diameter (●) *vs.* solution pH and (b) z-average diameter and polydispersity (■) *vs.* added KCl at pH 7 recorded for $PNMEP_{42}$-$PHPMA_{300}$ nanoparticles.

Thus, 0.1% w/w aqueous dispersions of $PNMEP_{42}$-$PHPMA_{300}$ nanoparticles were exposed to 10-200 mM KCl at pH 7. The DLS size distribution became significantly broader (*i.e.* higher polydispersities, *PDI*) above 60 mM KCl, indicating incipient flocculation. However, the z-average particle diameter did not increase significantly until the KCl concentration exceeded 100 mM (see Figure 2.12b). Nevertheless, it is clear that the colloidal stability of such dispersions is compromised in the presence of sufficient added salt. In order to confirm that PNMEP also

contributes to steric stabilisation, $PNMEP_{42}$-$PHPMA_{250}$ diblock copolymer nanoparticles were synthesised at 20% w/w in D_2O at pH 7.

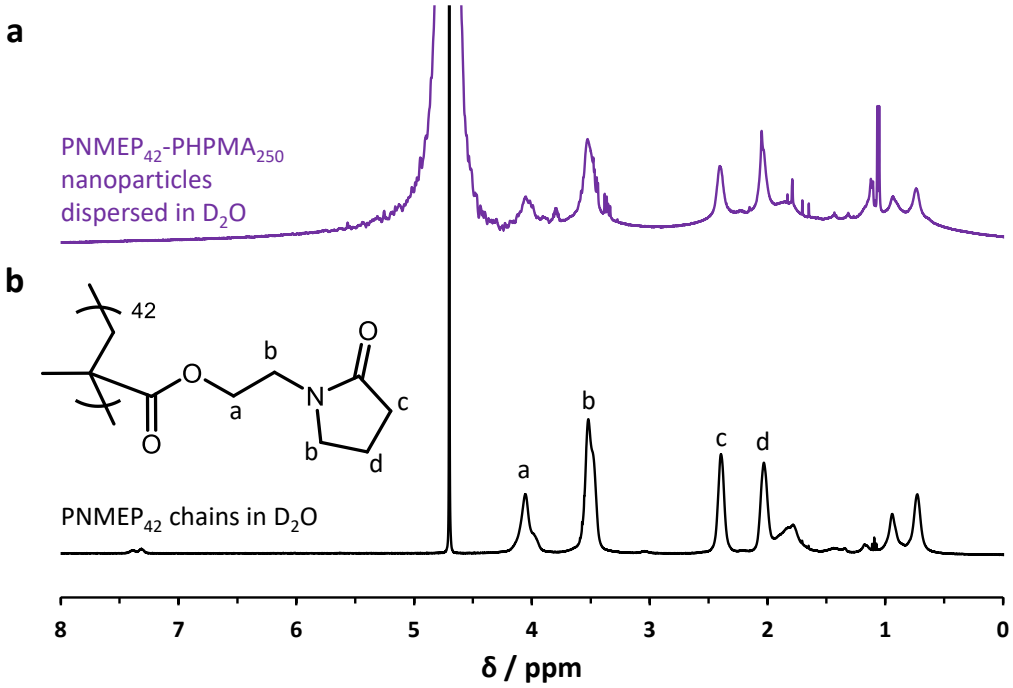

Figure 2.13. ^{1}H NMR spectra recorded in D_2O for (a) a 20% w/w dispersion of $PNMEP_{42}$-$PHPMA_{250}$ diblock copolymer nanoparticles in D_2O at pH 7 and (b) a $PNMEP_{42}$ macro-CTA dissolved in the same solvent. PNMEP signals are clearly visible at 4.1, 3.5 and 2.4 ppm, indicating that this hydrophilic block confers some degree of steric stabilisation, in addition to the charge stabilisation behaviour indicated in Figure 2.12. Thus, such nanoparticles are best described as electrosterically-stabilised.

^{1}H NMR spectroscopy studies of this dispersion confirmed the presence of the expected PNMEP signals at 4.1, 3.5 and 2.4 ppm (see Figure 2.13). This provides strong evidence that this hydrophilic block also acts as a steric stabiliser for these nanoparticles. Given the salt- and pH-sensitive colloidal stability behaviour discussed above, this suggests that these nanoparticles are best described as electrosterically-stabilised, rather than either charge-stabilised or sterically-stabilised.[52,53]

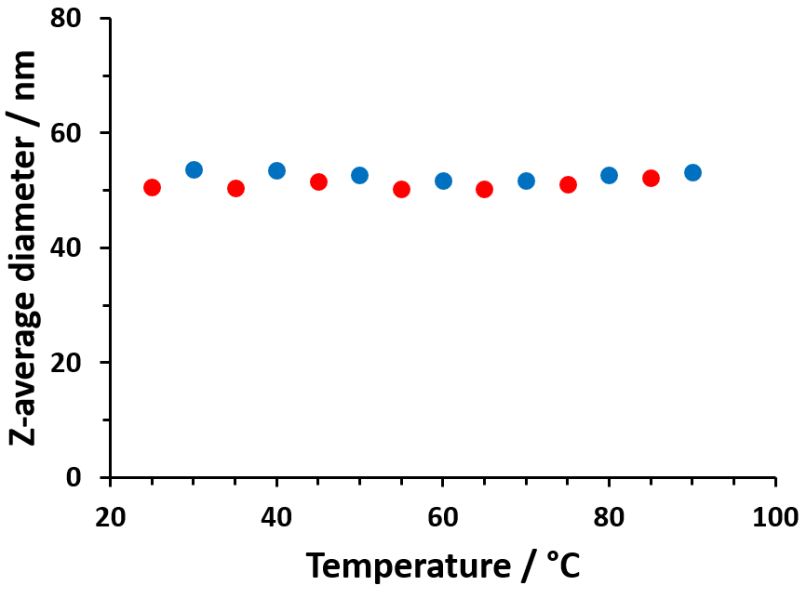

Figure 2.14. Variation in z-average diameter for a 0.1% w/w dispersion of $PNMEP_{42}$-$PHPMA_{250}$ diblock copolymer nanoparticles at pH 7 when heated from 25 to 90 °C (also the corresponding size data on cooling from 90 to 25 °C).

Finally, the thermoresponsive behaviour was briefly examined by variable temperature DLS of a 0.1% w/w dispersion of $PNMEP_{42}$-$PHPMA_{250}$ diblock copolymer nanoparticles at pH 7. The z-average diameter remained essentially constant over the entire temperature range, indicating that the particles are not thermoresponsive (Figure 2.14).

2.3.4 Synthesis of $PNMEP_{53}$-$PEEMA_x$ diblock copolymer nanoparticles *via* RAFT aqueous emulsion polymerisation of EEMA

A $PNMEP_{53}$ macro-CTA was prepared by RAFT ethanolic solution polymerisation of NMEP. ^{1}H NMR spectroscopy indicated a mean DP of 53 *via* end-group analysis after purification. Chloroform GPC analysis indicated an M_n of 6 100 g mol^{-1} and an M_w/M_n of 1.24.

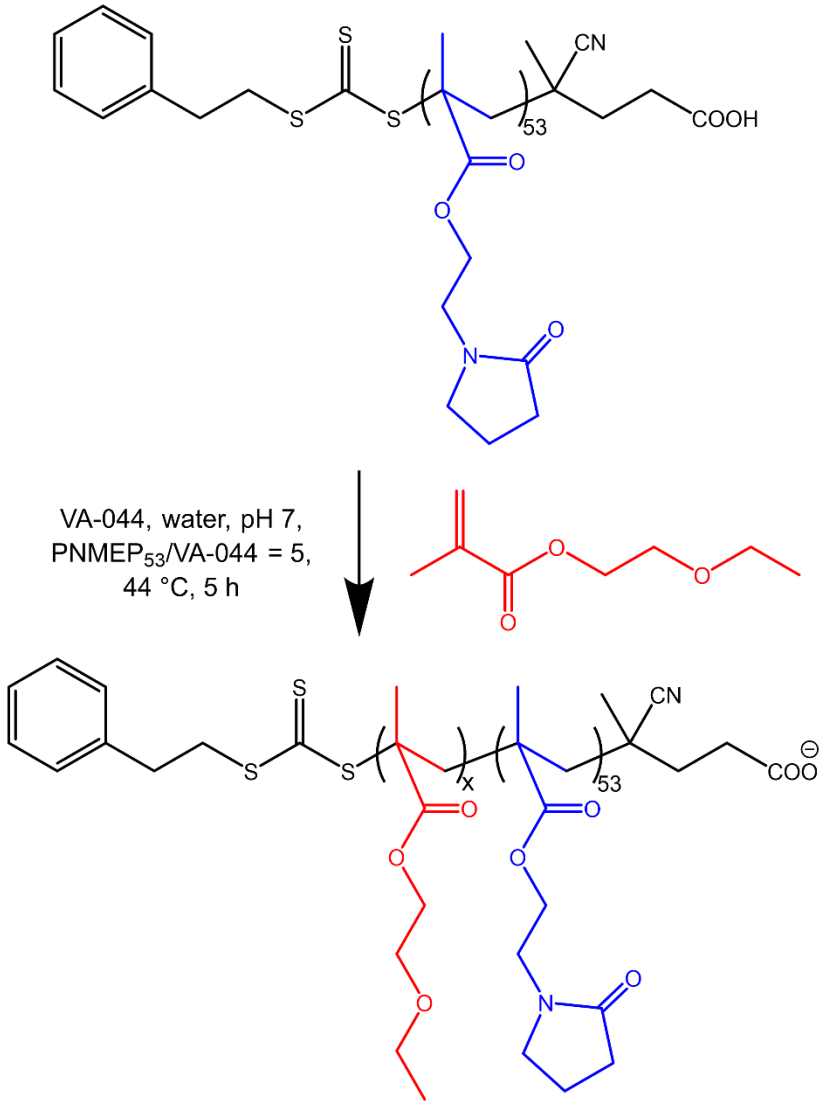

Scheme 2.3. Synthesis of $PNMEP_{53}$-$PEEMA_x$ diblock copolymers by RAFT aqueous emulsion polymerisation of EEMA at 44 °C at pH 7.

The $PNMEP_{53}$ precursor was subsequently chain-extended *via* RAFT aqueous emulsion polymerisation of EEMA (water solubility = 6.3 g dm^{-3}) at 20% w/w solids while varying the target PEEMA DP from 100 to 600 (Scheme 2.3 and Table 2.3). All reaction solutions were adjusted to pH 7.0 ± 0.1 using NaOH before the EEMA polymerisation was allowed to proceed for 5 h at 44 °C. More than 99% conversion was achieved in all cases as judged by ^{1}H NMR spectroscopy.

Chloroform GPC analyses indicated that the molecular weight increased linearly with DP (Figure 2.15a) and MWDs became significantly broader on increasing the target DP of the PEEMA core-forming block (Figure 2.15b).

Table 2.3. Summary of target $PNMEP_{53}$-$PEEMA_x$ diblock copolymer compositions, monomer conversions by ^1H NMR analysis, molecular weights (M_n) and dispersities (M_w/M_n) determined by chloroform GPC, and z-average particle diameter and dispersities (PDI) determined by DLS analysis of dilute aqueous dispersions at pH 7.

Target copolymer composition	Conversion[a] / %	GPC[b]		DLS[c]	
		M_n / g mol^{-1}	M_w/M_n	Z-average diameter / nm	PDI
$PNMEP_{53}$ precursor	69	6 100	1.24	n.d.	n.d.
$PNMEP_{53}$-$PEEMA_{100}$	>99	13 800	1.31	35	0.14
$PNMEP_{53}$-$PEEMA_{200}$	>99	20 700	1.49	42	0.09
$PNMEP_{53}$-$PEEMA_{300}$	>99	27 800	1.63	49	0.10
$PNMEP_{53}$-$PEEMA_{400}$	>99	31 500	1.72	55	0.09
$PNMEP_{53}$-$PEEMA_{500}$	>99	34 100	1.73	53	0.10
$PNMEP_{53}$-$PEEMA_{600}$	>99	37 400	1.96	66	0.08

[a]Determined by end-group analysis by ^1H NMR spectroscopy in d-chloroform [b]Determined by chloroform GPC analysis (relative to PMMA calibration standards). [c]Nanoparticle dispersions were diluted to 0.1% w/w using water (pH 7).

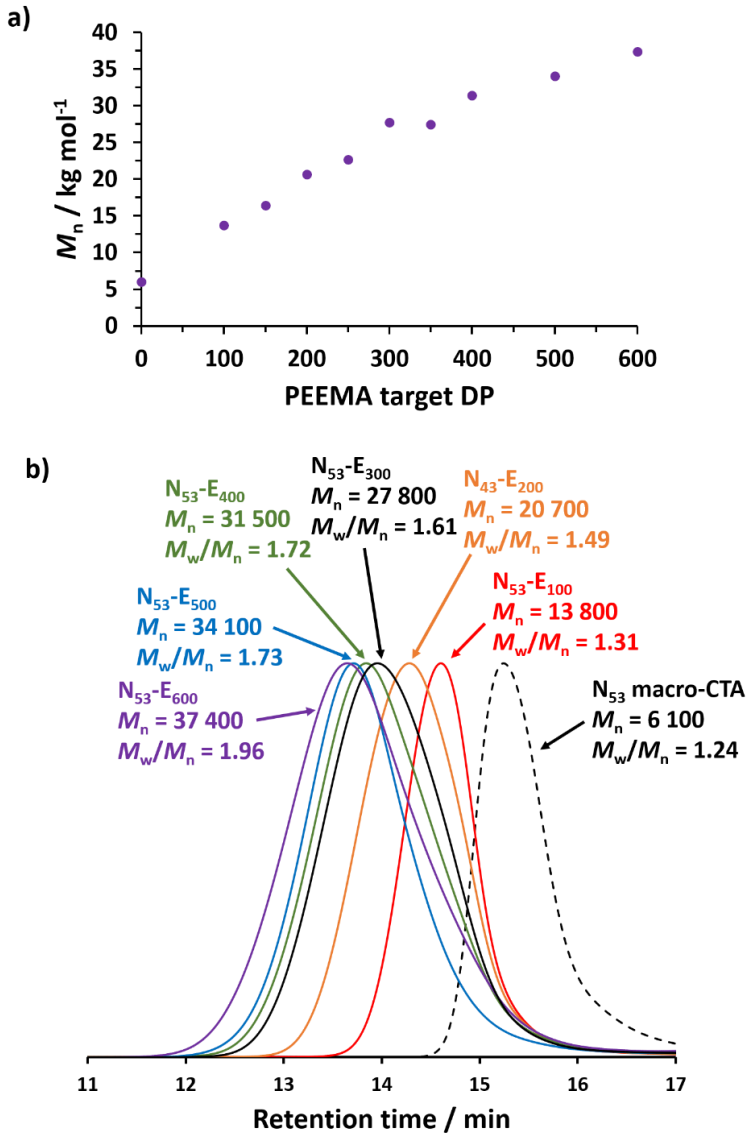

Figure 2.15. (a) Linear increase in molecular weight (M_n) with increasing PEEMA target DP as determined by chloroform GPC (R^2 = 0.96). (b) Overlaid GPC curves obtained for a series of $PNMEP_{53}$-$PEEMA_x$ diblock copolymers prepared by RAFT aqueous emulsion polymerisation of EEMA at 44 °C, and the corresponding $PNMEP_{53}$ precursor (refractive index detector; calibration using a series of near-monodisperse PMMA calibration standards). (For brevity, 'N' denoted PNMEP and 'E' denotes PEEMA).

All nanoparticles exhibited an exclusively spherical morphology as judged by TEM analysis, with some evidence for a minor population of relatively small particles (Figure 2.16). DLS studies indicated that the z-average particle diameter increased with target PEEMA DP and particle size distributions were reasonably uniform, with DLS polydispersity values below 0.10 in most cases.

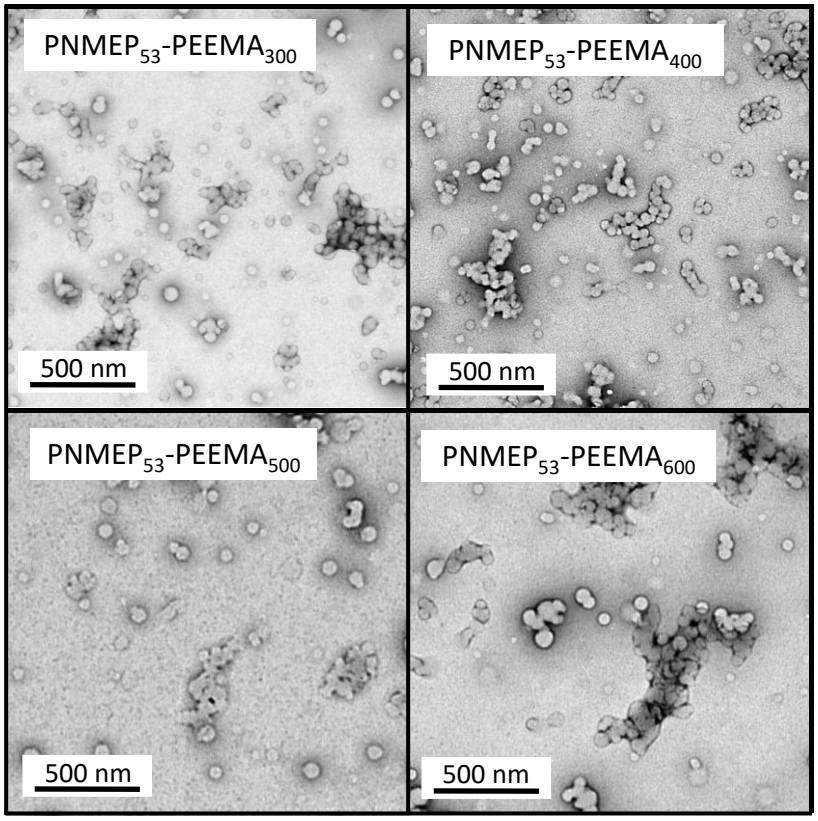

Figure 2.16. Representative TEM images showing spherical morphologies for $PNMEP_{53}$-$PEEMA_x$ diblock copolymer nanoparticles prepared at pH 7.

As discussed above, ionisation of the majority of the carboxylic acid end-groups is essential if the PNMEP precursor is to be used as a stabiliser block for aqueous PISA syntheses. The anionic surface charge leads to colloidally stable $PNMEP_{53}$-$PEEMA_{500}$ diblock copolymer nanoparticles at pH 7, which can be destabilised by lowering the aqueous dispersion pH. This leads to flocculation at 20 °C, as judged by DLS and aqueous electrophoresis studies, see Figure 2.17a. A monotonic reduction in zeta potential from approximately –36 mV at pH 8.0 to –13 mV at pH 4.6 was observed. Incipient flocculation occurred at the latter pH, which corresponds to protonation of most of the anionic carboxylate groups (as the pK_a of the $PNMEP_{53}$ homopolymer is 5.30). The nanoparticle zeta potential became progressively less negative on further lowering the dispersion pH, reaching a constant value of approximately –3 mV below pH 3.

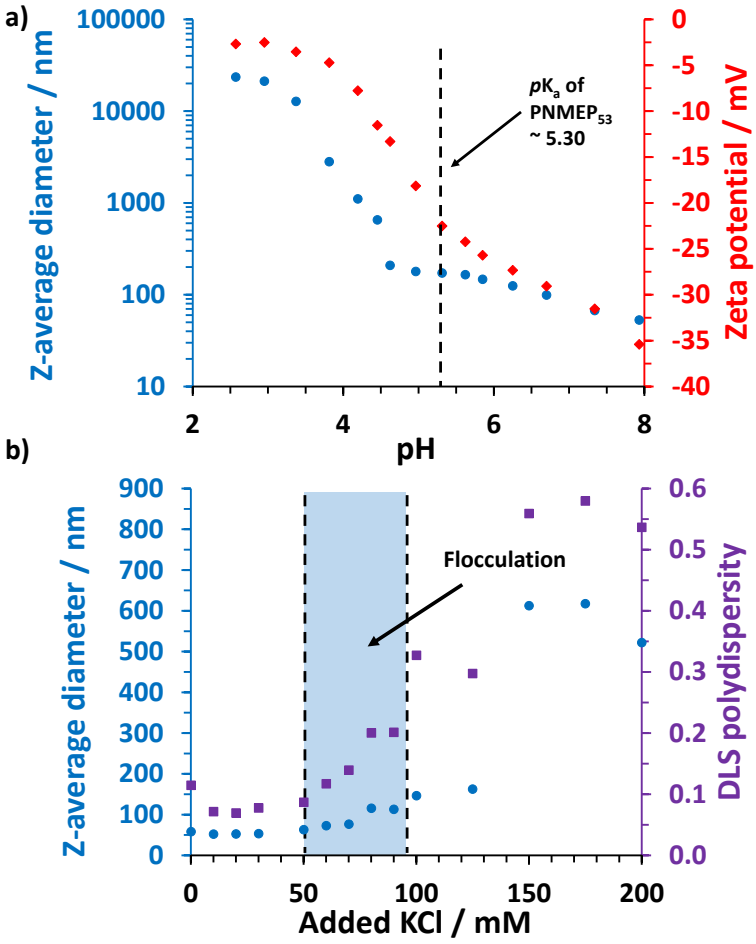

Figure 2.17. (a) Zeta potential (♦) and z-average diameter (●) *vs.* pH and b) z-average diameter and DLS polydispersity (■) *vs.* KCl concentration observed for a 0.1% w/w aqueous dispersion of PNMEP$_{53}$-PEEMA$_{500}$ diblock copolymer nanoparticles in the presence of 1 mM KCl as background electrolyte. The aqueous dispersion pH was adjusted using either 0.05 M or 0.01 M HCl.

To provide further evidence that the colloidal stability of these nanoparticles is indeed critically dependent on their anionic end-groups, their sensitivity to added electrolyte was examined (Figure 2.17b). Thus aqueous dispersions of PNMEP$_{53}$-PEEMA$_{500}$ diblock copolymer nanoparticles were diluted to 0.1% w/w using 10–200 mM KCl at pH 7. Particle size distributions became much broader for KCl concentrations above 60 mM, indicating incipient flocculation. However, the z-average particle diameter only increased substantially above 125 mM KCl. Nevertheless, it is clear that added salt compromises the colloidal stability of such nanoparticles.

2.4 Conclusions

A series of seven near-monodisperse $PNMEP_x$ homopolymers with mean DPs ranging from 19 to 89 were prepared *via* RAFT solution polymerisation of NMEP in ethanol at 70 °C using a carboxylic acid-based RAFT agent. Critical solution temperatures were determined for each $PNMEP_x$ homopolymer at pH 3 (where the carboxylic acid end-groups are present in their neutral form) and at pH 7 (where most of the carboxylic acid end-groups are ionised). End-group ionisation increased the hydrophilic character of each homopolymer significantly: no CP was observed on heating up to 90 °C for DPs greater than 50. The pK_a for each homopolymer was determined *via* acid titration and ranged from 5.07 to 5.44 for all DPs.

A $PNMEP_{42}$ macro-CTA was chain-extended *via* RAFT aqueous dispersion polymerisation of HPMA at 44 °C. A series of $PNMEP_{42}$-$PHPMA_x$ diblock copolymer nanoparticles were prepared at 20% w/w solids with the PHPMA DP systematically varied between 150 and 400. High monomer conversions were achieved in all cases and a linear correlation between GPC M_n and PHPMA DP was observed. TEM studies confirmed that the sole morphology was kinetically-trapped spheres and DLS studies indicated a monotonic increase in the hydrodynamic particle diameter with PHPMA DP. These nanoparticles became flocculated either below pH 4.5 (as a result of protonation of the anionic carboxylate end-groups) or on addition of 60 mM KCl (owing to charge screening).

PNMEP was also used as an electrosteric stabiliser to prepare a series of diblock copolymer nanoparticles at pH 7 *via* RAFT aqueous emulsion polymerisation of EEMA at 44 °C. More specifically, a $PNMEP_{53}$ precursor was chain-extended with the target PEEMA DP being varied between 100 and 600. High EEMA conversions were achieved in all cases and GPC studies confirmed a linear increase in molecular weight with PEEMA DP. A strong correlation between the mean nanoparticle diameter and the PEEMA DP was observed and TEM studies indicated kinetically-trapped spheres as the sole morphology. Like the $PNMEP_{42}$-$PHPMA_{300}$ nanoparticles, these $PNMEP_{53}$-$PEEMA_{500}$ nanoparticles became flocculated either on addition of 60 mM KCl or by adjusting the solution pH to below pH 4.5. Overall, such experiments confirm that the colloidal stability of these electrosterically-stabilised nanoparticles is critically dependent on the anionic charge located at the end of each stabiliser chain.

In summary, despite the inverse temperature solubility behaviour exhibited by PNMEP in aqueous solution, conferring appropriate hydrophilic end-groups enables use of this water-soluble

polymer as an electrosteric stabiliser for the preparation of block copolymer nanoparticles *via* PISA syntheses in aqueous solution at around neutral pH.

2.5 References

(1) Pelton, R. Temperature-Sensitive Aqueous Microgels. *Adv. Colloid Interface Sci.* **2000**, *85*, 1–33.

(2) Ganachaud, F.; Monteiro, M. J.; Gilbert, R. G.; Dourges, M. A.; Thang, S. H.; Rizzardo, E. Molecular Weight Characterization of Poly(N-Isopropylacrylamide) Prepared by Living Free-Radical Polymerization. *Macromolecules* **2000**, *33*, 6738–6745.

(3) Weaver, J. V. M.; Bannister, I.; Robinson, K. L.; Bories-Azeau, X.; Armes, S. P.; Smallridge, M.; McKenna, P. Stimulus-Responsive Water-Soluble Polymers Based on 2-Hydroxyethyl Methacrylate. *Macromolecules* **2004**, *37*, 2395–2403.

(4) Lutz, J. F. Polymerization of Oligo(Ethylene Glycol) (Meth)Acrylates: Toward New Generations of Smart Biocompatible Materials. *J. Polym. Sci. Part A Polym. Chem.* **2008**, *46*, 3459–3470.

(5) Bernaerts, K. V.; Fustin, C.-A.; Bomal-D'Haese, C.; Gohy, J.-F.; Martins, J. C.; Du Prez, F. E. Advanced Polymer Architectures with Stimuli-Responsive Properties Starting from Inimers. *Macromolecules* **2008**, *41*, 2593–2606.

(6) Eggers, S.; Fischer, B.; Abetz, V. Aqueous Solutions of Poly[2-(N-Morpholino)Ethyl Methacrylate]: Learning about Macromolecular Aggregation Processes from a Peculiar Three-Step Thermoresponsive Behavior. *Macromol. Chem. Phys.* **2016**, *217*, 735–747.

(7) Bütün, V.; Billingham, N. C.; Armes, S. P. Unusual Aggregation Behavior of a Novel Tertiary Amine Methacrylate-Based Diblock Copolymer: Formation of Micelles and Reverse Micelles in Aqueous Solution. *J. Am. Chem. Soc.* **1998**, *120*, 11818–11819.

(8) Halperin, A.; Kröger, M.; Winnik, F. M. Poly(*N* -Isopropylacrylamide) Phase Diagrams: Fifty Years of Research. *Angew. Chemie Int. Ed.* **2015**, *54*, 15342–15367.

(9) Gil, E. S.; Hudson, S. M. Stimuli-Reponsive Polymers and Their Bioconjugates. *Prog. Polym. Sci.* **2004**, *29*, 1173–1222.

(10) Yoshida, R.; Sakai, K.; Okano, T.; Sakurai, Y. Modulating the Phase Transition Temperature and Thermosensitivity in N-Isopropylacrylamide Copolymer Gels. *J. Biomater. Sci. Polym. Ed.* **1995**, *6*, 585–598.

(11) Feil, H.; Bae, Y. H.; Feijen, J.; Kim, S. W. Effect of Comonomer Hydrophilicity and Ionization on the Lower Critical Solution Temperature of N-Isopropylacrylamide Copolymers. *Macromolecules* **1993**, *26*, 2496–2500.

(12) Summers, M. J.; Phillips, D. J.; Gibson, M. I. "Isothermal" LCST Transitions Triggered by Bioreduction of Single Polymer End-Groups. *Chem. Commun.* **2013**, *49*, 4223–4225.

(13) Chung, J. E.; Yokoyama, M.; Aoyagi, T.; Sakurai, Y.; Okano, T. Effect of Molecular Architecture of Hydrophobically Modified Poly(N-Isopropylacrylamide) on the Formation of Thermoresponsive Core-Shell Micellar Drug Carriers. *J. Control. Release* **1998**, *53*, 119–130.

(14) Sun, J.; Peng, Y.; Chen, Y.; Liu, Y.; Deng, J.; Lu, L.; Cai, Y. Effect of Molecular Structure on Thermoresponsive Behaviors of Pyrrolidone-Based Water-Soluble Polymers. *Macromolecules* **2010**, *43*, 4041–4049.

(15) Iskander, G. M.; Baker, L. E.; Wiley, D. E.; Davis, T. P. Synthesis and Polymerization of New Pyrrolidone-Containing Methacrylate Monomers. *Polymer* **1998**, *39*, 4165–4169.

(16) Cunningham, V. J.; Derry, M. J.; Fielding, L. A.; Musa, O. M.; Armes, S. P. RAFT Aqueous Dispersion Polymerization of N -(2-(Methacryloyloxy)Ethyl)Pyrrolidone: A Convenient Low Viscosity Route to High Molecular Weight Water-Soluble Copolymers. *Macromolecules* **2016**, *49*, 4520–4533.

(17) Warren, N. J.; Armes, S. P. Polymerization-Induced Self-Assembly of Block Copolymer Nano-Objects via RAFT Aqueous Dispersion Polymerization. *J. Am. Chem. Soc.* **2014**, *136*, 10174–10185.

(18) Charleux, B.; Delaittre, G.; Rieger, J.; D'Agosto, F. Polymerization-Induced Self-Assembly: From Soluble Macromolecules to Block Copolymer Nano-Objects in One Step. *Macromolecules* **2012**, *45*, 6753–6765.

(19) Sun, J.-T.; Hong, C.-Y.; Pan, C.-Y. Formation of the Block Copolymer Aggregates via Polymerization-Induced Self-Assembly and Reorganization. *Soft Matter* **2012**, *8*, 7753.

(20) Canning, S. L.; Smith, G. N.; Armes, S. P. A Critical Appraisal of RAFT-Mediated Polymerization-Induced Self-Assembly. *Macromolecules* **2016**, *49*, 1985–2001.

(21) Cunningham, V. J.; Ning, Y.; Armes, S. P.; Musa, O. M. Poly(N-2-(Methacryloyloxy)Ethyl Pyrrolidone)-Poly(Benzyl Methacrylate) Diblock Copolymer Nano-Objects via RAFT Alcoholic Dispersion Polymerisation in Ethanol. *Polymer* **2016**, *106*, 189–199.

(22) Cunningham, V. J.; Armes, S. P.; Musa, O. M. Synthesis, Characterisation and Pickering Emulsifier Performance of Poly(Stearyl Methacrylate)–Poly(N-2-(Methacryloyloxy)Ethyl Pyrrolidone) Diblock Copolymer Nano-Objects via RAFT Dispersion Polymerisation in n-Dodecane. *Polym. Chem.* **2016**, *7*, 1882–1891.

(23) Hirao, A.; Kato, H.; Yamaguchi, K.; Nakahama, S. Polymerization of Monomers Containing Functional Groups Protected by Trialkylsilyl Groups. 5. Synthesis of Poly(2-Hydroxyethyl Methacrylate) with a Narrow Molecular Weight Distribution by Means of Anionic Living Polymerization. *Macromolecules* **1986**, *19*, 1294–1299.

(24) Han, S.; Hagiwara, M.; Ishizone, T. Synthesis of Thermally Sensitive Water-Soluble Polymethacrylates by Living Anionic Polymerizations of Oligo(Ethylene Glycol) Methyl Ether Methacrylates. *Macromolecules* **2003**, *36*, 8312–8319.

(25) Xia, Y.; Yin, X.; Burke, N. A. D.; Stöver, H. D. H. Thermal Response of Narrow-Disperse Poly(N-Isopropylacrylamide) Prepared by Atom Transfer Radical Polymerization. *Macromolecules* **2005**, *38*, 5937–5943.

(26) Bütün, V.; Armes, S. P.; Billingham, N. C. Synthesis and Aqueous Solution Properties of Near-Monodisperse Tertiary Amine Methacrylate Homopolymers and Diblock Copolymers. *Polymer* **2001**, *42*, 5993–6008.

(27) Ieong, N. S.; Hasan, M.; Phillips, D. J.; Saaka, Y.; O'Reilly, R. K.; Gibson, M. I. Polymers with Molecular Weight Dependent LCSTs Are Essential for Cooperative Behaviour. *Polym. Chem.* **2012**, *3*, 794–799.

(28) Xia, Y.; Burke, N. A. D.; And Stöver, H. D. H. End Group Effect on the Thermal Response of Narrow-Disperse Poly(N-Isopropylacrylamide) Prepared by Atom Transfer Radical Polymerization. *Macromolecules* **2006**, *39*, 2275–2283.

(29) Kujawa, P.; Segui, F.; Shaban, S.; Diab, C.; Okada, Y.; Tanaka, F.; Winnik, F. M. Impact of End-Group Association and Main-Chain Hydration on the Thermosensitive Properties of Hydrophobically Modified Telechelic Poly(N-Isopropylacrylamides) in Water. *Macromolecules* **2006**, *39*, 341–348.

(30) Luan, B.; Muir, B. W.; Zhu, J.; Hao, X. A RAFT Copolymerization of NIPAM and HPMA and Evaluation of Thermo-Responsive Properties of Poly(NIPAM-Co-HPMA). *RSC Adv.* **2016**, *6*, 89925–89933.

(31) Rymaruk, M. J.; Thompson, K. L.; Derry, M. J.; Warren, N. J.; Ratcliffe, L. P. D.; Williams, C. N.; Brown, S. L.; Armes, S. P. Bespoke Contrast-Matched Diblock Copolymer Nanoparticles Enable the Rational Design of Highly Transparent Pickering Double Emulsions. *Nanoscale* **2016**, *8*, 14497–14506.

(32) Lutz, J. F.; Akdemir, Ö.; Hoth, A. Point by Point Comparison of Two Thermosensitive Polymers Exhibiting a Similar LCST: Is the Age of Poly(NIPAM) Over? *J. Am. Chem. Soc.* **2006**, *128*, 13046–13047.

(33) Ferguson, C. J.; Hughes, R. J.; Nguyen, D.; Pham, B. T. T.; Gilbert, R. G.; Serelis, A. K.; Such, C. H.; Hawkett, B. S. Ab Initio Emulsion Polymerization by RAFT-Controlled Self-Assembly. *Macromolecules* **2005**, *38*, 2191–2204.

(34) Ganeva, D. E.; Sprong, E.; de Bruyn, H.; Warr, G. G.; Such, C. H.; Hawkett, B. S. Particle Formation in Ab Initio RAFT Mediated Emulsion Polymerization Systems. *Macromolecules* **2007**, *40*, 6181–6189.

(35) Semsarilar, M.; Ladmiral, V.; Blanazs, A.; Armes, S. P. Anionic Polyelectrolyte-Stabilized Nanoparticles via RAFT Aqueous Dispersion Polymerization. *Langmuir* **2012**, *28*, 914–922.

(36) Semsarilar, M.; Ladmiral, V.; Blanazs, A.; Armes, S. P. Cationic Polyelectrolyte-Stabilized Nanoparticles via RAFT Aqueous Dispersion Polymerization. *Langmuir* **2013**, *29*, 7416–7424.

(37) Chaduc, I.; Crepet, A.; Boyron, O.; Charleux, B.; D'Agosto, F.; Lansalot, M. Effect of the PH on the RAFT Polymerization of Acrylic Acid in Water. Application to the Synthesis of Poly(Acrylic Acid)-Stabilized Polystyrene Particles by RAFT Emulsion Polymerization. *Macromolecules* **2013**, *46*, 6013–6023.

(38) Wang, F.; Luo, Y.; Li, B.-G.; Zhu, S. Synthesis and Redispersibility of Poly(Styrene- *Block* - *n* -Butyl Acrylate) Core–Shell Latexes by Emulsion Polymerization with RAFT Agent–Surfactant Design. *Macromolecules* **2015**, *48*, 1313–1319.

(39) Cockram, A. A.; Neal, T. J.; Derry, M. J.; Mykhaylyk, O. O.; Williams, N. S. J.; Murray, M. W.; Emmett, S. N.; Armes, S. P. Effect of Monomer Solubility on the Evolution of Copolymer Morphology during Polymerization-Induced Self-Assembly in Aqueous Solution. *Macromolecules* **2017**, *50*, 796–802.

(40) Cockram, A. A.; Bradley, R. D.; Lynch, S. A.; Fleming, P. C. D.; Williams, N. S. J.; Murray, M. W.; Emmett, S. N.; Armes, S. P. Optimization of the High-Throughput Synthesis of Multiblock Copolymer Nanoparticles in Aqueous Media *via* Polymerization-Induced Self-

Assembly. *React. Chem. Eng.* **2018**, *3*, 645–657.

(41) Gurnani, P.; Bray, C. P.; Richardson, R. A. E.; Peltier, R.; Perrier, S. Heparin-Mimicking Sulfonated Polymer Nanoparticles via RAFT Polymerization-Induced Self-Assembly. *Macromol. Rapid Commun.* **2018**, 1800314.

(42) Lovett, J. R.; Warren, N. J.; Armes, S. P.; Smallridge, M. J.; Cracknell, R. B. Order–Order Morphological Transitions for Dual Stimulus Responsive Diblock Copolymer Vesicles. *Macromolecules* **2016**, *49*, 1016–1025.

(43) Lovett, J. R.; Warren, N. J.; Ratcliffe, L. P. D.; Kocik, M. K.; Armes, S. P. PH-Responsive Non-Ionic Diblock Copolymers: Ionization of Carboxylic Acid End-Groups Induces an Order-Order Morphological Transition. *Angew. Chemie Int. Ed.* **2015**, *54*, 1279–1283.

(44) Penfold, N. J. W.; Lovett, J. R.; Verstraete, P.; Smets, J.; Armes, S. P. Stimulus-Responsive Non-Ionic Diblock Copolymers: Protonation of a Tertiary Amine End-Group Induces Vesicle-to-Worm or Vesicle-to-Sphere Transitions. *Polym. Chem.* **2017**, *8*, 272–282.

(45) Penfold, N. J. W.; Lovett, J. R.; Warren, N. J.; Verstraete, P.; Smets, J.; Armes, S. P. PH-Responsive Non-Ionic Diblock Copolymers: Protonation of a Morpholine End-Group Induces an Order-Order Transition. *Polym. Chem.* **2016**, *7*, 79–88.

(46) Miasnikova, A.; Laschewsky, A. Influencing the Phase Transition Temperature of Poly(Methoxy Diethylene Glycol Acrylate) by Molar Mass, End Groups, and Polymer Architecture. *J. Polym. Sci. Part A Polym. Chem.* **2012**, *50*, 3313–3323.

(47) McCormick, C. L.; Lowe, A. B. Aqueous RAFT Polymerization: Recent Developments in Synthesis of Functional Water-Soluble (Co)Polymers with Controlled Structures. *Acc. Chem. Res.* **2004**, *37*, 312–325.

(48) Mertoglu, M.; Laschewsky, A.; Skrabania, K.; Wieland, C. New Water Soluble Agents for Reversible Addition-Fragmentation Chain Transfer Polymerization and Their Application in Aqueous Solutions. *Macromolecules* **2005**, *38*, 3601–3614.

(49) Khor, S. Y.; Truong, N. P.; Quinn, J. F.; Whittaker, M. R.; Davis, T. P. Polymerization-Induced Self-Assembly: The Effect of End Group and Initiator Concentration on Morphology of Nanoparticles Prepared via RAFT Aqueous Emulsion Polymerization. **2017**, *6*, 1013–1019.

(50) Biais, P.; Beaunier, P.; Stoffelbach, F.; Rieger, J. Loop-Stabilized BAB Triblock Copolymer Morphologies by PISA in Water. *Polym. Chem.* **2018**, *9*, 4483–4491.

(51) Cunningham, V. J.; Alswieleh, A. M.; Thompson, K. L.; Williams, M.; Leggett, G. J.; Armes, S. P.; Musa, O. M. Poly(Glycerol Monomethacrylate)–Poly(Benzyl Methacrylate) Diblock Copolymer Nanoparticles via RAFT Emulsion Polymerization: Synthesis, Characterization, and Interfacial Activity. *Macromolecules* **2014**, *47*, 5613–5623.

(52) Einarson, M. B.; Berg, J. C. Electrosteric Stabilization of Colloidal Latex Dispersions. *J. Colloid Interface Sci.* **1993**, *155*, 165–172.

(53) Save, M.; Manguian, M.; Chassenieux, C.; Charleux, B. Synthesis by RAFT of Amphiphilic Block and Comblike Cationic Copolymers and Their Use in Emulsion Polymerization for the Electrosteric Stabilization of Latexes. *Macromolecules* **2005**, *38*, 280–289.

Chapter 3.

RAFT dispersion polymerisation of lauryl methacrylate in ethanol-water binary mixtures: synthesis of diblock copolymer vesicles with deformable membranes

Reproduced in part with permission from [Gibson, R. R.; Cornel, E. J.; Musa, O. M.; Fernyhough A.; Armes, S. P. RAFT dispersion polymerisation of lauryl methacrylate in ethanol–water binary mixtures: synthesis of diblock copolymer vesicles with deformable membranes. *Polymer Chemistry*, **2020**, *11*, 1785-1796.

3.1 Introduction

Cunningham *et al.* reported using PNMEP as a steric stabiliser for the synthesis of diblock copolymer nano-objects *via* RAFT alcoholic dispersion polymerisation of BzMA.[1] Well-defined spheres, worms or vesicles could be obtained depending on the relative volume fractions of the PNMEP and PBzMA blocks (Figure 3.1). Moreover, this formulation provided the first example of a one-pot PISA synthesis in ethanol. However, relatively long reaction times (24 h) were required for high BzMA conversions at 70 °C.

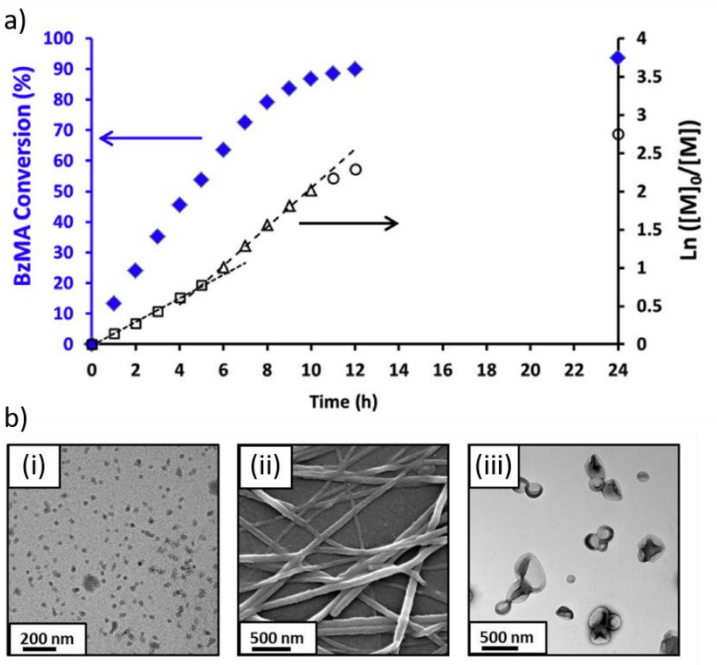

Figure 3.1. (a) Kinetic data obtained for the RAFT alcoholic dispersion polymerisation of BzMA at 70 °C targeting $PNMEP_{50}$-$PBzMA_{200}$ nano-objects at 20% w/w solids using a $PNMEP_{50}$ macro-CTA. Despite the rate enhancement observed after approximately 5 h, a relatively long reaction time is required for 95% conversion under such conditions. (b) TEM images obtained for (i) $PNMEP_{50}$-$PBzMA_{69}$ spheres, (ii) $PNMEP_{50}$-$PBzMA_{144}$ worms and $PNMEP_{50}$-$PBzMA_{188}$ vesicles using this PISA formulation.[1]

This problem is well-documented for various RAFT alcoholic dispersion formulations.[2–11] In this context, Zhang *et al.* reported the effect of adding water to the RAFT alcoholic dispersion polymerisation of BzMA on the final copolymer morphology.[2] Using just 5 % water as a co-solvent enabled either spheres, worms or vesicles to be obtained when increasing the target DP of the core-forming PBzMA block. Similarly, Jones and co-workers reported that the addition of increasing amounts of water to an alcoholic RAFT PISA formulation significantly increased the rate of polymerisation but limited the copolymer morphology to kinetically-trapped spheres.[6] The faster kinetics was attributed to a higher local monomer concentration caused by stronger partitioning of the BzMA monomer inside the growing nascent nanoparticles.

Lauryl methacrylate (LMA) is a commercially important hydrophobic monomer; PLMA-based copolymers have been used as viscosity modifiers in engine oil formulations.[12] Its relatively low T_g of -65 °C[13] affords excellent film-forming properties, which are utilised in the cosmetics industry for hair conditioning[14] and also to produce water-resistant barriers for skin care products.[15] Dong and co-workers reported the synthesis of PLMA-PNMEP diblock copolymers *via* RAFT *solution* polymerisation conducted in chloroform.[16–18] Unfortunately, only relatively low monomer conversions (typically < 86%) could be achieved within 24 h at 60 °C, regardless of the target copolymer composition. However, chloroform GPC studies confirmed that low-dispersity diblock copolymers were obtained (M_w/M_n < 1.21). Subsequently, these diblock copolymers were self-assembled in THF[16] or *n*-dodecane[17,18] to produce dilute dispersions of various types of nano-objects *via* traditional post-polymerisation processing.

Recently, Lowe and co-workers reported the PISA synthesis of well-defined spheres, worms or vesicles comprising low T_g core-forming blocks.[19] More specifically, RAFT dispersion polymerisation of 3-phenylpropyl methacrylate (PPPMA) in ethanol was conducted using a poly(2-(dimethylamino)ethyl methacrylate) (PDMA) steric stabiliser block. Interestingly, a reversible worm-to-sphere transition with concomitant degelation was observed on heating up to 70 °C (Figure 3.2). This was attributed in part to the relatively low T_g of the core-forming poly(3-phenylpropyl methacrylate) block, which was determined to be approximately 2 °C by differential scanning calorimetry (DSC) measurements.

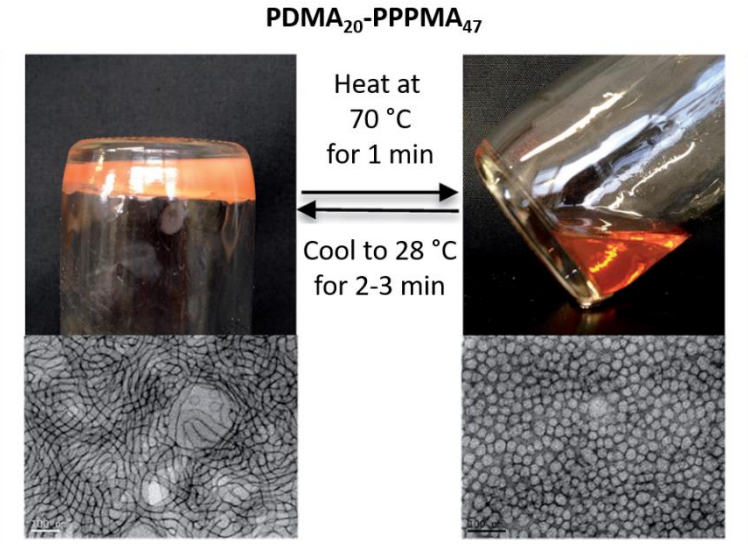

Figure 3.2. Digital photographs and corresponding TEM images recorded for a 21% w/w solution of $PDMA_{20}$-$PPPMA_{47}$ diblock copolymer worms (see main text for further details) in ethanol at room temperature and the same copolymer dispersion after heating to 70 °C, indicating a reversible worm-to-sphere reversible transition.[19]

Diblock copolymer nanoparticles comprising a relatively low T_g core-forming block are notoriously difficult to image using TEM owing to film formation during TEM grid preparation.[20,21] This problem can lead to incorrect assignment of the copolymer morphology. Erroneous morphologies can also be assigned in the case of relatively small vesicles because the characteristic collapse and deformation of such nano-objects that is typically observed under the ultrahigh vacuum conditions required for TEM analysis may not occur.[22] Given such problems, the Armes group has recommended that SAXS analysis should be employed to validate diblock copolymer morphologies, particularly if spheres are not expected based on the target copolymer composition.[22]

Herein we report the highly convenient PISA synthesis of LMA-rich PNMEP-PLMA diblock copolymer vesicles in ethanol-water mixtures. Bearing in mind potential industrial applications, RAFT chain-end removal strategies have been briefly explored for such diblock copolymer nanoparticles.

3.2 Experimental

3.2.1 Materials

N-(2-(Methacryloyloxy)ethyl pyrrolidone (NMEP; 98% purity) was kindly provided by Ashland Inc. (Delaware, USA) and was used without further purification. Lauryl methacrylate (LMA), ethanol (≥99.8%), 2-cyano-2-propyl benzodithioate (CPDB) and d_1-chloroform were purchased from Sigma Aldrich UK. 4,4'-Azobis(4-cyanovaleric acid) (ACVA; 99%) was purchased from Alfa Aesar (Heysham, UK)**.** d_6-Acetone and d_4-methanol was purchased from Goss Scientific Instruments Ltd. (Cheshire, UK). Deionised water was used for all experiments.

3.2.2 Synthesis of $PNMEP_{28}$ macro-CTA by RAFT solution polymerisation in ethanol

The protocol for the preparation of a $PNMEP_{28}$ macro-CTA is described below. NMEP (9.37 g, 47.4 mmol), CPDB RAFT agent (0.30 g, 1.36 mmol; target DP = 35), ACVA (76.0 mg, 0.27 mmol; CPDB/ACVA molar ratio = 5.0) and ethanol (14.59 g, 40% w/w solids) were weighed into a 50 mL round-bottom flask immersed in an ice bath and degassed with continuous stirring for 30 min. The reaction was allowed to proceed for 270 min in an oil bath set to 70 °C, resulting in a monomer conversion of 90% as judged by ^{1}H NMR spectroscopy. The polymerisation was then quenched by exposing the hot reaction solution to air and cooling to 20 °C. The crude polymer was precipitated into excess diethyl ether to remove residual monomer before freeze-drying from water to afford

a dry pink powder. The mean DP was calculated to be 28 by comparing the integrated aromatic protons arising from the dithiobenzoate RAFT end-groups at 7-8 ppm to the methylene proton signal next to the carbonyl at 2.5 ppm. GPC analysis using chloroform eluent indicated an M_n of 5 000 g mol^{-1} and an M_w/M_n of 1.23 against a series of ten near-monodisperse PMMA calibration standards.

3.2.3 Synthesis of PNMEP$_{28}$-PLMA$_x$ diblock copolymer nanoparticles *via* RAFT dispersion polymerisation of LMA in an ethanol-water mixture at 70 °C

A typical protocol for the synthesis of PNMEP$_{28}$-PLMA$_{87}$ (LMA/NMEP mass ratio = 4:1) is described as follows: PNMEP$_{28}$ macro-CTA (0.15 g, 26.10 µmol), LMA (0.58 g, 2.27 mmol; target DP = 87) and ACVA (1.50 mg, 5.22 µmol; 0.19 mL of a 7.89 g dm^{-3} ethanolic stock solution; PNMEP$_{28}$/ACVA molar ratio = 5.0) were dissolved in an 80:20 w/w ethanol-water mixture (2.92 g). The reaction vial was sealed and degassed under N_2 for 30 min before placing in a pre-heated oil bath set at 70 °C for 16 h. The polymerisation was quenched by exposing the hot reaction solution to air and cooling to 20 °C. The resulting diblock copolymer nanoparticles were characterised by ^{1}H NMR spectroscopy, DLS and TEM with 0.1% w/w dispersions being prepared *via* dilution using an 80:20 w/w ethanol-water mixture. Chloroform GPC analysis indicated an M_n of 19 800 g mol^{-1} and an M_w/M_n of 1.28. Other diblock compositions were prepared by adjusting the amount of LMA monomer to target LMA/NMEP mass ratios ranging between 2:1 and 7:1. For these additional syntheses, the volume of the continuous phase was adjusted to maintain an overall solids concentration of 20% w/w (see Table 3.1 for the corresponding DPs of the PLMA blocks). ^{1}H NMR analysis indicated that more than 98% monomer conversion was achieved in all cases.

3.2.4 Protocol for cleavage of RAFT end-groups from PNMEP$_{28}$-PLMA$_{87}$ diblock copolymer nanoparticles using blue LED light irradiation.

The dithiobenzoate end-groups within PNMEP$_{28}$-PLMA$_{87}$ vesicles were cleaved according to the following protocol. A 20% w/w copolymer dispersion (1.0 g) was diluted to 7.5% w/w using deionised water (1.7 g). This dispersion was then placed in a water-jacketed Schlenk tube wrapped in blue LED light strips (λ = 405 nm, 0.37 mW cm^{-2}) with the temperature of the recirculating water set to 50 °C. Aliquots of this reaction mixture were taken periodically and analysed using UV GPC (with the UV detector set at λ = 308 nm).

3.2.5 Copolymer characterisation

^{1}H NMR spectroscopy. d_4-Methanol was used to record ^{1}H NMR spectra of the $PNMEP_{28}$ macro-CTA and d_1-chloroform and d_6-acetone were used to analyse the $PNMEP_{28}$-$PLMA_x$ diblock copolymers in a 10:1 mass ratio. Spectra were recorded using a 400 MHz Bruker Avance 400 spectrometer with 64 scans being averaged per spectrum.

Gel permeation chromatography (GPC). Molecular weight data for both the PNMEP homopolymer precursor and the series of $PNMEP_{28}$-$PLMA_x$ diblock copolymers were obtained using chloroform GPC at 35 °C, with the eluent containing 0.25% triethylamine by volume. Two Polymer Laboratories PL gel 5 µm Mixed C columns were connected in series to a Varian 390 multi-detector suite (refractive index detector) and a Varian 290 LC pump injection module using a 1.0 mL min^{-1} flow rate. Ten near-monodisperse PMMA standards (M_n = 625 – 618 000 g mol^{-1}) were used for calibration and data were analysed using Varian Cirrus GPC software. UV GPC chromatograms were obtained simultaneously by detection at a fixed wavelength of 308 nm, which corresponds to the absorption maximum of the dithiobenzoate RAFT end-groups.

Dynamic light scattering (DLS). A Malvern Zetasizer NanoZS instrument was used to determine the intensity-average hydrodynamic diameter of the copolymer nanoparticles at 20 °C at a scattering angle of 173°. As-synthesised dispersions were diluted to 0.1% w/w using either an 80:20 w/w ethanol-water mixture, deionised water or pure ethanol and analysed using disposable 1.0 cm path length plastic cuvettes. Data were averaged over three consecutive measurements (with 10 sub-runs per run) for each sample. Sphere-equivalent intensity-average diameters were calculated for diblock copolymer nano-objects *via* the Stokes–Einstein equation, which assumes perfectly monodisperse, non-interacting spheres. Aqueous electrophoresis measurements were also conducted at 20 °C using the same instrument for 0.1% w/w nanoparticle dispersions prepared using 1 mM KCl as the diluent. The solution pH was adjusted using either HCl or KOH as required. Zeta potentials were calculated from the Henry equation using the Smoluchowski approximation.

Transmission electron microscopy (TEM). Copper/palladium grids were surface-coated in-house to produce a thin film of amorphous carbon before being plasma glow-discharged for 40 s producing a hydrophilic surface. A single droplet (15 µL) of a 0.1% w/w copolymer dispersion (prepared by serial dilution using an 80:20 w/w ethanol-water mixture) was placed on a grid for 60 s, blotted to remove the excess solution and then stained using an aqueous uranyl formate solution (0.75% w/v) for 20 s. Excess negative stain was removed by careful blotting and the grid was then dried

using a vacuum hose. A FEI Tecnai Spirit microscope operating at 80 kV equipped with a Gatan 1kMS600CW CCD camera was used to image the grids.

Small angle X-ray scattering (SAXS). SAXS patterns were recorded by Armes group members at a national synchrotron facility (station I22, Diamond Light Source, Didcot, Oxfordshire, UK) using monochromatic X-ray radiation (λ = 0.124 nm with q ranging from 0.01 to 2.00 nm^{-1} where $q = 4\pi\sin\Theta/\lambda$ is the length of the scattering vector and Θ is one-half of the scattering angle) and a 2D Pilatus 2M pixel detector (Dectris, Switzerland). A glass capillary of 2 mm diameter was used as a sample holder and all measurements were conducted on 1.0% w/w copolymer dispersions in 80:20 w/w ethanol-water mixtures. X-ray scattering data were reduced and normalised using standard routines by the beamline and were further analysed using Irena SAS macros for Igor Pro.

Reverse phase high performance liquid chromatography (Reverse phase HPLC). HPLC analysis was performed on an HP 1100 series LC equipped with a quadratic pump, an autosampler and a diode array detector. An Agilent Poroshell EC-C18 100 x 4.6 mm column with a particle size of 3.5 µm was used at 40 °C. The mobile phase consisted of water with 0.1% (v/v) orthophosphoric acid and acetonitrile run under gradient conditions (acetonitrile varied from 5% to 100% in 20 min with a 2-min hold at 100% before re-equilibriation at 5% for 5 min) at a flow rate of 0.40 mL min^{-1}, a run time of 27 min and an injection volume of 5 µL. The analyte was detected at a wavelength of 210 nm normalised against a 360 nm reference wavelength. Nanoparticle dispersions were diluted to 2.0% w/w using deionised water. The resulting dispersions were shaken for 20 min and decanted into centrifugal cut-off filters (Merck Amicon Ultra-4, 3 KDa nominal molecular weight) to remove high molecular weight material. These were centrifuged at an RCF of 8422 g (9000 rpm; rotor radius = 9.3 cm) for 20 min to produce approximately 4 mL of aqueous filtrate for evaluation of residual NMEP monomer. Concentration was measured based on the detector response to external NMEP standard solutions of known concentration.

Gas chromatography (GC). GC analysis for residual LMA was conducted using an Agilent 7890A series GC equipped with a Restek Rxi-624Sil-MS capillary column (30 m x 0.32 mm, D= 1.8 µm), hydrogen carrier gas and a flame ionisation detector (FID). Carrier gas velocity was fixed at 45.5 cm s^{-1}. The injection volume was fixed at 2 µL. The LMA content of reaction mixtures was calculated against the detector response towards a series of LMA external standard solutions of known concentration (5 - 100 µg mL^{-1}). The inlet temperature was fixed at 225 °C and the initial oven temperature was 100 °C. The oven programme was a 2 min isothermal hold followed by a 10 °C min^{-1} ramp to 300 °C and a 4 min hold. The detector temperature was maintained at 300 °C.

Samples were extracted using acetone (0.2 g in 2 mL) and filtered through a 0.45 µm PTFE filter prior to injection.

Differential Scanning Calorimetry (DSC). The T_gs for six PNMEP$_{28}$-PLMA$_x$ diblock copolymers were determined using a TA Instruments Discovery DSC 25 instrument from −90 to 100 °C at a heating/cooling rate of 10 °C min^{-1}. Each copolymer (10 mg) was dried for at least 24 h in a vacuum oven at 70 °C prior to analysis. Dried samples were sealed in a vented aluminium pan, and the instrument was calibrated for heat flow and temperature using both indium and zinc standards. Samples were annealed at 100 °C for 5 min before cooling to −90 °C and maintaining this temperature for 1 min. The T_g was then determined by heating the copolymer up to 100 °C and taken as a midpoint value.

3.3 Results and discussion

3.3.1 Preparation of PNMEP$_{28}$-PLMA$_x$ diblock copolymers *via* RAFT dispersion polymerisation of LMA

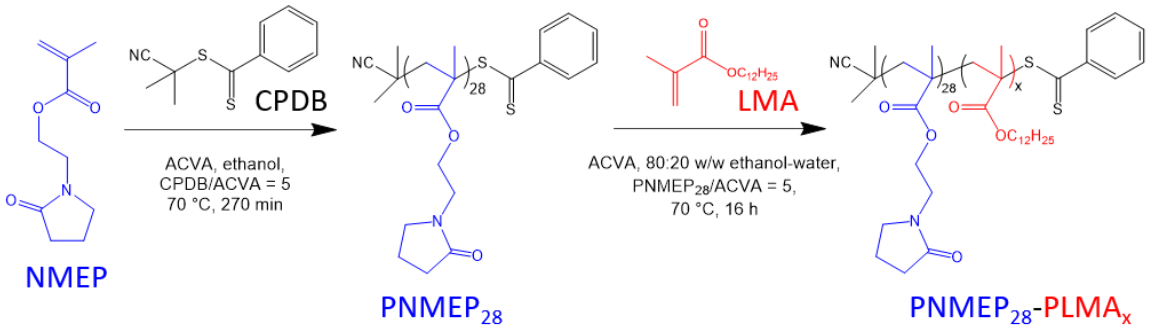

Scheme 3.1. Synthesis of a PNMEP$_{28}$ macro-CTA by RAFT solution polymerisation of NMEP in ethanol at 70 °C and subsequent synthesis of PNMEP$_{28}$-PLMA$_x$ diblock copolymer nano-objects by RAFT dispersion polymerisation of LMA in an 80:20 w/w ethanol-water mixture at 70 °C.

A PNMEP$_{28}$ macro-CTA was prepared by RAFT solution polymerisation of NMEP in ethanol at 70 °C using a CPDB RAFT agent, see Scheme 3.1. This polymerisation was allowed to progress for 270 min and was quenched at 90% conversion. The mean DP was determined to be 28 by end-group analysis using ^{1}H NMR spectroscopy (Figure 3.3). This PNMEP$_{28}$ macro-CTA was subsequently chain-extended *via* RAFT dispersion polymerisation of LMA at 20% w/w solids in an 80:20 w/w ethanol-water mixture at 70°C. The aqueous solubility of LMA is too low for an aqueous emulsion polymerisation formulation[23] while it is difficult to achieve high monomer conversions in pure ethanol owing to the relatively slow polymerisation kinetics under such conditions.[6,24] Thus, an 80:20 w/w ethanol-water mixture was selected for the RAFT dispersion polymerisation of LMA. This formulation enabled very high LMA conversions to be achieved within 11 h at 70 °C.

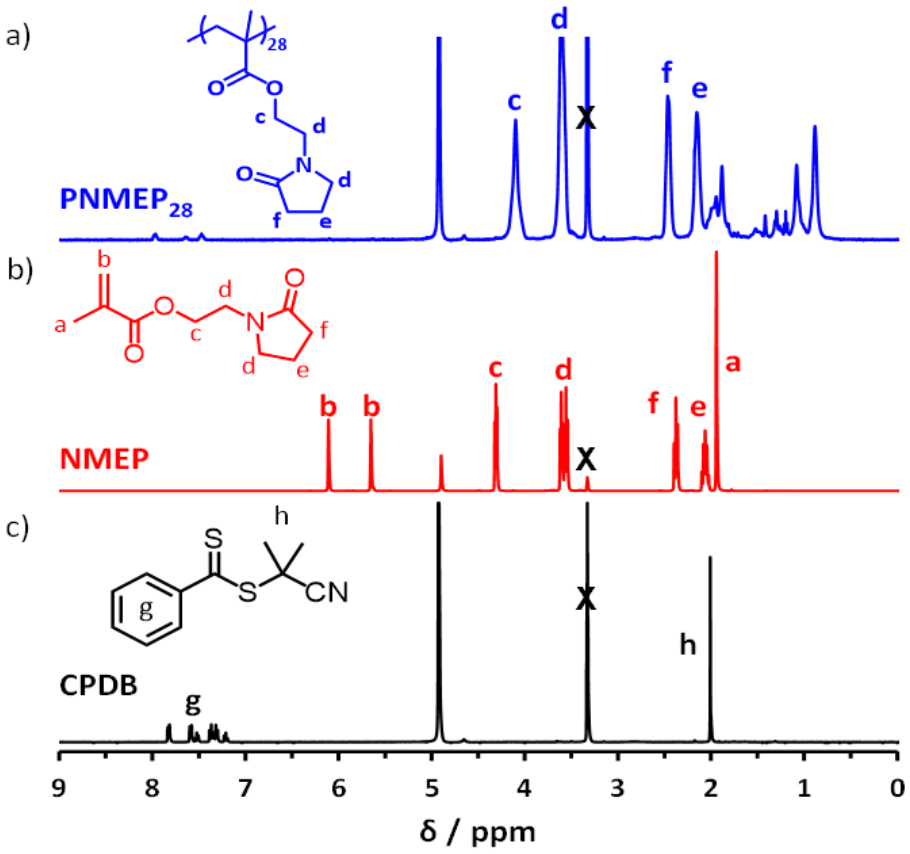

Figure 3.3. ^{1}H NMR spectra recorded in d_4-methanol for (a) $PNMEP_{28}$ macro-CTA, (b) NMEP monomer and (c) CPDB RAFT agent.

A series of $PNMEP_{28}$-$PLMA_x$ diblock copolymer nano-objects were synthesised by targeting PLMA/PNMEP mass ratios ranging from 2:1 to 7:1 using a 80:20 w/w ethanol-water mixture. Both high and low molecular weight shoulders are observed in the GPC curves obtained for all target diblock copolymers. Utilising UV GPC (Figure 3.4b), whereby the detector wavelength is tuned to the absorption of the dithiobenzoate chain-ends at 308 nm, it is clear that some of the polymer chains in both these minor populations possess a RAFT end-group. This suggests that the low molecular weight shoulder is simply the result of slow/incomplete reinitiation of the $PNMEP_{28}$ precursor, rather than premature loss of RAFT end-groups. We attribute the high molecular weight shoulder to chain transfer to polymer, rather than dimethacrylate impurities in the LMA monomer. High LMA conversions (>98%) were achieved in all cases as shown by ^{1}H NMR spectroscopy (Figure 3.5). However, this technique becomes rather insensitive for low concentrations of residual monomer (< 1%).

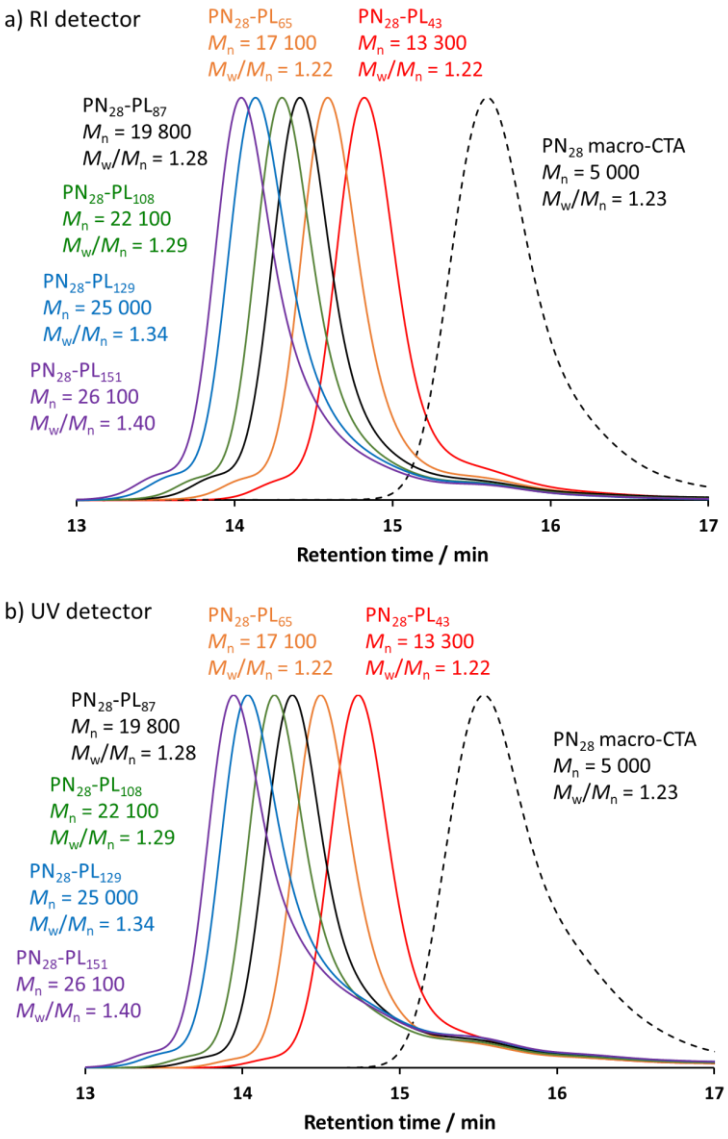

Figure 3.4. Chloroform GPC curves recorded for a series of $PNMEP_{28}$-$PLMA_x$ diblock copolymers and the corresponding $PNMEP_{28}$ precursor: (a) refractive index detector with calibration using a series of near-monodisperse PMMA standards; (b) UV detection at λ = 308 nm.(N.B. PN and PL are shorthand for PNMEP and PLMA.)

For potential industrial applications, the level of volatile organic compounds (VOCs) in such formulations is very important. Thus, gas chromatography (GC) analysis was used to quantify the residual unreacted LMA monomer while reverse-phase high performance liquid chromatography (HPLC) was utilised to determine residual NMEP monomer. GC analysis indicated LMA contents of less than 0.15% (1500 ppm) while HPLC indicated that less than 0.03% NMEP (300 ppm) remained in the original copolymer dispersions. For the two shortest diblock copolymers, GC analysis was not conducted owing to poor partitioning of these low molecular weight chains with the solvent.

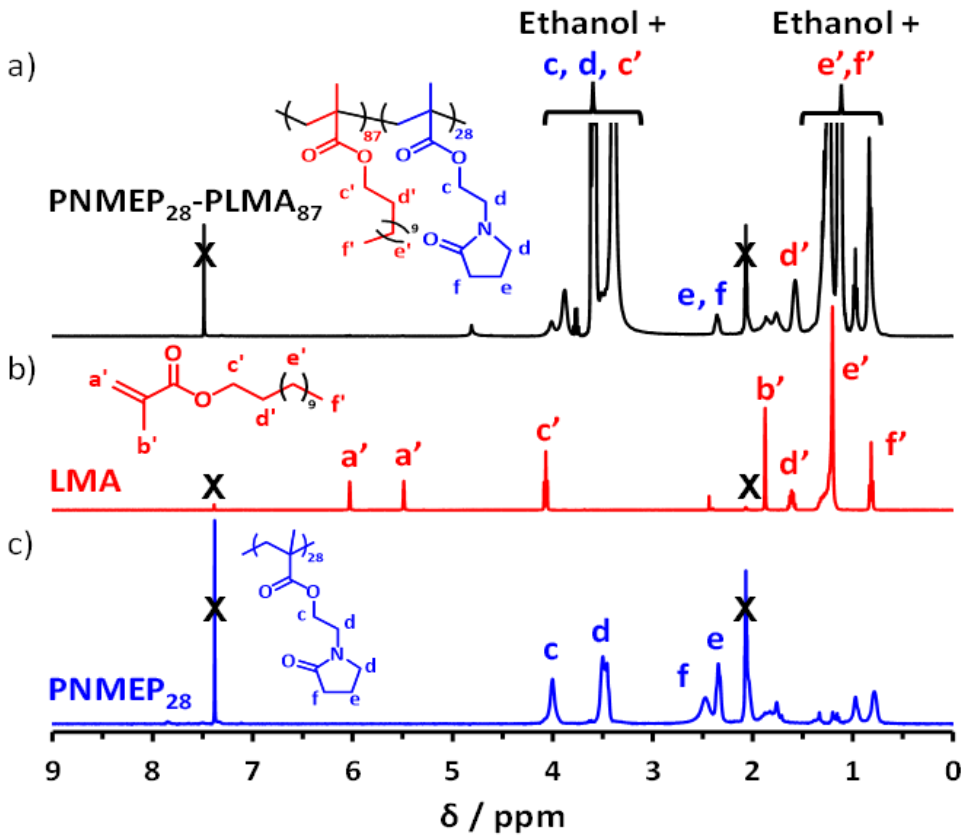

Figure 3.5. ^{1}H NMR spectra recorded in a 10:1 d_1-chloroform/d_6-acetone mixture for (a) $PNMEP_{28}$-$PLMA_{87}$ diblock copolymer, (b) LMA monomer and (c) $PNMEP_{28}$ macro-CTA.

The polymerisation kinetics were monitored for various ethanol-water mixtures (containing 0, 5, 10 or 20% water by mass) targeting a $PNMEP_{28}$-$PLMA_{87}$ diblock composition. It is clear that increasing the proportion of water as a co-solvent significantly increases the rate of LMA polymerisation, as previously reported by other workers.[2,6] For example, using an 80:20 w/w ethanol-water mixture enabled 99% LMA conversion to be achieved within 8.5 h. Hence this solvent composition was utilised for all of the PISA syntheses reported in this study.

Table 3.1. Summary of the target diblock copolymer compositions, LMA monomer conversions, residual levels of NMEP and LMA monomer, molecular weight data and T_g values.

Target diblock copolymer composition	LMA conversion[a] / %	Residual NMEP[b] / ppm	Residual LMA[c] / ppm	M_n[d] / g mol^{-1}	M_w/M_n[d]	PLMA T_g[e] / °C	PNMEP T_g / °C
$PNMEP_{28}$	N/A	n.d.	N/A	5 000	1.23	N/A	65
$PNMEP_{28}$-$PLMA_{43}$	>99	136	n.d.	13 300	1.22	-48	56
$PNMEP_{28}$-$PLMA_{65}$	>99	309	n.d.	17 100	1.22	-48	56
$PNMEP_{28}$-$PLMA_{87}$	>99	199	983	19 800	1.28	-46	52
$PNMEP_{28}$-$PLMA_{108}$	99	132	1037	22 100	1.29	-47	49
$PNMEP_{28}$-$PLMA_{129}$	99	155	1156	25 000	1.34	-48	49
$PNMEP_{28}$-$PLMA_{151}$	99	168	1153	26 100	1.40	-47	50

[a]Determined by ^{1}H NMR spectroscopy. [b]Determined by HPLC. [c]Determined by gas chromatography [d]Determined by chloroform GPC. [e]Determined by DSC. [N.B. 'n.d.' is shorthand for 'not determined'].

The corresponding semi-logarithmic plots (Figure 3.6b) indicate markedly faster polymerisations after nucleation as the proportion of water was increased. Prior to micellar nucleation, there appears to be no trend in the polymerisation rates observed as the water content is systematically increased (see inset in Figure 3.6b). However, a noticeable rate enhancement occurred at approximately the same LMA conversion for the 90:10 and 80:20 w/w solvent compositions, suggesting that a critical PLMA DP of 17 is required for nucleation. This is significantly lower than the critical DP of 160 reported by Jones and co-workers, for PBzMA chains grown from a PDMA precursor under the same conditions.[6] The rate enhancement was significantly higher for 20% w/w water compared to 10% w/w water, with the latter formulation only reaching an LMA conversion of 93% within the same 8.5 h time period.

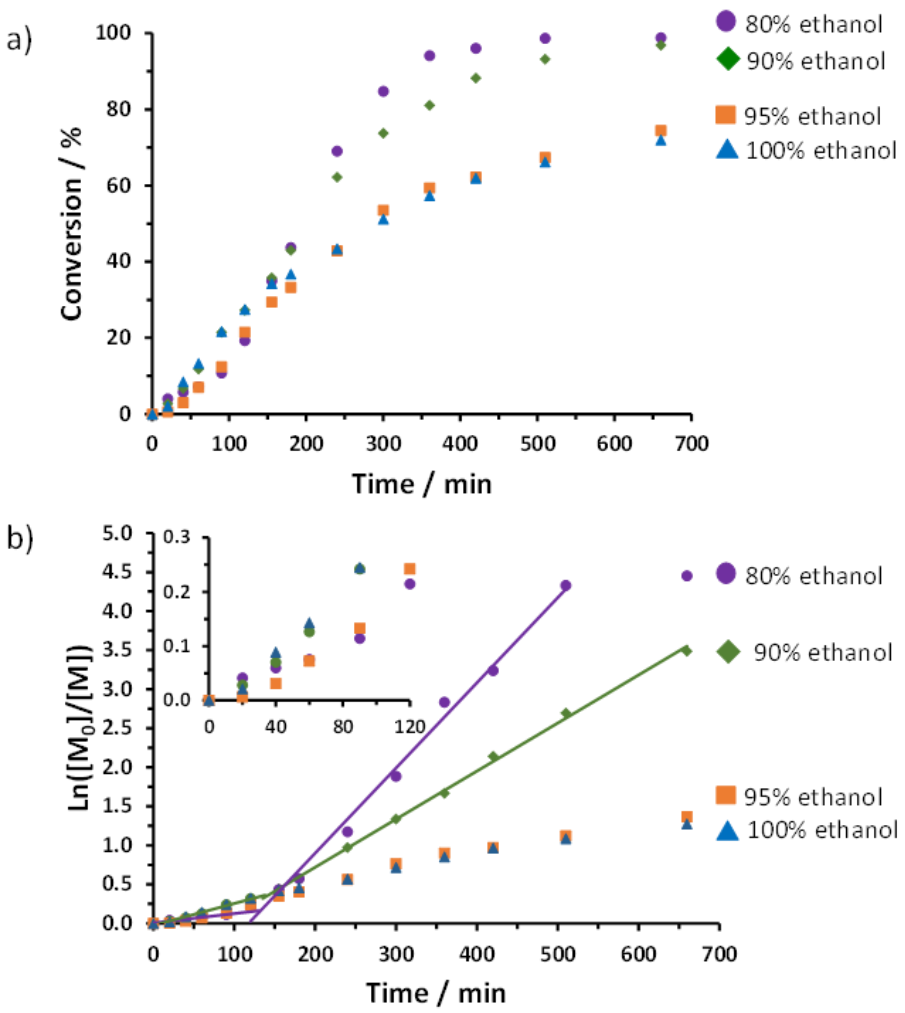

Figure 3.6. (a) Conversion *vs.* time curves obtained for the RAFT dispersion polymerisation of LMA at 70 °C using a $PNMEP_{28}$ macro-CTA and ACVA initiator ([PNMEP]/[ACVA] = 5.0) at 20% w/w solids. LMA conversions were determined by ^1H NMR spectroscopy. In each case, a $PNMEP_{28}$-$PLMA_{87}$ composition was targeted and the solvent composition was varied from absolute ethanol to an 80:20 w/w ethanol-water mixture. (b) The same data are presented as semi-logarithmic plots, with the data points obtained for the first two hours magnified in the inset.

However to ensure maximum conversion for all target diblock copolymers, each polymerisation was allowed to proceed overnight (16 h). The same diblock composition was also targeted using anhydrous ethanol. The conversion *vs.* time curve and semi-logarithmic plot was almost identical to that observed using either 5% w/w water or laboratory-grade ethanol (see Figures 3.6 and 3.7), suggesting that such low levels of water have a negligible effect on the polymerisation kinetics. The final LMA conversion obtained after 11 h at 70 °C for the laboratory-grade ethanol (designated 100% ethanol) was 72%, whereas 68% conversion was achieved for the anhydrous ethanol formulation under the same conditions.

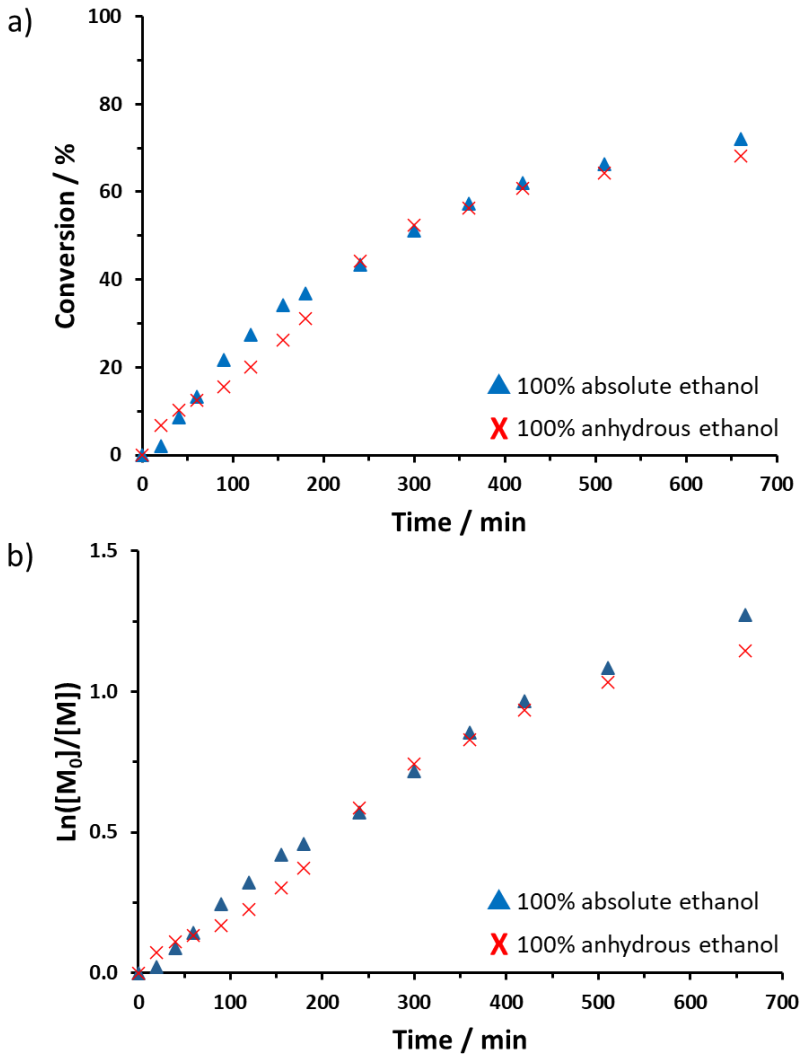

Figure 3.7. Conversion *vs.* time curves obtained by ^{1}H NMR spectroscopy studies of the RAFT dispersion polymerisation of LMA at 70 °C using a PNMEP$_{28}$ macro-CTA and ACVA initiator ([PNMEP$_{28}$]/[ACVA] molar ratio = 5.0) while targeting 20% w/w solids using either laboratory-grade ethanol or anhydrous ethanol. (b) Corresponding semi-logarithmic plots calculated for the same kinetic data.

The molecular weight and dispersity were plotted against conversion for the kinetics conducted using an 80:20 w/w ethanol-water mixture (Figure 3.8). The linear evolution in M_n with increasing conversion indicates good RAFT control. The observed deviation from the theoretical M_n at high conversions was not unexpected because molecular weights are calculated using PMMA calibration standards.

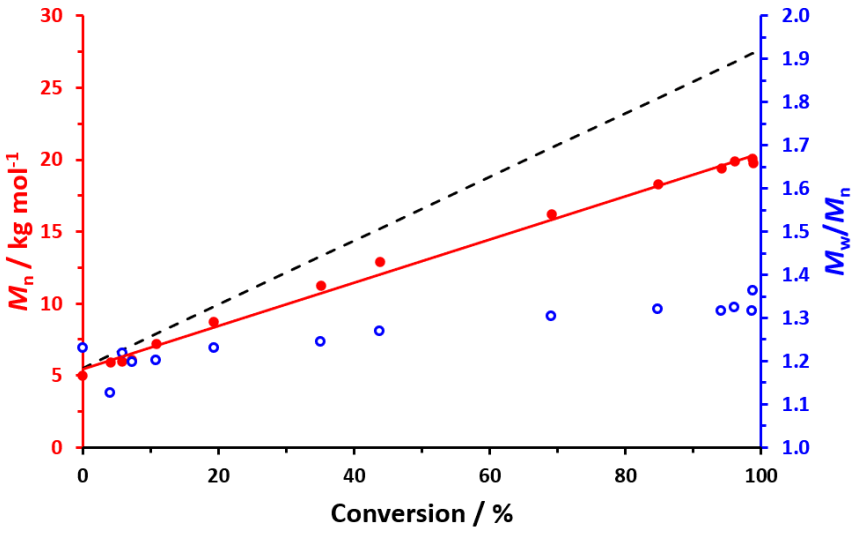

Figure 3.8. Evolution of M_n (●) and M_w/M_n (○) with conversion observed during the RAFT dispersion polymerisation of LMA at 70 °C targeting PNMEP$_{28}$-PLMA$_{87}$ in an 80:20 w/w ethanol-water mixture at 20% w/w solids. The theoretical M_n is indicated by the black dashed line.

The T_g associated with each PNMEP$_{28}$-PLMA$_x$ diblock copolymer was determined by DSC after annealing at 100 °C to remove traces of solvent (Figure 3.9). In all cases, these copolymers are distinctly PLMA-rich, which means that the T_g for the PNMEP cannot be easily detected. The T_g of the PNMEP$_{28}$ macro-CTA was 65 °C. For the diblock copolymer series, the PLMA$_x$ T_g was fairly constant at around -48 °C, which is somewhat higher than the reported literature value of –65 °C.[13] Similarly, the T_g of the PNMEP$_{28}$ block was suppressed by 10 - 15 °C for PLMA DPs above 87. The target diblock compositions are highly asymmetric in favour of PLMA, hence this block should be more easily detectable. This change in T_g for the PLMA and PNMEP blocks respectively indicated some degree of miscibility between the two blocks.

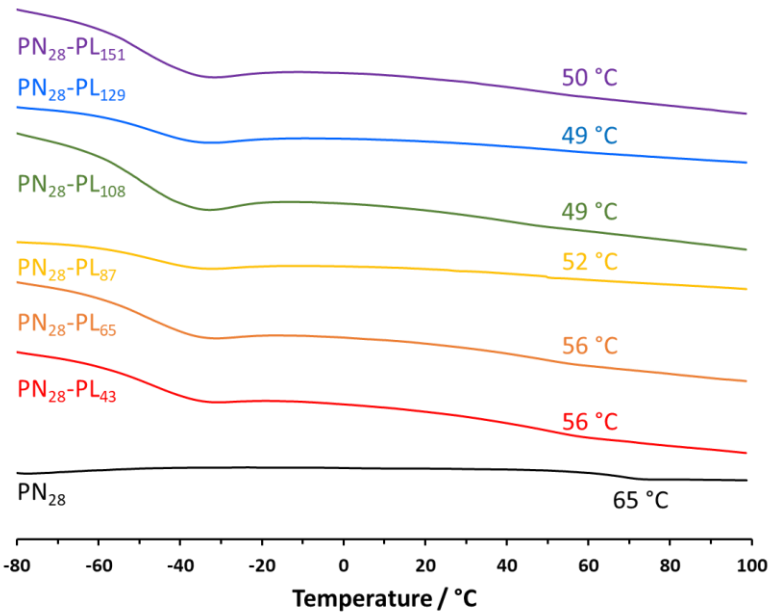

Figure 3.9. DSC traces obtained for the $PNMEP_{28}$ macro-CTA precursor and a series of $PNMEP_{28}$-$PLMA_x$ diblock copolymers using a heating rate of 10 °C min^{-1}.

In this context, a study of diblock copolymers comprising *tert*-butyldimethylsilyl methacrylate (TBDMSiMA) and poly(dimethylsiloxane) methacrylate (PDMSMA) by Lejars *et al.* is noteworthy.[25] These workers observed that the T_g of the PTBDMSiMA block (82 °C) was somewhat lower than that of the corresponding PTBDMSiMA homopolymer (105 °C), whereas the T_g for the PDMSMA block was higher than that of the corresponding homopolymer (-114 °C *vs.* -123 °C). Moreover, greater microphase separation was observed for longer PDMSMA blocks, so the T_g values for the individual blocks were closer to those for the corresponding homopolymers. It was concluded that the PDMSMA chains had a plasticising effect on the PTBDMSiMA block, which led to partial misciblity and hence only weak segregation. This behaviour is also observed for the $PNMEP_{28}$-$PLMA_x$ diblock copolymers as the T_g values for the $PLMA_x$ and $PNMEP_{28}$ blocks are increased and decreased respectively relative to their homopolymer T_g values.

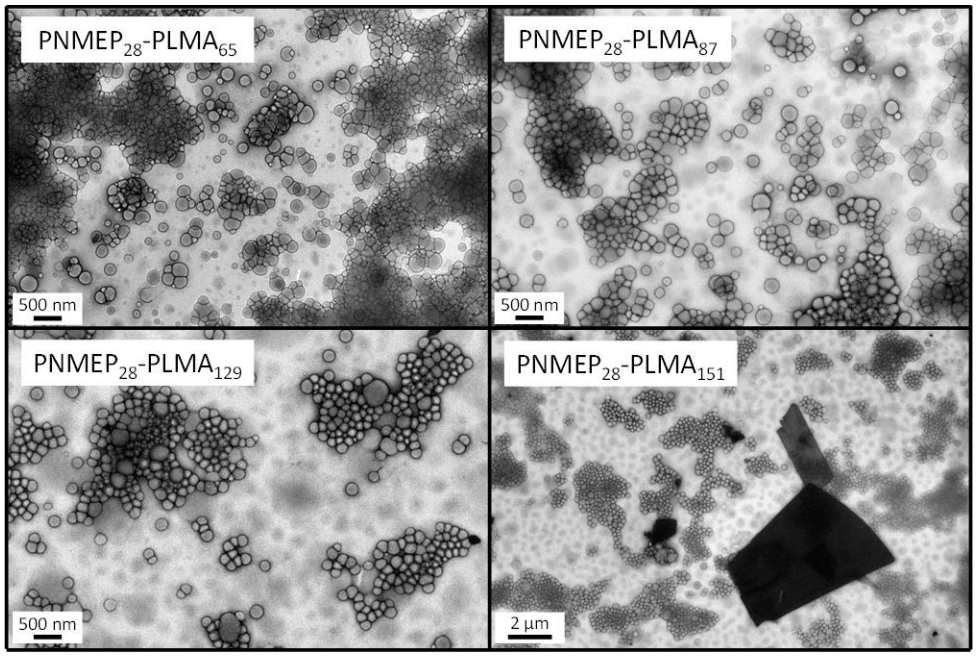

Figure 3.10. Representative TEM images recorded for dried dilute aqueous dispersions of PNMEP$_{28}$-PLMA$_x$ diblock copolymer nano-objects prepared *via* RAFT dispersion polymerisation of LMA in an 80:20 w/w ethanol-water mixture. A spherical morphology is observed in all cases with a minor population of lamellar sheets present in some samples. A lower magnification image is shown for PNMEP$_{28}$-PLMA$_{152}$ (note 2 µm scale bar) to more clearly show the relatively large lamellar sheets that are present in this dispersion. Subsequent SAXS studies indicated that some of the 'spheres' are actually vesicles (see Figures 3.11 and 3.12).

Despite the relatively low T_g values for the insoluble PLMA block, these diblock copolymer nano-objects could be imaged by TEM. For all targeted copolymer compositions, the predominant morphology appeared to be spheres (see Figure 3.10). However, minor populations of lamellar sheets were also observed in all cases. In many instances, PISA syntheses only produce kinetically-trapped spheres.[6,26–28] This is particularly true in the case of RAFT emulsion polymerisation,[27,29–35] but it is also well-known for RAFT dispersion polymerisation when using a relatively long steric stabiliser block[12,36–38] or when working at relatively low copolymer concentration.[36,39] However, so-called higher order morphologies such as worms, vesicles or lamellae can be obtained under appropriate conditions. [36,40–44] Typically, this involves using a suitable short steric stabiliser block and targeting a relatively long insoluble block at a sufficiently high copolymer concentration.[42,45–47] For such PISA formulations, the evolution in copolymer morphology always follows the same mechanistic pathway. Spheres are formed initially and, as the structure-directing insoluble block grows longer, worms are formed *via* the stochastic 1D fusion of multiple spheres, followed by vesicle formation *via* transient jellyfish-like intermediates if a sufficiently asymmetric diblock copolymer composition is targeted.[43,48,49] Under certain conditions, block copolymer lamellae (*i.e.* thin sheets or platelets) can also be formed.[50,51]

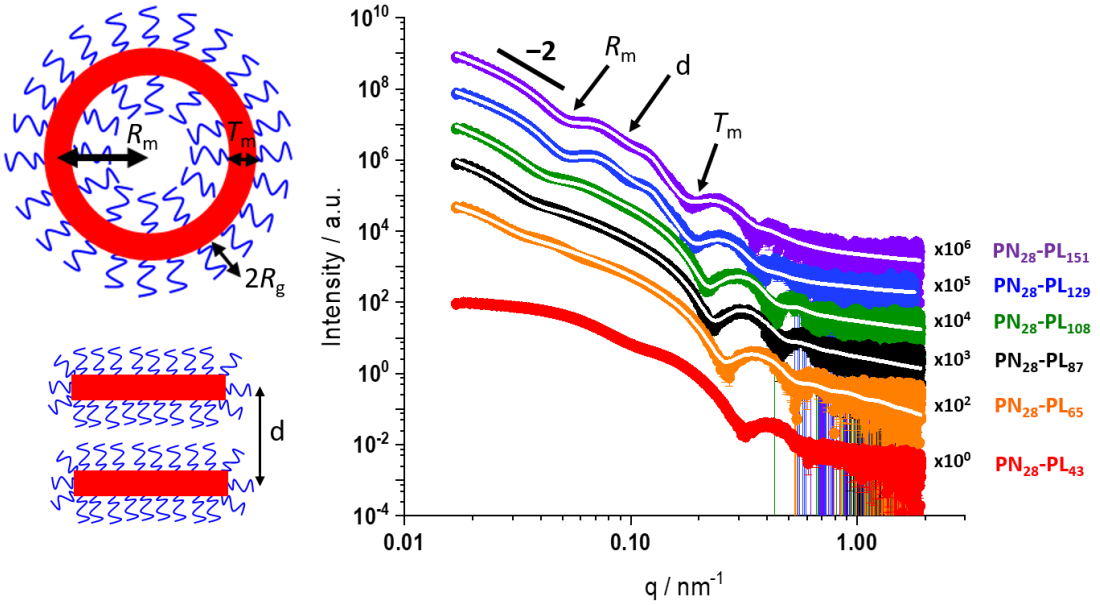

Figure 3.11. SAXS patterns recorded for 1.0% w/w copolymer dispersions in 80:20 w/w ethanol-water at 20 °C: $PNMEP_{28}$-$PLMA_{43}$ (red), $PNMEP_{28}$-$PLMA_{65}$ (orange), $PNMEP_{28}$-$PLMA_{87}$ (black), $PNMEP_{28}$-$PLMA_{108}$ (green), $PNMEP_{28}$-$PLMA_{129}$ (blue) and $PNMEP_{28}$-$PLMA_{151}$ (purple). The white lines indicate data fits obtained using a well-known vesicle model for five of the patterns.[52] See Figure 3.12 for the $PNMEP_{28}$-$PLMA_{43}$ fit. Each SAXS pattern is offset by an arbitrary factor for clarity. A cartoon for a vesicle and for stacked lamellae has been added to assist with picking out important features on the SAXS patterns where R_m is the distance from the centre of the vesicle to the middle of the membrane, T_m is the membrane thickness, R_g is the radius of gyration and d is the stacking distance between two lamella sheets.

In view of this literature precedent, it seemed rather surprising that spheres should co-exist with lamellae. Thus small angle X-ray scattering (SAXS) was used to examine these diblock copolymer morphologies in more detail. Satisfactory data fits could be obtained using a vesicle model (see Figure 3.11) for five of the six entries shown in Table 3.2. Moreover, the low *q* gradient was close to -2, which is consistent with the formation of vesicles (and lamellae).[53]

Table 3.2. Summary of TEM and SAXS data obtained for a series of six $PNMEP_{28}$-$PLMA_x$ diblock copolymer nano-objects.

Target diblock composition	TEM[a]	SAXS[b]				DLS[c]
	Number-average diameter / nm	Volume-average diameter / nm	R_g / nm	Membrane Thickness / nm	N_{agg}	Z-average diameter / nm
$PNMEP_{28}$-$PLMA_{43}$	66 ± 23	N/A	N/A	N/A	N/A	87 ± 30
$PNMEP_{28}$-$PLMA_{65}$	155 ± 58	174 ± 61	2.5	13.4 ± 1.1	32 500	170 ± 38
$PNMEP_{28}$-$PLMA_{87}$	181 ± 40	166 ± 48	2.2	16.5 ± 2.1	26 200	195 ± 48
$PNMEP_{28}$-$PLMA_{108}$	207 ± 77	161 ± 38	2.1	18.8 ± 2.3	21 500	224 ± 63
$PNMEP_{28}$-$PLMA_{129}$	200 ± 49	153 ± 25	2.6	22.7 ± 3.3	17 600	201 ± 53
$PNMEP_{28}$-$PLMA_{151}$	212 ± 64	150 ± 28	2.1	25.1 ± 4.4	15 700	216 ± 72

[a]At least 100 particles were analysed per sample. [b]SAXS measurements were performed on 1.0% w/w copolymer dispersions diluted using an 80:20 w/w ethanol-water mixture. R_g is the radius of gyration of the coronal stabiliser (PNMEP) chains and N_{agg} is the mean vesicle aggregation number. [c]Determined by DLS for nanoparticle dispersions diluted to 0.1% w/w using 80/20 ethanol-water.

Inspecting the first entry in Table 3.2 ($PNMEP_{28}$-$PLMA_{43}$), TEM studies initially suggested a broad size distribution of spheres (see inset of Figure 3.12a) but the corresponding SAXS pattern could not be fitted to a spherical model (see Figure 3.12b). Instead, this SAXS pattern was fitted using a two-population 'vesicle plus sphere' model to obtain a mean sphere diameter of 32 nm and a vesicle diameter of 76 nm with an associated membrane thickness of 10.0 nm (Figure 3.12a).

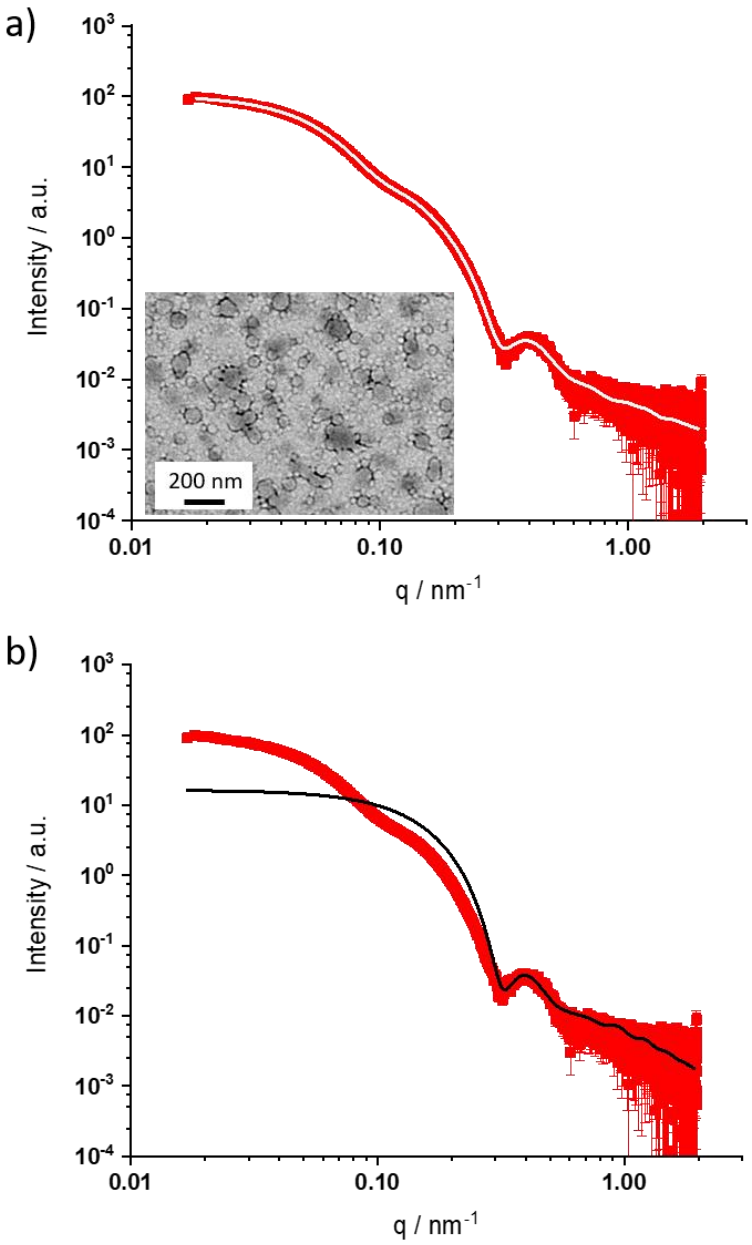

Figure 3.12. SAXS pattern recorded for a 1.0% w/w copolymer dispersion of $PNMEP_{28}$-$PLMA_{43}$ in 80:20 w/w ethanol-water at 20 °C. (a) The white line indicates the data fit obtained a spherical plus vesicle two-population model. Inset is a TEM image of the $PNMEP_{28}$-$PLMA_{43}$ diblock copolymer nanoparticles indicating the presence of small spheres and larger vesicles. (b) The solid black line indicates the unsatisfactory data fit obtained when attempting to use a spherical micelle model to fit this SAXS pattern.

TEM studies indicate an apparent increase in mean vesicle diameter when targeting higher DPs for the membrane-forming PLMA block. However, given the low T_g of the PLMA block these vesicles are expected to be rather deformable indeed there is no direct evidence for membranes in the TEM images. Moreover, the number-average vesicle diameters estimated by TEM exceed the volume-average diameters determined by SAXS. This is physically unrealistic, which again suggests significant deformation (flattening) of the original vesicle morphology during drying.

Moreover, when calculating mean TEM diameters only 100 vesicles were analysed per copolymer. Thus the TEM data are far less statistically robust than that obtained by SAXS, for which the X-ray scattering is averaged over many millions of vesicles. SAXS studies indicated a modest reduction in the mean vesicle diameter from 174 nm to 150 nm on increasing the PLMA DP (see entries 2-6 in Table 3.2). This is accompanied by a significant reduction in the vesicle polydispersity. Moreover, thicker vesicle membranes (from 13.4 nm to 25.1 nm) are obtained on increasing the PLMA DP, while there is a systematic reduction in the mean number (N_{agg}) from 32 500 to 15 700. DLS indicated a monotonic increase in vesicle diameter with increasing PLMA DP except for $PNMEP_{28}$-$PLMA_{108}$ which was slightly larger than expected. It should be noted that the polydispersity by SAXS and DLS for this particular sample was also greater than expected indicating the presence of some larger aggregates. A small volume of large aggregates has a greater effect on the diameter given by DLS as the light scattering is proportional to r^6 where r is the particle radius.[54] Interestingly, a structure peak is observed in the scattering patterns for the two most PLMA-rich diblock copolymer compositions (entries 5 and 6 in Table 3.2). This feature is tentatively assigned to lamellar stacking and suggests a mean inter-lamellar spacing of 51 and 53 nm for the PLMA DP of 129 and 151 respectively. To account for this lamella stacking, a Gaussian peak was added to the vesicle fit at 0.1 nm^{-1}.[55] However, this SAXS feature could instead indicate the presence of multilamellar vesicles. TEM analysis provides no evidence for such nano-objects but we are unable to categorically rule out this possibility.

The highly asymmetric nature of these diblock copolymers coupled with the weakly hydrophilic nature of the PNMEP stabiliser block[56] suggests that they should not be colloidally stable in water. In the previous chapter, it was shown that PNMEP could be used as an electrosteric stabiliser block for aqueous PISA syntheses.[28] However, colloidal stability was only conferred if the terminal carboxylic acid end-group on the PNMEP chain was in its ionised anionic form. Macroscopic precipitation was always observed if the aqueous solution pH was lower than pH 7. This is an example of so-called electrosteric stabilisation. In view of these prior observations, we did not expect the $PNMEP_{28}$-$PLMA_x$ nano-objects prepared in the present study to remain stable when diluted from their original 80:20 w/w ethanol-water mixture using deionised water. This is

because the CPDB RAFT agent used for such PISA syntheses does not confer any ionic end-groups to supplement the rather weak steric stabilisation provided by the non-ionic PNMEP chains. However, preliminary DLS experiments indicated that the colloidal stability of such nanoparticles was retained in dilute aqueous solution (Figure 3.13). Moreover, no aggregation was observed even when heating up to 90 °C, despite the well-documented LCST behaviour observed for PNMEP.[28,56]

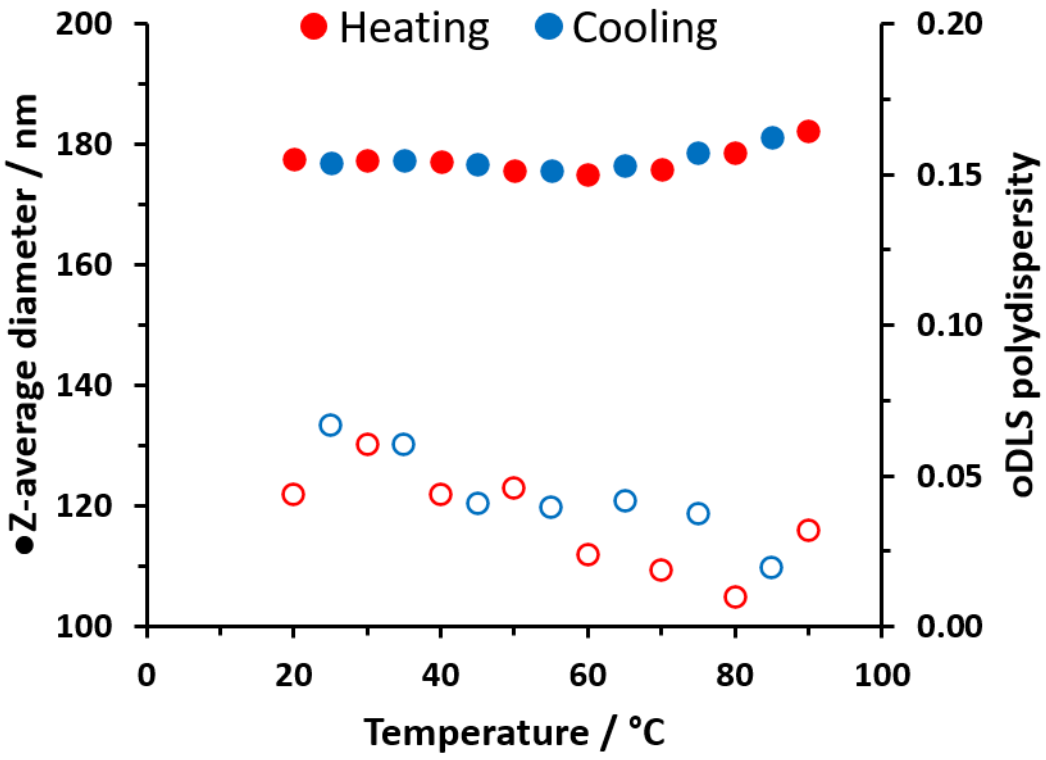

Figure 3.13. Z-average diameter obtained by DLS studies of a 0.1% w/w aqueous dispersion of $PNMEP_{28}$-$PLMA_{87}$ nanoparticles synthesised in an 80:20 w/w ethanol-water mixture on heating from 20 to 90 °C and the corresponding data on cooling from 90 to 25 °C. The z-average diameter and DLS polydispersity remains essentially constant over the entire temperature range, indicating an unexpected lack of thermoresponsive behaviour.

To better understand these unexpected observations, zeta potential measurements were undertaken. Given the non-ionic nature of the CPDB RAFT agent, the nanoparticle zeta potential was expected to be close to zero. Instead, a zeta potential of -46 mV was obtained at pH 7 (Figure 3.14). However, it is well known that a minor proportion of RAFT-synthesised polymer chains can be capped by end-groups originating from the initiator.[57] Thus, this negative surface charge is conferred by the carboxylic acid-based azo initiator (ACVA) used in the macro-CTA synthesis and this is sufficient to confer some charge stabilisation on the nanoparticles in water. Moreover, the sharp upturn in apparent particle size observed at lower pH occurs below pH 4.3. Given that the pK_a for carboxylic acid-capped non-ionic water-soluble polymer chains lies between 4.67[58] and

5.44,[28] this suggests that colloidal instability only occurs when most of the $PNMEP_{28}$ stabiliser chain-ends become protonated. In summary, the RAFT synthesis of the $PNMEP_{28}$ macro-CTA using CPDB combined with ACVA results in a significant proportion of carboxylic acid-terminated stabiliser chains, which is sufficient to account for the unexpected colloidal stability observed for the corresponding $PNMEP_{28}$-$PLMA_x$ vesicles when dispersed in dilute aqueous solution.

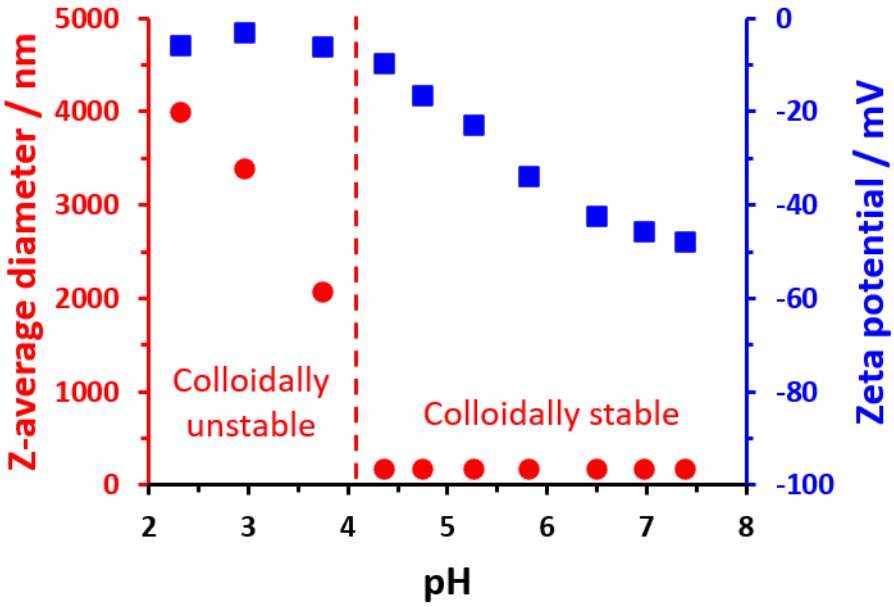

Figure 3.14. Zeta potential (■) and z-average diameter (●) *vs.* solution pH curves obtained for $PNMEP_{28}$-$PLMA_{87}$ vesicles prepared using a carboxylic acid-functionalised initiator (ACVA) for both blocks. At pH 7, the z-average diameter is 168 nm and the zeta potential is -46 mV.

3.3.2 RAFT end-group removal from PNMEP-PLMA diblock copolymer nano-objects using visible light irradiation

One well-known disadvantage of RAFT polymerisation is that the sulfur-based chain transfer agent confers both colour and malodour on the final copolymer.[59,60] In view of this, considerable effort has been devoted to the post-polymerisation removal of RAFT end-groups.[61,62] Most of these studies have involved either thermolysis or the use of selective reagents to cleave the organosulfur groups from the chain-ends.[63–66] Moreover, the vast majority of work in this area has focused on the modification of soluble chains,[67–75] with only a few studies examining RAFT end-group removal from block copolymer nano-objects.[76,77]

Mattson and co-workers used UV light (λ = 380nm) to remove terminal trithiocarbonate end-groups with a photoredox catalyst in solution (acetonitrile or *N,N*-dimethylacetamide).[73] This method was shown to be compatible with many monomer classes and did not require elevated

temperatures or deoxygenation. Discekici *et al.* were the first to report using visible light (λ = 465 nm) to remove trithiocarbonate end-groups from polystyrene chains dissolved in dichloromethane.[78] They found that using both an auxiliary amine and visible light was essential to produce a hydrogen chain-end; in the absence of light irradiation, aminolysis produced thiol end-groups.

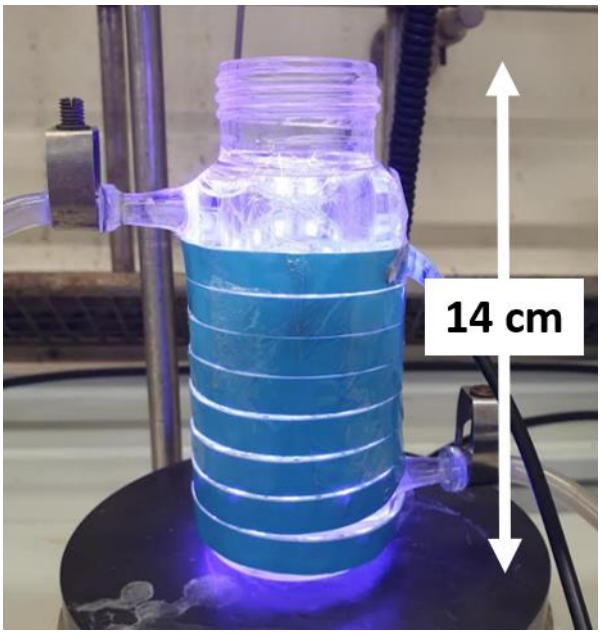

Figure 3.15. Digital photograph of the LED photoreactor used for removal of RAFT end-groups. The reactor consists of a water-jacketed Schlenk tube wrapped in blue LED light strips (λ = 405 nm, 0.37 mW cm^{-2}).

Matioszek and co-workers used ozonolysis to remove xanthate-based RAFT end-groups buried within the cores of relatively low molecular weight poly(*n*-butyl acrylate) latex particles in aqueous media.[76] Complete removal of these RAFT end-groups was observed by UV GPC analysis within 1 h at room temperature. Colloidal stability was maintained provided that the M_n of the latex was above 5 000 g mol^{-1}. Recently, Jesson *et al.* utilised H_2O_2 to remove RAFT chain-ends from aqueous dispersions of diblock copolymer nano-objects.[77] In this case, 96% removal of dithiobenzoate end-groups from weakly hydrophobic PHPMA cores was achieved within 8 h at 70 °C as judged by UV GPC analysis. However, this protocol required using excess H_2O_2 (H_2O_2/dithiobenzoate molar ratio = 5.0). Moreover, it was much more difficult to remove trithiocarbonate end-groups under the same conditions. Furthermore, removal of dithiobenzoate end-groups from PBzMA core-forming blocks proved to be problematic. Presumably, this is the result of restricted diffusion of the H_2O_2 reagent into such relatively hydrophobic nanoparticle cores. Both Matioszek and co-workers and Jesson *et al.* demonstrated that UV GPC was particularly useful for analysing the extent of removal of RAFT end-groups over time. This is

because this technique ensures separation of the copolymer chains from any UV-absorbing low MW products (*e.g.* benzoic acid) arising from chemical oxidation of the RAFT end-groups.

In view of this literature precedent, we examined the use of blue LED light (λ = 405 nm) to remove dithiobenzoate chain-ends from a 7.5% w/w aqueous dispersion of $PNMEP_{28}$-$PLMA_{87}$ diblock copolymer vesicles. This protocol was adopted because our preliminary experiments suggested that it was difficult for various chemical reagents (*e.g.* ACVA, Luperox, H_2O_2 and benzylamine) to diffuse into the highly hydrophobic PLMA membranes (see Figure 3.16 for the failed attempt to remove end-groups using excess ACVA). As far as we are aware, there are no literature reports of using visible light to remove RAFT end-groups from diblock copolymer nano-objects. In this context, it should be noted that visible light can be used to control the polymerisation of methacrylates in the absence of initiators by generating radicals by excitation of the spin-forbidden $n \rightarrow \pi^*$ transition.[79–83]

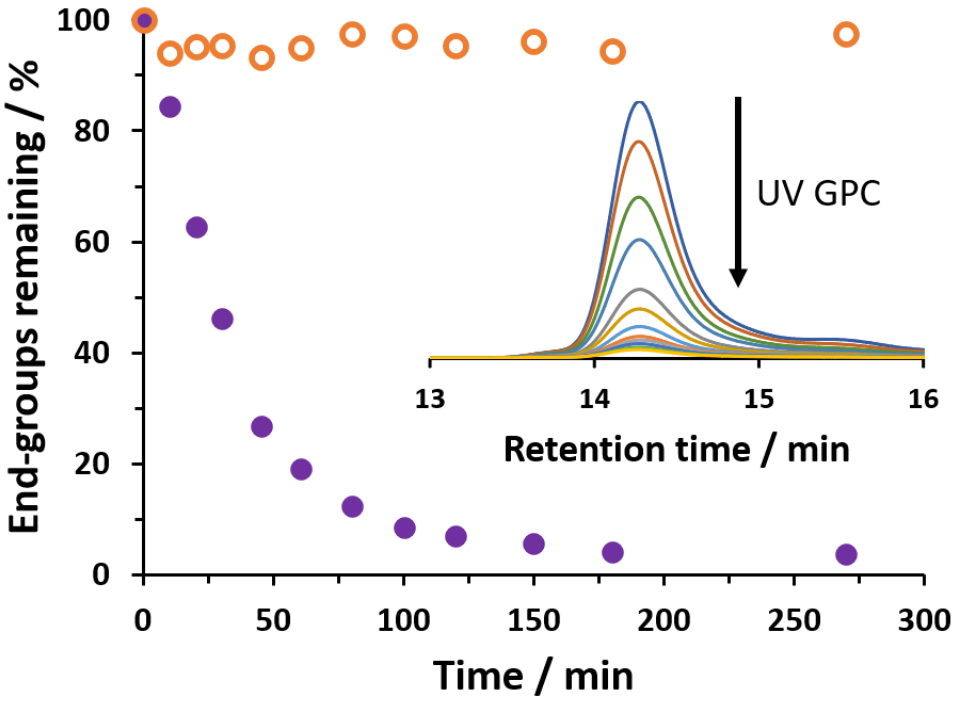

Figure 3.16. Relative reduction in dithiobenzoate end-group concentration over time for a 7.5% w/w aqueous dispersion of $PNMEP_{28}$-$PLMA_{87}$ vesicles after continuous irradiation for 4.5 h using blue LED light (λ = 405 nm, 0.37 mW cm^{-2}) at 50 °C (●) and the corresponding data when using 5 molar equivalents of H_2O_2 relative to the RAFT end-group at the same temperature (○). Inset shows the reduction in UV GPC signal over time during the LED irradiation experiment.

An aqueous dispersion of $PNMEP_{28}$-$PLMA_{87}$ diblock copolymer nanoparticles was diluted to 7.5% w/w using deionised water and exposed to 405 nm light at 50 °C with continuous stirring (Figure 3.15). The rate of RAFT end-group removal was monitored over 4.5 h using UV GPC (Figure 3.16). UV GPC chromatograms were normalised with respect to the refractive index signal. After 60 min,

81% of the RAFT end-groups were removed. After 3 h, only 4% of the original RAFT end-groups remained removing the inherent pink colour of the nanoparticle dispersion (Figure 3.17). Unlike the H_2O_2 protocol reported by Jesson and co-workers, this visible light irradiation method requires a lower temperature, significantly shorter reaction times and no additional reagents to remove more than 96% dithiobenzoate end-groups from an aqueous dispersion of methacrylic diblock copolymer nano-objects. It is perhaps also worth emphasising that the water-insoluble PLMA blocks used in the present study are significantly more hydrophobic than water-insoluble PHPMA and PBzMA blocks that comprised the cores of the nanoparticles reported by Jesson and co-workers.[77] In that prior study, ingress of the H_2O_2 reagent was relatively fast for the water-plasticised, weakly hydrophobic PHPMA cores but relatively slow for more hydrophobic PBzMA cores. This reagent mass transport problem does not apply to the LED irradiation method, allowing rapid removal of dithiobenzoate end-groups even from highly hydrophobic PLMA cores. Given the growing interest in PISA syntheses using flow chemistry, visible light could prove to be useful for removing RAFT end-groups on a large scale.[84,85]

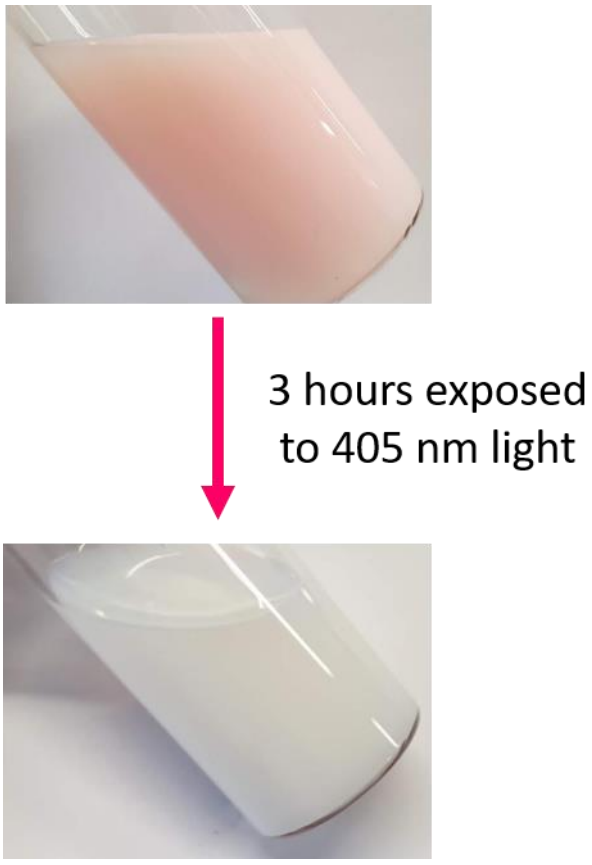

Figure 3.17. Digital photographs recorded for a 7.5% w/w aqueous dispersion of $PNMEP_{28}$-$PLMA_{87}$ vesicles recorded before (upper) and after (lower) exposure to blue LED light for 3 h at 50 °C. UV GPC studies (see Figure 3.16) confirm that this protocol is sufficient to remove almost all of the dithibenzoate end-groups, which is consistent with the observed loss in colour.

3.4 Conclusions

A $PNMEP_{28}$ macro-CTA was chain-extended with LMA in an 80:20 w/w ethanol-water mixture to produce a series of $PNMEP_{28}$-$PLMA_x$ diblock copolymer nano-objects. Despite the well-documented low T_g for the insoluble PLMA block, good-quality TEM images could be obtained for this PISA formulation. For x = 43, a mixed sphere and vesicle morphology was observed, while polydisperse vesicles were obtained for x values ranging between 65 and 151. However, no worm phase could be identified. SAXS studies confirmed the copolymer morphologies that could not be assigned by TEM alone. Slightly smaller vesicles with lower mean aggregation numbers and thicker membranes were obtained when targeting higher PLMA DPs. A minor population of sheet-like lamellae was observed for each target copolymer composition, with lamellar stacking leading to a structure peak in the scattering patterns recorded for $PNMEP_{28}$-$PLMA_{129}$ and $PNMEP_{28}$-$PLMA_{151}$. Unexpectedly, these $PNMEP_{28}$-$PLMA_x$ nanoparticles proved to be colloidally stable when diluted with deionised water to afford aqueous dispersions. Zeta potential studies indicate that such colloidal stability is conferred by initiator-derived carboxylic acid end-groups located on some of the non-ionic PNMEP stabiliser chains. Finally, 96% of the original dithiobenzoate chain-ends could be removed within 3 h at 50 °C *via* visible light irradiation of a 7.5% aqueous dispersion of $PNMEP_{28}$-$PLMA_{87}$ vesicles at a wavelength of 405 nm. This appears to be an attractive method for RAFT chain-end removal from diblock copolymer nano-objects, particularly for those with highly hydrophobic cores for which ingress of ionic reagents such as ACVA is relatively slow.

3.5 References

(1) Cunningham, V. J.; Ning, Y.; Armes, S. P.; Musa, O. M. Poly(N-2-(Methacryloyloxy)Ethyl Pyrrolidone)-Poly(Benzyl Methacrylate) Diblock Copolymer Nano-Objects via RAFT Alcoholic Dispersion Polymerisation in Ethanol. *Polymer* **2016**, *106*, 189–199.

(2) Zhang, X.; Rieger, J.; Charleux, B. Effect of the Solvent Composition on the Morphology of Nano-Objects Synthesized via RAFT Polymerization of Benzyl Methacrylate in Dispersed Systems. *Polym. Chem.* **2012**, *3*, 1502.

(3) Su, Y.; Xiao, X.; Li, S.; Dan, M.; Wang, X.; Zhang, W. Precise Evaluation of the Block Copolymer Nanoparticle Growth in Polymerization-Induced Self-Assembly under Dispersion Conditions. *Polym. Chem.* **2014**, *5*, 578–587.

(4) Gao, C.; Li, S.; Li, Q.; Shi, P.; Shah, S. A.; Zhang, W. Dispersion RAFT Polymerization: Comparison between the Monofunctional and Bifunctional Macromolecular RAFT Agents. *Polym. Chem.* **2014**, *5*, 6957–6966.

(5) Gao, C.; Wu, J.; Zhou, H.; Qu, Y.; Li, B.; Zhang, W. Self-Assembled Blends of AB/BAB Block Copolymers Prepared through Dispersion RAFT Polymerization. *Macromolecules* **2016**, *49*, 4490–4500.

(6) Jones, E. R.; Semsarilar, M.; Wyman, P.; Boerakker, M.; Armes, S. P. Addition of Water to an Alcoholic RAFT PISA Formulation Leads to Faster Kinetics but Limits the Evolution of

Copolymer Morphology. *Polym. Chem.* **2016**, *7*, 851–859.

(7) North, S. M.; Jones, E. R.; Smith, G. N.; Mykhaylyk, O. O.; Annable, T.; Armes, S. P. Adsorption of Small Cationic Nanoparticles onto Large Anionic Particles from Aqueous Solution: A Model System for Understanding Pigment Dispersion and the Problem of Effective Particle Density. *Langmuir* **2017**, *33*, 1275–1284.

(8) Van Nieuwenhove, I.; Maji, S.; Dash, M.; Van Vlierberghe, S.; Hoogenboom, R.; Dubruel, P. RAFT/MADIX Polymerization of N-Vinylcaprolactam in Water–Ethanol Solvent Mixtures. *Polym. Chem.* **2017**, *8*, 2433–2437.

(9) Tan, M.; Shi, Y.; Fu, Z.; Yang, W. *In Situ* Synthesis of Diblock Copolymer Nano-Assemblies *via* Dispersion RAFT Polymerization Induced Self-Assembly and Ag/Copolymer Composite Nanoparticles Thereof. *Polym. Chem.* **2018**, *9*, 1082–1094.

(10) Khan, H.; Cao, M.; Duan, W.; Ying, T.; Zhang, W. Synthesis of Diblock Copolymer Nano-Assemblies: Comparison between PISA and Micellization. *Polymer* **2018**, *150*, 204–213.

(11) Rubio, A.; Desnos, G.; Semsarilar, M. Nanostructured Membranes from Soft and Hard Nanoparticles Prepared via RAFT-Mediated PISA. *Macromol. Chem. Phys.* **2018**, *219*, 1800351.

(12) Fielding, L. A.; Lane, J. A.; Derry, M. J.; Mykhaylyk, O. O.; Armes, S. P. Thermo-Responsive Diblock Copolymer Worm Gels in Non-Polar Solvents. *J. Am. Chem. Soc.* **2014**, *136*, 5790–5798.

(13) Rogers, S.; Mandelkern, L. Glass Transitions of the Poly-(n-Alkyl Methacrylates). *J. Phys. Chem.* **1957**, *61*, 985–991.

(14) Lochhead, R. Y. The Role of Polymers in Cosmetics: Recent Trends. In *Cosmetic Nanotechnology*; American Chemical Society: Washington, USA, 2007; Vol. 961, pp 3–56.

(15) Zeng, F.; Zhang, L. *Water Resistant Personal Care Polymers, US9486399B2*; 2016.

(16) Zhang, J.; Zou, M.; Dong, J.; Li, X. Synthesis and Self-Assembly Behaviors of Well-Defined Poly(Lauryl Methacrylate)-Block-Poly[N-(2-Methacryloylxyethyl)Pyrrolidone] Copolymers. *Colloid Polym. Sci.* **2013**, *291*, 2653–2662.

(17) He, X.; Wang, B.; Li, X.; Dong, J. Converse Transitions between the Micelles and the Vesicles of Pyrrolidone-Based AIE Amphiphilic Copolymers in Polar and Apolar Solvents. *RSC Adv.* **2019**, *9*, 28102–28111.

(18) He, X.; Li, X.; Dong, J. Self-Assembly of Well-Defined Amphiphilic Poly(N-(2-Methacryloylxyethyl)Pyrrolidone)- Poly(Lauryl Methacrylate) Diblock Copolymers in Non-Polar Solvent. *Colloids Surfaces A Physicochem. Eng. Asp.* **2019**, *577*, 493–499.

(19) Pei, Y.; Dharsana, N. C.; Van Hensbergen, J. A.; Burford, R. P.; Roth, P. J.; Lowe, A. B. RAFT Dispersion Polymerization of 3-Phenylpropyl Methacrylate with Poly[2-(Dimethylamino)Ethyl Methacrylate] Macro-CTAs in Ethanol and Associated Thermoreversible Polymorphism. *Soft Matter* **2014**, *10*, 5787–5796.

(20) Byard, S. J.; Williams, M.; McKenzie, B. E.; Blanazs, A.; Armes, S. P. Preparation and Cross-Linking of All-Acrylamide Diblock Copolymer Nano-Objects via Polymerization-Induced Self-Assembly in Aqueous Solution. *Macromolecules* **2017**, *50*, 1482–1493.

(21) Byard, S. J.; O'Brien, C. T.; Derry, M. J.; Williams, M.; Mykhaylyk, O. O.; Blanazs, A.; Armes, S. P. Unique Aqueous Self-Assembly Behavior of a Thermoresponsive Diblock

Copolymer. *Chem. Sci.* **2020**, *11*, 396–402.

(22) Brotherton, E. E.; Hatton, F. L.; Cockram, A. A.; Derry, M. J.; Czajka, A.; Cornel, E. J.; Topham, P. D.; Mykhaylyk, O. O.; Armes, S. P. In Situ Small-Angle X-Ray Scattering Studies during Reversible Addition-Fragmentation Chain Transfer Aqueous Emulsion Polymerization. *J. Am. Chem. Soc.* **2019**, *141*, 13664–13675.

(23) Tauer, K.; Ali, A. M. I.; Yildiz, U.; Sedlak, M. On the Role of Hydrophilicity and Hydrophobicity in Aqueous Heterophase Polymerization. *Polymer.* **2005**, *46*, 1003–1015.

(24) Pei, Y.; Lowe, A. B. Polymerization-Induced Self-Assembly: Ethanolic RAFT Dispersion Polymerization of 2-Phenylethyl Methacrylate. *Polym. Chem.* **2014**, *5*, 2342–2351.

(25) Lejars, M.; Margaillan, A.; Bressy, C. Well-Defined Graft Copolymers of Tert-Butyldimethylsilyl Methacrylate and Poly(Dimethylsiloxane) Macromonomers Synthesized by RAFT Polymerization. *Polym. Chem.* **2013**, *4*, 3282.

(26) Rieger, J.; Stoffelbach, F.; Bui, C.; Alaimo, D.; Jérôme, C.; Charleux, B. Amphiphilic Poly(Ethylene Oxide) Macromolecular RAFT Agent as a Stabilizer and Control Agent in Ab Initio Batch Emulsion Polymerization. *Macromolecules* **2008**, *41*, 4065–4068.

(27) Rieger, J.; Zhang, W.; Stoffelbach, F.; Charleux, B. Surfactant-Free RAFT Emulsion Polymerization Using Poly(N,N -Dimethylacrylamide) Trithiocarbonate Macromolecular Chain Transfer Agents. *Macromolecules* **2010**, *43*, 6302–6310.

(28) Gibson, R. R.; Armes, S. P.; Musa, O. M.; Fernyhough, A. End-Group Ionisation Enables the Use of Poly(N -(2-Methacryloyloxy)Ethyl Pyrrolidone) as an Electrosteric Stabiliser Block for Polymerisation-Induced Self-Assembly in Aqueous Media. *Polym. Chem.* **2019**, *10*, 1312–1323.

(29) Ferguson, C. J.; Hughes, R. J.; Nguyen, D.; Pham, B. T. T.; Gilbert, R. G.; Serelis, A. K.; Such, C. H.; Hawkett, B. S. Ab Initio Emulsion Polymerization by RAFT-Controlled Self-Assembly. *Macromolecules* **2005**, *38*, 2191–2204.

(30) Chaduc, I.; Crepet, A.; Boyron, O.; Charleux, B.; D'Agosto, F.; Lansalot, M. Effect of the PH on the RAFT Polymerization of Acrylic Acid in Water. Application to the Synthesis of Poly(Acrylic Acid)-Stabilized Polystyrene Particles by RAFT Emulsion Polymerization. *Macromolecules* **2013**, *46*, 6013–6023.

(31) Cunningham, V. J.; Alswieleh, A. M.; Thompson, K. L.; Williams, M.; Leggett, G. J.; Armes, S. P.; Musa, O. M. Poly(Glycerol Monomethacrylate)–Poly(Benzyl Methacrylate) Diblock Copolymer Nanoparticles via RAFT Emulsion Polymerization: Synthesis, Characterization, and Interfacial Activity. *Macromolecules* **2014**, *47*, 5613–5623.

(32) Truong, N. P.; Dussert, M. V.; Whittaker, M. R.; Quinn, J. F.; Davis, T. P. Rapid Synthesis of Ultrahigh Molecular Weight and Low Polydispersity Polystyrene Diblock Copolymers by RAFT-Mediated Emulsion Polymerization. *Polym. Chem.* **2015**, *6*, 3865–3874.

(33) Akpinar, B.; Fielding, L. A.; Cunningham, V. J.; Ning, Y.; Mykhaylyk, O. O.; Fowler, P. W.; Armes, S. P. Determining the Effective Density and Stabilizer Layer Thickness of Sterically Stabilized Nanoparticles. *Macromolecules* **2016**, *49*, 5160–5171.

(34) Cockram, A. A.; Bradley, R. D.; Lynch, S. A.; Fleming, P. C. D.; Williams, N. S. J.; Murray, M. W.; Emmett, S. N.; Armes, S. P. Optimization of the High-Throughput Synthesis of Multiblock Copolymer Nanoparticles in Aqueous Media *via* Polymerization-Induced Self-Assembly. *React. Chem. Eng.* **2018**, *3*, 645–657.

(35) Jesson, C. P.; Cunningham, V. J.; Smallridge, M. J.; Armes, S. P. Synthesis of High Molecular Weight Poly(Glycerol Monomethacrylate) via RAFT Emulsion Polymerization of Isopropylideneglycerol Methacrylate. *Macromolecules* **2018**, *51*, 3221–3232.

(36) Blanazs, A.; Ryan, A. J.; Armes, S. P. Predictive Phase Diagrams for RAFT Aqueous Dispersion Polymerization: Effect of Block Copolymer Composition, Molecular Weight, and Copolymer Concentration. *Macromolecules* **2012**, *45*, 5099–5107.

(37) Derry, M. J.; Fielding, L. A.; Warren, N. J.; Mable, C. J.; Smith, A. J.; Mykhaylyk, O. O.; Armes, S. P. In Situ Small-Angle X-Ray Scattering Studies of Sterically-Stabilized Diblock Copolymer Nanoparticles Formed during Polymerization-Induced Self-Assembly in Non-Polar Media. *Chem. Sci.* **2016**, *7*, 5078–5090.

(38) Jones, E. R.; Mykhaylyk, O. O.; Semsarilar, M.; Boerakker, M.; Wyman, P.; Armes, S. P. How Do Spherical Diblock Copolymer Nanoparticles Grow during RAFT Alcoholic Dispersion Polymerization? *Macromolecules* **2016**, *49*, 172–181.

(39) Lopez-Oliva, A. P.; Warren, N. J.; Rajkumar, A.; Mykhaylyk, O. O.; Derry, M. J.; Doncom, K. E. B.; Rymaruk, M. J.; Armes, S. P. Polydimethylsiloxane-Based Diblock Copolymer Nano-Objects Prepared in Nonpolar Media via RAFT-Mediated Polymerization-Induced Self-Assembly. *Macromolecules* **2015**, *48*, 3547–3555.

(40) He, W. D.; Sun, X. L.; Wan, W. M.; Pan, C. Y. Multiple Morphologies of PAA-b-PSt Assemblies throughout RAFT Dispersion Polymerization of Styrene with PAA Macro-CTA. *Macromolecules* **2011**, *44*, 3358–3365.

(41) Wan, W. M.; Sun, X. L.; Pan, C. Y. Morphology Transition in RAFT Polymerization for Formation of Vesicular Morphologies in One Pot. *Macromolecules* **2009**, *42*, 4950–4952.

(42) Boissé, S.; Rieger, J.; Belal, K.; Di-Cicco, A.; Beaunier, P.; Li, M. H.; Charleux, B. Amphiphilic Block Copolymer Nano-Fibers via RAFT-Mediated Polymerization in Aqueous Dispersed System. *Chem. Commun.* **2010**, *46*, 1950–1952.

(43) Zehm, D.; Ratcliffe, L. P. D.; Armes, S. P. Synthesis of Diblock Copolymer Nanoparticles via RAFT Alcoholic Dispersion Polymerization: Effect of Block Copolymer Composition, Molecular Weight, Copolymer Concentration, and Solvent Type on the Final Particle Morphology. *Macromolecules* **2013**, *46*, 128–139.

(44) Yang, P.; Ratcliffe, L. P. D.; Armes, S. P. Efficient Synthesis of Poly(Methacrylic Acid)-Block-Poly(Styrene-Alt-N-Phenylmaleimide) Diblock Copolymer Lamellae Using RAFT Dispersion Polymerization. *Macromolecules* **2013**, *46*, 8545–8556.

(45) Zhang, X.; Boissé, S.; Zhang, W.; Beaunier, P.; D'Agosto, F.; Rieger, J.; Charleux, B. Well-Defined Amphiphilic Block Copolymers and Nano-Objects Formed *in Situ* via RAFT-Mediated Aqueous Emulsion Polymerization. *Macromolecules* **2011**, *44*, 4149–4158.

(46) Boissé, S.; Rieger, J.; Pembouong, G.; Beaunier, P.; Charleux, B. Influence of the Stirring Speed and CaCl2 Concentration on the Nano-Object Morphologies Obtained via RAFT-Mediated Aqueous Emulsion Polymerization in the Presence of a Water-Soluble MacroRAFT Agent. *J. Polym. Sci. Part A Polym. Chem.* **2011**, *49*, 3346–3354.

(47) Zhang, W.; D'Agosto, F.; Boyron, O.; Rieger, J.; Charleux, B. Toward a Better Understanding of the Parameters That Lead to the Formation of Nonspherical Polystyrene Particles via RAFT-Mediated One-Pot Aqueous Emulsion Polymerization. *Macromolecules* **2012**, *45*, 4075–4084.

(48) Blanazs, A.; Madsen, J.; Battaglia, G.; Ryan, A. J.; Armes, S. P. Mechanistic Insights for Block Copolymer Morphologies: How Do Worms Form Vesicles? *J. Am. Chem. Soc.* **2011**, *133*, 16581–16587.

(49) Derry, M. J.; Fielding, L. A.; Armes, S. P. Polymerization-Induced Self-Assembly of Block Copolymer Nanoparticles via RAFT Non-Aqueous Dispersion Polymerization. *Prog. Polym. Sci.* **2016**, *52*, 1–18.

(50) Yang, P.; Ratcliffe, L. P. D.; Armes, S. P. Efficient Synthesis of Poly(Methacrylic Acid)-*Block* -Poly(Styrene- *Alt* - *N* -Phenylmaleimide) Diblock Copolymer Lamellae Using RAFT Dispersion Polymerization. *Macromolecules* **2013**, *46*, 8545–8556.

(51) Yang, P.; Mykhaylyk, O. O.; Jones, E. R.; Armes, S. P. RAFT Dispersion Alternating Copolymerization of Styrene with *N* -Phenylmaleimide: Morphology Control and Application as an Aqueous Foam Stabilizer. *Macromolecules* **2016**, *49*, 6731–6742.

(52) Bang, J.; Jain, S.; Li, Z.; Lodge, T. P.; Pedersen, J. S.; Kesselman, E.; Talmon, Y. Sphere, Cylinder, and Vesicle Nanoaggregates in Poly(Styrene-b-Isoprene) Diblock Copolymer Solutions. *Macromolecules* **2006**, *39*, 5583.

(53) Glatter, O.; Kratky, O. *Small Angle X-Ray Scattering*; Academic Press: New York, USA, 1982.

(54) Stetefeld, J.; McKenna, S. A.; Patel, T. R. Dynamic Light Scattering: A Practical Guide and Applications in Biomedical Sciences. *Biophys. Rev.* **2016**, *8*, 409–427.

(55) Derry, M. J.; Mykhaylyk, O. O.; Ryan, A. J.; Armes, S. P. Thermoreversible Crystallization-Driven Aggregation of Diblock Copolymer Nanoparticles in Mineral Oil. *Chem. Sci.* **2018**, *9*, 4071–4082.

(56) Cunningham, V. J.; Derry, M. J.; Fielding, L. A.; Musa, O. M.; Armes, S. P. RAFT Aqueous Dispersion Polymerization of N -(2-(Methacryloyloxy)Ethyl)Pyrrolidone: A Convenient Low Viscosity Route to High Molecular Weight Water-Soluble Copolymers. *Macromolecules* **2016**, *49*, 4520–4533.

(57) Moad, G.; Rizzardo, E.; Thang, S. H. Toward Living Radical Polymerization. *Acc. Chem. Res.* **2008**, *41*, 1133–1142.

(58) Lovett, J. R.; Warren, N. J.; Ratcliffe, L. P. D.; Kocik, M. K.; Armes, S. P. PH-Responsive Non-Ionic Diblock Copolymers: Ionization of Carboxylic Acid End-Groups Induces an Order-Order Morphological Transition. *Angew. Chemie Int. Ed.* **2015**, *54*, 1279–1283.

(59) Perrier, S. 50th Anniversary Perspective: RAFT Polymerization A User Guide. *Macromolecules* **2017**, *50*, 7433–7447.

(60) Canning, S. L.; Smith, G. N.; Armes, S. P. A Critical Appraisal of RAFT-Mediated Polymerization-Induced Self-Assembly. *Macromolecules* **2016**, *49*, 1985–2001.

(61) Chong, Y. K.; Moad, G.; Rizzardo, E.; Thang, S. H. Thiocarbonylthio End Group Removal from RAFT-Synthesized Polymers by Radical-Induced Reduction. *Macromolecules* **2007**, *40*, 4446–4455.

(62) Willcock, H.; O'Reilly, R. K. End Group Removal and Modification of RAFT Polymers. *Polym. Chem.* **2010**, *1*, 149–157.

(63) Chong, B.; Moad, G.; Rizzardo, E.; Skidmore, M.; Thang, S. H. Thermolysis of RAFT-Synthesized Poly(Methyl Methacrylate). *Aust. J. Chem.* **2006**, *59*, 755–762.

(64) Patton, D. L.; Mullings, M.; Fulghum, T.; Advincula, R. C. A Facile Synthesis Route to Thiol-Functionalized α,ω-Telechelic Polymers via Reversible Addition Fragmentation Chain Transfer Polymerization. *Macromolecules* **2005**, *38*, 8597–8602.

(65) Carmean, R. N.; Figg, C. A.; Scheutz, G. M.; Kubo, T.; Sumerlin, B. S. Catalyst-Free Photoinduced End-Group Removal of Thiocarbonylthio Functionality. *ACS Macro Lett.* **2017**, *6*, 185–189.

(66) Cornel, E. J.; van Meurs, S.; Smith, T.; O'Hora, P. S.; Armes, S. P. In Situ Spectroscopic Studies of Highly Transparent Nanoparticle Dispersions Enable Assessment of Trithiocarbonate Chain-End Fidelity during RAFT Dispersion Polymerization in Nonpolar Media. *J. Am. Chem. Soc.* **2018**, *140*, 12980–12988.

(67) Qiu, X. P.; Winnik, F. M. Facile and Efficient One-Pot Transformation of RAFT Polymer End Groups via a Mild Aminolysis/Michael Addition Sequence. *Macromol. Rapid Commun.* **2006**, *27*, 1648–1653.

(68) Nebhani, L.; Sinnwell, S.; Inglis, A. J.; Stenzel, M. H.; Barner-Kowollik, C.; Barner, L. Efficient Surface Modification of Divinylbenzene Microspheres via a Combination of RAFT and Hetero Diels-Alder Chemistry. *Macromol. Rapid Commun.* **2008**, *29*, 1431–1437.

(69) Inglis, A. J.; Stenzel, M. H.; Barner-Kowollik, C. Ultra-Fast Raft-Hda Click Conjugation: An Efficient Route to High Molecular Weight Block Copolymersa. *Macromol. Rapid Commun.* **2009**, *30*, 1792–1798.

(70) Boyer, C.; Davis, T. P. One- Pot Synthesis and Biofunctionalization of Glycopolymers via RAFT Polymerization and Thiol-Ene Reactions. *Chem. Commun.* **2009**, No. 40, 6029–6031.

(71) Boyer, C.; Bulmus, V.; Davis, T. P. Efficient Usage of Thiocarbonates for Both the Production and the Biofunctionalization of Polymers. *Macromol. Rapid Commun.* **2009**, *30*, 493–497.

(72) Zhou, K.; Cao, H.; Gao, P.; Cui, Z.; Ding, Y.; Cai, Y. Autocatalytic Self-Sorting in Biomimetic Polymer. *Macromolecules* **2016**, *49*, 2189–2196.

(73) Mattson, K. M.; Pester, C. W.; Gutekunst, W. R.; Hsueh, A. T.; Discekici, E. H.; Luo, Y.; Schmidt, B. V. K. J.; McGrath, A. J.; Clark, P. G.; Hawker, C. J. Metal-Free Removal of Polymer Chain Ends Using Light. *Macromolecules* **2016**, *49*, 8162–8166.

(74) Lunn, D. J.; Discekici, E. H.; Read de Alaniz, J.; Gutekunst, W. R.; Hawker, C. J. Established and Emerging Strategies for Polymer Chain-End Modification. *J. Polym. Sci. Part A Polym. Chem.* **2017**, *55*, 2903–2914.

(75) Alagi, P.; Hadjichristidis, N.; Gnanou, Y.; Feng, X. Fast and Complete Neutralization of Thiocarbonylthio Compounds Using Trialkylborane and Oxygen: Application to Their Removal from RAFT-Synthesized Polymers. *ACS Macro Lett.* **2019**, *8*, 664–669.

(76) Matioszek, D.; Dufils, P. E.; Vinas, J.; Destarac, M. Selective and Quantitative Oxidation of Xanthate End-Groups of RAFT Poly(n-Butyl Acrylate) Latexes by Ozonolysis. *Macromol. Rapid Commun.* **2015**, *36*, 1354–1361.

(77) Jesson, C. P.; Pearce, C. M.; Simon, H.; Werner, A.; Cunningham, V. J.; Lovett, J. R.; Smallridge, M. J.; Warren, N. J.; Armes, S. P. H2O2 Enables Convenient Removal of RAFT End-Groups from Block Copolymer Nano-Objects Prepared via Polymerization-Induced Self- Assembly in Water. *Macromolecules* **2017**, *50*, 182–191.

(78) Discekici, E. H.; Shankel, S. L.; Anastasaki, A.; Oschmann, B.; Lee, I.-H.; Niu, J.; McGrath, A.

J.; Clark, P. G.; Laitar, D. S.; de Alaniz, J. R.; Hawker, C. J.; Lunn, D. J. Dual-Pathway Chain-End Modification of RAFT Polymers Using Visible Light and Metal-Free Conditions. *Chem. Commun.* **2017**, *53*, 1888–1891.

(79) McKenzie, T. G.; Fu, Q.; Wong, E. H. H.; Dunstan, D. E.; Qiao, G. G. Visible Light Mediated Controlled Radical Polymerization in the Absence of Exogenous Radical Sources or Catalysts. *Macromolecules* **2015**, *48*, 3864–3872.

(80) Jung, K.; Boyer, C.; Zetterlund, P. B. RAFT Iniferter Polymerization in Miniemulsion Using Visible Light. *Polym. Chem.* **2017**, *8*, 3965–3970.

(81) Carmean, R. N.; Becker, T. E.; Sims, M. B.; Sumerlin, B. S. Ultra-High Molecular Weights via Aqueous Reversible-Deactivation Radical Polymerization. *Chem* **2017**, *2*, 93–101.

(82) Lamb, J. R.; Qin, K. P.; Johnson, J. A. Visible-Light-Mediated, Additive-Free, and Open-to-Air Controlled Radical Polymerization of Acrylates and Acrylamides. *Polym. Chem.* **2019**, *10*, 1585–1590.

(83) Rubens, M.; Latsrisaeng, P.; Junkers, T. Visible Light-Induced Iniferter Polymerization of Methacrylates Enhanced by Continuous Flow. *Polym. Chem.* **2017**, *8*, 6496–6505.

(84) Lewis, R. W.; Evans, R. A.; Malic, N.; Saito, K.; Cameron, N. R. Ultra-Fast Aqueous Polymerisation of Acrylamides by High Power Visible Light Direct Photoactivation RAFT Polymerisation. *Polym. Chem.* **2018**, *9*, 60–68.

(85) Corrigan, N.; Zhernakov, L.; Hashim, M. H.; Xu, J.; Boyer, C. Flow Mediated Metal-Free PET-RAFT Polymerisation for Upscaled and Consistent Polymer Production. *React. Chem. Eng.* **2019**, *4*, 1216–1228.

Chapter 4.

RAFT dispersion polymerisation of *N,N*-dimethylacrylamide in a series of *n*-alkanes using a poly(*tert*-octyl acrylamide) steric stabiliser

Reproduced in part with permission from [Gibson, R. R.; Armes, S. P.; Musa, O. M.; Fernyhough A. RAFT dispersion polymerization of *N*,*N*-dimethylacrylamide in a series of *n*-alkanes using a thermoresponsive poly(*tert*-octyl acrylamide) steric stabilizer. *Polymer Chemistry,* **2021**, *12*, 2165-2174]

4.1 Introduction

Highly hydrophobic polymers are widely used for various applications, including self-cleaning surfaces,[1] anti-icing formulations,[2] anti-biofouling substrates[3–5] and the separation of oil and water.[6,7] *tert*-Octyl acrylamide (OAA) is a highly hydrophobic monomer that has been used as a comonomer in commercial products (*e.g.* hair-styling products).[8–10] However, there are surprisingly few reports of its homopolymerisation or physical properties in the academic literature.[11–16]

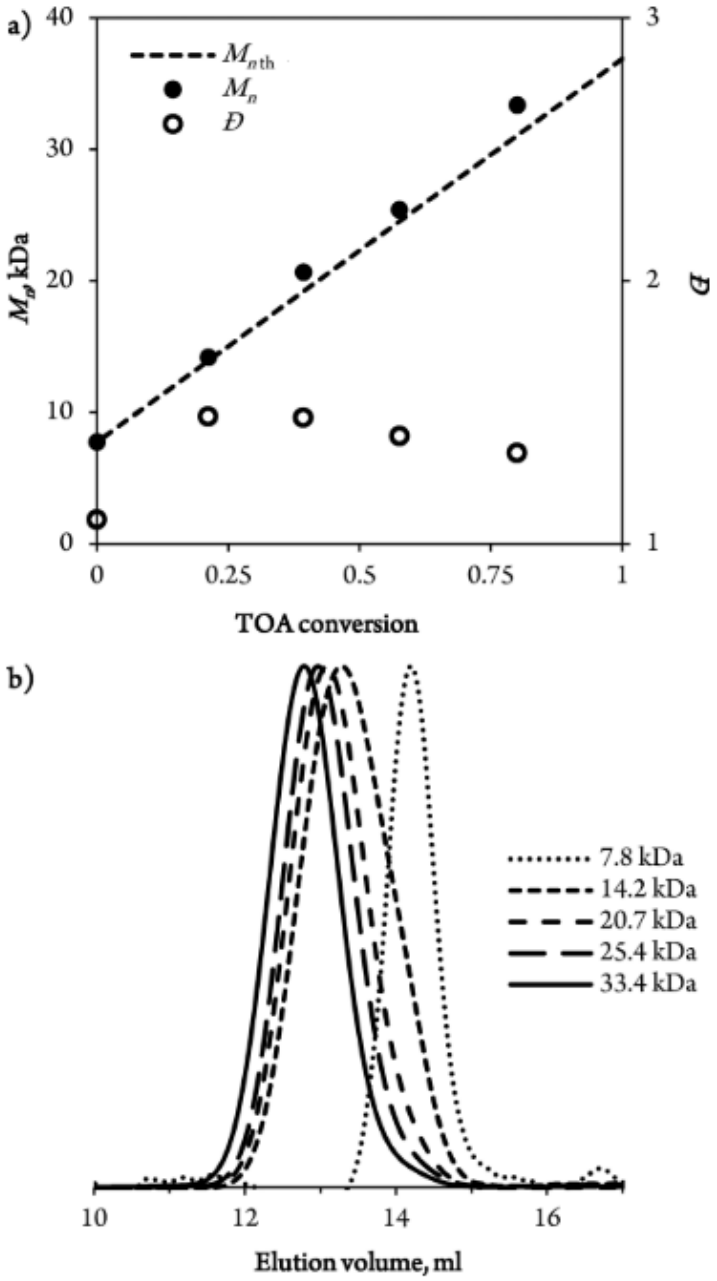

Figure 4.1. (a) Evolution of M_n and M_w/M_n with OAA conversion during the self-blocking polymerisation of POAA (7.8 kg mol^{-1}) and (b) the corresponding overlaid GPC traces.[17]

Remarkably, there appears to be only a single report of the reversible addition-fragmentation chain transfer (RAFT) solution polymerisation of OAA.[17] This involved using two tin-based RAFT agents, which enabled ^{119}Sn nuclear magnetic resonance (NMR) spectroscopy to be used to monitor chain-end fidelity during RAFT polymerisation. Chain extension experiments involving polymerisation of OAA using a POAA precursor led to around 80% within 13 h at 60 °C, while gel permeation chromatography (GPC) analysis indicated reasonably narrow molecular weight distributions (Figure 4.1).

Relatively long induction periods of up to 4.5 h were reported for such tin-based RAFT agents (Figure 4.2). In principle, using more conventional (*i.e.* metal-free) RAFT agents should enable the reaction conditions to be further optimised for the synthesis of POAA homopolymers, and perhaps also POAA-based block copolymers. This hypothesis is explored in the current study.

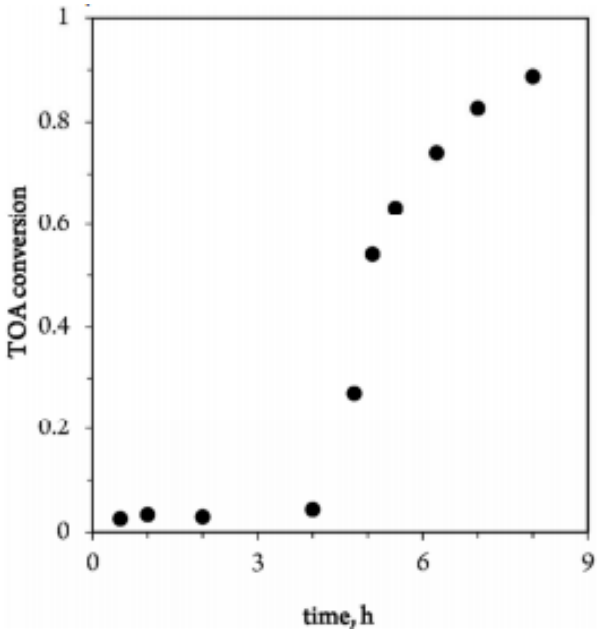

Figure 4.2. Kinetic plot for the RAFT solution polymerisation of OAA in 1,4-dioxane mediated by 1-phenylethyl triphenylstannylcarbodithioate chain transfer agent at 60 °C indicating an induction period of 4.5 h.[17]

Herein we report the synthesis of a series of well-defined POAA homopolymers *via* RAFT solution polymerisation in 1,4-dioxane and the subsequent synthesis of diblock copolymer nanoparticles *via* RAFT dispersion polymerisation of *N,N'*-dimethyl acrylamide (DMAC) in various non-polar solvents (*n*-heptane, *n*-octane, *n*-decane, *n*-dodecane, *n*-tetradecane or *n*-hexadecane). Turbidimetry studies indicated interesting differences in the temperature-dependent colloidal stability of such dispersions. An atom-efficient one-pot PISA protocol is demonstrated for the synthesis of $POAA_{82}$-$PDMAC_{100}$ nanoparticles prepared in *n*-heptane. Finally, $POAA_{85}$-$PDMAC_{150}$

were briefly evaluated for their performance as a putative Pickering emulsifier for *n*-heptane-water mixtures.

4.2 Experimental

4.2.1 Materials

tert-Octyl acrylamide (OAA; 98% purity) was kindly provided by Ashland Inc. (Delaware, USA) and was used without further purification. *N,N*-Dimethylacrylamide (DMAC), 2,2'-azobis(2-methylpropionitrile) (AIBN), 1,4-dioxane, *n*-octane, *n*-tetradecane, *n*-hexadecane, $CDCl_3$ and 2-(dodecylthiocarbonothioylthio)-2-methylpropionic acid (DDMAT) were purchased from Sigma Aldrich UK. *n*-Heptane, *n*-decane and *n*-dodecane were purchased from Alfa Aesar (Heysham, UK). Ethylene glycol diacrylate (EGDA) was purchased from Santa Cruz Biotechnology (Dallas, USA).

4.2.2 Synthesis of a $POAA_{85}$ macro-CTA by RAFT solution polymerisation of OAA in 1,4-dioxane

The protocol for the preparation of a $POAA_{85}$ macro-CTA is described below. OAA (20.11 g, 0.11 mol), DDMAT RAFT agent (0.40 g, 1.10 mmol; target DP = 100), AIBN (18.0 mg, 0.11 mmol; DDMAT/AIBN molar ratio = 10) and 1,4-dioxane (30.79 g, 40% w/w) were weighed into a 100 mL round-bottom flask and degassed under N_2 with continuous magnetic stirring for 20 min. The OAA polymerisation was allowed to proceed for 60 min in an oil bath set to 70 °C, before quenching by exposing the hot reaction solution to air while cooling to 20 °C. ^{1}H NMR spectroscopy studies indicated a final monomer conversion of 82%. The crude homopolymer was precipitated into excess methanol to remove residual OAA monomer before placing in a vacuum oven at 30 °C for three days to afford a dry yellow powder. The mean DP was calculated to be 85 by end-group analysis using UV spectroscopy (λ = 308 nm). Chloroform GPC analysis indicated an M_n of 9 900 g mol^{-1} and an M_w/M_n of 1.18 using a series of ten near-monodisperse poly(methyl methacrylate) (PMMA) calibration standards.

4.2.3 Synthesis of $POAA_{85}$-$PDMAC_x$ diblock copolymer nanoparticles *via* RAFT dispersion polymerisation of DMAC in various *n*-alkanes

A typical protocol for the synthesis of $POAA_{85}$-$PDMAC_{100}$ diblock copolymer nanoparticles in *n*-heptane was conducted as follows: $POAA_{85}$ macro-CTA (0.30 g, 18.8 µmol), DMAC (0.19 g, 1.88 mmol; target DP = 100) and AIBN (0.30 mg, 1.88 µmol; 0.03 g of a 10 mg g^{-1} stock solution of AIBN dissolved in DMAC; $POAA_{85}$/AIBN molar ratio = 10) were dissolved in *n*-heptane (1.95 g; targeting 20% w/w solids). The reaction vial was sealed and degassed *via* N_2 gas for 15 min at 20 °C before

being immersed in a pre-heated oil bath for 5 h at 70 °C. The DMAC polymerisation was quenched by exposing the hot reaction solution to air while cooling to 20 °C. The resulting diblock copolymer nanoparticles were characterised by ^{1}H NMR spectroscopy in $CDCl_3$, with 0.1% w/w dispersions being prepared by dilution with *n*-heptane for DLS and TEM studies. Chloroform GPC analysis indicated an M_n of 19 900 g mol^{-1} and an M_w/M_n of 1.19 (*vs.* a series of ten PMMA standards). Other diblock compositions were prepared by adjusting the amount of DMAC monomer to target the desired DP. For these additional syntheses, the volume of the continuous phase was adjusted to maintain an overall copolymer concentration of 20% w/w solids. ^{1}H NMR analysis indicated that at least 98% DMAC conversion was achieved in all cases. $POAA_{85}$-$PDMAC_x$ diblock copolymer nanoparticles were also prepared in *n*-octane, *n*-decane, *n*-dodecane, *n*-tetradecane and *n*-hexadecane. All synthetic parameters except for the volume of solvent were unchanged. Owing to the differing densities of these *n*-alkanes, the overall solution volume varied for these formulations.

4.2.4 One-pot synthesis of $POAA_{82}$-$PDMAC_{100}$ diblock copolymer nanoparticles *via* RAFT dispersion polymerisation of DMAC in *n*-heptane

OAA (0.40 g, 2.18 mmol), DDMAT RAFT agent (9.9 mg, 27.3 µmol; target DP = 80) and AIBN (0.40 mg, 2.7 µmol; DDMAT/AIBN molar ratio = 10) were dissolved in *n*-heptane (0.62 g; targeting 40% w/w solids) in a reaction vial. The resulting solution was then degassed for 20 min at 20 °C using a N_2 sparge before immersing the reaction vial in a pre-heated oil bath set at 70 °C. After 150 min, ^{1}H NMR studies indicated 98% OAA conversion and a mean DP of 82. Chloroform GPC analysis indicated an M_n of 8 100 g mol^{-1} and an M_w/M_n of 1.16. Next, deoxygenated *n*-heptane (3.00 mL; targeting 20% w/w solids) was added to dilute the reaction solution containing the $POAA_{82}$ macro-CTA and then deoxygenated DMAC (0.27 mL, 2.66 mmol; target DP = 100) was also added. The DMAC polymerisation was allowed to proceed for 5 h at 70 °C, resulting in a dispersion of $POAA_{82}$-$PDMAC_{100}$ diblock copolymer nanoparticles (M_n = 18 500 g mol^{-1} and M_w/M_n = 1.19 by chloroform GPC analysis using PMMA calibration standards).

4.2.5 Synthesis of core-crosslinked $POAA_{85}$-$PDMAC_{195}$-$PEGDA_{20}$ triblock copolymer nanoparticles *via* sequential RAFT dispersion polymerisation of DMAC and EGDA in *n*-heptane

A typical protocol for the synthesis of core-crosslinked $POAA_{85}$-$PDMAC_{195}$-$PEGDA_{20}$ nanoparticles was conducted as follows: $POAA_{85}$ macro-CTA (0.40 g, 25.1 µmol), DMAC (0.49 g, 4.89 mmol; target DP = 195) and AIBN (0.40 mg, 2.51 µmol; 0.04 g of a 10 mg g^{-1} stock solution of AIBN dissolved in DMAC; $POAA_{85}$/AIBN molar ratio = 10) were dissolved in *n*-heptane (3.88 g; targeting

20% w/w solids). The reaction vial was sealed and degassed under N_2 for 15 min at 20 °C before being placed in a pre-heated oil bath set at 70 °C for 195 min. EGDA (0.09 g, 0.50 mmol; target DP = 20; previously degassed with N_2 gas at 20 °C) was then added using a deoxygenated syringe/needle. EGDA polymerisation was allowed to proceed for 4 h before quenching by exposure of the hot reaction mixture to air while cooling to 20 °C. The resulting cross-linked triblock copolymer nanoparticles were diluted with *n*-heptane to afford a 0.1% w/w dispersion prior to characterisation by DLS and TEM.

4.2.6 Preparation of o/w emulsions using $POAA_{85}$-$PDMAC_{150}$ spheres

Water (2.0 mL) was homogenised with 2.0 mL of a dispersion of 0.075 – 1.000% w/w $POAA_{85}$-$PDMAC_{150}$ spheres in *n*-heptane for 2.0 min at 20 °C using an IKA Ultra-Turrax homogeniser at a shear rate of 13 500 rpm.

4.2.7 Copolymer characterisation

^{1}H NMR spectroscopy. Spectra were recorded for $POAA_x$ homopolymers and $POAA_{85}$-$PDMAC_x$ diblock copolymers dissolved in $CDCl_3$ using a 400 MHz Bruker Avance 400 spectrometer with 64 scans being averaged per spectrum.

UV spectroscopy. UV absorption spectra were recorded between 200 and 800 nm using a PC-controlled UV-1800 spectrophotometer at 25 °C equipped with a 1 cm path length cell. A Beer–Lambert curve was constructed using a series of fourteen DDMAT solutions of known concentration in chloroform. The absorption maximum at 308 nm assigned to the trithiocarbonate end-group was used for this calibration plot, and DDMAT concentrations were selected such that the absorbance at this wavelength always remained below unity. Subsequently, the mean DP for each of the five POAA homopolymers was determined using the molar extinction coefficient (ε) determined for DDMAT alone, for which ε = 15 210 ± 90 mol^{-1} dm^3 cm^{-1}.

Gel permeation chromatography (GPC). Molecular weight data for the five $POAA_x$ homopolymer precursors and the corresponding series of $POAA_{85}$-$PDMAC_x$ diblock copolymers were obtained using chloroform GPC at 35 °C, with the eluent containing 0.25% TEA by volume. Two Polymer Laboratories PL gel 5 µm Mixed C columns were connected in series to a Varian 390 multidetector suite (only the refractive index detector was used) and a Varian 290 LC pump injection module at a flow rate of 1.0 mL min^{-1}. Ten near-monodisperse PMMA standards (M_n = 625–618 000 g mol^{-1}) were used for calibration and data were analysed using Varian Cirrus GPC software supplied by the instrument manufacturer.

Dynamic light scattering (DLS). A Malvern Zetasizer NanoZS instrument was used to determine the intensity-average hydrodynamic diameter of the copolymer nanoparticles at 20 °C at a fixed scattering angle of 173°. As-synthesised dispersions were diluted to 0.1% w/w using *n*-heptane and analysed using a 1.0 cm path length glass cuvette. Data were averaged over three consecutive measurements (with 10 sub-runs per run) for each sample. Sphere-equivalent intensity-average diameters were calculated for nanoparticles using the Stokes−Einstein equation, which assumes perfectly monodisperse, non-interacting spheres.

Transmission electron microscopy (TEM). Copper/palladium grids were surface-coated in-house to produce a thin film of amorphous carbon. A 15 µL droplet of a 0.1% w/w copolymer dispersion (prepared by serial dilution using *n*-heptane) was placed on a grid using a micropipet, allowed to dry, and then stained by exposed to ruthenium(IV) oxide vapour for 7 min at 20 °C prior to analysis. A FEI Tecnai Spirit microscope operating at 80 kV and equipped with a Gatan 1kMS600CW CCD camera was used to image the nanoparticles.

Differential scanning calorimetry (DSC). Glass transition temperatures (T_g) for the five $POAA_x$ homopolymers were determined using a TA Instruments Discovery DSC 25 instrument operating from −50 °C to 120 °C at a heating/cooling rate of 10 °C min^{-1}. Each homopolymer (10 mg) was dried for at least 24 h in a vacuum oven at 30 °C prior to analysis. Dried samples were hermetically sealed in a vented aluminium pan, and the instrument was calibrated for heat flow and temperature using both indium and zinc standards. Samples were annealed at 100 °C for 5 min before cooling to −50 °C, with this latter temperature being maintained for 1 min. The T_g was then determined by heating the homopolymer up to 120 °C and determining the mid-point value. Heat flow was also monitored for *n*-dodecane alone, a 20% w/w solution of a $POAA_{85}$ homopolymer in *n*-dodecane and 20% w/w dispersions of $POAA_{85}$-$PDMAC_{150}$ diblock copolymer nanoparticles in *n*-dodecane on cooling from 120 °C to -50 °C at 10 °C min^{-1}.

Turbidimetry studies. These experiments were undertaken for $POAA_{85}$-$PDMAC_{100}$ diblock copolymer nanoparticles prepared directly in various *n*-alkanes. The corresponding *n*-alkane was used as a diluent to afford a 1.0% w/w dispersion in each case. A Varian Cary 300 Bio UV-visible spectrometer was used to record transmittance *vs.* temperature plots at a fixed wavelength of 600 nm. Each 1.0% w/w dispersion was equilibrated for 5 min at 90 °C and then cooled to either 20 or 2 °C at a rate of 1.0 °C per min with the transmittance being recorded at 1.0 °C intervals.

Optical microscopy

Optical microscopy images were recorded using a Cole–Palmer compound optical microscope equipped with an LCD tablet display and a Moticam BTW digital camera.

Laser diffraction

Each emulsion was sized by laser diffraction using a Malvern Mastersizer 3000 instrument equipped with a hydro EV wet sample dispersion unit, a red HeNe laser operating at 633 nm and a LED blue light source operating at 470 nm. The stirring rate was adjusted to 1500 rpm in order to avoid creaming of the emulsion droplets during analysis. After each measurement, the cell was rinsed once with ethanol and twice with deionised water and the laser was aligned centrally to the detector prior to data acquisition.

4.3 Results and Discussion

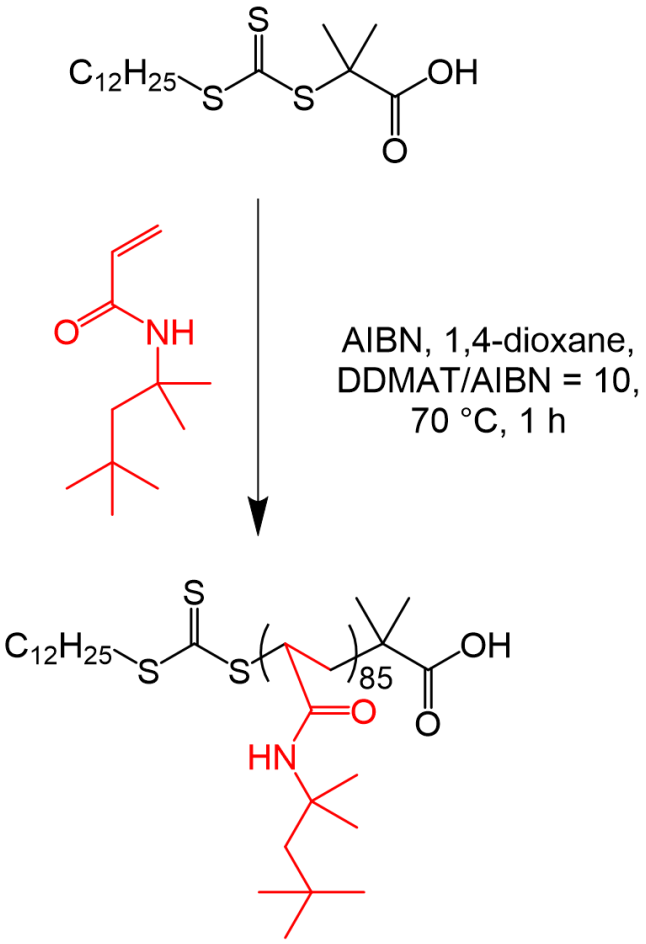

Scheme 4.1. Synthesis of a $POAA_{85}$ homopolymer by RAFT solution polymerisation of tert-octyl acrylamide (OAA) in 1,4-dioxane at 70 °C targeting 40% w/w solids.

A $POAA_{85}$ homopolymer was prepared by RAFT solution polymerisation of OAA in 1,4-dioxane at 70 °C using a DDMAT RAFT agent, see Scheme 4.1. ^{1}H NMR spectroscopy studies indicated that 82% OAA monomer conversion was achieved within 60 min and the mean DP was estimated to

be 85 by end-group analysis using unique NMR signals assigned to the RAFT chain-ends (Figure 4.3).

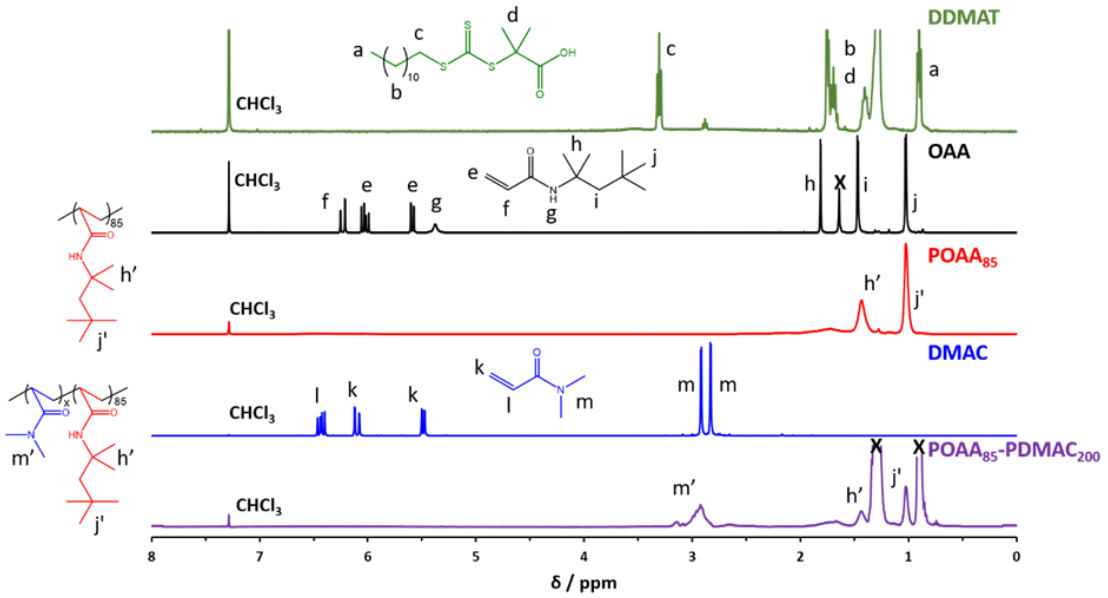

Figure 4.3. ^{1}H NMR spectra recorded in $CDCl_3$ for DDMAT RAFT agent (green), OAA monomer (black), a $POAA_{85}$ macro-CTA (red), DMAC monomer (blue) and a $POAA_{85}$-$PDMAC_{150}$ diblock copolymer (purple).

This approximate DP was confirmed by UV spectroscopy studies in chloroform. For this calculation (see Figure 4.4), it is assumed that all chains contain a trithiocarbonate end-group and the molar extinction coefficient, ε, for this chain-end is identical to that of DDMAT, for which ε = 15 210 ± 90 mol^{-1} dm^3 cm^{-1} at 308 nm. In practice, the wavelengths observed for the absorption maxima of these two species differ by just 2 nm (310 nm *vs.* 308 nm, respectively). This suggests that the corresponding molar extinction coefficients should be very similar.[18]

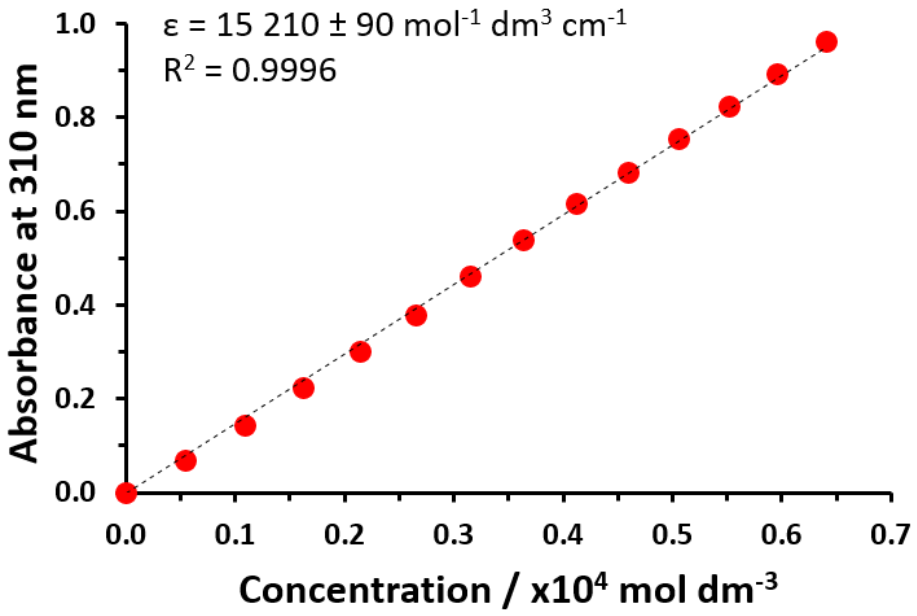

Figure 4.4. Beer-Lambert calibration plot constructed for the trithiocarbonate-based DDMAT RAFT agent in chloroform to calculate the molar extinction coefficient (ε) of the absorption maximum at 310 nm.

The mean degree of polymerisation (DP) was calculated by end-group analysis *via* UV spectroscopy using the following five equations [N.B. 'CTA' stands for chain transfer agent and 'poly' and 'mon' are shorthand for polymer and monomer, respectively]:

$$c_{CTA} = \frac{A}{\varepsilon \times l} \quad (1)$$

$$n_{CTA} = c_{CTA} \times V \quad (2)$$

$$n_{CTA} = n_{poly} \quad (3)$$

$$MW_{poly} = \left(\frac{m_{poly}}{n_{poly}}\right) - MW_{CTA} \quad (4)$$

$$DP = \frac{MW_{poly}}{MW_{mon}} \quad (5)$$

where *c* is concentration (mol dm^{-3}), *A* denotes absorbance, ε is the molar extinction coefficient (mol^{-1} dm^3 cm^{-1}), *l* is the path length (cm), *n* is the number of moles (mol), *V* is volume (dm^{-3}), *m* is mass (g) and *MW* is the molecular weight (g mol^{-1}). In this calculation, it was assumed that every polymer chain contained a RAFT end-group and that the molar extinction coefficient of the trithiocarbonate end-group on the polymer chain was identical to that of the original RAFT agent (DDMAT).

The RAFT polymerisation of OAA was also attempted using a xanthate-based chain transfer agent (CTA), (*S*)-2-(ethyl propionate)-(*O*-ethyl xanthate).[19] Unfortunately, this reaction proved to be unsuccessful as broad molecular weight distributions (M_w/M_n > 1.71) were obtained (by drip-feeding the OAA monomer into the reaction solution, *i.e.* under monomer-starved conditions), indicating little or no RAFT control.

Aliquots were periodically extracted during the RAFT homopolymerisation of OAA, with monomer conversions being determined by ^{1}H NMR spectroscopy (Figure 4.5a) and molecular weight data being obtained by GPC analysis using chloroform as an eluent. DDMAT/AIBN molar ratios of either 5 or 10 were explored, with a marginally faster rate of polymerisation being achieved when using more initiator (Figure 4.5). However, the final dispersities and conversions were very similar. Thus, using a DDMAT/AIBN molar ratio of 5.0 afforded 97% conversion, an M_n of 8 700 g mol^{-1} and an M_w/M_n of 1.18, whereas using a DDMAT/AIBN molar ratio of 10 produced 98% conversion, an M_n of 8 500 g mol^{-1} and an M_w/M_n of 1.16, see Figure 4.5b. For such homopolymerisations there was either little or no induction period (*e.g.* just 10 min when using a DDMAT/AIBN molar ratio of 10). In contrast, relatively long induction periods (up to 4.5 h) were reported for the only other literature example of the RAFT homopolymerisation of OAA.[17] Klumperman and co-workers have attributed similar observations to a so-called initialisation process.[20] This problem may well be related to the use of an organotin-based RAFT agent by Kulai and co-workers,[17] whereas a more conventional trithiocarbonate-based reagent was employed in the present study.

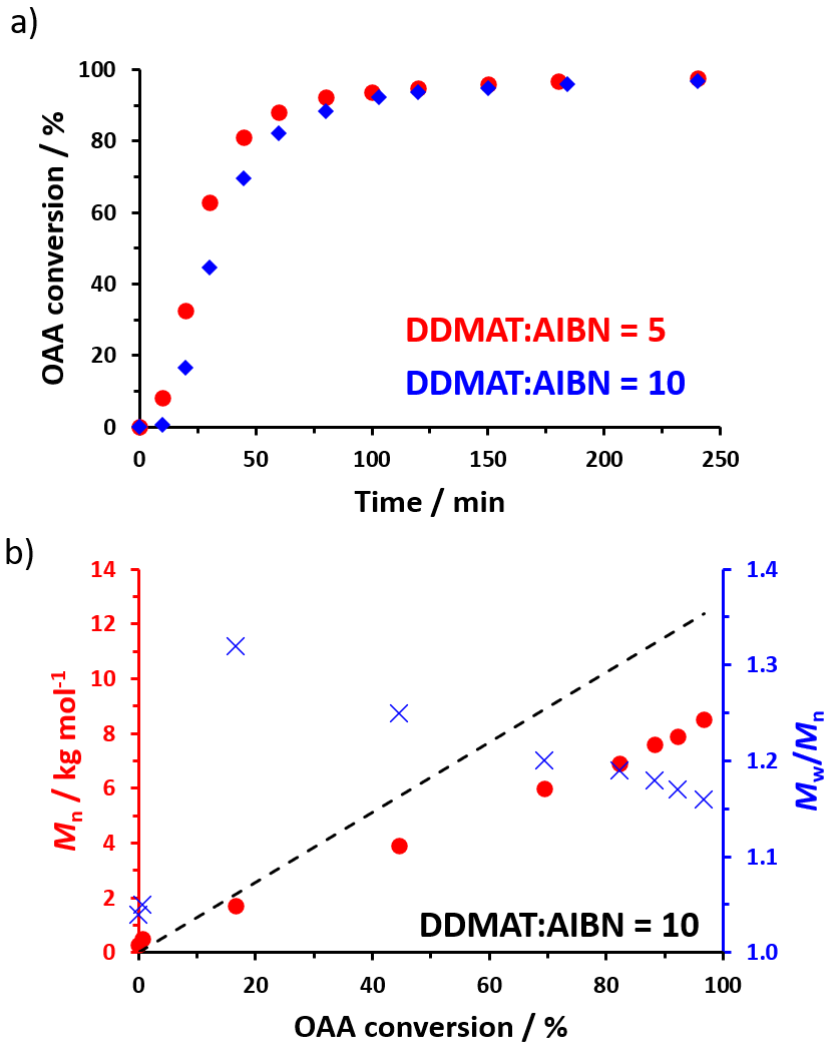

Figure 4.5. (a) Conversion *vs.* time curves obtained for the RAFT solution polymerisation of OAA at 70 °C in 1,4-dioxane using a DDMAT RAFT agent and AIBN initiator targeting a POAA DP of 70 at 40% w/w solids using a DDMAT/AIBN molar ratio of either 5 or 10. (b) Evolution of M_n and M_w/M_n with conversion observed during the RAFT solution polymerisation of OAA at 70 °C in 1,4-dioxane when targeting a POAA DP of 70 at 40% w/w solids using a DDMAT/AIBN molar ratio of 10. The dashed line indicates the theoretical M_n data. The experimental M_n data set falls below this theoretical line owing to a systematic GPC calibration error.

The T_g of each of the five $POAA_x$ homopolymers was determined using differential scanning calorimetry (DSC). The shortest homopolymer ($POAA_{22}$) had a T_g of 67 °C while the longest ($POAA_{99}$) had a T_g of 83 °C, indicating the expected weak molecular weight dependence (Figure 4.6).

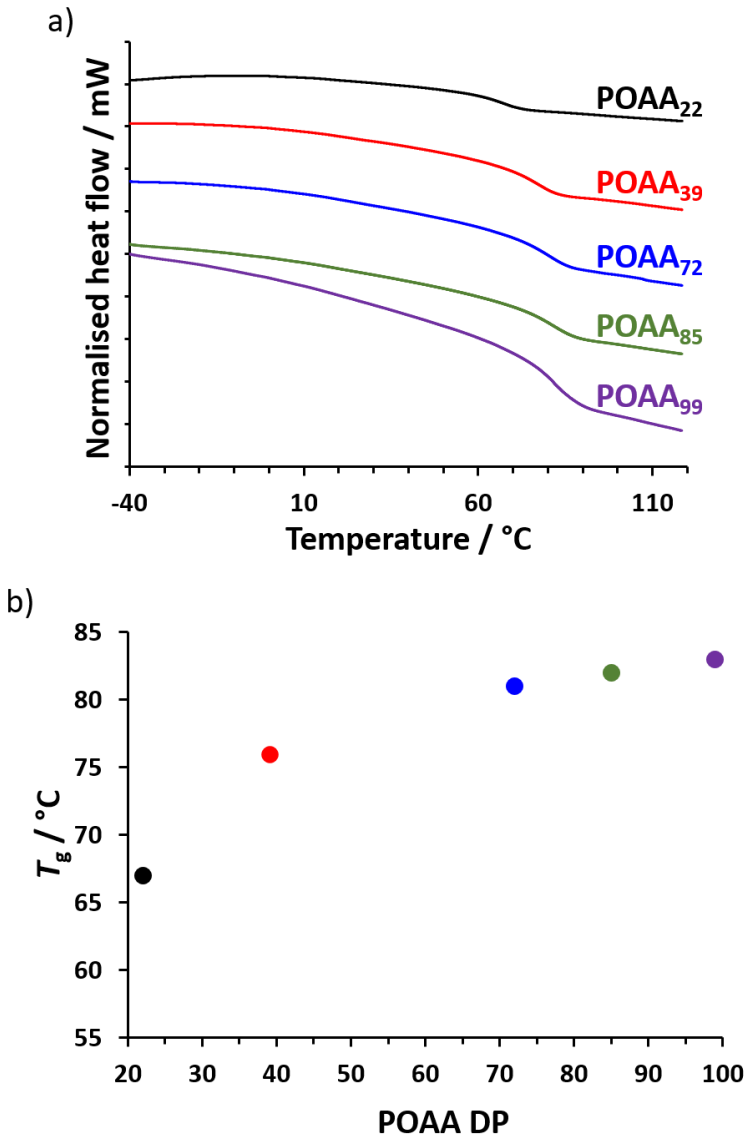

Figure 4.6. (a) Differential scanning calorimetry (DSC) traces recorded at a heating rate of 10 °C min^{-1} for a series of five $POAA_x$ homopolymers: x = 22 (black), 39 (red), 72 (blue), 85 (green) and 99 (purple). (b) Relationship between T_g and POAA DP plotted for the data shown in (a).

OAA monomer is a solid at room temperature, with DSC studies indicating a melting point of around 64 °C (see Figure 4.7). Preliminary attempts to polymerise OAA by RAFT aqueous emulsion polymerisation at 70 °C (*i.e.* above its melting point) using a water-soluble homopolymer precursor NAEP[21] were unsuccessful: there was either no polymerisation at all or OAA underwent conventional free radical polymerisation, with no RAFT control being achieved. This failure was attributed to the highly hydrophobic nature of OAA, which has five pendent methyl groups. Presumably, this means that its aqueous solubility is simply too low to enable its emulsion homopolymerisation. Similar problems are well-documented for other highly hydrophobic monomers such as LMA or SMA.[22]

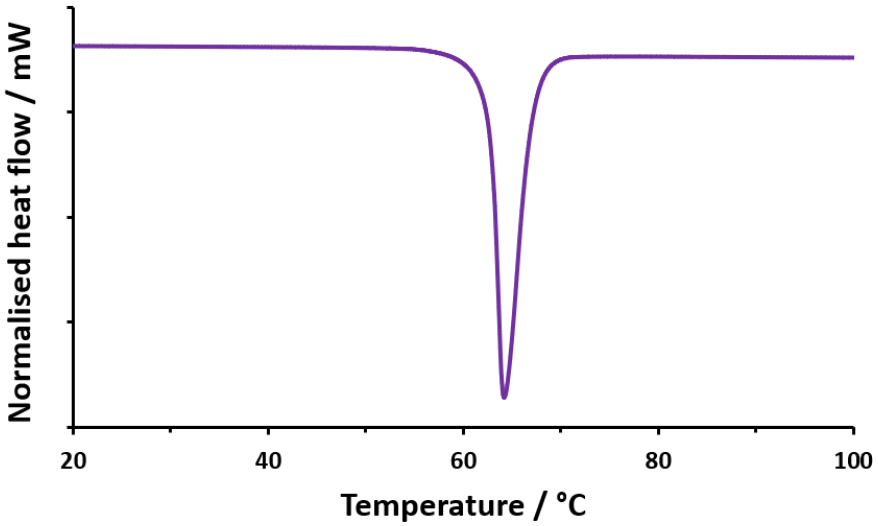

Figure 4.7. DSC curve recorded for OAA monomer (98% purity; as received from the manufacturer) indicating a melting point of approximately 64 °C.

Self-blocking studies were conducted to examine the fidelity of the RAFT chain-ends on the $POAA_{85}$ homopolymer. Accordingly, chain extension experiments targeting POAA DPs of 50, 100 or 150 were performed at 40% w/w solids in 1,4-dioxane.

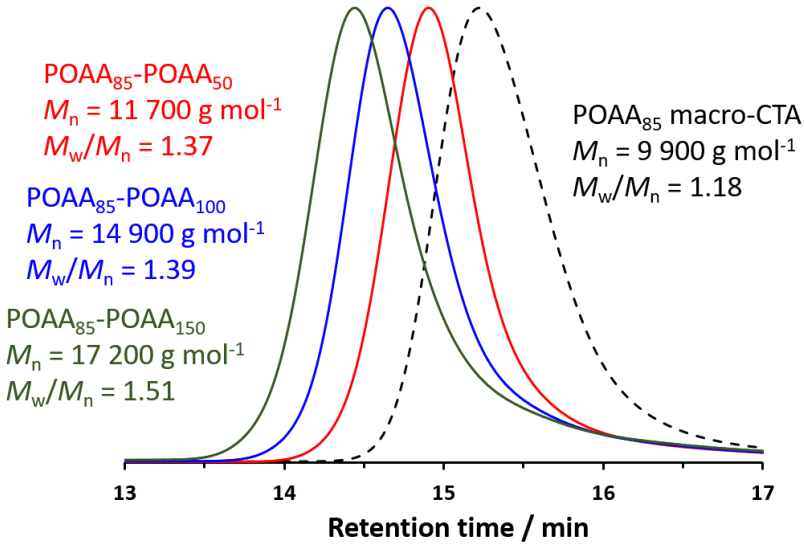

Figure 4.8. Chloroform GPC curves recorded for a $POAA_{85}$ precursor and the corresponding chain-extended $POAA_{85}$-$POAA_x$ homopolymers prepared by RAFT solution polymerisation of OAA at 70 °C in 1,4-dioxane, where x = 50 (red), 100 (blue) and 150 (green). The unimodal nature of the latter three traces indicates a relatively high blocking efficiency in each case.

In each case, more than 97% OAA conversion was achieved within 3 h at 70 °C while GPC analysis indicated that the whole MWD was shifted to higher molecular weight relative to that for the $POAA_{85}$ precursor (see Figure 4.8). Such high RAFT chain-end fidelity augurs well for the synthesis

of POAA-based diblock copolymers when using alternative acrylamides for the second-stage polymerisation. The observed increase in M_w/M_n after chain extension is comparable to that reported by Kulai and co-workers when performing self-blocking experiments.[17]

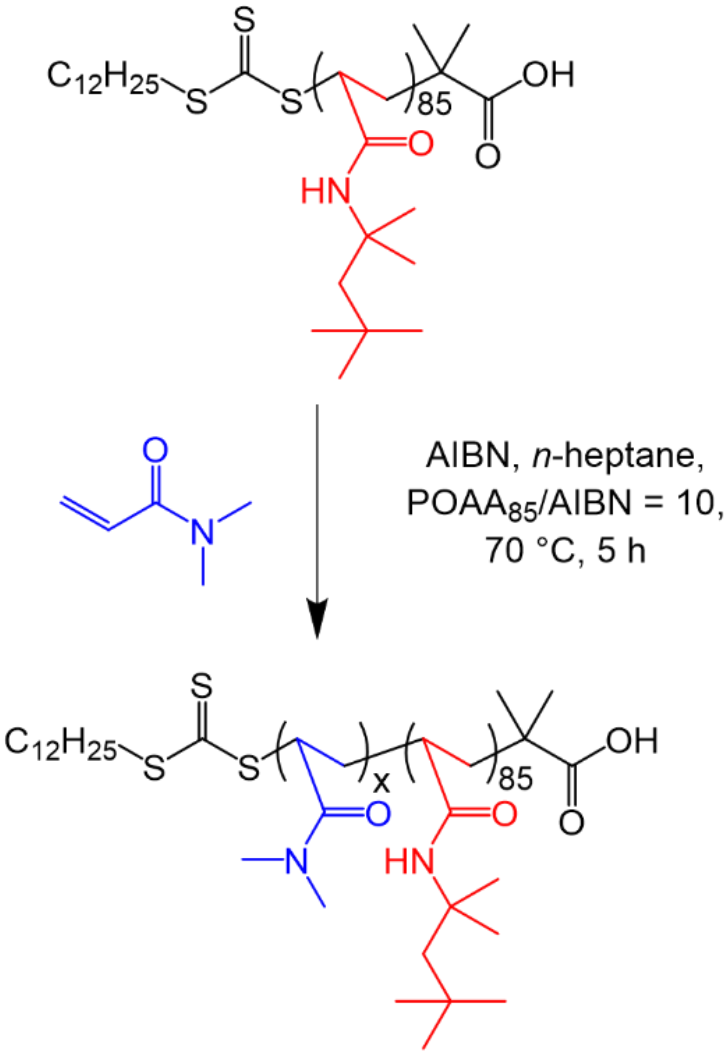

Scheme 4.2. Synthesis of a series of $POAA_{85}$-$PDMAC_x$ diblock copolymer nanoparticles by RAFT dispersion polymerisation of DMAC in *n*-heptane at 70 °C targeting 20% w/w solids.

To prepare sterically-stabilised diblock copolymer nanoparticles, the $POAA_{85}$ precursor was subsequently chain-extended *via* RAFT dispersion polymerisation of DMAC in *n*-heptane at 70 °C targeting 20% w/w solids (see Scheme 4.2). The polymerisation kinetics for this chain extension were monitored using ^{1}H NMR spectroscopy (Figure 4.9a) while chloroform GPC was used to monitor the evolution in M_n and M_w/M_n (Figure 4.9b). Essentially full DMAC conversion was achieved within 5 h with a linear increase in M_n being observed. The final $POAA_{85}$-$PDMAC_{100}$ diblock copolymer had an M_n of 21 900 g mol^{-1} and an M_w/M_n of 1.20. These data are consistent with a well-controlled RAFT polymerisation.

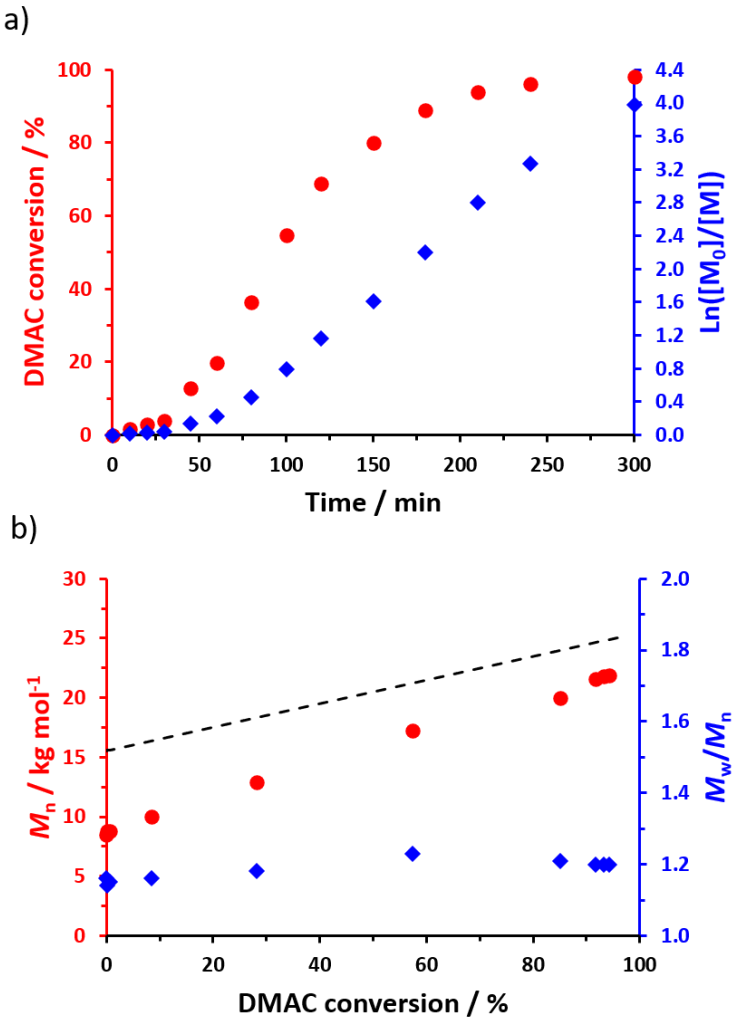

Figure 4.9. (a) Conversion *vs.* time curve with the corresponding semi-logarithmic plot obtained for the RAFT dispersion polymerisation of DMAC at 70 °C in *n*-heptane using a $POAA_{85}$ precursor and targeting a PDMAC DP of 100 at 20% w/w solids ($POAA_{85}$/AIBN molar ratio = 10). (b) Evolution of M_n and M_w/M_n with DMAC conversion for the same RAFT dispersion polymerisation. The dashed line indicates the theoretical M_n data. The experimental M_n data set falls below this theoretical line owing to a systematic GPC calibration error.

A series of $POAA_{85}$-$PDMAC_x$ diblock copolymer nanoparticles were prepared in *n*-heptane (Figure 4.10a) with a linear increase in M_n being observed when targeting higher PDMAC DPs. Reasonably good RAFT control was achieved, although a gradual increase in M_w/M_n is discernible when targeting longer PDMAC DPs. In all cases, high DMAC conversions (≥ 98%) were achieved as indicated by ^{1}H NMR analysis. A linear relationship was obtained between the z-average nanoparticle diameter determined by DLS and the target PDMAC DP up to a core DP of 175. Above a target PDMAC DP of 200, somewhat larger nanoparticles were obtained with slightly higher DLS polydispersities (Figure 4.10b). For such PISA syntheses, an increase in both nanoparticle diameter and polydispersity can indicate a (partial) change in copolymer morphology, *e.g.* the presence of some worms rather than just pure spheres.[23–27] However, close inspection of the

corresponding TEM images (Figure 4.11) did not provide any evidence for the presence of anisotropic nano-objects.

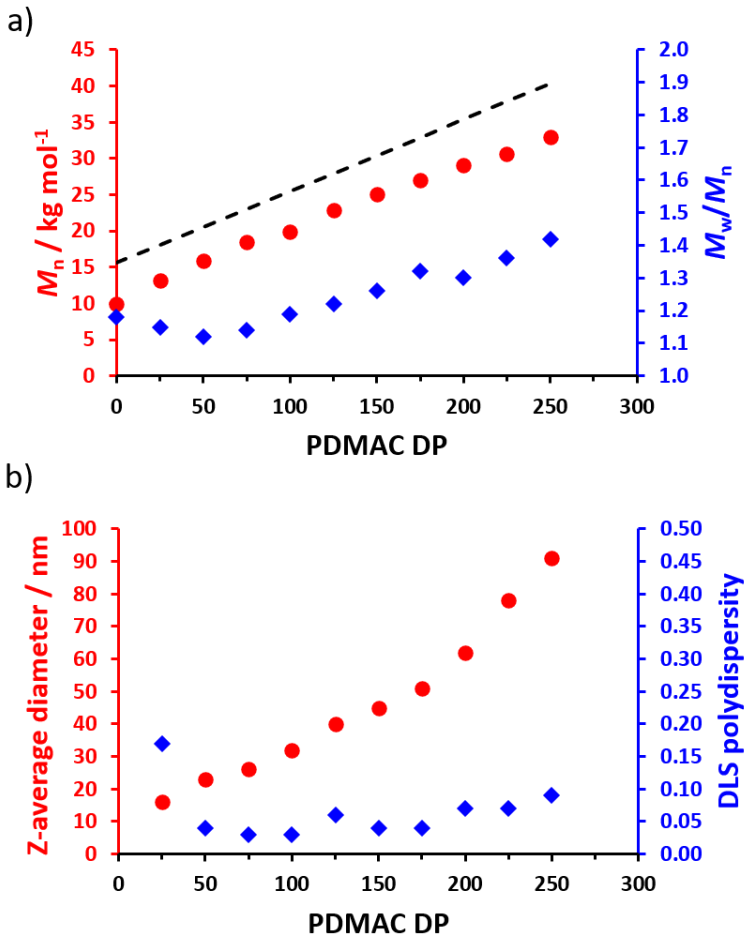

Figure 4.10. (a) Evolution in M_n and M_w/M_n with target PDMAC DP for a series of $POAA_{85}$-$PDMAC_x$ diblock copolymers (refractive index detector with calibration using a series of near-monodisperse PMMA standards). The M_n value for the corresponding $POAA_{85}$ precursor is also shown as a y-intercept. (b) Evolution in z-average diameter and DLS polydispersity with target PDMAC DP for a series of $POAA_{85}$-$PDMAC_x$ nano-objects. Each diblock copolymer dispersion was initially prepared at 20% w/w solids and then diluted to 0.1% w/w solids using *n*-heptane prior to analysis. The dashed line indicates the theoretical M_n data. The experimental M_n data set falls below this theoretical line owing to a systematic GPC calibration error.

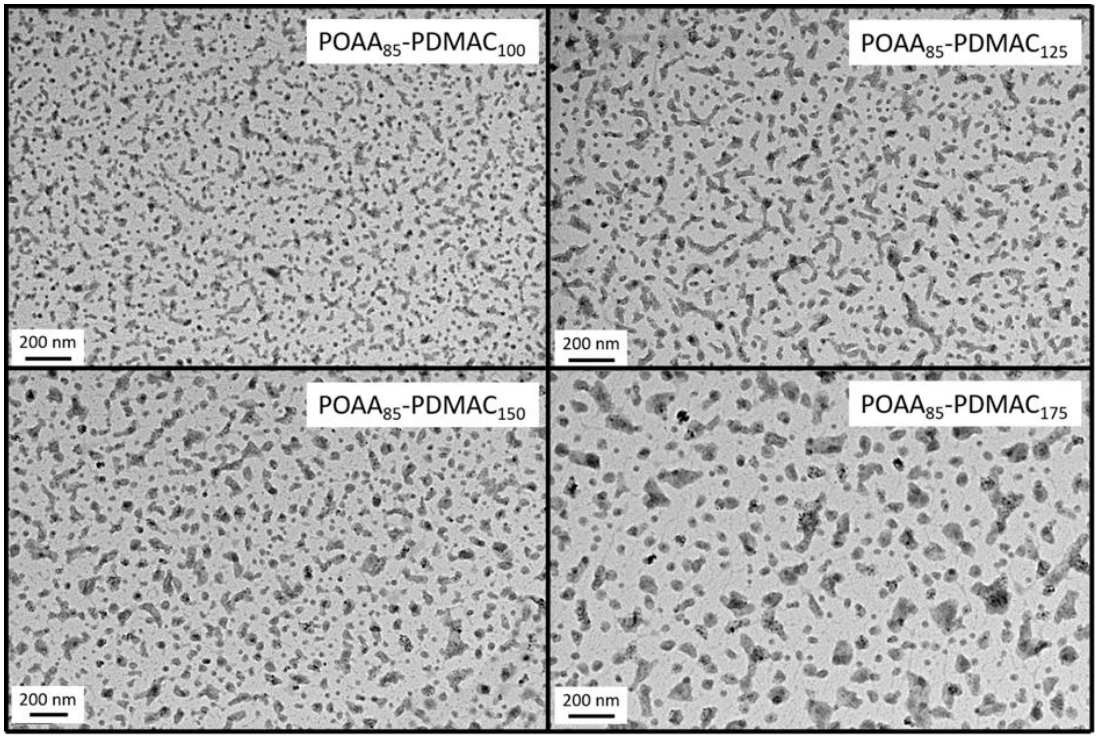

Figure 4.11. TEM images recorded for linear $POAA_{85}$-$PDMAC_x$ nano-objects to illustrate their tendency to undergo film formation on the TEM grid during sample preparation.

To examine the morphology of these $POAA_{85}$-$PDMAC_x$ nanoparticles, they were imaged using TEM (see Figure 4.11). Unfortunately, nanoparticle deformation tended to occur during drying. This problem was not foreseen because the T_g of PDMAC homopolymer has been reported to be 120 °C.[28] To address this issue, ethylene glycol diacrylate (EGDA) was added towards the end of the DMAC polymerisation when targeting a $POAA_{85}$-$PDMAC_{195}$ diblock copolymer. The resulting core-crosslinked $POAA_{85}$-$PDMAC_{195}$-$PEGDA_{20}$ triblock copolymer nano-objects were much more resistant to deformation during TEM grid preparation and exhibited a relatively well-defined spherical morphology (Figure 4.12).

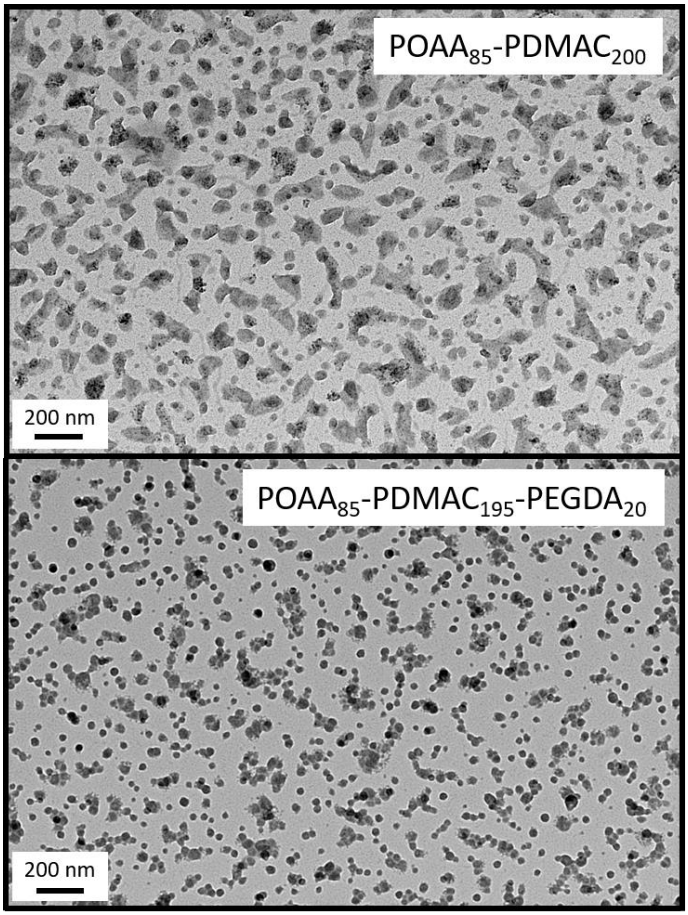

Figure 4.12. Representative TEM images recorded for linear $POAA_{85}$-$PDMAC_{200}$ and cross-linked $POAA_{85}$-$PDMAC_{195}$-$PEGDA_{20}$ nano-objects. The latter nanoparticles exhibit a relatively well-defined spherical morphology, whereas the former nanoparticles tend to undergo film formation on the TEM grid.

Moreover, the z-average diameter indicated by DLS studies of these crosslinked nanoparticles corresponded well with that observed for the comparable linear nanoparticles (65 nm *vs.* 62 nm respectively), see Table 4.1. The DLS diameter for the core-crosslinked $POAA_{85}$-$PDMAC_{195}$-$PEGDA_{20}$ spheres was also determined in chloroform. This solvent is a good solvent for both blocks, so nanogel swelling was anticipated under such conditions. Indeed, a significantly larger diameter (90 nm) was observed for such nanoparticles (Table 4.1).

Table 4.1. Summary of z-average diameters and polydispersities (PDI) determined by DLS studies of linear $POAA_{85}$-$PDMAC_{200}$ diblock copolymer nanoparticles and the corresponding core-crosslinked $POAA_{85}$-$PDMAC_{195}$-$PEGDA_{20}$ triblock copolymer nanoparticles in *n*-heptane (a poor solvent for PDMAC) and chloroform (a good solvent for PDMAC).

Target block copolymer composition	**Z-average diameter / nm (PDI)**	
	n-Heptane	Chloroform
$POAA_{85}$-$PDMAC_{200}$	62 (0.07)	/
$POAA_{85}$-$PDMAC_{195}$-$PEGDA_{20}$	65 (0.06)	90 (0.09)

To demonstrate the potential industrial relevance of such PISA formulations, an efficient one-pot synthetic protocol was developed to produce $POAA_{82}$-$PDMAC_{100}$ diblock copolymer nano-objects directly in *n*-heptane. First a $POAA_{82}$ precursor was prepared by RAFT solution polymerisation of OAA in *n*-heptane when targeting a DP of 80. An OAA conversion of 98% was achieved within 150 min with an M_n of 8 100 g mol^{-1} and an M_w/M_n of 1.16 being indicated by chloroform GPC analysis (Figure 4.13). A deoxygenated solution containing DMAC and *n*-heptane was added to this reaction solution to target $POAA_{82}$-$PDMAC_{100}$ nano-objects at 20% w/w solids. The DMAC polymerisation was allowed to proceed for 5 h at 70 °C. A final monomer conversion of more than 99% was determined by ^{1}H NMR analysis and chloroform GPC analysis indicated an M_n of 18 500 g mol^{-1} and an M_w/M_n of 1.16 for the final $POAA_{82}$-$PDMAC_{100}$ diblock copolymer chains (see Figure 4.13). The M_n and M_w/M_n data were comparable to the diblock copolymer nano-objects prepared by a two-step protocol. Similarly, the resulting spherical nanoparticles had a z-average diameter of 36 nm (DLS polydispersity = 0.20) compared to z-average diameter of 32 nm (DLS polydispersity = 0.03), see Figure 4.10b.

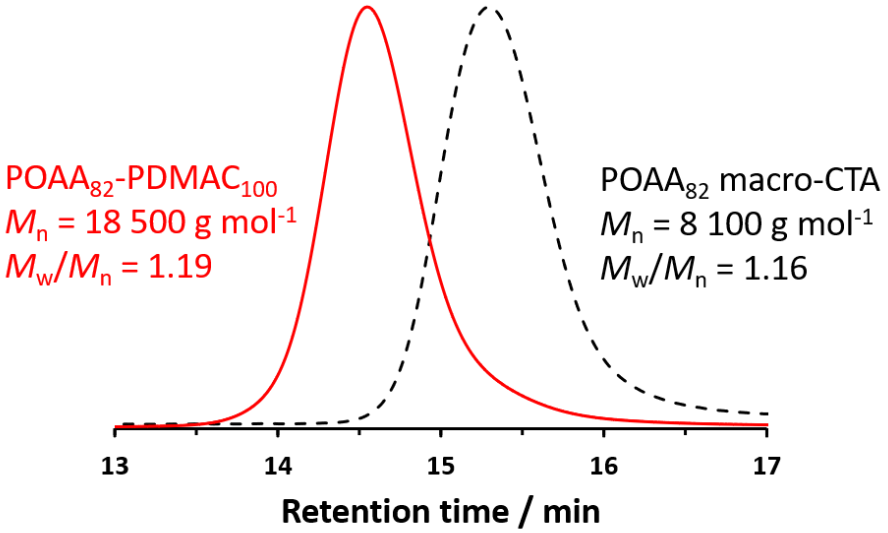

Figure 4.13. Chloroform GPC curves recorded for the initial $POAA_{82}$ precursor (98% conversion) and the final $POAA_{82}$-$PDMAC_{100}$ diblock copolymer (more than 99% conversion after 5 h at 70 °C) prepared by a one-pot protocol targeting 20% w/w solids in *n*-heptane *via* RAFT dispersion polymerisation.

The PISA synthesis of $POAA_{85}$-$PDMAC_{150}$ nanoparticles was also conducted in *n*-dodecane at 70 °C. As expected, a free-flowing turbid dispersion was observed at this reaction temperature. However, an opaque, free-standing paste was formed on cooling this 20% w/w dispersion to 20 °C (Figure 4.14).

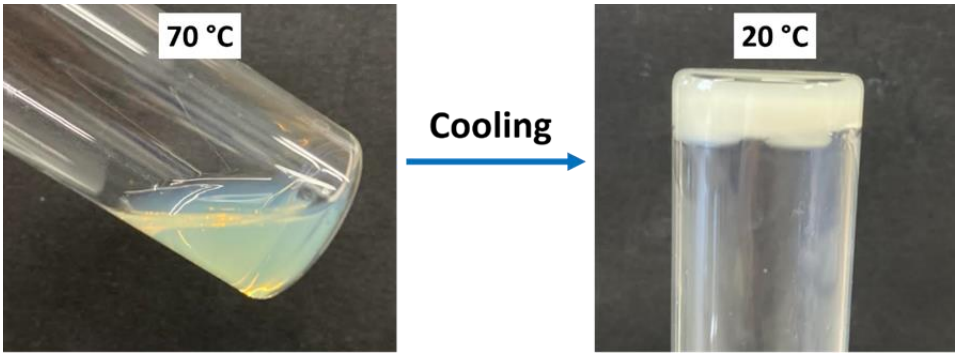

Figure 4.14. Digital photographs recorded for $POAA_{85}$-$PDMAC_{150}$ diblock copolymer nano-objects prepared in *n*-dodecane at 70 °C (reaction temperature) and at 20 °C. The increase in turbidity suggests thermoresponsive behaviour.

To further examine this unexpected behaviour, DLS particle size distributions were determined for $POAA_{85}$-$PDMAC_{150}$ nano-objects prepared in either *n*-heptane or *n*-dodecane at temperatures ranging from 80 °C to 20 °C (Figure 4.15). On cooling a dispersion of $POAA_{85}$-$PDMAC_{150}$ nanoparticles prepared in *n*-heptane, both the z-average diameter (~ 46 nm) and DLS polydispersity (~0.05) remained essentially constant across the whole temperature range. In

contrast, for the same nanoparticles prepared in *n*-dodecane, the apparent particle diameter increased dramatically from 52 nm (40-80 °C) to 276 nm (20 °C), indicating that aggregation occurs on cooling. Such aggregation was accompanied by a substantial increase in DLS polydispersity (from less than 0.10 to more than 0.57). However, this aggregation proved to be reversible on heating, indicating weak flocculation and minimal hysteresis.

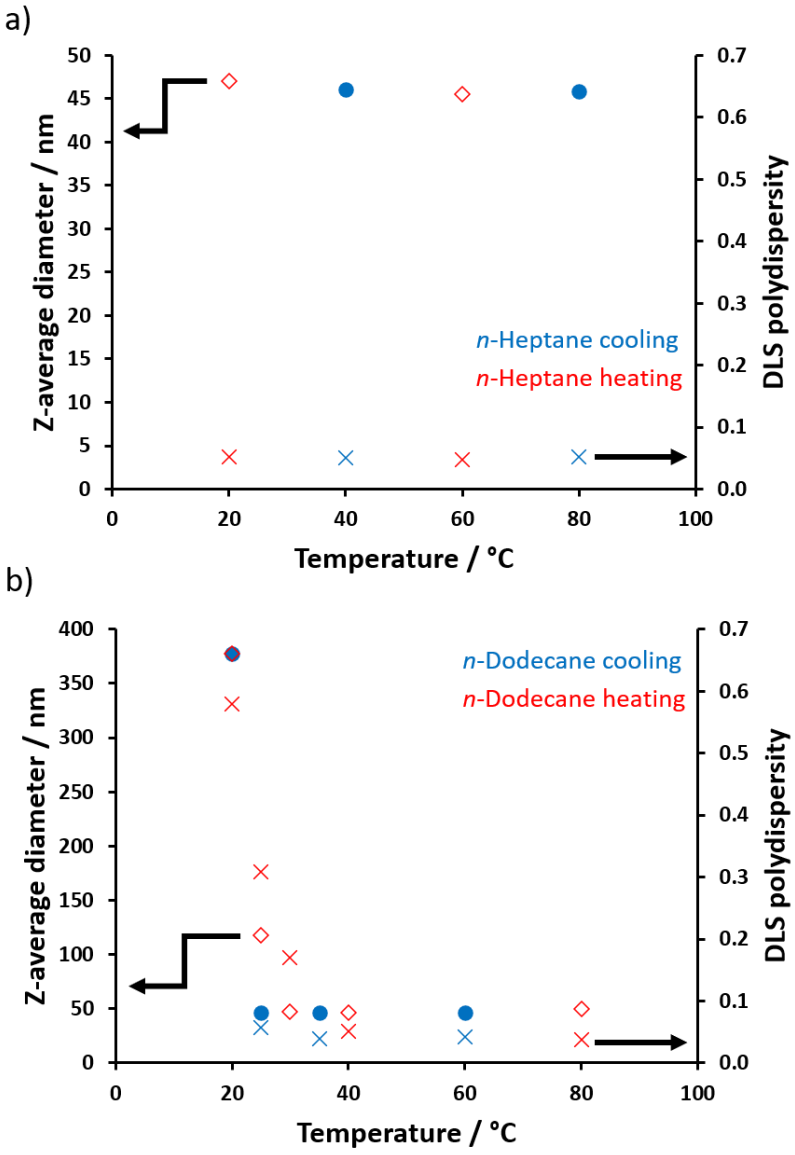

Figure 4.15. Temperature dependence of the z-average diameter and corresponding DLS polydispersity determined for the following 0.1% w/w copolymer dispersions: (a) $POAA_{85}$-$PDMAC_{150}$ nanoparticles prepared in *n*-heptane cooled from 80 to 20 °C and then heated from 20 to 80 °C; (b) $POAA_{85}$-$PDMAC_{150}$ nanoparticles prepared in *n*-dodecane cooled from 80 °C to 20 °C then heated from 20 °C to 80 °C. These DLS experiments confirm that these nanoparticles exhibit thermoreversible flocculation with minimal hysteresis in *n*-dodecane but no aggregation occurs in *n*-heptane.

In principle, such thermoresponsive behaviour might be an example of crystallisation-driven aggregation, whereby an initially stable colloidal dispersion becomes aggregated owing to

crystallisation between neighbouring steric stabiliser chains.[29] However, DSC studies indicated no crystallisation event when cooling either a 20% w/w dispersion of $POAA_{85}$-$PDMAC_{150}$ nanoparticles in *n*-dodecane or a 20% w/w solution of $POAA_{85}$ homopolymer in *n*-dodecane from 120 °C to –50 °C (see Figure 4.16). This suggests that the thermoreversible flocculation observed for the $POAA_{85}$-$PDMAC_{150}$ nanoparticles in *n*-dodecane is simply due to the upper critical solution temperature (UCST)-like behaviour of the POAA stabiliser chains, which become less solvated at lower temperature. If this is the case, then $POAA_{85}$ *homopolymer* should exhibit UCST behaviour, *i.e.* it should be soluble in *n*-dodecane at 80 °C but precipitate on cooling to 20 °C.

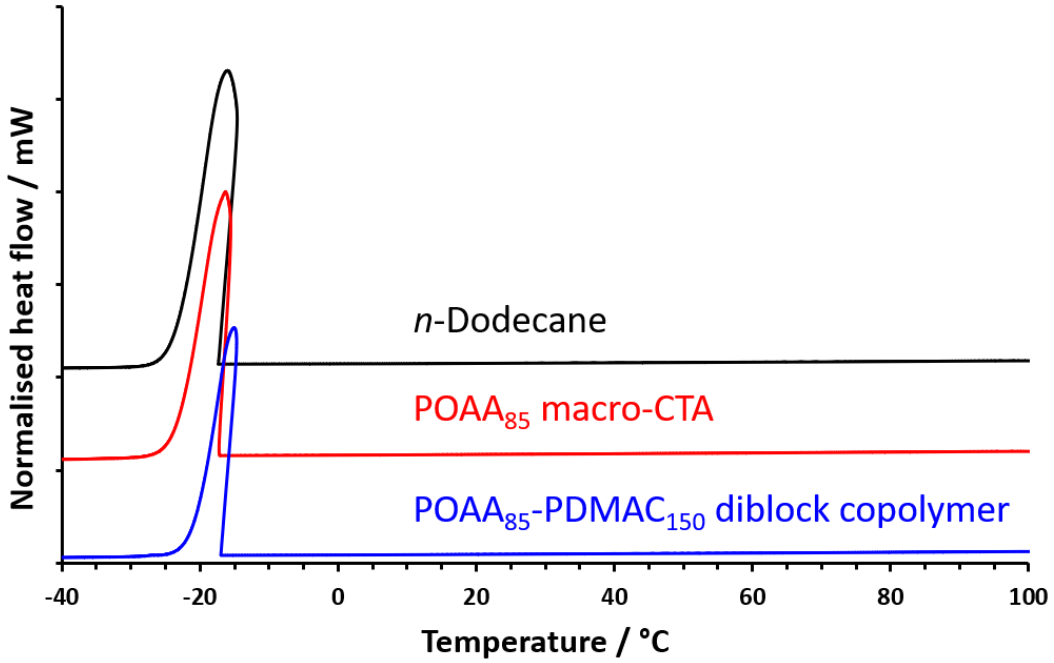

Figure 4.16. DSC curves recorded for *n*-dodecane (black), a 20% w/w solution of $POAA_{85}$ macro-CTA in *n*-dodecane (red) and a 20% w/w dispersion of $POAA_{85}$-$PDMAC_{150}$ nanoparticles in *n*-dodecane (blue) when cooling from 100 °C to –40 °C at 10 °C min^{-1}. The strong exotherm observed at around –20 °C is attributed to the freezing point of *n*-dodecane (usually observed at –9 °C but shifted in this data set owing to the relatively fast cooling rate). Importantly, these DSC curves do not provide any evidence for crystallisation of either the POAA homopolymer or POAA-stabilised nanoparticles in *n*-dodecane.

Perhaps surprisingly, turbidimetry studies conducted on $POAA_{85}$ homopolymer in various *n*-alkanes did not provide any evidence for UCST-type behaviour. More specifically, this homopolymer remained soluble between 20 and 90 °C when dissolved in *n*-heptane, *n*-octane, *n*-decane and *n*-dodecane. However, visual inspection confirms that this homopolymer is indeed insoluble in *n*-tetradecane and *n*-hexadecane at 20 °C (see Figure 4.17). Unfortunately, we have been unable to determine the critical flocculation temperature for such phase separation *via* turbidimetry.

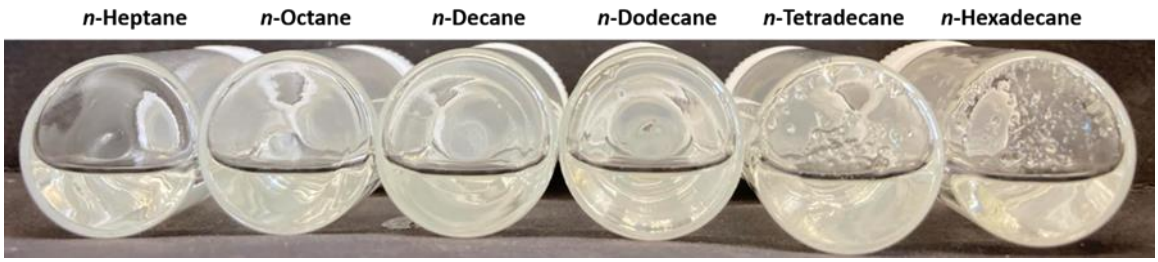

Figure 4.17. Digital photographs recorded for $POAA_{85}$ macro-CTA when added at 1.0% w/w concentration in turn to six different *n*-alkanes at 20 °C. This homopolymer is fully soluble in *n*-heptane, *n*-octane, *n*-decane and *n*-dodecane but it is clearly insoluble in *n*-tetradecane and *n*-hexadecane at this temperature.

Moreover, DSC analysis of a 50% w/w solution of $POAA_{85}$ homopolymer in either *n*-tetradecane or *n*-hexadecane indicated no UCST behaviour (Figure 4.18) when heating from –60 °C to 100 °C. Instead, only a strong endothermic peak corresponding to the melting point of the solvent is observed at 7 °C for *n*-tetradecane and 18 °C for *n*-hexadecane, respectively.

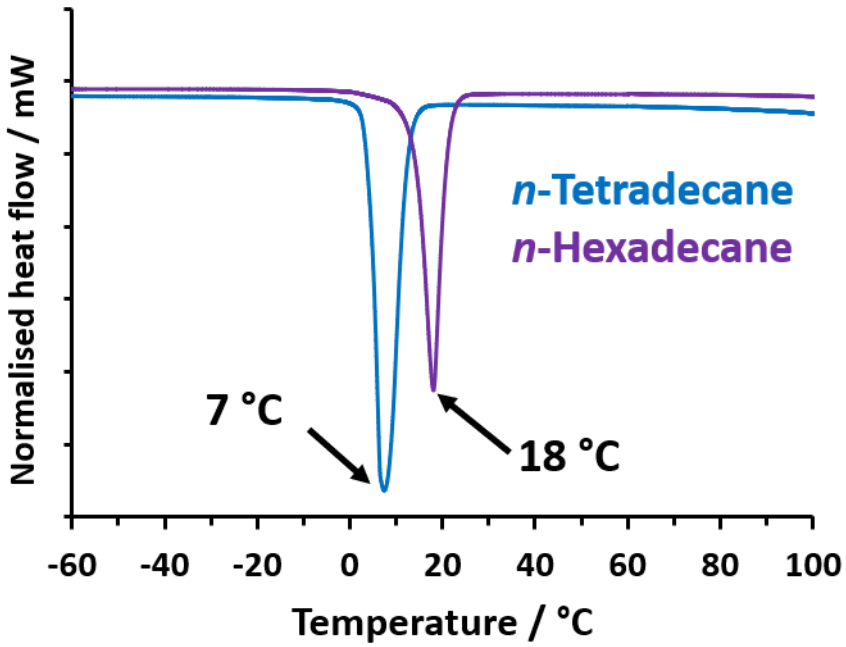

Figure 4.18. DSC curves recorded for a 50% w/w solution of $POAA_{85}$ macro-CTA in either *n*-tetradecane (blue) or *n*-hexadecane (purple) when heating from –60 °C to 100 °C at 10 °C min^{-1}. The strong endotherms observed at around 7 °C and 18 °C are assigned to the melting points of *n*-tetradecane and *n*-hexadecane, respectively.

Many polymers exhibit temperature-dependent solubility in various solvents.[30–39] For example, it is well known that poly(*N*-isopropylacrylamide) (PNIPAM) exhibits a lower critical solution temperature (LCST) of around 32 °C in aqueous solution.[40,41] In contrast, UCST behaviour is much more typical for polymers in organic solvents, with relatively few examples being reported in aqueous solution.[33] A well-documented example of a UCST system is polystyrene/cyclohexane;

this polymer is soluble in hot cyclohexane but becomes insoluble on cooling below 35 °C.[35–37] According to Imre and co-workers, styrene oligomers exhibit UCST behaviour in *n*-alkanes.[38] Similarly, poly(ethylene oxide) exhibits UCST behaviour in ethanol.[39] Moreover, several research groups have prepared so-called 'schizophrenic' diblock copolymers where UCST-type behaviour is observed for one block and LCST-type behaviour is obtained for the other block. If the UCST lies below the LCST, there is an intermediate temperature range over which the diblock copolymer chains are molecularly dissolved but two different types of micelles are formed below the UCST and above the LCST, respectively.[42–44]

$POAA_{85}$-$PDMAC_x$ nanoparticles prepared in *n*-dodecane *n*-tetradecane or *n*-hexadecane invariably formed waxy pastes on cooling, indicating UCST-like thermoreversible flocculation. To further investigate this phenomenon, $POAA_{85}$-$PDMAC_{150}$ nanoparticles were prepared directly in turn in each of the six *n*-alkanes *via* PISA.

Relatively good RAFT control (high blocking efficiencies, similar M_n values, unimodal MWDs and relatively low M_w/M_n values) was achieved during the RAFT dispersion polymerisation of DMAC using a $POAA_{85}$ macro-CTA in *n*-heptane, *n*-octane, *n*-decane, *n*-dodecane or *n*-tetradecane (Figure 4.19a). In marked contrast, only poor RAFT control (inefficient chain extension, bimodal MWD and a relatively high M_w/M_n of 1.58) was observed when the same synthetic protocol was conducted in *n*-hexadecane. Presumably, this is related to the UCST behaviour of the $POAA_{85}$ steric stabiliser block, which exhibits only marginal solubility in this solvent at 70 °C. Initially, the DMAC monomer acts as a co-solvent and ensures solubility of the $POAA_{85}$ precursor in *n*-hexadecane. However, as the DMAC polymerisation proceeds, the monomer concentration falls and the solvency gradually worsens, which leads to nanoparticle flocculation as well as loss of RAFT control. To combat this problem, the PISA synthesis of $POAA_{85}$-$PDMAC_{150}$ in *n*-hexadecane was also attempted at 90 °C, which is well above the UCST of 55 °C exhibited by the diblock copolymer nanoparticles in this solvent when cooling at 5 °C min^{-1} (see Figure 4.19b). This latter protocol produced a slightly higher M_n of 20 000 g mol^{-1} but the MWD remained bimodal and relatively broad (M_w/M_n = 1.76).

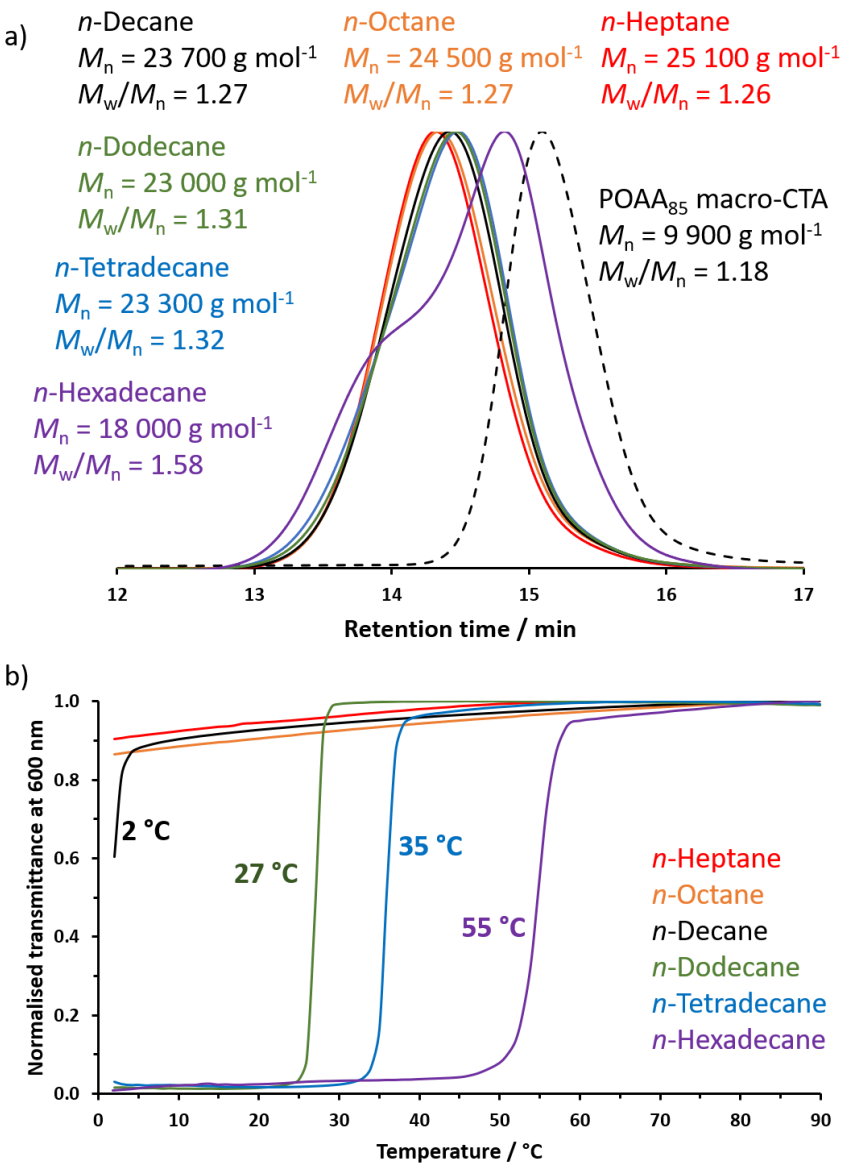

Figure 4.19. (a) Chloroform GPC curves recorded for a series of POAA$_{85}$-PDMAC$_{150}$ diblock copolymers prepared by RAFT dispersion polymerisation of DMAC using a POAA$_{85}$ precursor at 70 °C in *n*-heptane (red), *n*-octane (orange), *n*-decane (black), *n*-dodecane (green), *n*-tetradecane (blue) or *n*-hexadecane (purple). The GPC curve for the POAA$_{85}$ precursor (dashed black line) is also included as a reference. (b) Normalised transmittance (λ = 600 nm) against temperature curves recorded for 1.0% w/w dispersions of POAA$_{85}$-PDMAC$_{150}$ nanoparticles on cooling from 90 °C to 2 °C.

The turbidity of the above six POAA$_{85}$-PDMAC$_{150}$ dispersions was evaluated in turn at an arbitrary wavelength of 600 nm on cooling from 90 to 20 °C (Figure 4.19b). Initially, each of these 1.0% w/w dispersions exhibited high transmittance, indicating minimal light scattering and good colloidal stability. In the case of *n*-hexadecane, when cooling at 1 °C min^{-1} the dispersion became relatively opaque below 67 °C owing to the onset of aggregation (see Figure 4.20 for the effect cooling ramp rate has on the mid-point aggregation temperature in *n*-hexadecane). On cooling the dispersion further, the nanoparticles sedimented to the bottom of the cuvette, resulting in a

final non-zero transmittance (see inset in Figure 4.20) therefore the data shown in Figure 4.19b was recorded at a cooling ramp of 5 °C min^{-1}.

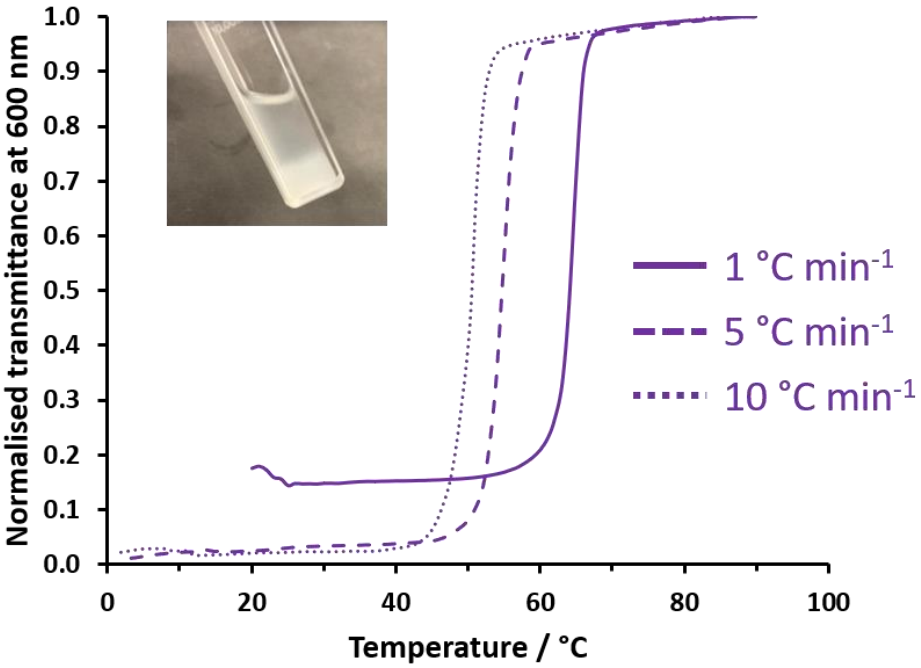

Figure 4.20. Normalised transmittance (λ = 600 nm) against temperature curves recorded for 1.0% w/w dispersions of $POAA_{85}$-$PDMAC_{150}$ nanoparticles synthesised in *n*-hexadecane on cooling from 90 °C to 20 or 2 °C at cooling ramp rates of 1, 5 and 10 °C min^{-1}. The inset image is a digital photograph of the cuvette after a 1 °C min^{-1} cooling experiment indicating macroscopic sedimentation of the copolymer nanoparticle aggregates.

In contrast, the critical flocculation temperature observed for such $POAA_{85}$-$PDMAC_{150}$ nanoparticles is approximately 35 °C in *n*-tetradecane and 27 °C in *n*-dodecane. (N.B. In all cases, nanoparticle light scattering means that such dispersions never become fully transparent even at 90 °C, hence the turbidity data have been normalised with respect to the highest transmittance value). Bearing in mind the difference in nanoparticle concentration and cooling rate, the increase in turbidity observed at around 27 °C for *n*-dodecane is reasonably consistent with the onset of flocculation indicated by DLS studies in the same solvent below 25 °C (see Figure 4.15b). The onset of nanoparticle aggregation in *n*-decane was observed below 5 °C, which is close to the minimum temperature for the instrument set-up. Accordingly, an ice bath was used to lower the temperature of this 1.0% w/w nanoparticle dispersion to –1 °C, which resulted in macroscopic precipitation (see Figure 4.21). Only minimal changes in turbidity are observed for $POAA_{85}$-$PDMAC_{150}$ nanoparticles in *n*-octane and *n*-heptane, suggesting that colloidal stability is retained in these lower *n*-alkanes.

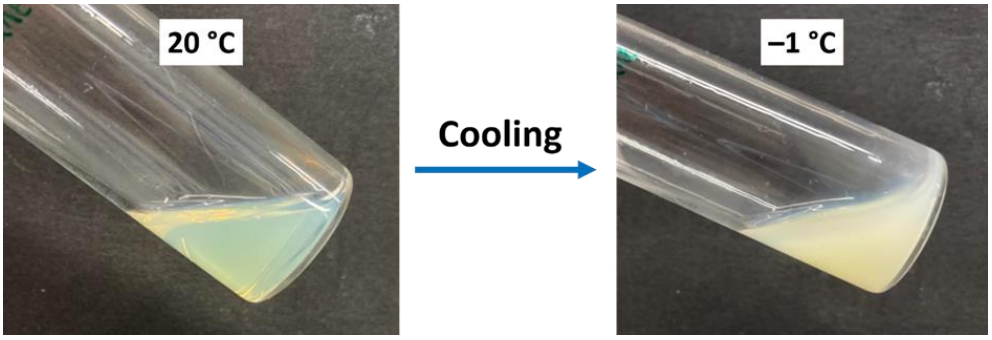

Figure 4.21. Digital photographs recorded for $POAA_{85}$-$PDMAC_{150}$ diblock copolymer nano-objects prepared in *n*-decane at 20 °C and –1 °C. The increase in turbidity suggests thermoresponsive behaviour for this dispersion.

In principle, PISA enables the rational synthesis of a wide range of sterically-stabilised diblock copolymer nano-objects of tunable surface wettability that can be used as emulsifiers instead of traditional surfactants.[45–47] Ramsden[48] and Pickering[49] were the first to demonstrate that colloidal particles can be used to stabilise emulsions (now commonly known as Pickering emulsions). There are many examples of using inorganic particles such as silica,[50,51] iron oxide,[52] titanium dioxide[53] and clays[54–56] but there are also various reports of emulsifiers based on organic copolymer latexes.[57–63] Particle adsorption at the oil-water interface reduces the effective surface area between these two immiscible liquids, which in turn lowers the free energy of the system.[64] The particle contact angle (θ) is linked to the surface wettability of the particles and normally dictates the type of emulsion that is formed.[64–66] For θ > 90°, water-in-oil (w/o) emulsions are formed because the particles are hydrophobic and so prefer to reside mainly in the oil phase. Conversely, oil-in-water (o/w) emulsions are produced when using hydrophilic particles (θ < 90°) that prefer the aqueous phase.

For example, Cunningham and co-workers prepared poly(stearyl methacrylate)-poly(2-(*N*-methacryloyloxyethyl pyrrolidone) [PSMA-PNMEP] spherical nanoparticles *via* RAFT dispersion polymerisation of NMEP in *n*-dodecane and examined their performance as putative Pickering emulsifiers.[26] Thus, on addition of an equal volume of water to a 1.0% w/w dispersion of 23 nm diameter $PSMA_{14}$-$PNMEP_{49}$ spheres in *n*-dodecane, high shear homogenisation led to the formation of oil-in-water (o/w) emulsions. This was unexpected because the original PSMA-PNMEP spheres were highly hydrophobic, which should normally favor the formation of water-in-oil (w/o) emulsions. Under high shear conditions, diblock copolymer nanoparticles have been known to dissociate into amphiphilic chains stabilising droplets like traditional surfactants.[67–69] However, closer examination of this system indicated that *in situ* nanoparticle inversion occurred during high shear homogenisation, leading to the formation of *hydrophilic* $PNMEP_{49}$-$PSMA_{14}$ nanoparticles.

Bearing in mind this prior literature,[26] the performance of these $POAA_{85}$-$PDMAC_x$ nanoparticles as putative Pickering emulsifiers was briefly investigated. Accordingly, $POAA_{85}$-$PDMAC_{150}$ nanoparticles were prepared on a three-gram scale in *n*-heptane to provide sufficient material for a series of experiments. This solvent was selected because we wanted to ensure a high degree of dispersion for the nanoparticles at ambient temperature. The nanoparticle concentration was systematically lowered from 1.0% w/w to 0.075% w/w prior to addition of deionised water and high shear homogenisation at a constant *n*-heptane volume fraction of 0.50 (Figure 4.22). The electrical conductivity for an emulsion obtained using 1.0% w/w $POAA_{85}$-$PDMAC_{150}$ copolymer was determined to be 1.85×10^{-4} S m^{-1}, which is comparable to that of deionised water alone (1.77×10^{-4} S m^{-1}). This indicates the formation of an o/w emulsion. The so-called 'drop test' method (which involves taking an aliquot of the emulsion and determining whether it disperses more readily when added to either water or *n*-heptane) was used to confirm that o/w emulsions were always produced regardless of the nanoparticle concentration.

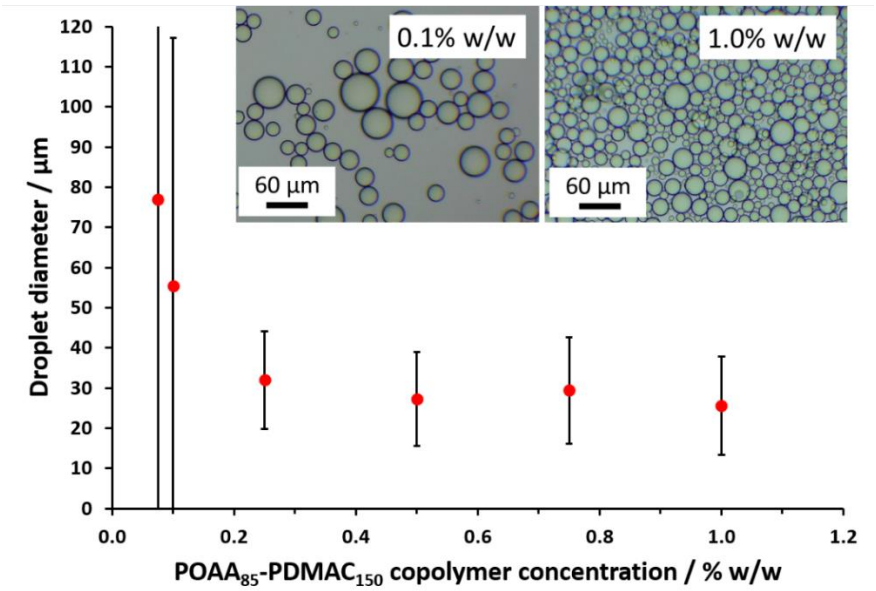

Figure 4.22. Variation in volume-average droplet diameter (as determined by laser diffraction) for a series of o/w emulsions obtained by high-shear homogenisation when systematically varying the $POAA_{85}$-$PDMAC_{150}$ nanoparticle concentration at a constant *n*-heptane volume fraction of 0.50. The error bars indicate the droplet polydispersity rather than the error in the measurements. Inset: optical micrographs recorded at nanoparticle concentrations of 0.1% and 1.0% w/w, respectively.

Laser diffraction was used to size these emulsions (see Figure 4.22). At higher nanoparticle concentrations, the volume-average droplet diameter remained constant at around 25-30 µm. However, both the mean droplet diameter and the standard deviation increased when nanoparticle concentrations were reduced below 0.25% w/w. Relatively large, polydisperse droplets with relatively poor stability towards droplet coalescence were obtained at the lowest

nanoparticle concentration investigated (0.075% w/w). The upturn in droplet size at lower nanoparticle concentration is characteristic of a genuine Pickering emulsion.[26,69–71]This implies that the original linear $POAA_{85}$-$PDMAC_{150}$ nanoparticles survive the high-shear homogenisation conditions intact. However, in view of the highly hydrophobic nature of these nanoparticles, we had expected the formation of w/o Pickering emulsions, rather than o/w emulsions. In principle, there are two possible explanations for this surprising observation. First, *in situ* nanoparticle inversion might have occurred during homogenisation, thus converting the *hydrophobic* $POAA_{85}$-$PDMAC_{150}$ nanoparticles into *hydrophilic* $PDMAC_{150}$-$POAA_{85}$ nanoparticles (see Figure 4.23a). This transformation would certainly account for the formation of an o/w Pickering emulsion. Moreover, as discussed above, Cunningham and co-workers provides a useful precedent for the inversion of similar linear diblock copolymer nanoparticles under comparable conditions.[26] Alternatively, it is perfectly feasible that the hydrophobic $POAA_{85}$-$PDMAC_{150}$ nanoparticles simply adsorb at the *inner surface* of the oil droplets (see Figure 4.23b).[72] It should be noted that the DDMAT RAFT agent that was used to synthesise the diblock copolymers confers a carboxylic acid group to the terminus of the POAA stabiliser block. This hydrophilic group may become ionised in the aqueous phase resulting in stabilisation of the droplets due to electrostatic repulsion, preventing their coalescence.

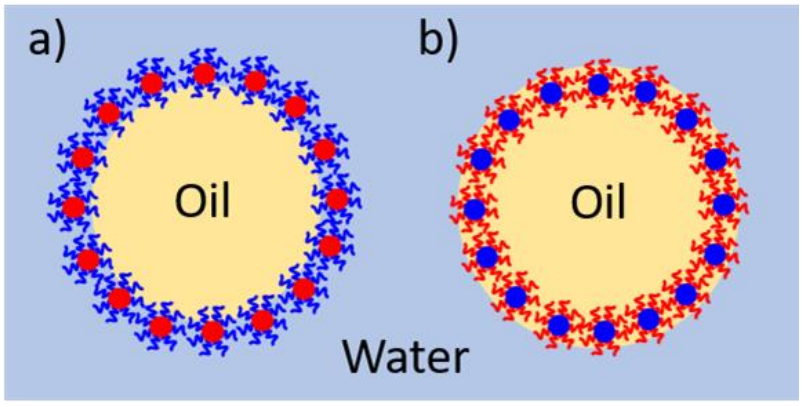

Figure 4.23. Schematic representation of the two possible explanations for the o/w Pickering emulsions that are formed after high-shear homogenisation of an equal volume of deionised water and a 1.0% w/w dispersion of *hydrophobic* $POAA_{85}$-$PDMAC_{150}$ nanoparticles in *n*-heptane. (a) *In situ* nanoparticle inversion during homogenisation produces *hydrophilic* $PDMAC_{150}$-$POAA_{85}$ nanoparticles that then adsorb at the outer surface of the oil droplets. (b) The original *hydrophobic* $POAA_{85}$-$PDMAC_{150}$ nanoparticles adsorb at the *inner surface* of the oil droplets. The experimental data suggest that the second explanation is most likely to be correct. [N.B. Both schematic cartoons have been simplified for clarity. In scenario A, the excess (non-adsorbed) hydrophilic nanoparticles in the aqueous continuous phase have been omitted. Similarly, the excess (non-adsorbed) hydrophobic particles present within the oil droplet are not shown in scenario B].

To distinguish between these two scenarios, core-crosslinked $POAA_{85}$-$PDMAC_{195}$-$PEGDA_{20}$ nanoparticles were used to prepare Pickering emulsions (Figure 4.24). DLS studies confirmed that, unlike the corresponding linear nanoparticles, such nanoparticles swelled appreciably but did not

dissolve when diluted with chloroform, which is a good solvent for both blocks (see Table 4.1). Again, the nanoparticle concentration was systematically lowered from 1.0% w/w to 0.075% w/w when performing high-shear homogenisation at a constant oil volume fraction of 0.50. The 'drop test' method confirmed the formation of o/w emulsions in all cases. Moreover, an upturn in droplet diameter was observed at lower nanoparticle concentrations, which is characteristic of Pickering emulsions.[71,73] Importantly, such core-crosslinked nanoparticles cannot undergo inversion to form *hydrophilic* PDMAC-stabilised nanoparticles that might adsorb at the outer surface of the oil droplets (see Figure 4.23a). Thus, we conclude that the original linear *hydrophobic* $POAA_{85}$-$PDMAC_{150}$ nanoparticles must instead adsorb at the *inner surface* of the oil droplets, (see Figure 4.23b).

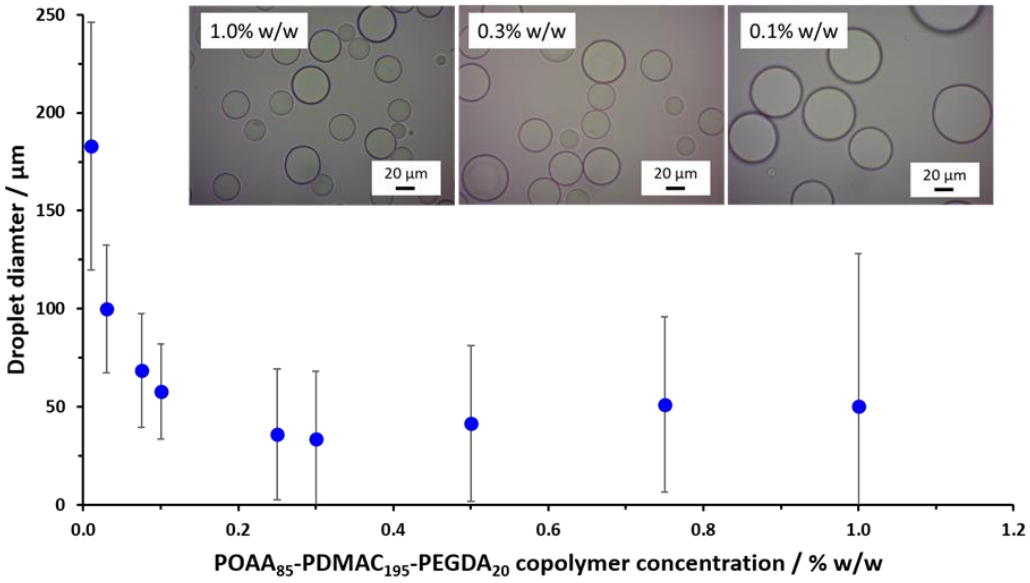

Figure 4.24. Variation in volume-average droplet diameter (as determined by laser diffraction) for the o/w Pickering emulsions obtained when varying the concentration of the core-crosslinked $POAA_{85}$-$PDMAC_{195}$-$PEGDA_{20}$ nanoparticles in *n*-heptane while conducting high-shear homogenisation of an equivolume mixture of this dispersion and deionised water. The error bars indicate the droplet polydispersity rather than the error in the measurements. Inset: optical micrographs recorded at nanoparticle concentrations of 0.1%, 0.3% and 1.0% w/w, respectively.

Finally, the relative volume fraction of *n*-heptane was varied while fixing the $POAA_{85}$-$PDMAC_{150}$ nanoparticle concentration at 1.0% w/w with respect to the oil phase. Again, only o/w Pickering emulsions were obtained for *n*-heptane volume fractions up to 0.60, with mean droplet diameters remaining approximately constant at 15 to 26 µm regardless of the *n*-heptane volume fraction. An unstable w/o emulsion was produced when attempting homogenisation at an *n*-heptane volume fraction of either 0.65 or 0.70. The same experiment was also conducted for the core-crosslinked $POAA_{85}$-$PDMAC_{195}$-$PEGDA_{20}$ nanoparticles using an *n*-heptane volume fraction of

either 0.60 or 0.70. Interestingly, the drop test method indicated the formation of a w/o Pickering emulsion in this case.

4.4 Conclusions

RAFT solution homopolymerisation of a highly hydrophobic acrylamide-based monomer, OAA, has been conducted in 1,4-dioxane. GPC studies indicate that good control over the MWD can be achieved when using a suitable trithiocarbonate-based RAFT agent. Five well-defined $POAA_x$ homopolymers were prepared by varying the [OAA]/[DDMAT agent] molar ratio and their respective mean DPs were calculated by end-group analysis using UV spectroscopy. DSC studies indicate a modest increase in T_g when targeting higher POAA DPs. A $POAA_{85}$ precursor was subsequently employed for the RAFT dispersion polymerisation of DMAC in *n*-heptane. A series of sterically-stabilised $POAA_{85}$-$PDMAC_x$ diblock copolymer spheres was produced with high DMAC conversions being achieved in all cases (≥ 98% within 5 h at 70 °C). An increase in both z-average diameter and molecular weight was observed when targeting higher PDMAC DP, albeit at the expense of reduced RAFT control. TEM studies of the linear diblock nanoparticles proved to be problematic owing to film formation during sample preparation. Thus, EGDA was employed as a bifunctional crosslinker and added towards the end of the DMAC polymerisation to produce covalently-stabilised nanoparticles. This strategy enabled a well-defined spherical morphology to be confirmed by TEM while also producing nanogels that swelled when dispersed in chloroform, which is a good solvent for both blocks. $POAA_{82}$-$PDMAC_{100}$ nanoparticles could also be prepared using an atom-efficient one-pot protocol that augurs well for potential industrial scale-up for such PISA formulations.

The temperature-dependent colloidal stability of a range of $POAA_{85}$-$PDMAC_{150}$ nanoparticles prepared in a homologous series of *n*-alkanes (*n*-heptane, *n*-octane, *n*-decane, *n*-dodecane, *n*-tetradecane or *n*-hexadecane) was investigated using turbidimetry. When prepared in lower *n*-alkanes, the nanoparticles remained well-dispersed at all temperatures. However, reversible flocculation of the nanoparticles occurred on cooling from 70 °C to 20 °C for higher *n*-alkanes, with progressively higher critical flocculation temperatures being observed when increasing the *n*-alkyl chain length. This UCST-like behaviour is attributed to poor solvation of the $POAA_{85}$ stabiliser block at lower temperature, which is consistent with the insolubility of this precursor in *n*-tetradecane and *n*-hexadecane at 20 °C.

$POAA_{85}$-$PDMAC_{150}$ spheres prepared in *n*-heptane were selected as a putative Pickering emulsifier. We hypothesised that employing such hydrophobic nanoparticles should lead to the formation of w/o emulsions. Unexpectedly, addition of an equal volume of water followed by high-shear

homogenisation always produced o/w emulsions. Laser diffraction and optical microscopy studies indicated that larger droplets were obtained when using lower nanoparticle concentrations. This implies that the nanoparticles remain intact after homogenisation to produce genuine Pickering emulsions. Thus, either the hydrophobic $POAA_{85}$-$PDMAC_{150}$ spheres are adsorbed at the *inner* surface of the oil droplets or nanoparticle inversion has occurred during high-shear homogenisation to form *hydrophilic* $PDMAC_{85}$-$POAA_{150}$ spheres that then adsorb at the *outer* surface of the oil droplets. Accordingly, core-crosslinked $POAA_{85}$-$PDMAC_{195}$-$PEGDA_{20}$ spheres were prepared in *n*-heptane to discriminate between these two possibilities. In this case, high-shear homogenisation at various copolymer concentrations again produced o/w Pickering emulsions. As these covalently-stabilised hydrophobic nanoparticles cannot undergo inversion to form hydrophilic nanoparticles, this suggests that such Pickering emulsions must be formed by nanoparticle adsorption at the *inner* surface of the oil droplets.

4.5 References

(1) Kim, D. Y.; Lee, J. G.; Joshi, B. N.; Latthe, S. S.; Al-Deyab, S. S.; Yoon, S. S. Self-Cleaning Superhydrophobic Films by Supersonic-Spraying Polytetrafluoroethylene-Titania Nanoparticles. *J. Mater. Chem. A* **2015**, *3*, 3975–3983.

(2) Tang, Y.; Zhang, Q.; Zhan, X.; Chen, F. Superhydrophobic and Anti-Icing Properties at Overcooled Temperature of a Fluorinated Hybrid Surface Prepared via a Sol-Gel Process. *Soft Matter* **2015**, *11*, 4540–4550.

(3) Thallinger, B.; Prasetyo, E. N.; Nyanhongo, G. S.; Guebitz, G. M. Antimicrobial Enzymes: An Emerging Strategy to Fight Microbes and Microbial Biofilms. *Biotechnol. J.* **2013**, *8*, 97–109.

(4) Vaterrodt, A.; Thallinger, B.; Daumann, K.; Koch, D.; Guebitz, G. M.; Ulbricht, M. Antifouling and Antibacterial Multifunctional Polyzwitterion/Enzyme Coating on Silicone Catheter Material Prepared by Electrostatic Layer-by-Layer Assembly. *Langmuir* **2016**, *32*, 1347–1359.

(5) Spasova, M.; Manolova, N.; Markova, N.; Rashkov, I. Superhydrophobic PVDF and PVDF-HFP Nanofibrous Mats with Antibacterial and Anti-Biofouling Properties. *Appl. Surf. Sci.* **2016**, *363*, 363–371.

(6) Li, J.; Yan, L.; Li, H.; Li, J.; Zha, F.; Lei, Z. A Facile One-Step Spray-Coating Process for the Fabrication of a Superhydrophobic Attapulgite Coated Mesh for Use in Oil/Water Separation. *RSC Adv.* **2015**, *5*, 53802–53808.

(7) Jayaramulu, K.; Datta, K. K. R.; Rösler, C.; Petr, M.; Otyepka, M.; Zboril, R.; Fischer, R. A. Biomimetic Superhydrophobic/Superoleophilic Highly Fluorinated Graphene Oxide and ZIF-8 Composites for Oil-Water Separation. *Angew. Chemie Int. Ed.* **2016**, *55*, 1178–1182.

(8) Micchelli, A. L.; Legato, G. J.; Ganslaw, S. H.; Schuler, L. D.; Brunswick, N. Hair Fixing Compositions Containing N-Alkyl Acrylamide or Methacrylamide Interpolymer. 3927199, August 13, 1975.

(9) Krohn, R.; Schulze zur Wiesche, E. Active Substance Composition for Changing the Shape of Hair. WO 2020089367, May 7, 2020.

(10) Metten, D.; Scheffler, R.; Lange, J. B.; Martinez, C. Sprayable Cosmetic Agent for Treatment of Keratin Fibers, Comprising Fibers, Ethanol, Polymers and Propellant. WO 2018177722, October 4, 2018.

(11) Shi, W.; Palmer, C. P. Effect of Pendent Group Structures on the Chemical Selectivity and Performance of Sulfonated Copolymers as Novel Pseudophases in Electrokinetic Chromatography. *Electrophoresis* **2002**, *23*, 1285–1295.

(12) Rumyantsev, M.; Kazantsev, O. A.; Kamorina, S. I.; Kamorin, D. M.; Sivokhin, A. P. FT-IR and Computer Modeling Study of Hydrogen Bonding in N-Alkyl Acrylamide–Toluene Binary Mixtures. *J. Mol. Struct.* **2016**, *1121*, 86–92.

(13) Bork, J. F.; Wyman, D. P.; Coleman, L. E. Nitrogen-Containing Monomers. III. Reactivity Ratios of N-Alkyl Acrylamides with Vinyl Monomers. *J. Appl. Polym. Sci.* **1963**, *7*, 451–459.

(14) Gouveia, L. M.; Paillet, S.; Khoukh, A.; Grassl, B.; Müller, A. J. The Effect of the Ionic Strength on the Rheological Behavior of Hydrophobically Modified Polyacrylamide Aqueous Solutions Mixed with Sodium Dodecyl Sulfate (SDS) or Cetyltrimethylammonium p-Toluenesulfonate (CTAT). *Colloids Surfaces A Physicochem. Eng. Asp.* **2008**, *322*, 211–218.

(15) Penott-Chang, E. K.; Gouveia, L.; Fernández, I. J.; Müller, A. J.; Díaz-Barrios, A.; Sáez, A. E. Rheology of Aqueous Solutions of Hydrophobically Modified Polyacrylamides and Surfactants. *Colloids Surfaces A Physicochem. Eng. Asp.* **2007**, *295*, 99–106.

(16) Barabanova, A. I.; Bune, E. V.; Gromov, A. V.; Gromov, V. F. Hydrophobic Interactions in the Radical Polymerization of Acrylamide Derivatives. *Eur. Polym. J.* **2000**, *36*, 479–483.

(17) Kulai, I.; Brusylovets, O.; Voitenko, Z.; Harrisson, S.; Mazières, S.; Destarac, M. RAFT Polymerization with Triphenylstannylcarbodithioates (Sn-RAFT). *ACS Macro Lett.* **2015**, *4*, 809–813.

(18) Skrabania, K.; Miasnikova, A.; Bivigou-Koumba, A. M.; Zehm, D.; Laschewsky, A. Examining the UV-Vis Absorption of RAFT Chain Transfer Agents and Their Use for Polymer Analysis. *Polym. Chem.* **2011**, *2*, 2074–2083.

(19) Patel, V. K.; Mishra, A. K.; Vishwakarma, N. K.; Biswas, C. S.; Ray, B. (S)-2-(Ethyl Propionate)-(O-Ethyl Xanthate) and (S)-2-(Ethyl Isobutyrate)-(O-Ethyl Xanthate)-Mediated RAFT Polymerization of N-Vinylpyrrolidone. *Polym. Bull.* **2010**, *65*, 97–110.

(20) Klumperman, B.; van den Dungen, E. T. A.; Heuts, J. P. A.; Monteiro, M. J. RAFT-Mediated Polymerization-A Story of Incompatible Data? *Macromol. Rapid Commun.* **2010**, *31*, 1846–1862.

(21) Deane, O. J.; Musa, O. M.; Fernyhough, A.; Armes, S. P. Synthesis and Characterization of Waterborne Pyrrolidone-Functional Diblock Copolymer Nanoparticles Prepared via Surfactant-Free RAFT Emulsion Polymerization. *Macromolecules* **2020**, *53*, 1422–1434.

(22) Rimmer, S.; Tattersall, P. The Inclusion of β Cyclodextrin Provides a Supramolecular Solution to the Problem of Polymerization of Dodecyl and Octadecyl Methacrylates in Aqueous Emulsion. *Polymer.* **1999**, *40*, 5729–5731.

(23) Fielding, L. A.; Derry, M. J.; Ladmiral, V.; Rosselgong, J.; Rodrigues, A. M.; Ratcliffe, L. P. D.; Sugihara, S.; Armes, S. P. RAFT Dispersion Polymerization in Non-Polar Solvents: Facile

Production of Block Copolymer Spheres, Worms and Vesicles in n-Alkanes. *Chem. Sci.* **2013**, *4*, 2081–2087.

(24) Kang, Y.; Pitto-Barry, A.; Willcock, H.; Quan, W. D.; Kirby, N.; Sanchez, A. M.; O'Reilly, R. K. Exploiting Nucleobase-Containing Materials-from Monomers to Complex Morphologies Using RAFT Dispersion Polymerization. *Polym. Chem.* **2015**, *6*, 106–117.

(25) Canning, S. L.; Cunningham, V. J.; Ratcliffe, L. P. D.; Armes, S. P. Phenyl Acrylate Is a Versatile Monomer for the Synthesis of Acrylic Diblock Copolymer Nano-Objects: Via Polymerization-Induced Self-Assembly. *Polym. Chem.* **2017**, *8*, 4811–4821.

(26) Cunningham, V. J.; Armes, S. P.; Musa, O. M. Synthesis, Characterisation and Pickering Emulsifier Performance of Poly(Stearyl Methacrylate)–Poly(N-2-(Methacryloyloxy)Ethyl Pyrrolidone) Diblock Copolymer Nano-Objects via RAFT Dispersion Polymerisation in n-Dodecane. *Polym. Chem.* **2016**, *7*, 1882–1891.

(27) Qu, S.; Liu, R.; Duan, W.; Zhang, W. RAFT Dispersion Polymerization in the Presence of Block Copolymer Nanoparticles and Synthesis of Multicomponent Block Copolymer Nanoassemblies. *Macromolecules* **2019**, *52*, 5168–5176.

(28) Xie, X.; Hogen-Esch, T. E. Anionic Synthesis of Narrow Molecular Weight Distribution Water-Soluble Poly(N,N-Dimethylacrylamide) and Poly(N-Acryloyl-N'-Methylpiperazine). *Macromolecules* **1996**, *29*, 1746–1752.

(29) Derry, M. J.; Mykhaylyk, O. O.; Ryan, A. J.; Armes, S. P. Thermoreversible Crystallization-Driven Aggregation of Diblock Copolymer Nanoparticles in Mineral Oil. *Chem. Sci.* **2018**, *9*, 4071–4082.

(30) Pelton, R. Temperature-Sensitive Aqueous Microgels. *Adv. Colloid Interface Sci.* **2000**, *85*, 1–33.

(31) Weaver, J. V. M.; Bannister, I.; Robinson, K. L.; Bories-Azeau, X.; Armes, S. P.; Smallridge, M.; McKenna, P. Stimulus-Responsive Water-Soluble Polymers Based on 2-Hydroxyethyl Methacrylate. *Macromolecules* **2004**, *37*, 2395–2403.

(32) Bernaerts, K. V.; Fustin, C.-A.; Bomal-D'Haese, C.; Gohy, J.-F.; Martins, J. C.; Du Prez, F. E. Advanced Polymer Architectures with Stimuli-Responsive Properties Starting from Inimers. *Macromolecules* **2008**, *41*, 2593–2606.

(33) Seuring, J.; Agarwal, S. Polymers with Upper Critical Solution Temperature in Aqueous Solution. *Macromol. Rapid Commun.* **2012**, *33*, 1898–1920.

(34) Roy, D.; Brooks, W. L. A.; Sumerlin, B. S. New Directions in Thermoresponsive Polymers. *Chem. Soc. Rev.* **2013**, *42*, 7214–7243.

(35) Saeki, S.; Kuwahara, N.; Konno, S.; Kaneko, M. Upper and Lower Critical Solution Temperatures in Polystyrene Solutions. II. *Macromolecules* **1973**, *6*, 589–593.

(36) Vshivkov, S. A.; Safronov, A. P. The Conformational Coil-Globule Transition of Polystyrene in Cyclohexane Solution. *Macromol. Chem. Phys.* **1997**, *198*, 3015–3023.

(37) Siporska, A.; Szydlowski, J.; Rebelo, L. P. N. Solvent H/D Isotope Effects on Miscibility and θ-Temperature in the Polystyrene-Cyclohexane System. *Phys. Chem. Chem. Phys.* **2003**, *5*, 2996–3002.

(38) Imre, A. R.; Van Hook, W. A.; Chang, B. H.; Bae, Y. C. The Effect of Alkane Chain Length on the Liquid-Liquid Critical Temperatures of Oligostyrene/Linear-Alkane Mixtures.

Monatshefte fur Chemie **2003**, *134*, 1529–1539.

(39) Ho, D. L.; Hammouda, B.; Kline, S. R.; Chen, W. R. Unusual Phase Behavior in Mixtures of Poly(Ethylene Oxide) and Ethyl Alcohol. *J. Polym. Sci. Part B Polym. Phys.* **2006**, *44*, 557–564.

(40) Heskins, M.; Guillet, J. E. Solution Properties of Poly(N-Isopropylacrylamide). *J. Macromol. Sci. Part A - Chem.* **1968**, *2*, 1441–1455.

(41) Schild, H. G. Poly(N-Isopropylacrylamide): Experiment, Theory and Application. *Prog. Polym. Sci.* **1992**, *17*, 163–249.

(42) Kotsuchibashi, Y.; Ebara, M.; Aoyagi, T.; Narain, R. Recent Advances in Dual Temperature Responsive Block Copolymers and Their Potential as Biomedical Applications. *Polymers.* **2016**, *8*, 380–405.

(43) Arotçaréna, M.; Heise, B.; Ishaya, S.; Laschewsky, A. Switching the inside and the Outside of Aggregates of Water-Soluble Block Copolymers with Double Thermoresponsivity. *J. Am. Chem. Soc.* **2002**, *124*, 3787–3793.

(44) Weaver, J. V. M.; Armes, S. P.; Bütün, V. Synthesis and Aqueous Solution Properties of a Well-Defined Thermo-Responsive Schizophrenic Diblock Copolymer. *Chem. Commun.* **2002**, *2*, 2122–2123.

(45) Govorun, E. N.; Erukhimovich, I. Emulsion Stabilization by Diblock Copolymers: Droplet Curvature Effect. *Langmuir* **1999**, *15*, 8392–8398.

(46) Romet-Lemonne, G.; Daillant, J.; Guenoun, P.; Yang, J.; Holley, D. W.; Mays, J. W. Oil-in-Water Microemulsions Stabilized by Charged Diblock Copolymers. *J. Chem. Phys.* **2005**, *122*, 064703.

(47) Marchal, F.; Roudot, A.; Pantoustier, N.; Perrin, P.; Daillant, J.; Guenoun, P. Emulsion Stabilization and Inversion Using a PH- and Temperature-Sensitive Amphiphilic Copolymer. *J. Phys. Chem. B* **2007**, *111*, 13151–13155.

(48) Ramsden, W. Separation of Solids in the Surface-Layers of Solutions and 'Suspensions' (Observations on Surface-Membranes, Bubbles, Emulsions, and Mechanical Coagulation).—Preliminary Account. *Proc. R. Soc. London* **1903**, *72*, 156–164.

(49) Pickering, S. U. CXCVI. - Emulsions. *J. Chem. Soc. Trans.* **1907**, *91*, 2001–2021.

(50) Binks, B. P.; Lumsdon, S. O. Effects of Oil Type and Aqueous Phase Composition on Oil-Water Mixtures Containing Particles of Intermediate Hydrophobicity. *Phys. Chem. Chem. Phys.* **2000**, *2*, 2959–2967.

(51) Binks, B. P.; Lumsdon, S. O. Catastrophic Phase Inversion of Water-in-Oil Emulsions Stabilized by Hydrophobie Silica. *Langmuir* **2000**, *16*, 2539–2547.

(52) Madivala, B.; Vandebril, S.; Fransaer, J.; Vermant, J. Exploiting Particle Shape in Solid Stabilized Emulsions. *Soft Matter* **2009**, *5*, 1717–1727.

(53) Chen, T.; Colver, P. J.; Bon, S. A. F. Organic–Inorganic Hybrid Hollow Spheres Prepared from TiO2-Stabilized Pickering Emulsion Polymerization. *Adv. Mater.* **2007**, *19*, 2286–2289.

(54) Williams, M.; Armes, S. P.; York, D. W. Clay-Based Colloidosomes. *Langmuir* **2012**, *28*, 1142–1148.

(55) Cauvin, S.; Colver, P. J.; Bon, S. A. F. Pickering Stabilized Miniemulsion Polymerization: Preparation of Clay Armored Latexes. *Macromolecules* **2005**, *38*, 7887–7889.

(56) Bon, S. A. F.; Colver, P. J. Pickering Miniemulsion Polymerization Using Laponite Clay as a Stabilizer. *Langmuir* **2007**, *23*, 8316–8322.

(57) Velev, O. D.; Furusawa, K.; Nagayama, K. Assembly of Latex Particles by Using Emulsion Droplets as Templates. 1. Microstructured Hollow Spheres. *Langmuir* **1996**, *12*, 2374–2384.

(58) Velev, O. D.; Nagayama, K. Assembly of Latex Particles by Using Emulsion Droplets. 3. Reverse (Water in Oil) System. *Langmuir* **1997**, *13*, 1856–1859.

(59) Binks, B. P.; Lumsdon, S. O. Pickering Emulsions Stabilized by Monodisperse Latex Particles: Effects of Particle Size. *Langmuir* **2001**, *17*, 4540–4547.

(60) Aveyard, R.; Binks, B. P.; Clint, J. H.; Fletcher, P. D.; Horozov, T. S.; Neumann, B.; Paunov, V. N.; Annesley, J.; Botchway, S. W.; Nees, D.; Parker, A. W.; Ward, A. D.; Burgess, A. N. Measurement of Long-Range Repulsive Forces between Charged Particles at an Oil-Water Interface. *Phys. Rev. Lett.* **2002**, *88*, 2461021–2461024.

(61) Binks, B. P.; Murakami, R.; Armes, S. P.; Fujii, S. Temperature-Induced Inversion of Nanoparticle-Stabilized Emulsions. *Angew. Chemie* **2005**, *117*, 4873–4876.

(62) Fujii, S.; Cai, Y.; Weaver, J. V. M.; Armes, S. P. Syntheses of Shell Cross-Linked Micelles Using Acidic ABC Triblock Copolymers and Their Application as PH-Responsive Particulate Emulsifiers. *J. Am. Chem. Soc.* **2005**, *127*, 7304–7305.

(63) Reynaert, S.; Moldenaers, P.; Vermant, J. Control over Colloidal Aggregation in Monolayers of Latex Particles at the Oil-Water Interface. *Langmuir* **2006**, *22*, 4936–4945.

(64) Binks, B. P. Particles as Surfactants—Similarities and Differences. *Curr. Opin. Colloid Interface Sci.* **2002**, *7*, 21–41.

(65) Binks, B. P.; Yin, D. Pickering Emulsions Stabilized by Hydrophilic Nanoparticles:: In Situ Surface Modification by Oil. *Soft Matter* **2016**, *12*, 6858–6867.

(66) Wu, J.; Ma, G.-H. Recent Studies of Pickering Emulsions: Particles Make the Difference. *Small* **2016**, *12*, 4633–4648.

(67) Thompson, K. L.; Chambon, P.; Verber, R.; Armes, S. P. Can Polymersomes Form Colloidosomes? *J. Am. Chem. Soc.* **2012**, *134*, 12450–12453.

(68) Thompson, K. L.; Mable, C. J.; Cockram, A.; Warren, N. J.; Cunningham, V. J.; Jones, E. R.; Verber, R.; Armes, S. P. Are Block Copolymer Worms More Effective Pickering Emulsifiers than Block Copolymer Spheres? *Soft Matter* **2014**, *10*, 8615–8626.

(69) Mable, C. J.; Warren, N. J.; Thompson, K. L.; Mykhaylyk, O. O.; Armes, S. P. Framboidal ABC Triblock Copolymer Vesicles: A New Class of Efficient Pickering Emulsifier. *Chem. Sci.* **2015**, *6*, 6179–6188.

(70) Morse, A. J.; Armes, S. P.; Thompson, K. L.; Dupin, D.; Fielding, L. A.; Mills, P.; Swart, R. Novel Pickering Emulsifiers Based on PH-Responsive Poly(2- (Diethylamino)Ethyl Methacrylate) Latexes. *Langmuir* **2013**, *29*, 5446–5475.

(71) Binks, B. P.; Whitby, C. P. Silica Particle-Stabilized Emulsions of Silicone Oil and Water: Aspects of Emulsification. *Langmuir* **2004**, *20*, 1130–1137.

(72) Bon, S. A. F.; Mookhoek, S. D.; Colver, P. J.; Fischer, H. R.; van der Zwaag, S. Route to Stable Non-Spherical Emulsion Droplets. *Eur. Polym. J.* **2007**, *43*, 4839–4842.

(73) Rymaruk, M. J.; Thompson, K. L.; Derry, M. J.; Warren, N. J.; Ratcliffe, L. P. D.; Williams, C. N.; Brown, S. L.; Armes, S. P. Bespoke Contrast-Matched Diblock Copolymer Nanoparticles Enable the Rational Design of Highly Transparent Pickering Double Emulsions. *Nanoscale* **2016**, *8*, 14497–14506.

Chapter 5.

RAFT non-aqueous emulsion polymerisation of *N*-(2-acryloyloxy) ethyl pyrrolidone to produce PSMA-PNAEP diblock copolymer nano-objects in non-polar media

5.1 Introduction

NMEP has been suggested as a more readily copolymerisable methacrylic analogue (MAM-type monomer) to the highly biocompatible LAM-type monomer, NVP.[1–3] Cunningham *et al.* reported on the RAFT dispersion polymerisation of NMEP in non-polar media using a PSMA macro-CTA: such PISA formulations provided access to spherical, worm-like and vesicular nano-objects.[1] The polymerisation of NMEP was much faster than that of BzMA for syntheses conducted under precisely the same conditions; this striking difference was attributed to the much more polar nature of the former monomer. PNMEP has been utilised as a steric stabiliser for ethanolic RAFT dispersion polymerisation[2,4] and the RAFT aqueous solution polymerisation of NMEP has also been reported.[2,4,5] Unlike PNVP, PNMEP exhibits LCST behaviour in water (see Chapter 2). Cunningham *et al.* exploited this to devise a low-viscosity route to high molecular weight PNMEP *via* RAFT aqueous dispersion polymerisation.[6] Here the PNMEP chains were weakly hydrophobic (and hence formed dehydrated cores of relatively large spheres) when prepared at 70 °C (*i.e.* above the LCST of PNMEP) but became water-soluble on cooling to ambient temperature (*i.e.* below the LCST of PNMEP). However, if PNMEP is to be used as an *electrosteric stabiliser* block for RAFT aqueous dispersion (or emulsion) polymerisation, a suitable carboxylic acid-functionalised RAFT agent should be used to introduce a terminal anionic charge by adjusting the solution pH so as to ensure end-group ionisation (see Chapter 2).[5] Recently, an acrylic analogue of NMEP, NAEP, has been developed. Unlike PNMEP, the corresponding homopolymer (PNAEP) is much more hydrophilic and no LCST behaviour is observed in aqueous solution at elevated temperature.[7] This has enabled the straightforward use of PNAEP as a steric stabiliser for the RAFT aqueous emulsion polymerisation of styrene and/or *n*-butyl acrylate.[8] A second advantage of NAEP over NMEP is its much faster rate of homopolymerisation,[7] which simply reflects the much higher k_p values observed for acrylic monomers compared to their methacrylic analogues.[9] For example, when using an ascorbic acid/potassium persulfate redox couple in aqueous solution in combination with a trithiocarbonate-based RAFT agent (DDMAT) and targeting a PNAEP DP of 80, more than 99% NAEP conversion was achieved within 5 min at 30 °C. Moreover, GPC analysis indicated a final M_n of 12 300 g mol^{-1} and an M_w/M_n of 1.15, which indicates a well-controlled RAFT polymerisation.

Currently, there are no literature reports of PISA syntheses that use NAEP as a core-forming block. Indeed, there are far fewer examples of PISA syntheses involving acrylic monomers compared to methacrylic monomers, particularly for non-aqueous formulations. This is perhaps surprising, because low T_g film-forming diblock copolymer nanoparticles are potentially useful for paints and coatings applications.[10,11] Charleux and co-workers were the first to report an all-acrylic PISA

formulation: in this case, poly(2-ethylhexyl acrylate)-poly(methyl acrylate) (PEHA-PMA) diblock copolymer nanoparticles were targeted in *iso*-dodecane.[12–14] However, only spherical nanoparticles could be obtained and GPC analysis indicated relatively poor control over the MWD, particularly when using a dithiobenzoate-based CTA (M_w/M_n > 6.00 at ≥ 85% conversion) compared to a trithiocarbonate-based macro-CTA (M_w/M_n = 1.21 for 100% conversion). In retrospect, this is not too surprising given that aromatic dithioesters are known to be problematic for high k_p acrylic monomers.[15]

Similarly, Ratcliffe and co-workers prepared all-acrylic diblock copolymer nano-objects by RAFT dispersion polymerisation of benzyl acrylate (BzA) using a relatively short poly(lauryl acrylate) precursor in various alkanes.[16] More specifically, spheres, worms or vesicles could be obtained in *n*-heptane, *n*-dodecane or *iso*-hexadecane at 80 °C. Broader MWDs were observed when polymerisations were conducted at lower concentration, this was attributed to chain transfer to solvent, as reported by Veloso and co-workers.[17] However, it is also well-documented that acrylates can undergo significant branching *via* chain transfer to polymer, which also broadens the MWD.[18–20]

Owing to their relatively low T_g, imaging acrylic nanoparticles using TEM can be problematic. For example, the PLA-PBzA nano-objects described above had to be imaged using cryo-TEM owing to the film-forming nature of the PBzA block (T_g = 6 °C).[16] To overcome this problem, an acrylic polymer with a relatively high T_g can be targeted, at least for model studies. Suitable examples here include poly(phenyl acrylate) (PPhA) (T_g = 50 °C),[21] and poly(isobornyl acrylate) (PIBOA) (T_g = 94 °C).[22] Thus Canning *et al.* chain-extended a PLA precursor *via* RAFT dispersion polymerisation of PhA in *n*-heptane: in this case, high-quality images of the resulting high T_g nano-objects could be recorded using conventional TEM (Figure 5.1).[21] Spheres, worms and vesicles could each be produced at 25% w/w solids simply by varying the target DP of the structure-directing PPhA block. However, GPC analysis revealed a high molecular weight shoulder for each copolymer, which suggested that chain transfer to polymer occurred during this PISA formulation.

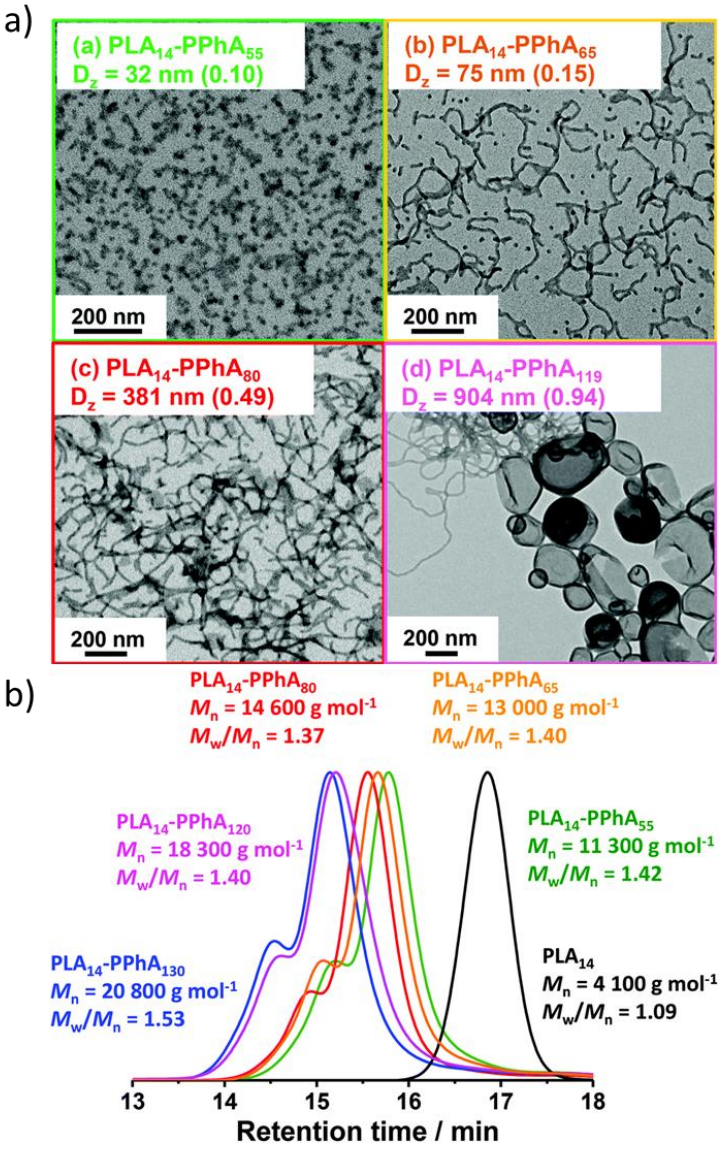

Figure 5.1. (a) TEM images recorded for PLA_{14}-$PPhA_x$ diblock copolymer nano-objects prepared in *n*-heptane by RAFT dispersion polymerisation of PhA at 80 °C and (b) the corresponding THF GPC curves of the copolymers with data being relative to a series of PMMA calibrants.[21]

RAFT polymerisations typically utilise a thermally activated azo or peroxide initiator.[23] However, it is also feasible for such reactions to proceed *via* light irradiation using either a photocatalyst or a photoinitiator.[24,25] In fact, the RAFT agent itself can be used as an iniferter: once cleaved, the resulting carbon-centred radical initiates chain growth while the sulfur-centred radical undergoes reversible termination with the active chain. Otsu and co-workers were the first to describe this thiocarbonylthio compound as a so-called 'photoiniferter', which denotes **photo**lysis **ini**tiates polymerisation, chain trans**fer** mediates chain length, and reversible **ter**mination deactivates chain growth.[26–28]

Iniferter polymerisation enables high chain-end fidelity to be achieved along with exquisite control over block order as demonstrated by Easterling and co-workers.[29] This team hypothesised that photolysis of C–S bonds generated macroradical intermediates (R groups) that are normally disfavoured by the RAFT mechanism, which in principle might allow inversion of the block sequence to produce LAM-MAM diblock copolymers. Conventional RAFT polymerisations require a continuous radical flux from the thermal decomposition of either azo or peroxide initiators to compensate for background radical termination. This results in the formation of a (minor) population of relatively short polymer chains that broadens the MWD and limits the formation of high MW chains.[30] Moreover, attaining high DPs requires thousands of activation-deactivation cycles; this inevitably results in some degree of radical termination and transfer, which severely limits access to high MW.[31] Acrylates and acrylamides both exhibit high propagation rate constant (k_p) values and are capable of achieving high conversions under relatively mild polymerisation conditions. Hence these two monomer classes are particularly amenable to RAFT iniferter polymerisation. Utilising the high k_p values of water-soluble monomers and excluding conventional initiators minimises bimolecular termination and enables the preparation of ultrahigh molecular weight polymers (M_n > 10^6 g mol^{-1}).[32,33] However, one major drawback of RAFT iniferter polymerisation is that relatively small reaction volumes and optically clear solutions are required to allow for sufficient light penetration. Given that PISA formulations typically produce rather turbid dispersions of diblock copolymer nano-objects, it may not be feasible to conduct such syntheses using RAFT iniferter polymerisation. However, there are several literature examples of successful photo-PISA.[34–36] Moreover, the Armes group has recently devised highly transparent PISA formulations by matching the refractive index of the nanoparticles to that of the solvent at the polymerisation temperature.[37]

Herein, a PSMA precursor is used to control the RAFT *non-aqueous* emulsion polymerisation of NAEP in *n*-dodecane to produce spherical nanoparticles. It should be noted that non-aqueous emulsion polymerisations, where the monomer droplets are polymerisable, are quite rare[38–41] and should not be confused with non-aqueous mini-emulsion formulations in which the monomer is solubilised within oil droplets.[42,43] Preliminary experiments indicated that PISA syntheses based on RAFT iniferter polymerisations were also feasible in *n*-dodecane at 80 °C using 405 nm light as the initiation source. The low T_g of these $PSMA_{36}$-$PNAEP_x$ diblock copolymers was evaluated by DSC and the spherical nanoparticles were sized by DLS, TEM and SAXS. Finally, $PSMA_{36}$-$PNAEP_{70}$ spheres were briefly evaluated for their performance as a putative Pickering emulsifier for *n*-dodecane/water mixtures.

5.2 Experimental

5.2.1 Materials

Chloroform and triethylamine (TEA) were purchased from Alfa Aesar (Haysham, UK). *n*-Dodecane, toluene, ethanol, d_1-chloroform, stearyl methacrylate (SMA) and azobisisobutyronitrile (AIBN) were purchased from Sigma Aldrich (Dorset, UK). *N*-(2-Acryloyloxy)ethyl pyrrolidone (NAEP; 95% purity) was donated by Ashland (NJ, USA) and was further purified in-house by dilution with chloroform followed by sequential washes with 5% Na_2CO_3 solution, saturated NaCl solution, and finally deionised water. Repeated washes with water were performed until the aqueous NAEP solution exhibited neutral pH. This solution was then dried over anhydrous $MgSO_4$ to remove the water. 4-Cyano-4-(2-phenylethanesulfanylthiocarbonyl)sulfanylpentanoic acid (PETTC) RAFT agent was prepared as previously reported.[44] d_2-Dichloromethane was purchased from Goss Scientific Instruments Ltd. (Cheshire, UK). Ethylene glycol diacrylate (EGDA) was purchased from Santa Cruz Biotechnology (Dallas, USA).

5.2.2 Synthesis of a $PSMA_x$ precursor by RAFT solution polymerisation in toluene

The $PSMA_{36}$ precursor was prepared as described below. SMA (36.0 g, 0.11 mol), PETTC RAFT agent (0.60 g, 1.77 mmol; target DP = 60), AIBN (58.1 mg, 0.35 mmol; PETTC/AIBN molar ratio = 5) and toluene (36.6 g, 50% w/w solids) were weighed into a 250 mL round-bottom flask and degassed under N_2 with continuous magnetic stirring for 30 min. The SMA polymerisation was allowed to proceed for 260 min in an oil bath set to 70 °C, resulting in a final monomer conversion of 71% as judged by ^{1}H NMR spectroscopy. Quenching was achieved by exposing the hot reaction solution to air and cooling to 20 °C. The crude polymer was precipitated into excess cold ethanol to remove residual monomer before placing in a vacuum oven at 30 °C for 72 h to afford an orange waxy solid. The mean DP was calculated to be 36 by ^{1}H NMR analysis by comparing the aromatic protons of the RAFT end-group at 7.3 ppm to the two oxymethylene protons of PSMA at 3.8-4.1 ppm. Chloroform GPC analysis indicated an M_n of 10 200 g mol^{-1} and an M_w/M_n of 1.18 using a series of ten near-monodisperse PMMA calibration standards. A second PSMA precursor with a mean DP of 8 was also synthesised using the same synthetic protocol but adjusting the SMA/PETTC molar ratio to target a DP of 5. In this case, chloroform GPC analysis indicated an M_n of 2 500 g mol^{-1} and an M_w/M_n of 1.26.

5.2.3 Synthesis of $PSMA_x$-$PNAEP_y$ diblock copolymer nanoparticles by RAFT non-aqueous emulsion polymerisation of NAEP in *n*-dodecane

A typical protocol for the synthesis of $PSMA_{36}$-$PNAEP_{60}$ nano-objects *via* RAFT non-aqueous emulsion polymerisation of NAEP in *n*-dodecane was conducted as follows. The $PSMA_{36}$ precursor

(0.15 g, 12.0 µmol), NAEP (0.12 g, 0.72 mmol; target DP = 60) and T21s initiator (0.50 mg, 2.99 µmol; 0.05 g of a 10 mg g^{-1} stock solution of T21s dissolved in *n*-dodecane; $PSMA_{36}$/T21s molar ratio = 4.0) were dissolved in *n*-dodecane (1.10 g). The reaction vial was sealed and degassed under N_2 for 20 min before being placed in a pre-heated oil bath set at 90 °C for 5 h. The NAEP polymerisation was quenched by exposing the hot reaction solution to air and cooling to 20 °C. The resulting diblock copolymer chains were characterised by ^{1}H NMR spectroscopy and chloroform GPC while 0.1% w/w dispersions of the nano-objects were prepared by dilution with *n*-dodecane prior to analysis by DLS and TEM. Chloroform GPC analysis indicated an M_p of 23 000 g mol^{-1} and an M_w/M_n of 1.50 (calculated using a series of ten near-monodisperse PMMA calibration standards and refractive index detector). Other diblock copolymer compositions were prepared by adjusting the amount of NAEP monomer to target a range of DPs. For these additional syntheses, the volume of the continuous phase was adjusted to maintain an overall copolymer concentration of 20% w/w solids. ^{1}H NMR analysis indicated that at least 99% NAEP conversion was achieved in all cases. Finally, a similar series of $PSMA_8$-$PNAEP_x$ diblock copolymer nanoparticles were also synthesised in *n*-dodecane using the $PSMA_8$ precursor.

5.2.4 Synthesis of $PSMA_{36}$-$PNAEP_x$ diblock copolymers by RAFT iniferter solution polymerisation of NAEP in toluene

A typical protocol for the synthesis of $PSMA_{36}$-$PNAEP_{50}$ *via* RAFT iniferter solution polymersation of NAEP in toluene was conducted as follows. The $PSMA_{36}$ precursor (0.20 g, 16.0 µmol) and NAEP (0.14 g, 0.80 mmol; target DP = 50) were dissolved in toluene (0.79 g, 30% w/w solids). The reaction vial was sealed and degassed under N_2 for 20 min before being placed in a water-jacketed LED reactor (see Figure 3.15) (λ = 405 nm) at 30 °C for 7.5 h. The NAEP polymerisation was quenched by exposing the reaction solution to air and cooling to 20 °C. The resulting diblock copolymer chains were characterised by ^{1}H NMR spectroscopy and chloroform GPC analysis. The latter technique indicated an M_n of 15 400 g mol^{-1} and a M_w/M_n of 1.18 (*vs.* PMMA standards), while ^{1}H NMR analysis indicated that a final NAEP conversion of 33% was achieved within 7.5 h at 30 °C. $PSMA_{36}$-$PNAEP_{60}$ diblock copolymer nano-objects were also synthesised in *n*-dodecane, with the temperature of the water-jacketed LED reactor being set to either 80 or 70 °C as required.

5.2.5 Synthesis of core-crosslinked $PSMA_{36}$-$PNAEP_{60}$-$PEGDA_{10}$ triblock copolymer nanoparticles

A typical protocol for the synthesis of core-crosslinked $PSMA_{36}$-$PNAEP_{60}$-$PEGDA_{10}$ spherical nanoparticles was conducted as follows. The $PSMA_{36}$ precursor (0.50 g, 40.0 µmol), NAEP (0.44 g, 2.39 mmol; target DP = 60) and T21s initiator (1.60 mg, 9.99 µmol; 0.16 g of a 10 mg g^{-1} stock

solution of T21s dissolved in *n*-dodecane; $PSMA_{36}$/T21s molar ratio = 4.0) were dissolved in *n*-dodecane (4.03 g). The reaction vial was sealed and degassed under N_2 for 20 min before being placed in a pre-heated oil bath set at 90 °C for 1 h. EGDA (0.07 g, 0.40 mmol; target DP = 10; previously degassed with N_2 gas at 20 °C) was then added using a deoxygenated syringe/needle. The EGDA polymerisation was allowed to proceed for 5 h before quenching by exposing the hot reaction mixture to air while cooling to 20 °C. The resulting crosslinked spherical triblock copolymer nanoparticles were diluted with *n*-dodecane to afford a 0.1% w/w dispersion prior to characterisation by DLS and TEM.

5.2.6 Preparation of o/w (and w/o/w) emulsions using $PSMA_{36}$-$PNAEP_{70}$ spheres

Water (2.0 mL) was homogenised with 2.0 mL of a dispersion containing 0.025 – 1.0% w/w $PSMA_{36}$-$PNAEP_{70}$ spheres in *n*-dodecane for 2.0 min at 20 °C using an IKA Ultra-Turrax homogeniser at a shear rate of 13 500 rpm.

5.2.7 Copolymer characterisation

^{1}H NMR spectroscopy. Spectra were recorded for $PSMA_x$ homopolymers dissolved in CD_2Cl_2 and $PSMA_{36}$-$PNAEP_x$ diblock copolymers dissolved in $CDCl_3$ using a 400 MHz Bruker Avance 400 spectrometer with 64 scans being averaged per spectrum.

Gel permeation chromatography (GPC). Molecular weight data for the $PSMA_x$ homopolymer precursors and the corresponding series of $PSMA_{36}$-$PNAEP_x$ diblock copolymers were obtained using chloroform GPC at 35 °C, with the eluent containing 0.25% TEA by volume. Two Polymer Laboratories PL gel 5 µm Mixed C columns were connected in series to a Varian 390 multidetector suite (only the refractive index detector was used) and a Varian 290 LC pump injection module at a flow rate of 1.0 mL min^{-1}. Ten near-monodisperse PMMA standards (M_n = 625 - 618 000 g mol^{-1}) were used for calibration and data were analysed using Varian Cirrus GPC software supplied by the instrument manufacturer.

Dynamic light scattering (DLS). A Malvern Zetasizer NanoZS instrument was used to determine the intensity-average hydrodynamic diameter of the copolymer nanoparticles at 20 °C at a fixed scattering angle of 173°. As-synthesised dispersions were diluted to 0.1% w/w using *n*-dodecane and analysed using a 1.0 cm path length glass cuvette. Data were averaged over three consecutive measurements (with 10 sub-runs per run) for each sample. Sphere-equivalent intensity-average diameters were calculated for nanoparticles using the Stokes–Einstein equation, which assumes perfectly monodisperse, non-interacting spheres.

Transmission electron microscopy (TEM). Copper/palladium grids were surface-coated in-house to produce a thin film of amorphous carbon. A 15 µL droplet of a 0.1% w/w copolymer dispersion

(prepared by serial dilution using *n*-dodecane) was placed on a grid using a micropipet, allowed to dry, and then stained by exposed to ruthenium(IV) oxide vapour for 7 min at 20 °C prior to analysis. A FEI Tecnai Spirit microscope operating at 80 kV and equipped with a Gatan 1kMS600CW CCD camera was used to image the nanoparticles.

Differential scanning calorimetry (DSC). Glass transition temperatures (T_g) for the $PSMA_{36}$ homopolymer and corresponding $PSMA_{36}$-$PNAEP_x$ diblock copolymers were determined using a TA Instruments Discovery DSC 25 instrument operating from −50 °C to 100 °C at a heating/cooling rate of 10 °C min^{-1}. Each sample (10 mg) was dried for at least 24 h in a vacuum oven at 30 °C prior to analysis before they were hermetically sealed in a vented aluminium pan. The instrument was calibrated for heat flow and temperature using both indium and zinc standards. Samples were annealed at 100 °C for 5 min before cooling to −50 °C, with this latter temperature being maintained for 1 min. The T_g was then determined by heating the polymers up to 100 °C and defining the mid-point value.

Small angle X-ray scattering (SAXS). SAXS patterns were recorded by Armes group members at either a national synchrotron facility (station I22, Diamond Light Source, Didcot, Oxfordshire, UK) using monochromatic X-ray radiation (λ = 0.124 nm with q ranging from 0.01 to 2.00 nm^{-1}) and a 2D Pilatus 2M pixel detector (Dectris, Switzerland) or a Xeuss 2.0 SAXS instrument (Xenocs, France) equipped with a liquid gallium MetalJet X-ray source (Excillum, Sweden, λ = 0.134 nm), two sets of motorized scatterless slits for beam collimation and a Dectris Pilatus 1 M pixel detector (sample-to-detector distance = 5.102 m with q ranging from 0.02 nm^{-1} to 1.3 nm^{-1}). Where $q = 4\pi\sin\Theta/\lambda$ is the length of the scattering vector and Θ is one-half of the scattering angle). A glass capillary of 2 mm diameter was used as a sample holder and all measurements were conducted on 1.0% w/w copolymer dispersions in *n*-dodecane. X-ray scattering data were reduced and normalised using standard routines by the beamline or using the Foxtrot software package supplied with the Xeuss 2.0 instrument and further analysed (background subtraction and data modelling) using Irena SAS macros for Igor Pro.[45]

Optical microscopy. Optical microscopy images were recorded using a Cole–Palmer compound optical microscope equipped with an LCD tablet display and a Moticam BTW digital camera.

Laser diffraction. Each emulsion was sized by laser diffraction using a Malvern Mastersizer 3000 instrument equipped with a hydro EV wet sample dispersion unit, a red HeNe laser operating at 633 nm and a LED blue light source operating at 470 nm. The stirring rate was adjusted to 1500 rpm in order to avoid creaming of the emulsion droplets during analysis. After each

measurement, the cell was rinsed once with ethanol and twice with deionised water and the laser was aligned centrally to the detector prior to data acquisition.

Fluorescence microscopy. Fluorescence microscopy images of the w/o/w double Pickering emulsions were recorded using a Zeiss Axio Scope A1 microscope equipped with an AxioCam 1Cm1 monochrome camera. Nile Red dye was dissolved in *n*-dodecane prior to high-shear homogenisation and the resulting oil droplets were imaged using Zeiss filter set 43 HE (excitation 550/25 nm and emission 605/70 nm). Images were captured and processed using ZEN lite 2012 software.

5.3 Results and Discussion

Cunningham and co-workers demonstrated that $PSMA_{14}$ is an effective steric stabiliser block for the RAFT dispersion polymerisation of NMEP in *n*-dodecane to form spheres, worms and vesicles.[1] Accordingly, a $PSMA_8$ oligomer was prepared using PETTC as a RAFT agent. After purification to remove residual SMA monomer, this precursor was subsequently used to prepare $PSMA_8$-$PNAEP_x$ diblock copolymer nano-objects in *n*-dodecane. Chloroform GPC curves indicated reasonably high blocking efficiency and a linear increase in M_n with PNAEP DP (Figure 5.2a) was observed. However, the relatively broad MWDs (M_w/M_n > 1.40) indicated rather poor RAFT control and the presence of a high molecular weight shoulder suggested chain transfer to polymer. Moreover, incipient flocculation was observed for all target PNAEP DPs when using this oligomeric $PSMA_8$ precursor. These nanoparticle aggregates were observed on dilution with *n*-dodecane for DLS analysis (Figure 5.2b), particularly when targeting higher DPs (*e.g.* DP = 150).

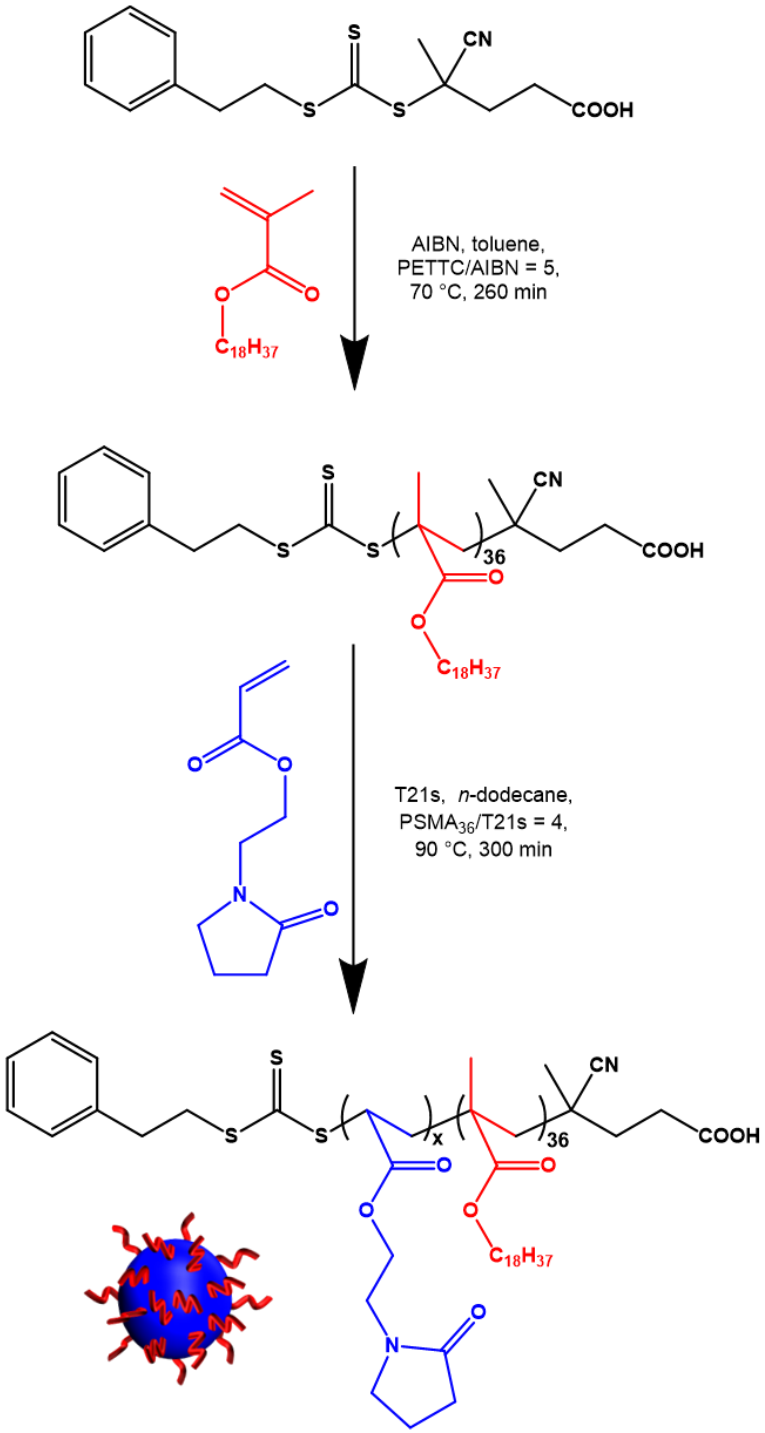

Scheme 5.1. Synthesis of a $PSMA_{36}$ precursor by RAFT solution polymerisation of SMA in toluene at 70 °C and its subsequent chain extension *via* RAFT non-aqueous emulsion polymerisation of NAEP in *n*-dodecane at 90 °C when targeting 20% w/w solids.

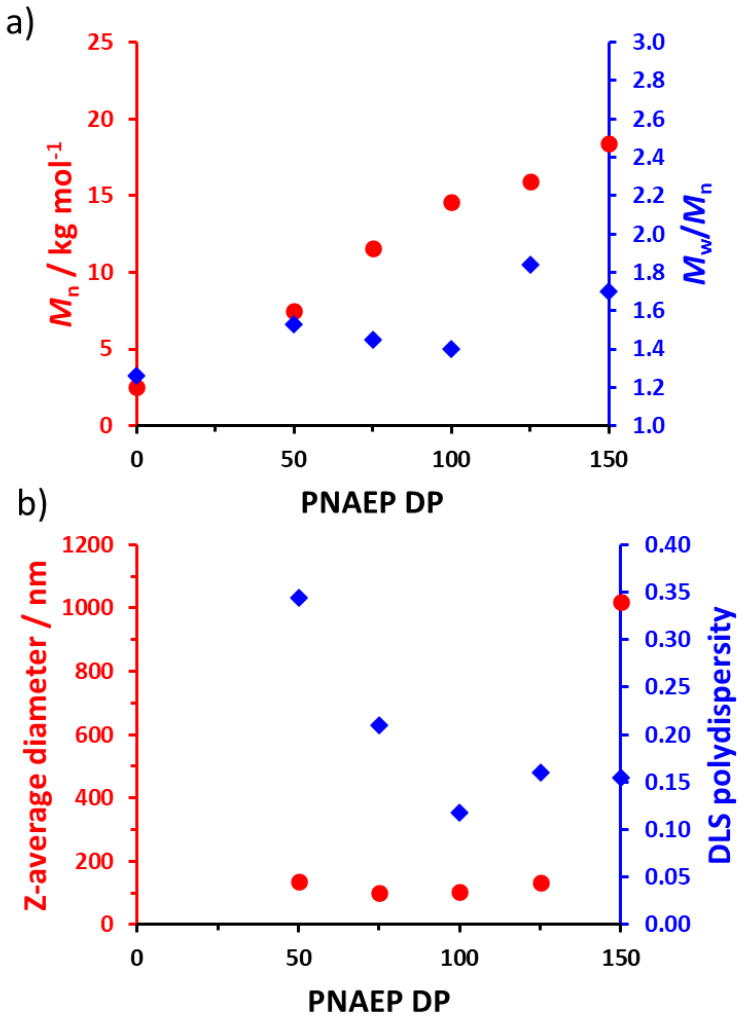

Figure 5.2. (a) Evolution in M_n and M_w/M_n with target PNAEP DP for a series of $PSMA_8$-$PNAEP_x$ diblock copolymers synthesised at 90 °C in *n*-dodecane using a $PSMA_8$/T21s molar ratio of 4.0 and the corresponding $PSMA_8$ precursor (refractive index detector with calibration using a series of near-monodisperse PMMA standards). (b) Evolution in z-average diameter (and the corresponding DLS polydispersity) with increasing target PNAEP DP for a series of $PSMA_8$-$PNAEP_x$ diblock copolymers diluted from 20 to 0.1% w/w solids using *n*-dodecane.

Literature precedent suggested that a longer PSMA stabiliser should facilitate greater colloidal stability.[46–49] Similar observations were reported for aqueous dispersions of PEG-PHPMA nano-objects, whereby using a PEG DP of 45 merely produced macroscopic flocculation whereas a PEG DP of 113 enabled stable colloidal dispersions to be obtained.[50]

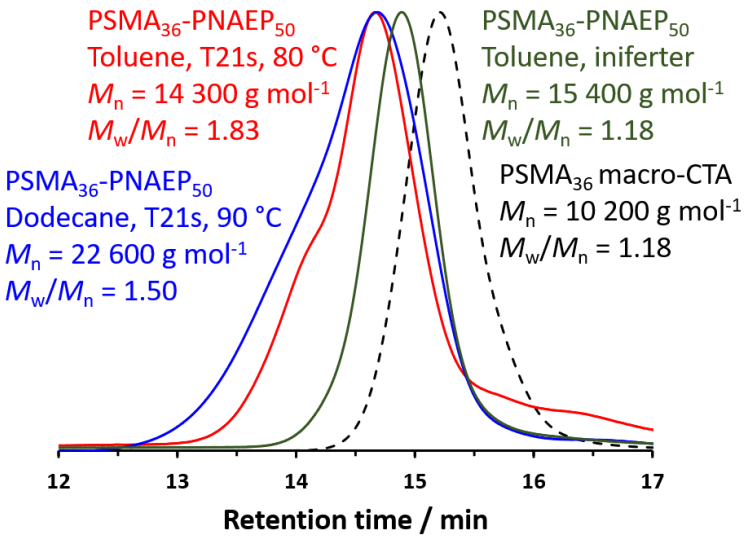

Figure 5.3. Chloroform GPC curves recorded for a $PSMA_{36}$ precursor and the corresponding chain-extended $PSMA_{36}$-$PNAEP_{50}$ diblock copolymers prepared by RAFT polymerisation of NAEP using a $PSMA_{36}$/T21s molar ratio of 4.0 in toluene at 80 °C (red), using a $PSMA_{36}$/T21s molar ratio of 4.0 in *n*-dodecane at 90 °C (blue) or by RAFT iniferter polymerisation in toluene at 30 °C (green). These GPC traces indicate relatively high blocking efficiencies but the presence of a high molecular weight shoulder for the T21s-initiated syntheses suggest some chain transfer to polymer in this case.

A $PSMA_{36}$ precursor was chain-extended with NAEP targeting a DP of 50 (i) by iniferter RAFT polymerisation in toluene at 30 °C, (ii) at 80 °C in the same solvent using T21s initiator and (iii) by non-aqueous emulsion polymerisation in *n*-dodecane at 90 °C using T21s initiator (Figure 5.3 and Table 5.1, see entries 1-3). In each case, a high blocking efficiency was achieved but a high MW shoulder was visible in the GPC curves recorded for the T21s-initiated syntheses. The iniferter polymerisation conducted in toluene resulted in a clear, viscous polymer solution and DLS studies indicated that only molecularly dissolved chains were present (so no particle nucleation occurred under such conditions). In this case, the absence of a high MW shoulder indicates better control over the NAEP polymerisation, but only 33% NAEP conversion was achieved within 7.5 h. In contrast, for the RAFT iniferter polymerisation conducted in *n*-dodecane at 30 °C resulted in no chain extension of the PSMA precursor and a precipitate phase of unreacted immiscible NAEP monomer instead. This was unexpected as successful chain extension was achieved using the T21s initiator in *n*-dodecane. This difference was attributed to the significantly higher reaction temperature employed (90 °C), which most likely leads to a greater proportion of the immiscible NAEP monomer becoming soluble in the *n*-dodecane continuous phase. It is perhaps noteworthy that such high temperatures are usually avoided when polymerising acrylic monomers because this often leads to inferior control.[19,20,51]

Table 5.1. Summary of the synthesis parameters, NAEP conversions, GPC data and DLS analyses for a series of $PSMA_{36}$-$PNAEP_x$ diblock copolymers prepared by RAFT polymerisation. The final physical appearance of each formulation is also indicated.

Entry number	Target composition	Temperature / °C	Initiator (CTA:I ratio)	Solvent	Solids concentration / % w/w	Reaction time / h	Conversion[a] / %	M_n[b] / g mol^{-1}	M_w/M_n[b]	Z-average diameter[c] / nm (PDI)	Visual appearance
1	$PSMA_{36}$-$PNAEP_{50}$	80	T21s (4)	Toluene	20	7.0	87	14 300	1.83	222 (0.54)	Hazy
2	$PSMA_{36}$-$PNAEP_{50}$	30	Iniferter	Toluene	30	7.5	33	15 400	1.18	No particles	Clear and viscous
3	$PSMA_{36}$-$PNAEP_{50}$	90	T21s (4)	*n*-Dodecane	20	2.0	99	22 600	1.50	45 (0.17)	Turbid and colloidal
4	$PSMA_{36}$-$PNAEP_{60}$	80	Iniferter	*n*-Dodecane	30	6.0	>99	21 500	1.33	120 (0.61)	Aggregation
5	$PSMA_{36}$-$PNAEP_{60}$	80	Iniferter	*n*-Dodecane	20	6.0	>99	24 000	1.43	69 (0.23)	Aggregation
6	$PSMA_{36}$-$PNAEP_{60}$	70	Iniferter	*n*-Dodecane	20	6.0	91	23 700	1.48	84 (0.21)	Aggregation
7	$PSMA_{36}$-$PNAEP_{60}$	90	T21s (4)	*n*-Dodecane	20	2.0	99	23 000	1.50	52 (0.10)	Colloidal
8	$PSMA_{36}$-$PNAEP_{60}$	90	T21s (10)	*n*-Dodecane	20	4.0	94	23 900	1.40	52 (0.23)	Colloidal, some aggregation
9	$PSMA_{36}$-$PNAEP_{60}$	90	T21s (20)	*n*-Dodecane	20	6.0	24	13 400	1.17	248 (0.58)	Clear with brown precipitation

[a]NAEP conversion determined by ^{1}H NMR spectroscopy in d_1-chloroform. [b]Determined by chloroform GPC (relative to PMMA calibration standards). [c]Determined by DLS for nanoparticle dispersions diluted to 0.1% w/w using *n*-dodecane.

However, for the PSMA-PNAEP synthesis conducted in *n*-dodecane, a relatively high temperature was required because NAEP is immiscible with *n*-dodecane; this makes this formulation a rare example of a *non-aqueous* emulsion polymerisation. Solubility experiments indicated that the solubility of NAEP in *n*-dodecane at 20°C was only 0.25% by volume. At the reaction temperature of 90 °C used for the T21S initiator, the NAEP solubility in *n*-dodecane increased to 4.9% by volume. These observations are consistent with the empirical finding that high temperatures are required for the efficient RAFT polymerisation of NAEP in *n*-dodecane.

In view of the relatively low solubility of NAEP in *n*-dodecane, the RAFT iniferter polymerisation of NAEP was conducted at elevated temperatures (see Figure 5.4 and Table 5.1, entries 4-6). A recirculating water bath was used to control the temperature of the LED reactor and the maximum accessible temperature using this set-up was 80 °C.

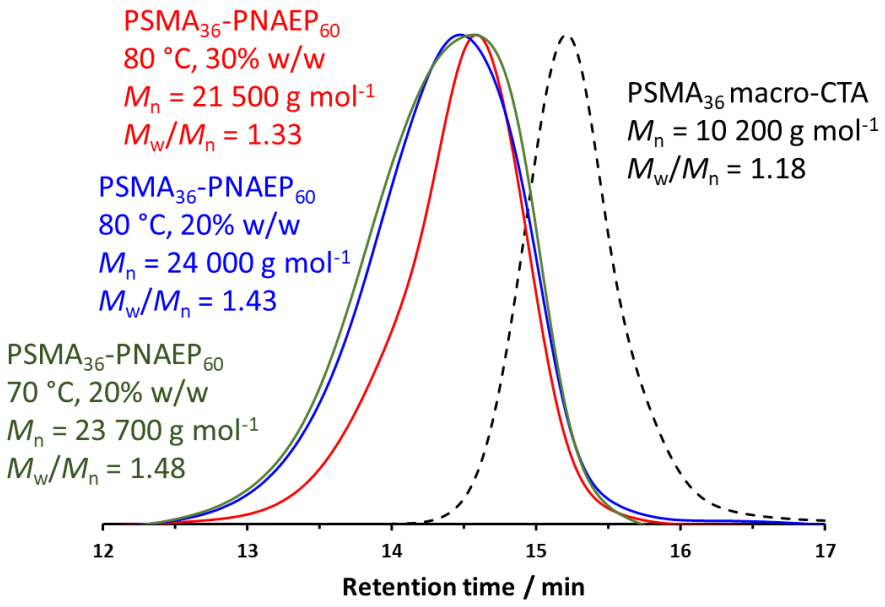

Figure 5.4. Chloroform GPC curves recorded for a $PSMA_{36}$ precursor and the corresponding $PSMA_{36}$-$PNAEP_{60}$ diblock copolymers prepared by RAFT iniferter polymerisation of NAEP in *n*-dodecane at 80 °C when targeting 30% w/w solids (red trace), at 80 °C when targeting 20% w/w solids (blue trace) and at 70 °C when targeting 20% w/w solids (green traces). These GPC data indicate that relatively high blocking efficiencies can be achieved under such conditions.

Initially, $PSMA_{36}$-$PNAEP_{60}$ nanoparticles were synthesised at 30% w/w solids and 80 °C. A high blocking efficiency and more than 99% NAEP conversion was achieved within 6 h, with a final M_w/M_n of 1.33. However, the resulting nanoparticles were extremely polydisperse as judged by DLS studies (z-average diameter = 120 nm; DLS polydispersity = 0.61). Moreover, macroscopic sedimentation of these nanoparticles was observed over time. To address this colloidal instability problem, the same synthesis was conducted targeting 20% w/w solids. Again, more than 99% NAEP conversion was achieved but the final M_w/M_n increased up to 1.43, indicating reduced RAFT

control. However, a z-average diameter of 69 nm and a corresponding DLS polydispersity of 0.23 was recorded, which suggests the formation of more well-defined nanoparticles. Nevertheless, nanoparticle sedimentation was still observed over time. Finally, $PSMA_{36}$-$PNAEP_{60}$ nanoparticles were prepared targeting 20% w/w solids at 70 °C. In this case, the final NAEP conversion was only 91% after 6 h and the final M_w/M_n was 1.48, which suggests that better RAFT control is achieved at elevated temperature. This counter-intuitive result may be related to the low solubility of NAEP in *n*-dodecane. RAFT iniferter polymerisations often exhibit exquisite control with narrow MWDs even for UHMW polymers.[52] This is due to the slower rate of termination exhibited when using photolysis of the RAFT CTA as opposed to an exogeneous radical source. It was therefore expected that RAFT iniferter polymerisation would result in narrower MWDs for $PSMA_{36}$-$PNAEP_x$ diblock copolymers than was actually observed by GPC ($M_w/M_n \leq 1.48$). However, chain transfer to polymer is well-documented for the polymerisation of acrylates and this problem is exacerbated at high temperatures.[51]

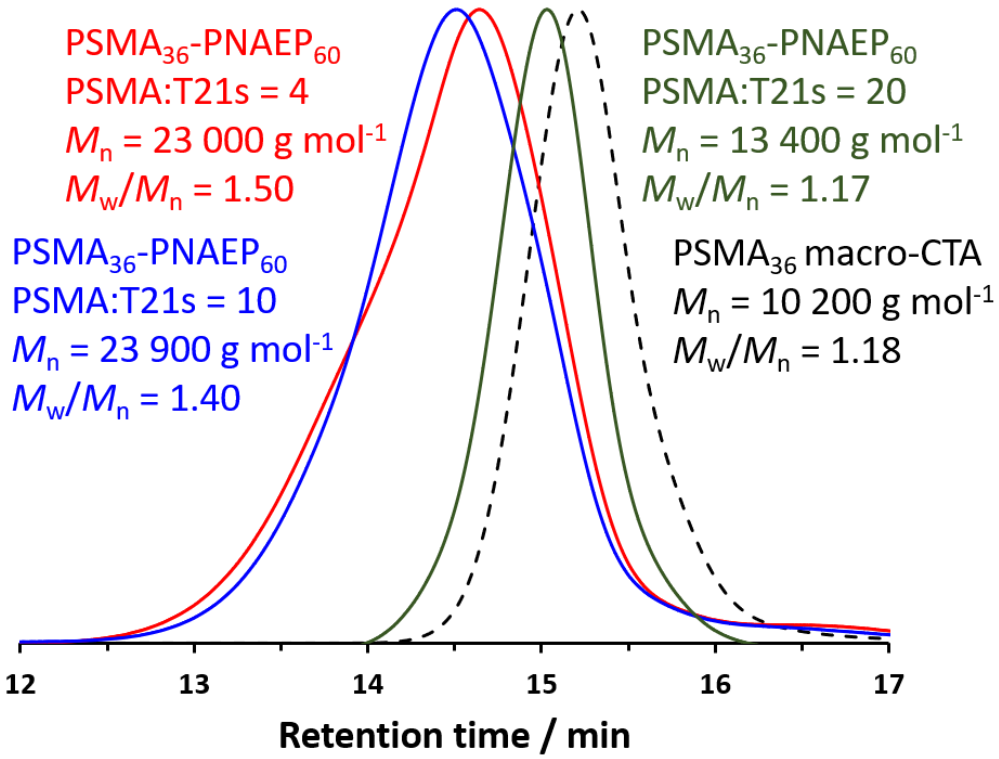

Figure 5.5. Chloroform GPC curves recorded for a $PSMA_{36}$ precursor and the corresponding $PSMA_{36}$-$PNAEP_{60}$ diblock copolymers prepared by RAFT non-aqueous emulsion polymerisation of NAEP in *n*-dodecane using a 4:1 $PSMA_{36}$/T21s molar ratio at 90 °C (red trace), a 10:1 $PSMA_{36}$/T21s molar ratio at 90 °C (blue trace) and using a 20:1 $PSMA_{36}$/T21s molar ratio at 90 °C (green trace).

As stated above, high temperatures do not usually favour the well-controlled polymerisation of acrylates. Nevertheless, this seems to be a prerequisite to ensure sufficient NAEP solubility in *n*-dodecane. Thus several synthetic parameters were varied to optimise such formulations (Table 5.1, entries 7-9). For example, the $PSMA_{36}$/T21s molar ratio was varied from 4.0 to 20.0 when

targeting $PSMA_{36}$-$PNAEP_{60}$ diblock copolymers because higher ratios should provide greater RAFT control and hence narrower MWDs.[53,54] The data shown in Figure 5.5 support this hypothesis: GPC analysis indicates that the M_w/M_n is reduced from 1.50 to 1.40 when the $PSMA_{36}$/T21s molar ratio is increased from 4.0 to 10.0. However, this also led to a significantly slower rate of polymerisation: the final NAEP conversion was lowered from >99% within 2 h to only 94% within 4 h, see entries 7 and 8 in Table 5.1. Indeed, when using a $PSMA_{36}$/T21s molar ratio of 20.0, only 24% NAEP conversion could be achieved within 6 h. Clearly, this approach is rather limited in scope if efficient polymerisations are desired. Moreover, higher molar ratios led to broader particle size distributions. When using a $PSMA_{36}$/T21s ratio of 4.0, DLS studies indicated a z-average diameter of 52 nm and a DLS polydispersity of 0.10, suggesting relatively well-defined spheres. However, the DLS polydispersity increased to 0.23 for a $PSMA_{36}$/T21s ratio of 10.0 for approximately the same z-average diameter. Finally, the $PSMA_{36}$-$PNAEP_{60}$ diblock copolymers were synthesised in *n*-dodecane using a $PSMA_{36}$/T21s ratio of 4.0 at 70 °C. At 70 °C, the solubility of NAEP in *n*-dodecane is around 2.9% v/v. However, this seems to be insufficient to enable its efficient non-aqueous polymerisation since ^{1}H NMR studies indicated no discernible conversion within 6 h at this temperature. Similar observations were made at 80 °C. However, the solubility of NAEP in *n*-dodecane is around 4.9% v/v at 90 °C, which is sufficient to enable its non-aqueous emulsion polymerisation at this temperature. On the basis of these preliminary studies, it was decided that the best compromise between MWD control, NAEP conversion and DLS polydispersity for $PSMA_{36}$-$PNAEP_{60}$ nanoparticles was achieved when using a $PSMA_{36}$/T21s ratio of 4.0 at 90 °C.

Aliquots were periodically extracted during the RAFT solution homopolymerisation of SMA in toluene at 70 ℃, with monomer conversions being determined by ^{1}H NMR spectroscopy (Figure 5.6a) and molecular weight data being obtained by GPC analysis using chloroform as an eluent (Figure 5.6b).

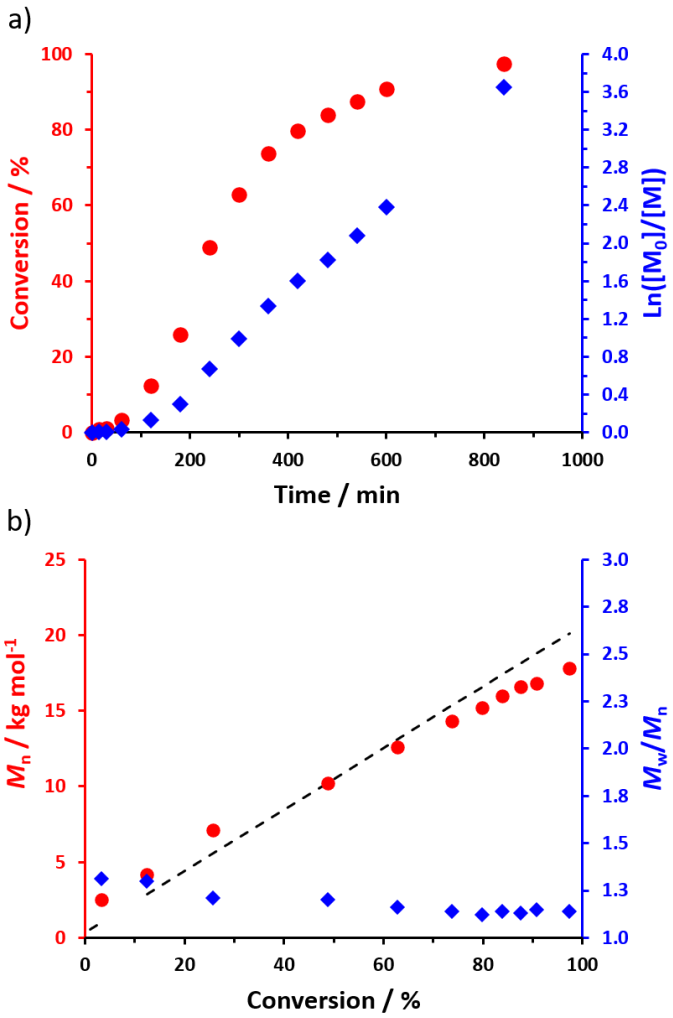

Figure 5.6. (a) Conversion *vs.* time curves obtained for the RAFT solution polymerisation of SMA at 70 °C in toluene using a PETTC RAFT agent and AIBN initiator targeting a PSMA DP of 60 at 50% w/w solids using a PETTC/AIBN molar ratio of 5. (b) Corresponding evolution in M_n and M_w/M_n with conversion observed for the same polymerisation. The dashed line indicates the theoretical M_n data. The experimental M_n data set differs from this theoretical line owing to a systematic GPC calibration error.

To prepare sterically-stabilised diblock copolymer nanoparticles, the $PSMA_{36}$ precursor was subsequently chain-extended *via* RAFT non-aqueous emulsion polymerisation of NAEP in *n*-dodecane at 90 °C targeting 20% w/w solids (see Scheme 5.1). The polymerisation kinetics for this chain extension were monitored using ^{1}H NMR spectroscopy (Figure 5.7a) while chloroform GPC was used to monitor the evolution in M_n and M_w/M_n (Figure 5.7b). Essentially full NAEP conversion was achieved within 1 h with a linear increase in M_n being observed. The final $PSMA_{36}$-$PNAEP_{60}$ diblock copolymer had an M_n of 24 100 g mol^{-1} and an M_w/M_n of 1.48. Relatively little NAEP was consumed within the first 20 min, indicating an initial induction period. However, the subsequent polymerisation proceeded rapidly, with 69% conversion being observed after 30 min.

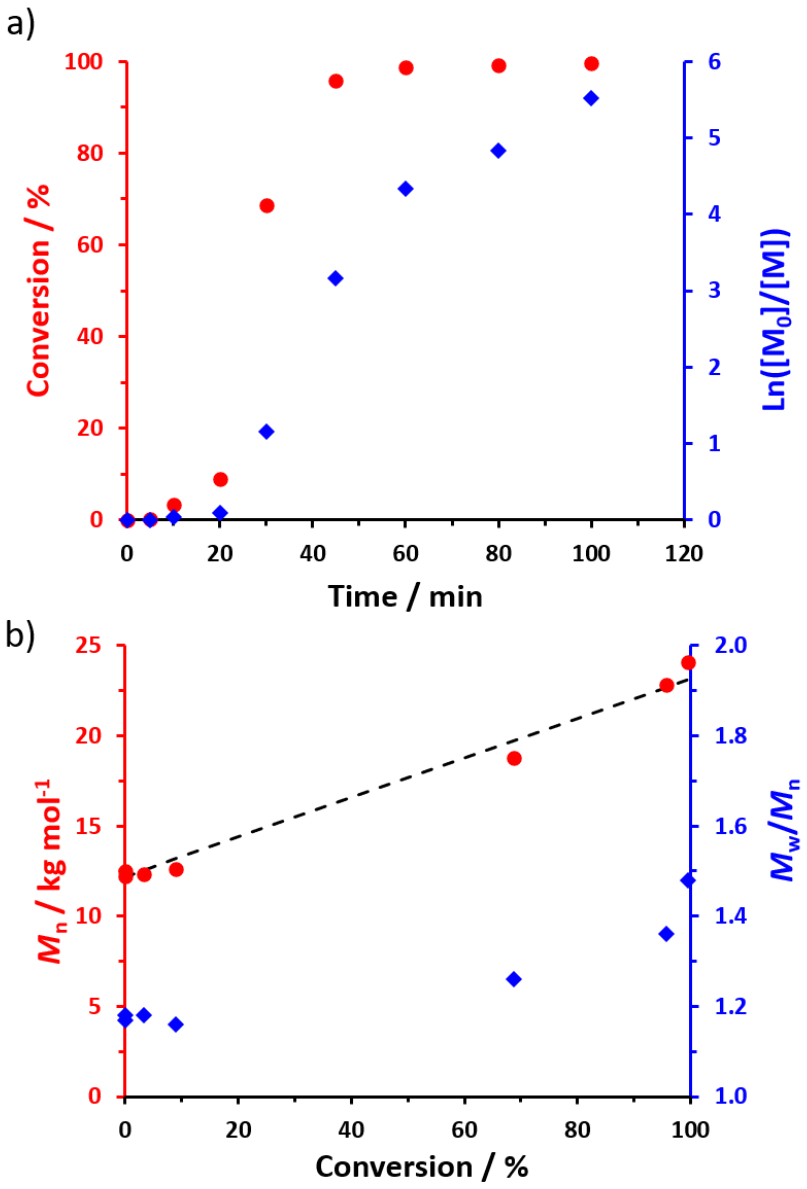

Figure 5.7. (a) Conversion *vs.* time curve and corresponding semi-logarithmic plot obtained for the RAFT non-aqueous emulsion polymerisation of NAEP at 90 °C in *n*-dodecane using a $PSMA_{36}$ precursor and targeting a PNAEP DP of 60 at 20% w/w solids using a $PSMA_{36}$/T21s molar ratio of 4.0. (b) Evolution of M_n and M_w/M_n with NAEP conversion for the same PISA formulation. The dashed line indicates the theoretical M_n data. Given that this GPC protocol uses a series of PMMA calibration standards, the good agreement between the experimental M_n data set and the theoretical line is merely fortuitous in this particular case.

A series of $PSMA_{36}$-$PNAEP_x$ nanoparticles were prepared in *n*-dodecane (Scheme 5.1). In all cases, high NAEP conversions (≥ 98%) were achieved as indicated by ^{1}H NMR analysis. A linear relationship was obtained between the z-average nanoparticle diameter determined by DLS and the PNAEP DP when targeting DPs up to 500 (Figure 5.8a). Inspecting this data set, it seems that systematic variation of the PNAEP DP alone enables reasonably well-defined nanoparticles (DLS polydispersities < 0.10) to be prepared over a relatively wide size range (from around 40 to 260 nm). Moreover, a linear increase in M_n and M_p was observed when targeting PNAEP DPs up to DP

70 (Figure 5.8b) and reasonably good RAFT control was achieved for target PNAEP DPs up to 60 (M_w/M_n < 1.50). Moreover, there appears to be an inflection point for the M_n and M_p and M_w/M_n data sets above a target PNAEP DP of 60. This interesting feature is not currently understood. It should be noted that GPC analysis was not attempted on $PSMA_{36}$-$PNAEP_x$ diblock copolymers for x values above 110 owing to solubility concerns. Presumably, this problem is related to inter-chain crosslinking *via* chain transfer to polymer, which becomes more observable when targeting longer chains.

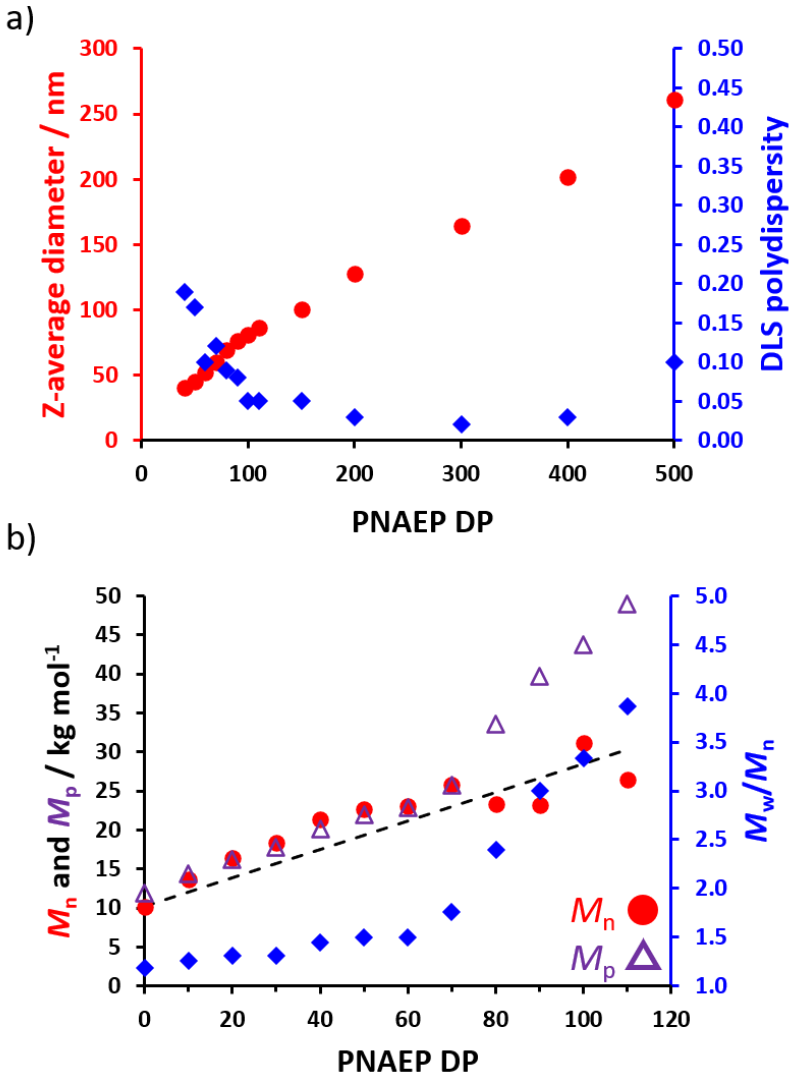

Figure 5.8. (a) Evolution in z-average diameter (and DLS polydispersity) with target PNAEP DP for a series of $PSMA_{36}$-$PNAEP_x$ nanoparticles diluted from 20% to 0.1% w/w solids using *n*-dodecane. (b) Evolution in M_n (red filled circle), M_p (purple open triangle) and M_w/M_n with target PNAEP DP for a series of $PSMA_{36}$-$PNAEP_x$ diblock copolymers prepared at 90 °C in *n*-dodecane using a $PSMA_{36}$/T21s molar ratio of 4.0 and the corresponding $PSMA_{36}$ precursor (refractive index detector with calibration using a series of near-monodisperse PMMA standards). The dashed line indicates the theoretical M_n data. The experimental M_n data set differs from this theoretical line owing to a systematic GPC calibration error.

The $PSMA_{36}$ precursor and two $PSMA_{36}$-$PNAEP_x$ diblock copolymers were characterised using differential scanning calorimetry (DSC). The $PSMA_{36}$ semi-crystalline precursor had a melting

temperature (T_m) of 30 °C (black trace), which has been previously reported by Semsarilar and co-workers.[55] The $PSMA_{36}$-$PNAEP_{60}$ diblock copolymer exhibited a T_g of –7 °C for the PNAEP block (red trace) while the $PSMA_{36}$-$PNAEP_{200}$ diblock copolymer had a T_g of –3 °C (blue trace), indicating only a weak molecular weight dependence (Figure 5.9a).[7] Such low T_g values mean that TEM imaging is very difficult for PNAEP-core nanoparticles owing to their deformation during TEM grid preparation (Figure 5.9b). This problem is well-documented for diblock copolymer nano-objects comprising low T_g core-forming blocks.[4,56,57]

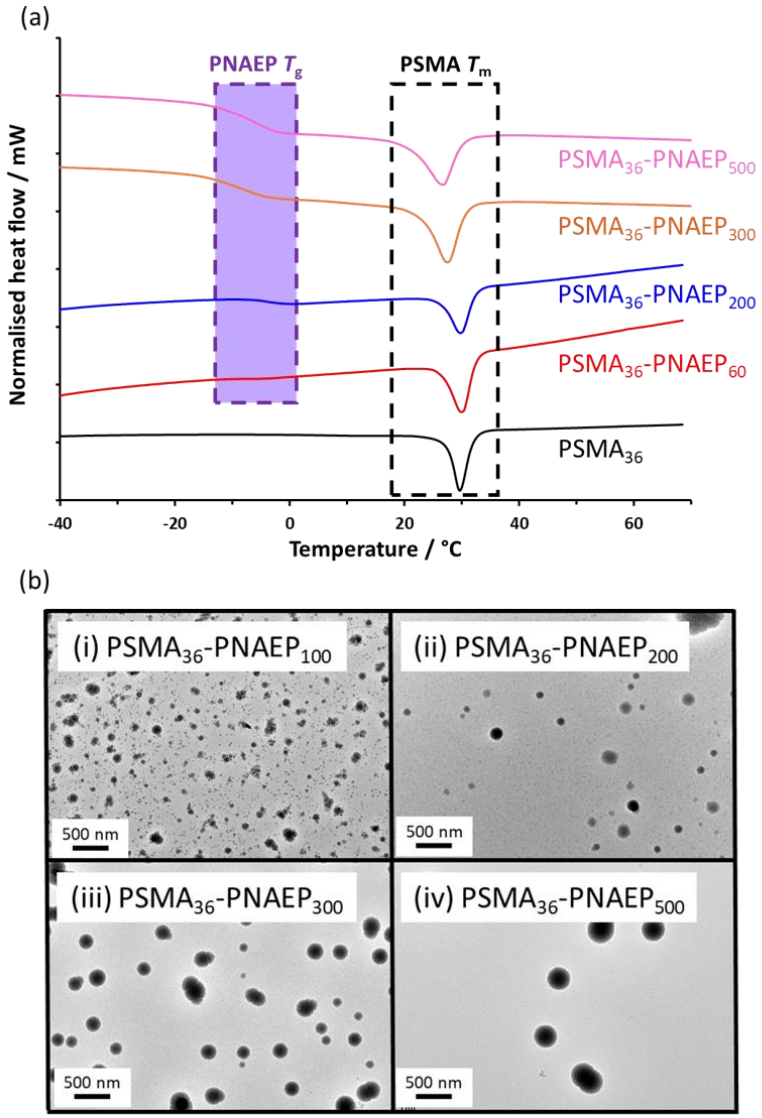

Figure 5.9. (a) Differential scanning calorimetry (DSC) curves recorded at a heating rate of 10 °C min^{-1} for the $PSMA_{36}$ precursor (black trace), $PSMA_{36}$-$PNAEP_{60}$ diblock copolymer (red trace), $PSMA_{36}$-$PNAEP_{200}$ diblock copolymer (blue trace), $PSMA_{36}$-$PNAEP_{300}$ diblock copolymer (orange trace).and $PSMA_{36}$-$PNAEP_{500}$ diblock copolymer (pink trace). (b) Representative TEM images recorded for $PSMA_{36}$-$PNAEP_{100}$, $PSMA_{36}$-$PNAEP_{200}$, $PSMA_{36}$-$PNAEP_{300}$ and $PSMA_{36}$-$PNAEP_{500}$ diblock copolymer spheres. Such nanoparticles tend to undergo film formation during TEM grid preparation owing to the relatively low T_g of the core-forming PNAEP block.

To address this issue, a bifunctional comonomer, EGDA, was added towards the end of the NAEP polymerisation when targeting a $PSMA_{36}$-$PNAEP_{60}$ diblock copolymer. As expected, the resulting core-crosslinked $PSMA_{36}$-$PNAEP_{60}$-$PEGDA_{10}$ triblock copolymer nano-objects were less prone to deformation during TEM grid preparation and hence exhibited a more well-defined spherical morphology (Figure 5.10). Moreover, the z-average diameter indicated by DLS studies of these crosslinked nanoparticles was consistent with that observed for the linear non-crosslinked nanoparticles (57 nm *vs.* 52 nm, respectively). The DLS diameter for the core-crosslinked $PSMA_{36}$-$PNAEP_{60}$-$PEGDA_{10}$ spheres was also determined in chloroform as well as *n*-dodecane (Table 5.2). The former solvent is a good solvent for both blocks, so core swelling was anticipated under such conditions. Indeed, a significantly larger diameter (84 nm) was observed for such nanogels.

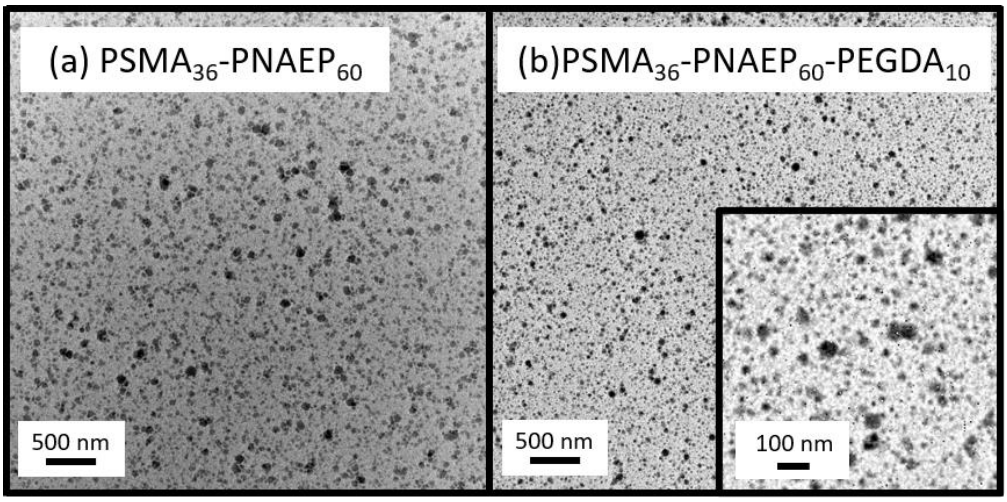

Figure 5.10. Representative TEM images recorded for linear $PSMA_{36}$-$PNAEP_{60}$ and cross-linked $PSMA_{36}$-$PNAEP_{60}$-$PEGDA_{10}$ nano-objects. The latter nanoparticles exhibit a more well-defined spherical morphology, whereas the former tend to undergo deformation during TEM grid preparation. Inset image shows nano-objects at a greater magnification.

Table 5.2. Summary of z-average diameters and DLS polydispersities (PDI) determined for linear $PSMA_{36}$-$PNAEP_{60}$ diblock copolymer nanoparticles and the corresponding core-crosslinked $PSMA_{36}$-$PNAEP_{60}$-$PEGDA_{10}$ triblock copolymer nanoparticles in *n*-dodecane (a poor solvent for PNAEP) and chloroform (a good solvent for PNAEP).

Diblock copolymer composition	**DLS diameter / nm (PDI)**	
	n-Dodecane	Chloroform
$PSMA_{36}$-$PNAEP_{60}$	52 (0.10)	/
$PSMA_{36}$-$PNAEP_{60}$-$PEGDA_{10}$	57 (0.09)	84 (0.06)

Small angle X-ray scattering (SAXS) was used to examine these diblock copolymer spheres in more detail. SAXS patterns were recorded for 1.0% w/w dispersions in *n*-dodecane. Satisfactory data fits could be obtained using a well-known spherical micelle model[58] (see Figure 5.11a) for all five types of diblock copolymer nanoparticles. Moreover, the low *q* gradient (Guinier region) tended

to zero, which is consistent with the formation of isotropic spheres. The position of the local minima observed at low *q* is inversely proportional to the particle radius (Equation 5.1), so such minima shift to lower *q* for larger particles.[59]

$$d = \frac{4.49}{q} \qquad 5.1$$

The R_g for $PSMA_{36}$ was estimated to be 1.5 nm using Equations 5.2 and 5.3 shown below.

$$L_{PSMA} = PSMA\ DP \times 0.255 \qquad 5.2$$

$$R_g = \left(L_{PSMA} \times \frac{1.53}{6}\right)^{\frac{1}{2}} \qquad 5.3$$

Here, L_{PSMA} is the contour length of the PSMA chain calculated by multiplying the PSMA DP by the contour length per monomer repeat unit (0.255 nm). The latter is defined by assuming an all-*trans* conformation for the relevant carbon bonds. A Kuhn length of 1.53 nm is used in this calculation, which corresponds to the literature value for poly(methyl methacrylate).[60] Clearly, this value is only an approximation to the true Kuhn length for PSMA.

Each of these scattering patterns was fitted according to a suitable spherical micelle model. The R_g for the $PSMA_{36}$ stabiliser block was fixed using the estimated theoretical value of 1.5 nm. The mean solvent volume fraction within the nanoparticle cores (x_{sol}) was zero, as expected for the PNAEP chains in the presence of *n*-dodecane. As expected, such SAXS analysis indicated an increase in sphere diameter with PNAEP DP. However, satisfactory fits using the spherical micelle model could not be obtained for PNAEP DPs > 300 at higher *q* region ($q > 0.2$). For these larger spheres, SAXS patterns were recorded at two different camera lengths (1.84 and 6.25 m) and these two data sets were combined prior to modelling, which may contribute to this deviation. DLS diameters were significantly greater than those determined by SAXS (Figure 5.11b). This is not unexpected, since the former technique reports a hydrodynamic z-average diameter whereas the latter technique reports a volume-average diameter. For this series of experiments, the DLS diameter was almost double the SAXS diameter. This may indicate the presence of larger spheres or aggregates: unlike SAXS, DLS is particularly sensitive to larger particles because light scattering scales as r^6, where *r* is the particle radius.[61]

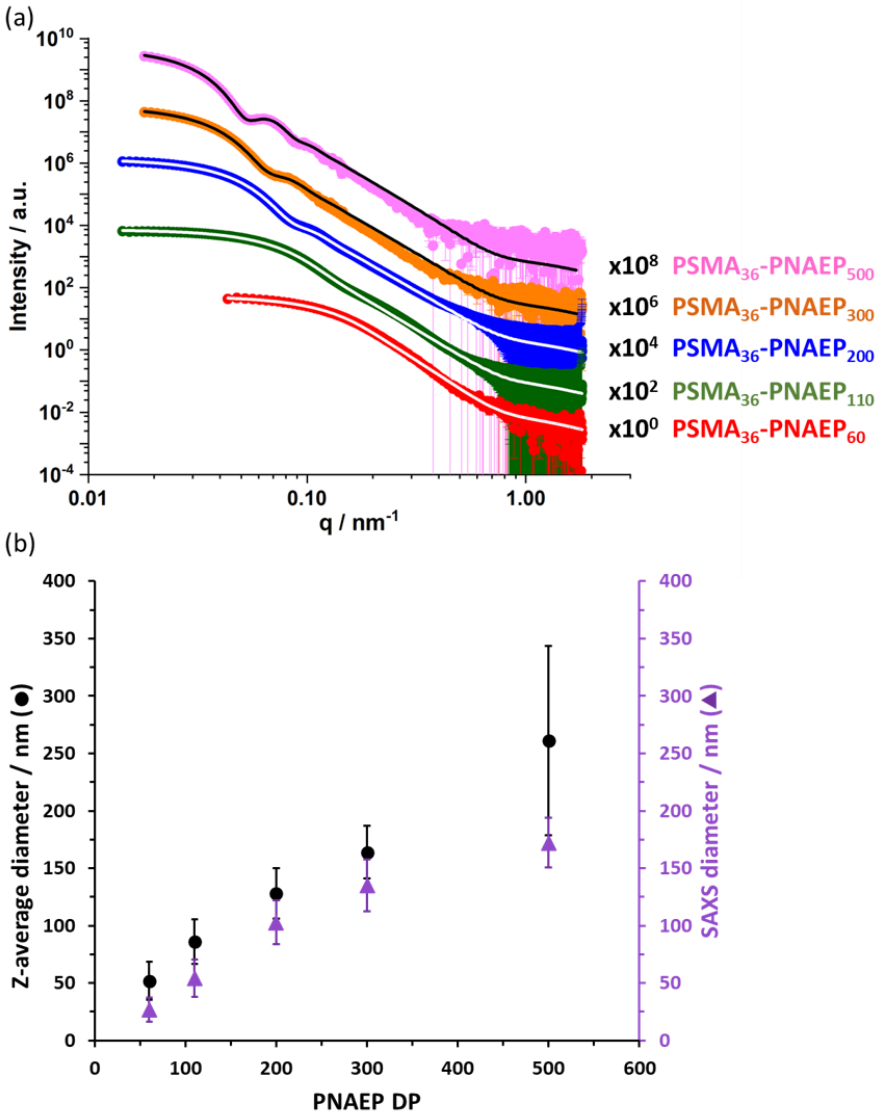

Figure 5.11. (a) SAXS patterns recorded for 1.0% w/w diblock copolymer dispersions in *n*-dodecane at 20 °C: $PSMA_{36}$-$PNAEP_{60}$ (red), $PSMA_{36}$-$PNAEP_{110}$ (green), $PSMA_{36}$-$PNAEP_{200}$ (blue), $PSMA_{36}$-$PNAEP_{300}$ (orange) and $PSMA_{36}$-$PNAEP_{500}$ (pink). Data fits obtained using a well-known spherical micelle model for each of these three patterns are indicated by either white lines (for satisfactory fits) or black lines (for unsatisfactory fits at high *q*).[58] Each SAXS pattern is offset by an arbitrary factor for the sake of clarity. (b) Corresponding sphere diameters determined by DLS (black circles) and SAXS (violet triangles) analysis, respectively. The error bars shown are the standard deviations for the nanoparticle diameter and hence indicate the width of each particle size distribution, rather than the experimental error.

Cunningham and co-workers prepared PSMA-PNMEP spherical nanoparticles *via* RAFT dispersion polymerisation of NMEP in *n*-dodecane and examined their performance as putative Pickering emulsifiers.[1] For example, addition of an equal volume of water to a 1.0% w/w dispersion of 23 nm diameter $PSMA_{14}$-$PNMEP_{49}$ spheres in *n*-dodecane followed by high-shear homogenisation led to the formation of oil-in-water (o/w) emulsions. This was unexpected because such *hydrophobic* nanoparticles normally favour the formation of water-in-oil (w/o) emulsions).[62] After

further investigation, it was concluded that *in situ* nanoparticle inversion occurred during homogenisation, leading to the formation of *hydrophilic* $PNMEP_{49}$-$PSMA_{14}$ nanoparticles that subsequently acted as a Pickering emulsifier.

Similar Pickering emulsifier studies were undertaken using the $POAA_{85}$-$PDMAC_{150}$ spheres prepared in *n*-heptane (see Chapter 4). Again, it was predicted that such *hydrophobic* nanoparticles should lead to the production of w/o emulsions but o/w emulsions were formed instead. To determine whether these new diblock copolymer nanoparticles had also inverted *in situ* to form *hydrophilic* $PDMAC_{195}$-$POAA_{85}$ nanoparticles, core-crosslinked triblock copolymer particles were prepared by adding EGDA towards the end of the DMAC polymerisation. Accordingly, core-crosslinked $POAA_{85}$-$PDMAC_{195}$-$PEGDA_{20}$ spheres were produced in *n*-heptane. In this case, high-shear homogenisation using a range of copolymer concentrations invariably produced o/w Pickering emulsions. Since such covalently-stabilised hydrophobic nanoparticles cannot undergo *in situ* inversion to form hydrophilic nanoparticles, this suggests that such Pickering emulsions must be formed by nanoparticle adsorption at the *inner* surface of the oil droplets. In retrospect, is it possible that nanoparticles adsorption from within the oil droplets could actually explain the data reported by Cunningham and co-workers (o/w emulsions produced for hydrophobic nanoparticles) seen for $PSMA_{14}$-$PNMEP_{49}$ diblock copolymers which was attributed to *in situ* micelle inversion.[1]

Accordingly, $PSMA_{36}$-$PNAEP_{70}$ nanoparticles were prepared in *n*-dodecane for evaluation as a putative Pickering emulsifier. The copolymer concentration was systematically lowered from 1.0% w/w to 0.025% w/w by dilution with *n*-dodecane to produce a series of dispersions. Then deionised water was added to each dispersion in turn to obtain a constant *n*-dodecane volume fraction of 0.50 and high-shear homogenisation was conducted in each case (Figure 5.12). The electrical conductivity for an emulsion obtained using 1.0% w/w $PSMA_{36}$-$PNMEP_{70}$ diblock copolymer nanoparticles was determined to be 3.22×10^{-4} S m^{-1}, which is comparable to that of deionised water alone (3.83×10^{-4} S m^{-1}). It should be noted that the non-aqueous conductivity of *n*-dodecane is 1.1×10^{-11} S m^{-1}).[63] This indicates the formation of an o/w emulsion. The so-called 'drop test' method (which involves taking an aliquot of the emulsion and determining whether it disperses more readily when added to either water or *n*-dodecane) was used to confirm that o/w emulsions were always produced regardless of the nanoparticle concentration.

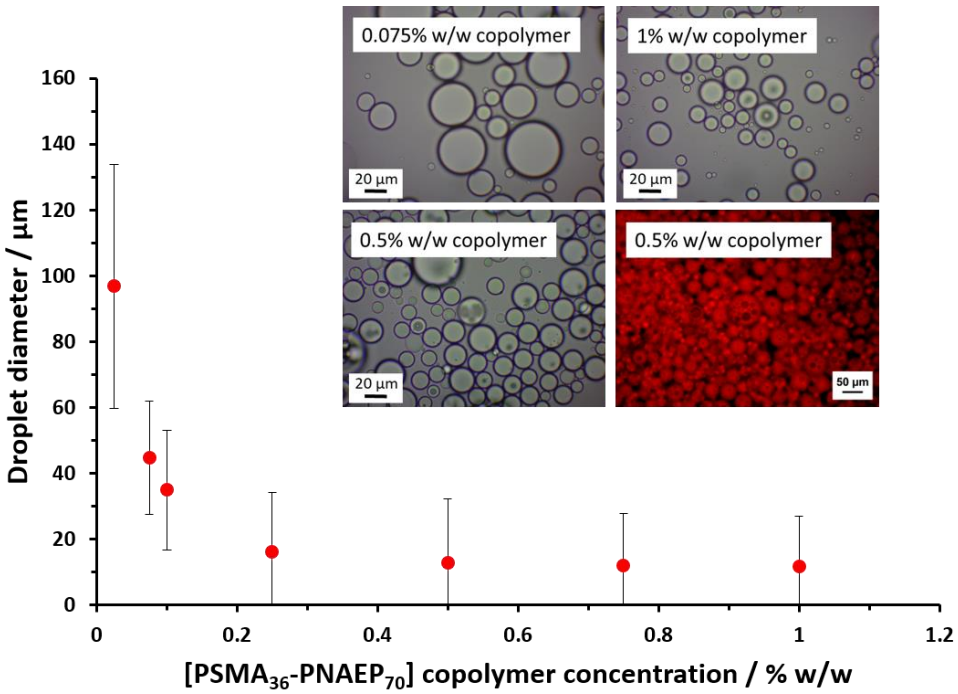

Figure 5.12. Variation in volume-average droplet diameter (as determined by laser diffraction) for a series of o/w Pickering emulsions obtained by high-shear homogenisation when systematically varying the $PSMA_{36}$-$PNAEP_{70}$ copolymer concentration at a constant *n*-dodecane volume fraction of 0.50. The error bars indicate the droplet polydispersity rather than the error in the measurements. Inset: optical micrographs recorded at copolymer concentrations of 0.075%, 0.50% and 1.0% w/w, respectively. For 0.50% w/w copolymer concentration, the oil phase is labelled with a water-insoluble dye (Nile Red) to aid the identification of w/o/w double emulsions by fluorescence microscopy.

Close inspection of optical images recorded for the emulsions generated using copolymer concentrations ≥ 0.5% w/w reveals the presence of small droplets within larger droplets. This suggests the formation of double emulsions. To further investigate this observation, Nile Red was dissolved in *n*-dodecane containing 0.50% w/w copolymer prior to homogenisation with water to enable fluorescence microscopy studies (Figure 5.12). This water-insoluble dye label is exclusively located in the droplet phase, demonstrating that an o/w emulsion is obtained in this case. Close inspection revealed that water droplets were present within these oil droplets, confirming the formation of a w/o/w double emulsion. This is somewhat surprising: normally, a w/o emulsion must be produced first before re-emulsification in the presence of further water to form w/o/w emulsions.[64] Moreover, the production of Pickering double emulsions usually requires two types of particles of differing wettability (*i.e. hydrophilic* particles to produce o/w and *hydrophobic* particles to stabilise w/o emulsions).[65–68] Nevertheless, there are a few literature reports of such complex Pickering double emulsions being formed during a single emulsification step.[69–72] For example, György and co-workers obtained w/o/w double emulsions when using *hydrophobic* $PSMA_9$-$PHPMA_{50}$ diblock copolymer nanoparticles prepared in mineral oil.[73] More specifically, high oil volume fractions (> 0.50), high shear rates (> 13 500 rpm) and high copolymer

concentrations (> 0.5% w/w) enabled the direct formation of w/o/w double emulsions in one step. Similarly, optical microscopy studies of the present system indicate that w/o/w double emulsions are only obtained when using $PSMA_{36}$-$PNAEP_{70}$ copolymer concentrations greater than 0.5% w/w.

Laser diffraction was used to size the emulsion droplets (see Figure 5.12). At higher copolymer concentrations, the volume-average droplet diameter remained constant at around 12 μm. However, both the mean diameter and the standard deviation increased as the copolymer concentration was lowered to 0.25% w/w. Large, polydisperse droplets with relatively poor stability towards coalescence were obtained at or below 0.1% w/w copolymer concentration. This upturn in droplet size at lower copolymer concentrations is characteristic of Pickering emulsions because there are fewer nanoparticles to stabilise the additional interfacial area created during high-shear homogenisation.[74–77] This implies that the original linear $PSMA_{36}$-$PNAEP_{70}$ nanoparticles survive the high-shear homogenisation conditions intact. However, in view of their highly hydrophobic nature, we had expected such nanoparticles to form w/o Pickering emulsions, rather than o/w emulsions. In principle, there are two possible explanations for this surprising observation. *In situ* nanoparticle inversion might have occurred during homogenisation, thus converting the *hydrophobic* $PSMA_{36}$-$PNAEP_{70}$ nanoparticles into *hydrophilic* $PNAEP_{70}$-$PSMA_{36}$ nanoparticles. Alternatively, the hydrophobic $PSMA_{36}$-$PNAEP_{70}$ nanoparticles simply adsorb at the *inner surface* of the oil droplets.[78]

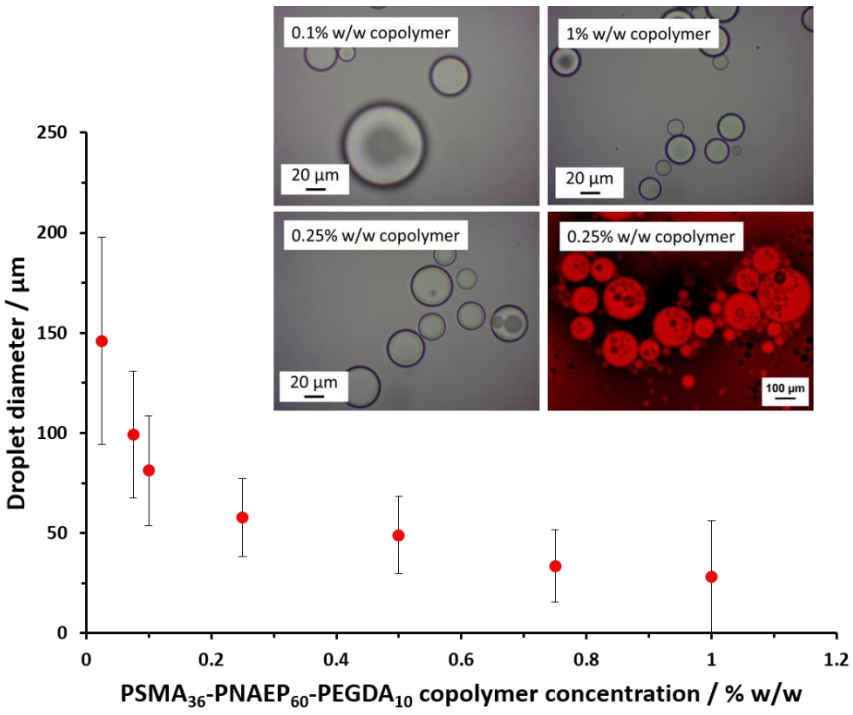

Figure 5.13. Variation in volume-average droplet diameter (as determined by laser diffraction) for a series of o/w Pickering emulsions obtained by high-shear homogenisation when systematically varying the $PSMA_{36}$-$PNAEP_{60}$-$PEGDA_{10}$ copolymer concentration at a constant *n*-dodecane volume fraction of 0.50. The error bars indicate the droplet polydispersity rather than the error in the measurements. Inset: optical micrographs recorded at copolymer concentrations of 0.1%, 0.25% and 1.0% w/w. At 0.25% w/w copolymer concentration, a water-insoluble dye (Nile Red) was dissolved in the oil phase to aid the identification of w/o/w double emulsions using fluorescence microscopy.

To distinguish between these two scenarios, core-crosslinked $PSMA_{36}$-$PNAEP_{60}$-$PEGDA_{10}$ nanoparticles were used to prepare emulsions *via* high-shear homogenisation. The upturn in droplet diameter observed at lower copolymer concentrations confirmed their Pickering-type character (see Figure 5.13). DLS studies indicated that, unlike the corresponding linear nanoparticles, such covalently-stabilised nanoparticles swelled appreciably but did not dissolve when diluted with chloroform, which is a good solvent for both blocks (Table 5.2). This suggests that the degree of core-crosslinking was sufficient to ensure their structural integrity. Accordingly, the copolymer concentration was systematically lowered from 1.0% w/w to 0.025% w/w when performing high-shear homogenisation at a constant oil volume fraction of 0.50. The 'drop test' method confirmed the formation of o/w emulsions in all cases. Importantly, such core-crosslinked nanoparticles cannot undergo inversion to form *hydrophilic* PNAEP-stabilised nanoparticles that could in principle adsorb at the outer surface of the oil droplets. Thus, this suggests that the original linear *hydrophobic* $PSMA_{36}$-$PNAEP_{70}$ nanoparticles must adsorb at the *inner surface* of the oil droplets, rather than undergo *in situ* inversion.

As for the linear $PSMA_{36}$-$PNAEP_{70}$ nanoparticles, optical microscopy studies of these core-crosslinked $PSMA_{36}$-$PNAEP_{60}$-$PEGDA_{10}$ nanoparticles indicated the formation of w/o/w double emulsions, which was confirmed by fluorescence microscopy studies when Nile Red dye was added to the oil phase (Figure 5.13). However, such complex emulsions were formed at somewhat lower copolymer concentrations; close inspection of the relevant optical micrographs suggest that w/o/w double emulsions can be formed at copolymer concentrations as low as 0.1% w/w.

Finally, the relative volume fraction of *n*-dodecane was varied while fixing the linear non-crosslinked $PSMA_{36}$-$PNAEP_{70}$ copolymer concentration at 1.0% w/w with respect to the oil phase (Figure 5.14). In this series of experiments, w/o/w Pickering double emulsions were obtained for *n*-dodecane volume fractions up to 0.60, with mean droplet diameters increasing from 6 µm to 19 µm when adjusting the oil volume fraction from 0.30 to 0.60. However, an w/o emulsion was produced when attempting homogenisation at an *n*-dodecane volume fraction of 0.65 and 0.70. Nevertheless, it is clear that relatively concentrated w/o/w Pickering double emulsions can be accessed with this simple protocol.

Emulsions prepared using 1% w/w $PSMA_{36}$-$PNAEP_{70}$ nanoparticles for oil volume fractions of either 0.50 or 0.70 were allowed to stand for 72 h to enable the droplets to either cream or sediment, respectively. These two emulsion formulations were chosen because an oil volume fraction of 0.50 gives an o/w emulsion and a volume fraction of 0.70 produces a w/o emulsion (see Figure 14a). DLS analysis was performed on each continuous phase after removal of the droplet phase. For the oil-continuous phase derived from the w/o emulsion, DLS studies confirmed strong light scattering (derived count rate = 10 000 kcps) and the presence of nanoparticles (z-average diameter = 55 nm; DLS polydispersity = 0.08) that were strikingly similar in size compared to the original nanoparticles (z-average diameter = 60 nm and DLS polydispersity = 0.12). Conversely, DLS studies of the aqueous continuous phase isolated from the o/w emulsion suggested that no nanoparticles were present because a much lower derived count rate of only 600 kcps was observed in this case. These experiments provide convincing evidence that the o/w Pickering emulsions are stabilised by hydrophobic $PSMA_{36}$-$PNAEP_{70}$ nanoparticles adsorbing at the oil/water interface from within the droplets and do not undergo *in situ* inversion to from hydrophilic $PNAEP_{70}$-$PSMA_{36}$ nanoparticles.

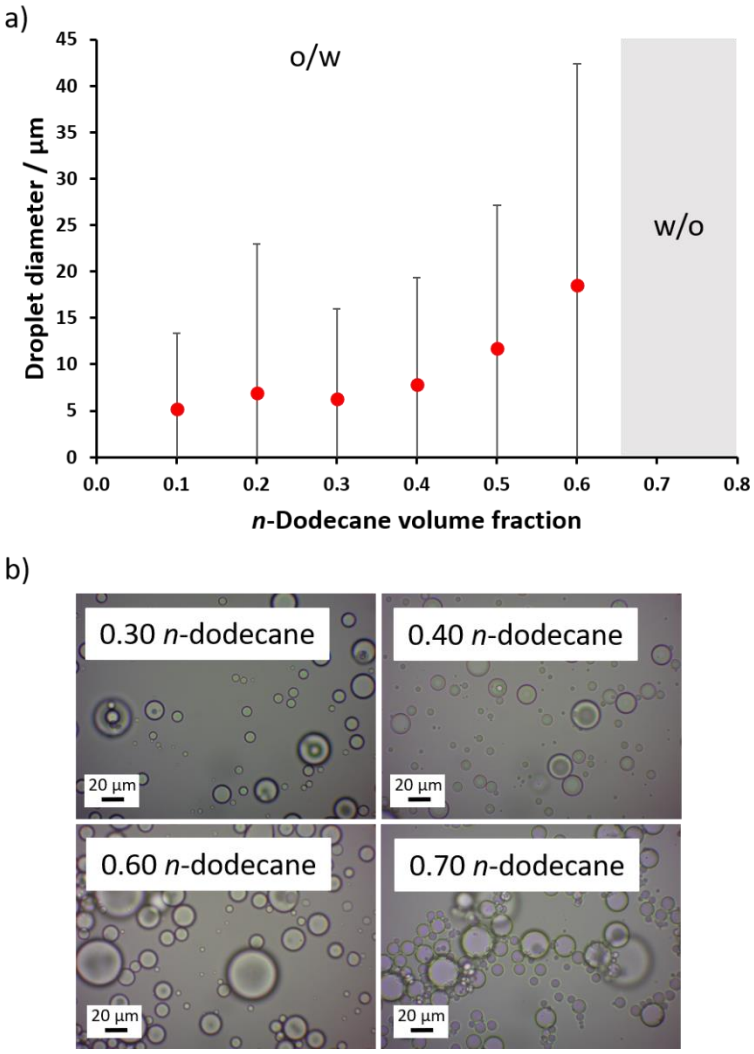

Figure 5.14. (a) Variation in volume-average droplet diameter (as determined by laser diffraction) for a series of o/w Pickering emulsions obtained by high-shear homogenisation when systematically varying the volume fraction of *n*-dodecane at a constant $PSMA_{36}$-$PNAEP_{70}$ copolymer concentration of 1.0% w/w. The error bars indicate the droplet polydispersity, rather than the error in the measurements. (b) Optical micrographs recorded for Pickering emulsions prepared at *n*-dodecane volume fractions of 0.10, 0.20, 0.30, 0.40, 0.60, 0.65 and 0.70, respectively.

5.4 Conclusions

A $PSMA_{36}$ precursor was employed for the RAFT non-aqueous emulsion polymerisation of NAEP in *n*-dodecane to produce a series of sterically-stabilised $PSMA_{36}$-$PNAEP_x$ diblock copolymer spheres with high NAEP conversions being achieved in all cases (≥ 98% within 5 h at 90 °C). Systematic increases in both z-average diameter and M_p were observed when targeting higher PNAEP DPs, but only relatively poor RAFT control could be achieved. TEM studies of the linear diblock nanoparticles proved to be problematic owing to film formation during TEM grid preparation. Thus, EGDA was employed as a bifunctional crosslinker and added towards the end of the NAEP polymerisation to produce covalently-stabilised nanoparticles. This strategy enabled

a well-defined spherical morphology to be confirmed by TEM while also producing core-crosslinked nanogels that swelled when dispersed in chloroform, which is a good solvent for both blocks. In addition, SAXS was also employed to confirm this spherical morphology as each scattering pattern could be satisfactorily fitted using a suitable scattering model for spherical micelles.

$PSMA_{36}$-$PNAEP_{70}$ spheres prepared in *n*-dodecane were evaluated as a putative Pickering emulsifier. We hypothesised that employing such hydrophobic nanoparticles should lead to the formation of w/o emulsions. Unexpectedly, addition of an equal volume of water followed by high-shear homogenisation always produced o/w emulsions. Laser diffraction and optical microscopy studies indicated that larger droplets were formed on lowering the copolymer concentration. According to prior studies by the Armes group,[68,77,79] this indicates that the nanoparticles remain intact after homogenisation to produce genuine Pickering emulsions. Thus, either the hydrophobic $PSMA_{36}$-$PNAEP_{70}$ spheres are adsorbed at the *inner* surface of the oil droplets or nanoparticle inversion has occurred during high-shear homogenisation to form *hydrophilic* $PNAEP_{70}$-$PSMA_{36}$ spheres that then adsorb at the *outer* surface of the oil droplets. Accordingly, core-crosslinked $PSMA_{36}$-$PNAEP_{60}$-$PEGDA_{10}$ spheres were prepared in *n*-dodecane to discriminate between these two possibilities. In this case, high-shear homogenisation at various copolymer concentrations again produced o/w Pickering emulsions. As these covalently-stabilised hydrophobic nanoparticles cannot undergo inversion to form hydrophilic nanoparticles, this suggests that such Pickering emulsions must be formed by nanoparticle adsorption at the *inner* surface of the oil droplets. For both types of Pickering emulsifiers, certain experimental conditions (*e.g.* copolymer concentrations ≥ 0.5% w/w for the linear nanoparticles, ≥ 0.1% w/w for the core-crosslinked nanoparticles, or when using oil volume fractions ≤ 0.60) produced w/o/w *double* emulsions, rather than o/w emulsions.

5.5 References

(1) Cunningham, V. J.; Armes, S. P.; Musa, O. M. Synthesis, Characterisation and Pickering Emulsifier Performance of Poly(Stearyl Methacrylate)–Poly(N-2-(Methacryloyloxy)Ethyl Pyrrolidone) Diblock Copolymer Nano-Objects via RAFT Dispersion Polymerisation in n-Dodecane. *Polym. Chem.* **2016**, *7*, 1882–1891.

(2) Cunningham, V. J.; Ning, Y.; Armes, S. P.; Musa, O. M. Poly(N-2-(Methacryloyloxy)Ethyl Pyrrolidone)-Poly(Benzyl Methacrylate) Diblock Copolymer Nano-Objects via RAFT Alcoholic Dispersion Polymerisation in Ethanol. *Polymer* **2016**, *106*, 189–199.

(3) Cunningham, V. J.; Derry, M. J.; Fielding, L. A.; Musa, O. M.; Armes, S. P. RAFT Aqueous Dispersion Polymerization of N -(2-(Methacryloyloxy)Ethyl)Pyrrolidone: A Convenient Low Viscosity Route to High Molecular Weight Water-Soluble Copolymers.

Macromolecules **2016**, *49*, 4520–4533.

(4) Gibson, R. R.; Cornel, E. J.; Musa, O. M.; Fernyhough, A.; Armes, S. P. RAFT Dispersion Polymerisation of Lauryl Methacrylate in Ethanol–Water Binary Mixtures: Synthesis of Diblock Copolymer Vesicles with Deformable Membranes. *Polym. Chem.* **2020**, *11*, 1785–1796.

(5) Gibson, R. R.; Armes, S. P.; Musa, O. M.; Fernyhough, A. End-Group Ionisation Enables the Use of Poly(N -(2-Methacryloyloxy)Ethyl Pyrrolidone) as an Electrosteric Stabiliser Block for Polymerisation-Induced Self-Assembly in Aqueous Media. *Polym. Chem.* **2019**, *10*, 1312–1323.

(6) Jesson, C. P.; Cunningham, V. J.; Smallridge, M. J.; Armes, S. P. Synthesis of High Molecular Weight Poly(Glycerol Monomethacrylate) via RAFT Emulsion Polymerization of Isopropylideneglycerol Methacrylate. *Macromolecules* **2018**, *51*, 3221–3232.

(7) Deane, O. J.; Lovett, J. R.; Musa, O. M.; Fernyhough, A.; Armes, S. P. Synthesis of Well-Defined Pyrrolidone-Based Homopolymers and Stimulus-Responsive Diblock Copolymers via RAFT Aqueous Solution Polymerization of 2-(N-Acryloyloxy)Ethylpyrrolidone. *Macromolecules* **2018**, *51*, 7756–7766.

(8) Deane, O. J.; Musa, O. M.; Fernyhough, A.; Armes, S. P. Synthesis and Characterization of Waterborne Pyrrolidone-Functional Diblock Copolymer Nanoparticles Prepared via Surfactant-Free RAFT Emulsion Polymerization. *Macromolecules* **2020**, *53*, 1422–1434.

(9) Beuermann, S.; Buback, M. Rate Coefficients of Free-Radical Polymerization Deduced from Pulsed Laser Experiments. *Prog. Polym. Sci.* **2002**, *27*, 191–254.

(10) Chenal, M.; Bouteiller, L.; Rieger, J. Ab Initio RAFT Emulsion Polymerization of Butyl Acrylate Mediated by Poly(Acrylic Acid) Trithiocarbonate. *Polym. Chem.* **2013**, *4*, 752–762.

(11) Zhang, X.; Boissé, S.; Bui, C.; Albouy, P. A.; Brûlet, A.; Li, M. H.; Rieger, J.; Charleux, B. Amphiphilic Liquid-Crystal Block Copolymer Nanofibers via RAFT-Mediated Dispersion Polymerization. *Soft Matter* **2012**, *8*, 1130–1141.

(12) Houillot, L.; Bui, C.; Save, M.; Charleux, B.; Farcet, C.; Moire, C.; Raust, J.-A.; Rodriguez, I. Synthesis of Well-Defined Polyacrylate Particle Dispersions in Organic Medium Using Simultaneous RAFT Polymerization and Self-Assembly of Block Copolymers. A Strong Influence of the Selected Thiocarbonylthio Chain Transfer Agent. *Macromolecules* **2007**, *40*, 6500–6509.

(13) Raust, J. A.; Houillot, L.; Save, M.; Charleux, B.; Moire, C.; Farcet, C.; Pasch, H. Two Dimensional Chromatographic Characterization of Block Copolymers of 2-Ethylhexyl Acrylate and Methyl Acrylate, P2EHA-b-PMA, Produced via RAFT-Mediated Polymerization in Organic Dispersion. *Macromolecules* **2010**, *43*, 8755–8765.

(14) Houillot, L.; Bui, C.; Farcet, C.; Moire, C.; Raust, J. A.; Pasch, H.; Save, M.; Charleux, B. Dispersion Polymerization of Methyl Acrylate in Nonpolar Solvent Stabilized by Block Copolymers Formed in Situ via the RAFT Process. *ACS Appl. Mater. Interfaces* **2010**, *2*, 434–442.

(15) Keddie, D. J.; Moad, G.; Rizzardo, E.; Thang, S. H. RAFT Agent Design and Synthesis. *Macromolecules* **2012**, *45*, 5321–5342.

(16) Ratcliffe, L. P. D.; McKenzie, B. E.; Le Bouëdec, G. M. D.; Williams, C. N.; Brown, S. L.; Armes, S. P. Polymerization-Induced Self-Assembly of All-Acrylic Diblock Copolymers via

RAFT Dispersion Polymerization in Alkanes. *Macromolecules* **2015**, *48*, 8594–8607.

(17) Veloso, A.; García, W.; Agirre, A.; Ballard, N.; Ruipérez, F.; De La Cal, J. C.; Asua, J. M. Determining the Effect of Side Reactions on Product Distributions in RAFT Polymerization by MALDI-TOF MS. *Polym. Chem.* **2015**, *6*, 5437–5450.

(18) Ahmad, N. M.; Heatley, F.; Britton, D.; Lovell, P. A. Chain Transfer to Polymer in Emulsion Polymerization. *Macromol. Symp.* **1999**, *143*, 231–241.

(19) Heatley, F.; Lovell, P. A.; Yamashita, T. Chain Transfer to Polymer in Free-Radical Solution Polymerization of 2-Ethylhexyl Acrylate Studied by NMR Spectroscopy. *Macromolecules* **2001**, *34*, 7636–7641.

(20) Ahmad, N. M.; Charleux, B.; Farcet, C.; Ferguson, C. J.; Gaynor, S. G.; Hawkett, B. S.; Heatley, F.; Klumperman, B.; Konkolewicz, D.; Lovell, P. A.; Matyjaszewski, K.; Venkatesh, R. Chain Transfer to Polymer and Branching in Controlled Radical Polymerizations of N-Butyl Acrylate. *Macromol. Rapid Commun.* **2009**, *30*, 2002–2021.

(21) Canning, S. L.; Cunningham, V. J.; Ratcliffe, L. P. D.; Armes, S. P. Phenyl Acrylate Is a Versatile Monomer for the Synthesis of Acrylic Diblock Copolymer Nano-Objects: Via Polymerization-Induced Self-Assembly. *Polym. Chem.* **2017**, *8*, 4811–4821.

(22) Tan, J.; Huang, C.; Liu, D.; Zhang, X.; Bai, Y.; Zhang, L. Alcoholic Photoinitiated Polymerization-Induced Self-Assembly (Photo-PISA): A Fast Route toward Poly(Isobornyl Acrylate)-Based Diblock Copolymer Nano-Objects. *ACS Macro Lett.* **2016**, *5*, 894–899.

(23) Perrier, S. 50th Anniversary Perspective: RAFT Polymerization A User Guide. *Macromolecules* **2017**, *50*, 7433–7447.

(24) Chen, M.; Zhong, M.; Johnson, J. A. Light-Controlled Radical Polymerization: Mechanisms, Methods, and Applications. *Chem. Rev.* **2016**, *116*, 10167–10211.

(25) Li, S.; Han, G.; Zhang, W. Photoregulated Reversible Addition-Fragmentation Chain Transfer (RAFT) Polymerization. *Polym. Chem.* **2020**, *11*, 1830–1844.

(26) Otsu, T.; Yoshida, M. Role of Initiator-transfer Agent-terminator (Iniferter) in Radical Polymerizations: Polymer Design by Organic Disulfides as Iniferters. *Macromol. Rapid Commun.* **1982**, *3*, 127–132.

(27) Otsu, T.; Kuriyama, A. Living Mono- and Biradical Polymerizations in Homogeneous System Synthesis of AB and ABA Type Block Copolymers. *Polym. Bull.* **1984**, *11*, 135–142.

(28) Otsu, T. Iniferter Concept and Living Radical Polymerization. *J. Polym. Sci. Part A Polym. Chem.* **2000**, *38*, 2121–2136.

(29) Easterling, C. P.; Xia, Y.; Zhao, J.; Fanucci, G. E.; Sumerlin, B. S. Block Copolymer Sequence Inversion through Photoiniferter Polymerization. *ACS Macro Lett.* **2019**, *8*, 1461–1466.

(30) Nicolaÿ, R.; Kwak, Y.; Matyjaszewski, K. A Green Route to Well-Defined High-Molecular-Weight (Co)Polymers Using ARGET ATRP with Alkyl Pseudohalides and Copper Catalysis. *Angew. Chemie Int. Ed.* **2010**, *49*, 541–544.

(31) An, Z. 100th Anniversary of Macromolecular Science Viewpoint: Achieving Ultrahigh Molecular Weights with Reversible Deactivation Radical Polymerization. *ACS Macro Lett.* **2020**, *9*, 350–357.

(32) Read, E.; Guinaudeau, A.; Wilson, D. J.; Cadix, A.; Violleau, F.; Destarac, M. Low Temperature RAFT/MADIX Gel Polymerisation: Access to Controlled Ultra-High Molar

Mass Polyacrylamides. *Polym. Chem.* **2014**, *5*, 2202–2207.

(33) Carmean, R. N.; Sims, M. B.; Figg, C. A.; Hurst, P. J.; Patterson, J. P.; Sumerlin, B. S. Ultrahigh Molecular Weight Hydrophobic Acrylic and Styrenic Polymers through Organic-Phase Photoiniferter-Mediated Polymerization. *ACS Macro Lett.* **2020**, 613–618.

(34) Yeow, J.; Sugita, O. R.; Boyer, C. Visible Light-Mediated Polymerization-Induced Self-Assembly in the Absence of External Catalyst or Initiator. *ACS Macro Lett.* **2016**, *5*, 558–564.

(35) Tan, J.; Liu, D.; Bai, Y.; Huang, C.; Li, X.; He, J.; Xu, Q.; Zhang, X.; Zhang, L. An Insight into Aqueous Photoinitiated Polymerization-Induced Self-Assembly (Photo-PISA) for the Preparation of Diblock Copolymer Nano-Objects. *Polym. Chem.* **2017**, *8*, 1315–1327.

(36) Blackman, L. D.; Doncom, K. E. B.; Gibson, M. I.; O'Reilly, R. K. Comparison of Photo- and Thermally Initiated Polymerization-Induced Self-Assembly: A Lack of End Group Fidelity Drives the Formation of Higher Order Morphologies. *Polym. Chem.* **2017**, *8*, 2860–2871.

(37) György, C.; Derry, M. J.; Cornel, E. J.; Armes, S. P. Synthesis of Highly Transparent Diblock Copolymer Vesicles via RAFT Dispersion Polymerization of 2,2,2-Trifluoroethyl Methacrylate in n -Alkanes. *Macromolecules* **2021**, *54*, 1159–1169.

(38) Landfester, K.; Willert, M.; Antonietti, M. Preparation of Polymer Particles in Nonaqueous Direct and Inverse Miniemulsions. *Macromolecules* **2000**, *33*, 2370–2376.

(39) You, X.; Dimonie, V. L.; Klein, A. Nonaqueous Emulsion Copolymerization of Ethyl Methacrylate/Lauryl Methacrylate in Propylene Glycol. I. Evaluation of Stabilizing Efficiency for PEO-PS-PEO Triblock Copolymers. *J. Appl. Polym. Sci.* **2001**, *80*, 1951–1962.

(40) Hariri, K.; Al Akhrass, S.; Delaite, C.; Moireau, P.; Riess, G. Polymerizable Oil-in-Oil Emulsions: Poly(Vinyl Pyrrolidone) Dispersions in Reactive PDMS Medium. *Polym. Int.* **2007**, *56*, 1200–1205.

(41) Daraba, O. M.; Cadinoiu, A. N.; Rata, D. M.; Atanase, L. I.; Vochita, G. Antitumoral Drug-Loaded Biocompatible Polymeric Nanoparticles Obtained by Non-Aqueous Emulsion Polymerization. *Polymers* **2020**, *12*, 1018–1034.

(42) Müller, K.; Klapper, M.; Müllen, K. Synthesis of Conjugated Polymer Nanoparticles in Non-Aqueous Emulsions. *Macromol. Rapid Commun.* **2006**, *27*, 586–593.

(43) Müller, K.; Klapper, M.; Müllen, K. Polyester Nanoparticles by Non-Aqueous Emulsion Polycondensation. *J. Polym. Sci. Part A Polym. Chem.* **2007**, *45*, 1101–1108.

(44) Jones, E. R.; Semsarilar, M.; Blanazs, A.; Armes, S. P. Efficient Synthesis of Amine-Functional Diblock Copolymer Nanoparticles via RAFT Dispersion Polymerization of Benzyl Methacrylate in Alcoholic Media. *Macromolecules* **2012**, *45*, 5091–5098.

(45) Ilavsky, J.; Jemian, P. R. Irena : Tool Suite for Modeling and Analysis of Small-Angle Scattering. *J. Appl. Crystallogr.* **2009**, *42*, 347–353.

(46) Pei, Y.; Sugita, O. R.; Thurairajah, L.; Lowe, A. B. Synthesis of Poly(Stearyl Methacrylate-b-3-Phenylpropyl Methacrylate) Nanoparticles in n-Octane and Associated Thermoreversible Polymorphism. *RSC Adv.* **2015**, *5*, 17636–17646.

(47) Pei, Y.; Thurairajah, L.; Sugita, O. R.; Lowe, A. B. RAFT Dispersion Polymerization in Nonpolar Media: Polymerization of 3-Phenylpropyl Methacrylate in n -Tetradecane with Poly(Stearyl Methacrylate) Homopolymers as Macro Chain Transfer Agents. *Macromolecules* **2015**, *48*, 236–244.

(48) Derry, M. J.; Fielding, L. A.; Warren, N. J.; Mable, C. J.; Smith, A. J.; Mykhaylyk, O. O.; Armes, S. P. In Situ Small-Angle X-Ray Scattering Studies of Sterically-Stabilized Diblock Copolymer Nanoparticles Formed during Polymerization-Induced Self-Assembly in Non-Polar Media. *Chem. Sci.* **2016**, *7*, 5078–5090.

(49) Parker, B. R.; Derry, M. J.; Ning, Y.; Armes, S. P. Exploring the Upper Size Limit for Sterically Stabilized Diblock Copolymer Nanoparticles Prepared by Polymerization-Induced Self-Assembly in Non-Polar Media. *Langmuir* **2020**, *36*, 3730–3736.

(50) Penfold, N. J. W.; Whatley, J. R.; Armes, S. P. Thermoreversible Block Copolymer Worm Gels Using Binary Mixtures of PEG Stabilizer Blocks. *Macromolecules* **2019**, *52*, 1653–1662.

(51) Britton, D.; Heatley, F.; Lovell, P. A. Chain Transfer to Polymer in Free-Radical Bulk and Emulsion Polymerization of Vinyl Acetate Studied by NMR Spectroscopy. *Macromolecules* **1998**, *31*, 2828–2837.

(52) Carmean, R. N.; Becker, T. E.; Sims, M. B.; Sumerlin, B. S. Ultra-High Molecular Weights via Aqueous Reversible-Deactivation Radical Polymerization. *Chem* **2017**, *2*, 93–101.

(53) Gody, G.; Maschmeyer, T.; Zetterlund, P. B.; Perrier, S. Rapid and Quantitative One-Pot Synthesis of Sequence-Controlled Polymers by Radical Polymerization. *Nat. Commun.* **2013**, *4*, 2505.

(54) Guimarães, T. R.; Khan, M.; Kuchel, R. P.; Morrow, I. C.; Minami, H.; Moad, G.; Perrier, S.; Zetterlund, P. B. Nano-Engineered Multiblock Copolymer Nanoparticles via Reversible Addition–Fragmentation Chain Transfer Emulsion Polymerization. *Macromolecules* **2019**, *52*, 2965–2974.

(55) Semsarilar, M.; Penfold, N. J. W.; Jones, E. R.; Armes, S. P. Semi-Crystalline Diblock Copolymer Nano-Objects Prepared via RAFT Alcoholic Dispersion Polymerization of Stearyl Methacrylate. *Polym. Chem.* **2015**, *6*, 1751–1757.

(56) Byard, S. J.; Williams, M.; McKenzie, B. E.; Blanazs, A.; Armes, S. P. Preparation and Cross-Linking of All-Acrylamide Diblock Copolymer Nano-Objects via Polymerization-Induced Self-Assembly in Aqueous Solution. *Macromolecules* **2017**, *50*, 1482–1493.

(57) Byard, S. J.; O'Brien, C. T.; Derry, M. J.; Williams, M.; Mykhaylyk, O. O.; Blanazs, A.; Armes, S. P. Unique Aqueous Self-Assembly Behavior of a Thermoresponsive Diblock Copolymer. *Chem. Sci.* **2020**, *11*, 396–402.

(58) Pedersen, J. S. Form Factors of Block Copolymer Micelles with Spherical, Ellipsoidal and Cylindrical Cores. *J. Appl. Crystallogr.* **2000**, *33*, 637–640.

(59) Li, M.; Liu, Y.; Nie, H.; Bansil, R.; Steinhart, M. Kinetics of Hexagonal−Body-Centered Cubic Transition in a Triblock Copolymer in a Selective Solvent: Time-Resolved Small-Angle X-Ray Scattering Measurements and Model Calculations. *Macromolecules* **2007**, *40*, 9491–9502.

(60) Fetters, L. J.; Lohse, D. J.; Colby, R. H. Chain Dimensions and Entanglement Spacings. In *Physical Properties of Polymers Handbook*; Springer: New York, USA, 2007; pp 447–454.

(61) Stetefeld, J.; McKenna, S. A.; Patel, T. R. Dynamic Light Scattering: A Practical Guide and Applications in Biomedical Sciences. *Biophys. Rev.* **2016**, *8*, 409–427.

(62) Thompson, K. L.; Fielding, L. A.; Mykhaylyk, O. O.; Lane, J. A.; Derry, M. J.; Armes, S. P. Vermicious Thermo-Responsive Pickering Emulsifiers. *Chem. Sci.* **2015**, *6*, 4207–4214.

(63) Taylor, S. E.; Zeng, H. Electrical Conductivity and Viscosity in Binary Organic Liquid Mixtures: Participation of Molecular Interactions and Nanodomains. *Colloids and Interfaces* **2020**, *4*, 44.

(64) Garti, N. Double Emulsions - Scope, Limitations and New Achievements. *Colloids Surfaces A Physicochem. Eng. Asp.* **1997**, *123–124*, 233–246.

(65) Zou, S.; Wang, C.; Gao, Q.; Tong, Z. Surfactant-Free Multiple Pickering Emulsions Stabilized by Combining Hydrophobic and Hydrophilic Nanoparticles. *J. Dispers. Sci. Technol.* **2013**, *34*, 173–181.

(66) Williams, M.; Warren, N. J.; Fielding, L. A.; Armes, S. P.; Verstraete, P.; Smets, J. Preparation of Double Emulsions Using Hybrid Polymer/Silica Particles: New Pickering Emulsifiers with Adjustable Surface Wettability. *ACS Appl. Mater. Interfaces* **2014**, *6*, 20919–20927.

(67) Williams, M.; Armes, S. P.; Verstraete, P.; Smets, J. Double Emulsions and Colloidosomes-in-Colloidosomes Using Silica-Based Pickering Emulsifiers. *Langmuir* **2014**, *30*, 2703–2711.

(68) Thompson, K. L.; Mable, C. J.; Lane, J. A.; Derry, M. J.; Fielding, L. A.; Armes, S. P. Preparation of Pickering Double Emulsions Using Block Copolymer Worms. *Langmuir* **2015**, *31*, 4137–4144.

(69) Nonomura, Y.; Kobayashi, N.; Nakagawa, N. Multiple Pickering Emulsions Stabilized by Microbowls. *Langmuir* **2011**, *27*, 4557–4562.

(70) Hong, L.; Sun, G.; Cai, J.; Ngai, T. One-Step Formation of W/O/W Multiple Emulsions Stabilized by Single Amphiphilic Block Copolymers. *Langmuir* **2012**, *28*, 2332–2336.

(71) Tu, F.; Lee, D. One-Step Encapsulation and Triggered Release Based on Janus Particle-Stabilized Multiple Emulsions. *Chem. Commun.* **2014**, *50*, 15549–15552.

(72) Clegg, P. S.; Tavacoli, J. W.; Wilde, P. J. One-Step Production of Multiple Emulsions: Microfluidic, Polymer-Stabilized and Particle-Stabilized Approaches. *Soft Matter* **2016**, *12*, 998–1008.

(73) György, C.; Hunter, S. J.; Girou, C.; Derry, M. J.; Armes, S. P. Synthesis of Poly(Stearyl Methacrylate)-Poly(2-Hydroxypropyl Methacrylate) Diblock Copolymer Nanoparticles: Via RAFT Dispersion Polymerization of 2-Hydroxypropyl Methacrylate in Mineral Oil. *Polym. Chem.* **2020**, *11*, 4579–4590.

(74) Binks, B. P.; Whitby, C. P. Silica Particle-Stabilized Emulsions of Silicone Oil and Water: Aspects of Emulsification. *Langmuir* **2004**, *20*, 1130–1137.

(75) Morse, A. J.; Armes, S. P.; Thompson, K. L.; Dupin, D.; Fielding, L. A.; Mills, P.; Swart, R. Novel Pickering Emulsifiers Based on PH-Responsive Poly(2- (Diethylamino)Ethyl Methacrylate) Latexes. *Langmuir* **2013**, *29*, 5446–5475.

(76) Mable, C. J.; Warren, N. J.; Thompson, K. L.; Mykhaylyk, O. O.; Armes, S. P. Framboidal ABC Triblock Copolymer Vesicles: A New Class of Efficient Pickering Emulsifier. *Chem. Sci.* **2015**, *6*, 6179–6188.

(77) Thompson, K. L.; Mable, C. J.; Cockram, A.; Warren, N. J.; Cunningham, V. J.; Jones, E. R.; Verber, R.; Armes, S. P. Are Block Copolymer Worms More Effective Pickering Emulsifiers than Block Copolymer Spheres? *Soft Matter* **2014**, *10*, 8615–8626.

(78) Bon, S. A. F.; Mookhoek, S. D.; Colver, P. J.; Fischer, H. R.; van der Zwaag, S. Route to

Stable Non-Spherical Emulsion Droplets. *Eur. Polym. J.* **2007**, *43*, 4839–4842.

(79) Thompson, K. L.; Chambon, P.; Verber, R.; Armes, S. P. Can Polymersomes Form Colloidosomes? *J. Am. Chem. Soc.* **2012**, *134*, 12450–12453.

Chapter 6.

Conclusions and prospect

This Thesis focuses on the controlled radical polymerisation of three commercially relevant monomers provided by Ashland Speciality Ingredients: NMEP, NAEP and OAA. RAFT polymerisation was used to synthesise amphiphilic diblock copolymers that undergo PISA to form spheres, vesicles or lamellae in a range of solvents. RAFT-mediated PISA is remarkably tolerant of monomer functionality and enables the reproducible synthesis of a wide range of diblock copolymer nano-objects in various media[1,2] simply by varying the target diblock composition and copolymer concentration.[3–6] Initially, PNMEP was employed as a stabiliser block for PISA syntheses. In Chapter 2, kinetically-trapped spheres were obtained in aqueous media and it was demonstrated that colloidal stability can only be achieved by introducing anionic carboxylate groups at the end of the PNMEP chains. This is not particularly surprising, because it is well-documented that suitable end-groups can enhance the hydrophilic character of a water-soluble polymer.[7] Such end-group ionisation is critical because it significantly raises the CP exhibited by the weakly hydrophilic PNMEP stabiliser chains, which possess inverse temperature solubility (*i.e.* LCST-type behaviour) in aqueous solution. For example, increasing the pH of a 1% w/w aqueous solution of $PNMEP_{53}$ homopolymer from pH 3 to pH 7 raised its CP from 64 °C to more than 90 °C. Moreover, lowering the dispersion pH below the pK_a of the PNMEP stabiliser chains or addition of low levels of salt (which causes charge screening) was sufficient to induce incipient flocculation. However, colloidal stability was not solely owing to charge stabilisation: ^{1}H NMR studies indicated that the PNMEP block acts as an *electrosteric* stabiliser because it is relatively well-solvated under the PISA synthesis conditions. It was also hypothesised that the terminal anionic charge was responsible for the kinetically-trapped spherical morphology. In principle, conducting such PISA syntheses in the presence of sufficient added salt should enable access to higher order morphologies (*i.e.* worms or vesicles).[8,9]

Ionisation of terminal carboxylic acid end-groups has been exploited to increase the hydrophilic character of another water-soluble polymer, poly(2-hydroxyethyl acrylate) or PHEA. For PHEA DPs ≤ 105, end-group ionisation of the carboxylic acid chain-ends was required to ensure the colloidal stability of PHEA-based diblock copolymer nanoparticles. However, when using a longer $PHEA_{140}$ stabiliser block, purely steric stabilisation was sufficient to prevent nanoparticle aggregation.[10]

In Chapter 3, vesicles and lamellae were produced by the RAFT dispersion polymerisation of LMA to produce highly asymmetric diblock copolymers in an 80:20 w/w ethanol-water mixture. According to kinetic studies conducted using ^{1}H NMR spectroscopy, micellar nucleation occurred when the growing PLMA chains attained a mean DP of 17. Surprisingly, vesicles were obtained even when targeting relatively low PLMA DPs (for which spheres and worms would be normally expected). Moreover, no evidence for a viscous reaction mixture (usually indicative of a worm-

like morphology) was observed at intermediate LMA conversions. This was unexpected, as the evolution of copolymer morphology generally involves initially spheres, then worms and finally vesicles for such RAFT dispersion polymerisations.[11] Presumably, these observations are related to the comparatively high molecular weight of the LMA monomer, which makes it much more difficult to pinpoint the worm morphology. In principle, further insights could be gained by using *in situ* SAXS to monitor the PISA synthesis of PNMEP-PLMA vesicles to determine if worm-like intermediates are formed.

The inherent colour and malodour conferred by the organosulfur-based RAFT chain-ends are undesirable for commercial applications, thus a suitable end-group removal protocol was briefly explored.[12,13] There are numerous literature studies concerning the removal of RAFT groups from soluble chains[14–16] but far fewer reports explore such end-group removal from diblock copolymer nanoparticles. Moreover, any small molecule reagent must be able to diffuse into the interior of the nanoparticles to access the RAFT chain-ends.[17,18] As an alternative strategy, visible light was shown to be an effective and efficient method for RAFT end-group removal from a 7.5% w/w aqueous dispersion of diblock copolymer vesicles. On exposure to blue light (λ = 405 nm) at 50 °C, UV GPC analysis indicated that 96% of the original dithiobenzoate end-groups were removed within 4 h. A comparative experiment using excess ACVA initiator at 70 °C resulted in almost no end-group removal over the same timescale, presumably because this ionic reagent cannot readily penetrate the highly hydrophobic PLMA membranes. These experiments confirm the advantages of using visible light to remove RAFT end-groups without recourse to chemical reagents. Clearly, further studies are warranted to study the effect of varying the wavelength and intensity of the visible light, the reaction temperature, the copolymer concentration and the copolymer morphology on the kinetics of end-group removal. Does the turbidity of the copolymer dispersion affect light penetration and, if so, does this reduce the overall efficiency of end-group removal? Similarly, can trithiocarbonate or xanthate end-groups be removed as efficiently as dithiobenzoates?

In Chapter 4, POAA is employed as a steric stabiliser for the PISA synthesis of PDMAC-core nanoparticles in various *n*-alkanes. In this context, it is perhaps worth emphasising that there are currently no literature reports of POAA-based diblock copolymers, whether by PISA or by RAFT solution polymerisation or by any other controlled radical polymerisation technique. Interestingly, the colloidal stability of these nanoparticles depends on the precise nature of the solvent used for their synthesis. Thus, spherical nanoparticles that remained colloidally stable between 20 and 90 °C were obtained when using *n*-heptane, *n*-octane or *n*-decane. However, for higher *n*-alkanes, the nanoparticles remained stable when synthesised at 70 °C but flocculated on

cooling. This interesting UCST-like phenomenon was observed by variable temperature turbidimetry and DLS experiments. Using a POAA precursor with a DP of 85 resulted in kinetically-trapped spherical nanoparticles. This is most likely because this relatively long steric stabiliser block inhibits 1D sphere-sphere fusion, which is considered to be a prerequisite for worm formation.[19] An important extension of this work could be to determine whether the solubility of the POAA stabiliser block depends on its DP. More specifically, it would be interesting to explore whether using a shorter POAA stabiliser might provide access to higher order morphologies or whether a longer POAA stabiliser might allow stable colloidal dispersions to be obtained at ambient temperature when using higher *n*-alkanes. In principle, higher order morphologies might also be accessed by statistical copolymerisation of suitable oil-soluble monomers such as 2-ethylhexyl acrylate or lauryl acrylate with OAA to suppress the UCST-type behaviour exhibited by the POAA stabiliser block.

Given the strongly amphiphilic nature of these nanoparticles (POAA is extremely hydrophobic whereas PDMAC is highly water-soluble), their performance as Pickering emulsifiers was explored. Accordingly, $POAA_{85}$-$PDMAC_{150}$ spheres were prepared in *n*-heptane to ensure no nanoparticle aggregation. The copolymer concentration was systematically lowered from 1% w/w to 0.1% w/w by diluting the original 20% w/w nanoparticle dispersion with *n*-heptane prior to homogenisation with water to produce 50% v/v o/w emulsions. Laser diffraction studies indicated that the droplet diameter increased at low copolymer concentrations, which is characteristic of Pickering emulsions.[20,21] As the spherical nanoparticles were highly hydrophobic, it was hypothesised that either they adsorbed onto the inner surface of the oil droplets (*i.e.* remained solely located within the dispersed phase) or they underwent micellar inversion *in situ* during high-shear homogenisation to form *hydrophilic* $PDMAC_{150}$-$POAA_{85}$ diblock copolymer nanoparticles. Further studies using core-crosslinked $POAA_{85}$-$PDMAC_{195}$-$PEGDA_{20}$ triblock copolymers that were unable to undergo micellar inversion also produced o/w Pickering emulsions, suggesting that the original linear nanoparticles most likely adsorb onto the inner surface of the oil droplets. $POAA_{85}$-$PDMAC_{150}$ nanoparticles synthesised in higher *n*-alkanes exhibit UCST-like behaviour. This observation leads to the following question: if o/w emulsions were prepared using such nanoparticles above their CP and then allowed to cool, would the oil droplets become flocculated?

Much of the work in this Thesis utilises NMEP. Its acrylic analogue, NAEP, has been much less extensively researched and the relatively few literature examples of its polymerisation invariably use water. Indeed, NAEP is significantly more hydrophilic than NMEP: it does not possess LCST-type behaviour in aqueous solution so it can serve as an effective steric stabiliser for aqueous

PISA formulations.[22] In Chapter 5, a PSMA stabiliser block is used to conduct the RAFT polymerisation of NAEP in *n*-dodecane. Again, only kinetically-trapped spheres were obtained.

Owing to the limited solubility of NAEP in *n*-dodecane, a relatively high reaction temperature (90 °C) was required for the synthesis of these diblock copolymer nanoparticles. This PISA formulation is best described as a rare example of a *non-aqueous* emulsion polymerisation. In the PISA literature, it is well-known that RAFT aqueous emulsion polymerisations are often limited to kinetically-trapped spheres. Interestingly, Cockram and co-workers have suggested that the aqueous solubility of the monomer may be a key parameter in this context, with higher solubilities providing access to worms or vesicles.[23,24] Thus it would be interesting to examine whether increasing the NAEP monomer solubility (either by raising the reaction temperature used for *n*-dodecane or by selecting lower *n*-alkanes such as *n*-heptane) could be utilised to access worms or vesicles for this unusual PISA formulation. In this context, it would also be fascinating to attempt the RAFT non-aqueous emulsion polymerisation of other polar monomers such as 2-hydroxyethyl methacrylate (HEMA) in such *n*-alkanes when employing suitable soluble precursors such as PSMA or PLMA.

Preliminary experiments were conducted using a trithiocarbonate-capped precursor for RAFT iniferter polymerisations. Solution polymerisations conducted in toluene at 30 °C were relatively slow, with only 33% NAEP conversion being achieved within 7.5 h, albeit with good MWD control (M_w/M_n = 1.18). The RAFT iniferter polymerisation of NAEP in *n*-dodecane required higher temperatures (70 or 80 °C), which led to more extensive chain transfer to polymer and hence significantly broader MWDs ($1.33 \leq M_w/M_n \leq 1.48$). $PSMA_{36}$-$PNAEP_{70}$ nanoparticles could also be used to stabilise Pickering emulsions. As in Chapter 4, the hydrophobic nanoparticles surprisingly formed o/w Pickering emulsions rather than w/o emulsions, suggesting their adsorption at the inner surface of the oil droplets. Interestingly, $PSMA_{36}$-$PNAEP_{70}$ nanoparticles produced w/o/w Pickering emulsions *directly* when conducting high-shear homogenisation at a copolymer concentration of at least 0.5% w/w or when employing oil volume fractions of no more than 0.60.

Chapter 5 illustrated that PISA *via* RAFT iniferter polymerisation is feasible using a trithiocarbonate CTA in *n*-dodecane. This suggests that the scope of PISA syntheses using iniferter polymerisation is worthy of further exploration. In principle, visible light irradiation might be used to first polymerise the monomer and then subsequently cleave the RAFT end-groups under monomer-starved conditions in a convenient one-pot formulation to produce an aqueous dispersion of diblock copolymer nanoparticles for which dialysis would be required to remove small molecule side-products. However, the technical problem here would be to ensure that little

or no end-group removal occurred on the time scale of the polymerisation, otherwise this would lead to a significantly longer DP for the structure-directing block. The removal of dithiobenzoate RAFT end-groups *via* visible light irradiation in non-polar media is likely to be less efficient than in aqueous media, which may favour PISA syntheses conditions *via* iniferter polymerisation under such conditions.

6.1 References

(1) Moad, G.; Rizzardo, E.; Thang, S. H. Living Radical Polymerization by the RAFT Process a Third Update. *Aust. J. Chem.* **2012**, *65*, 985–1076.

(2) Perrier, S. 50th Anniversary Perspective: RAFT Polymerization A User Guide. *Macromolecules* **2017**, *50*, 7433–7447.

(3) Warren, N. J.; Armes, S. P. Polymerization-Induced Self-Assembly of Block Copolymer Nano-Objects via RAFT Aqueous Dispersion Polymerization. *J. Am. Chem. Soc.* **2014**, *136*, 10174–10185.

(4) Canning, S. L.; Smith, G. N.; Armes, S. P. A Critical Appraisal of RAFT-Mediated Polymerization-Induced Self-Assembly. *Macromolecules* **2016**, *49*, 1985–2001.

(5) D'Agosto, F.; Rieger, J.; Lansalot, M. RAFT-Mediated Polymerization-Induced Self-Assembly. *Angew. Chemie - Int. Ed.* **2020**, *59*, 8368–8392.

(6) Blanazs, A.; Ryan, A. J.; Armes, S. P. Predictive Phase Diagrams for RAFT Aqueous Dispersion Polymerization: Effect of Block Copolymer Composition, Molecular Weight, and Copolymer Concentration. *Macromolecules* **2012**, *45*, 5099–5107.

(7) Summers, M. J.; Phillips, D. J.; Gibson, M. I. "Isothermal" LCST Transitions Triggered by Bioreduction of Single Polymer End-Groups. *Chem. Commun.* **2013**, *49*, 4223–4225.

(8) Semsarilar, M.; Ladmiral, V.; Blanazs, A.; Armes, S. P. Anionic Polyelectrolyte-Stabilized Nanoparticles via RAFT Aqueous Dispersion Polymerization. *Langmuir* **2012**, *28*, 914–922.

(9) Semsarilar, M.; Ladmiral, V.; Blanazs, A.; Armes, S. P. Cationic Polyelectrolyte-Stabilized Nanoparticles via RAFT Aqueous Dispersion Polymerization. *Langmuir* **2013**, *29*, 7416–7424.

(10) Beattie, D. L. Preparation of Diblock Copolymer Nano-Objects via Polymerisation-Induced Self-Assembly in Aqueous Media, PhD Thesis, The University of Sheffield, 2021.

(11) Blanazs, A.; Madsen, J.; Battaglia, G.; Ryan, A. J.; Armes, S. P. Mechanistic Insights for Block Copolymer Morphologies: How Do Worms Form Vesicles? *J. Am. Chem. Soc.* **2011**, *133*, 16581–16587.

(12) Willcock, H.; O'Reilly, R. K. End Group Removal and Modification of RAFT Polymers. *Polym. Chem.* **2010**, *1*, 149–157.

(13) Moad, G.; Rizzardo, E.; Thang, S. H. End-Functional Polymers, Thiocarbonylthio Group Removal/Transformation and Reversible Addition-Fragmentation-Chain Transfer (RAFT) Polymerization. *Polym. Int.* **2011**, *60*, 9–25.

(14) Boyer, C.; Bulmus, V.; Davis, T. P. Efficient Usage of Thiocarbonates for Both the Production and the Biofunctionalization of Polymers. *Macromol. Rapid Commun.* **2009**, *30*, 493–497.

(15) Mattson, K. M.; Pester, C. W.; Gutekunst, W. R.; Hsueh, A. T.; Discekici, E. H.; Luo, Y.; Schmidt, B. V. K. J.; McGrath, A. J.; Clark, P. G.; Hawker, C. J. Metal-Free Removal of Polymer Chain Ends Using Light. *Macromolecules* **2016**, *49*, 8162–8166.

(16) Lunn, D. J.; Discekici, E. H.; Read de Alaniz, J.; Gutekunst, W. R.; Hawker, C. J. Established and Emerging Strategies for Polymer Chain-End Modification. *J. Polym. Sci. Part A Polym. Chem.* **2017**, *55*, 2903–2914.

(17) Matioszek, D.; Dufils, P. E.; Vinas, J.; Destarac, M. Selective and Quantitative Oxidation of Xanthate End-Groups of RAFT Poly(n-Butyl Acrylate) Latexes by Ozonolysis. *Macromol. Rapid Commun.* **2015**, *36*, 1354–1361.

(18) Jesson, C. P.; Pearce, C. M.; Simon, H.; Werner, A.; Cunningham, V. J.; Lovett, J. R.; Smallridge, M. J.; Warren, N. J.; Armes, S. P. H2O2 Enables Convenient Removal of RAFT End-Groups from Block Copolymer Nano-Objects Prepared via Polymerization-Induced Self- Assembly in Water. *Macromolecules* **2017**, *50*, 182–191.

(19) Fielding, L. A.; Lane, J. A.; Derry, M. J.; Mykhaylyk, O. O.; Armes, S. P. Thermo-Responsive Diblock Copolymer Worm Gels in Non-Polar Solvents. *J. Am. Chem. Soc.* **2014**, *136*, 5790–5798.

(20) Binks, B. P.; Whitby, C. P. Silica Particle-Stabilized Emulsions of Silicone Oil and Water: Aspects of Emulsification. *Langmuir* **2004**, *20*, 1130–1137.

(21) Thompson, K. L.; Mable, C. J.; Cockram, A.; Warren, N. J.; Cunningham, V. J.; Jones, E. R.; Verber, R.; Armes, S. P. Are Block Copolymer Worms More Effective Pickering Emulsifiers than Block Copolymer Spheres? *Soft Matter* **2014**, *10*, 8615–8626.

(22) Deane, O. J.; Musa, O. M.; Fernyhough, A.; Armes, S. P. Synthesis and Characterization of Waterborne Pyrrolidone-Functional Diblock Copolymer Nanoparticles Prepared via Surfactant-Free RAFT Emulsion Polymerization. *Macromolecules* **2020**, *53*, 1422–1434.

(23) Cockram, A. A.; Neal, T. J.; Derry, M. J.; Mykhaylyk, O. O.; Williams, N. S. J.; Murray, M. W.; Emmett, S. N.; Armes, S. P. Effect of Monomer Solubility on the Evolution of Copolymer Morphology during Polymerization-Induced Self-Assembly in Aqueous Solution. *Macromolecules* **2017**, *50*, 796–802.

(24) Brotherton, E. E.; Hatton, F. L.; Cockram, A. A.; Derry, M. J.; Czajka, A.; Cornel, E. J.; Topham, P. D.; Mykhaylyk, O. O.; Armes, S. P. In Situ Small-Angle X-Ray Scattering Studies during Reversible Addition-Fragmentation Chain Transfer Aqueous Emulsion Polymerization. *J. Am. Chem. Soc.* **2019**, *141*, 13664–13675.

Chapter 7.

Appendix

7.1 Structural models for Small Angle X-ray Scattering (SAXS) analysis

In general, the intensity of X-rays scattered by a dispersion of nano-objects [usually represented by the scattering cross section per unit sample volume, $\frac{d\Sigma}{d\Omega}(q)$] can be expressed as:

$$\frac{d\Sigma}{d\Omega}(q) = NS(q)\int_0^\infty \dots \int_0^\infty F(q, r_1, \dots, r_k)^2 \Psi(r_1, \dots, r_k) dr_1 \dots dr_k \qquad 7.1$$

where $F(q, r_1, \dots, r_k)$ is the form factor, $r_1, \dots, r_k$ is a set of *k* parameters describing the structural morphology, $\Psi(r_1, \dots, r_k)$ is the distribution function, S(q) is the structure factor and *N* is the nano-object number density per unit volume expressed as:

$$N = \frac{\varphi}{\int_0^\infty \dots \int_0^\infty V(r_1,\dots,r_k)\Psi(r_1,\dots,r_k) dr_1 \dots dr_k} \qquad 7.2$$

where $V(r_1, \dots, r_k)$ is volume of the nano-object and φ is their volume fraction in the dispersion. For all SAXS experiments conducted herein, a dilute copolymer concentration of 1.0 % w/w was utilised. As such, for all analysis and modelling it was assumed that S(q) = 1.

Sphere model

The spherical micelle form factor equation for Equation 1 is given by:[1]

$$F_{sph}(q) = N_s^2 \beta_s^2 A_s^2(q, R_s) + N_s \beta_c^2 F_c(q, R_g) + (q) \qquad 7.3$$

Where R_s is the core radius of the spherical micelle, R_g, is the radius of gyration of the corona block. The core block and the corona block X-ray scattering length contrast is given by $\beta_s = V_s(\xi_s - \xi_{sol})$ and $\beta_s = V_c(\xi_c - \xi_{sol})$, respectively. Here ξ_s, ξ_c and ξ_{sol} are the X-ray scattering length densities of the core-forming block, the coronal stabiliser block and the solvent. V_s and V_c are the volumes of the core-forming block and the coronal stabiliser block, respectively. Using the molecular weights of the each block and their respective mass densities), the individual block volumes can be calculated from $V = \frac{M_{n,pol}}{N_A \rho}$, where $M_{n,pol}$ corresponds to the number-average molecular weight of the block determined by ^{1}H NMR spectroscopy.

The sphere form factor amplitude is used for the amplitude of the core self-term:

$$A_c(q, R_s) = \Phi(qR_s)\exp\left(-\frac{q^2\sigma^2}{2}\right) \qquad 7.4$$

Where $\Phi(qR_s) = \frac{3[\sin(qR_s) - qR_s\cos(qR_s)]}{(qR_s)^3}$. A sigmoidal interface between the two blocks was assumed for the spherical micelle form factor (Equation 4). This is described by the exponent term with a width σ accounting for a decaying scattering length density at the micellar interface. This σ value was fixed at 2.2 during fitting.

The form factor amplitude of the spherical micelle corona is:

$$A_c(q) = \frac{\int_{R_s}^{R_s+2s} \mu_c(r)\frac{\sin(qr)}{qr} r^2 dr}{\int_{R_s}^{R_s+2s} \mu_c(r) r^2 dr} exp\left(-\frac{q^2\sigma^2}{2}\right) \qquad 7.5$$

The radial profile, $\mu_c(r)$, can be expressed by a linear combination of two cubic b splines, with two fitting parameters *s* and *a* corresponding to the width of the profile and the weight coefficient, respectively. This information can be found elsewhere,[2,3] as can the approximate

integrated form of Equation 5. The self-correlation term for the corona block is given by the Debye function:

$$F_c(q, R_g) = \frac{2[\exp(-q^2R_g^2)-1+q^2R_g^2]}{q^4R_g^2} \qquad 7.6$$

Where R_g is the radius of gyration of the coronal block. The aggregation number of the spherical micelle is:

$$N_s = (1 - x_{sol})\frac{\frac{4}{3}\pi R_S^3}{V_s} \qquad 7.7$$

Where x_{sol} is the volume fraction of solvent in the micelle core. An effective structure factor expression proposed for interacting spherical micelles[4] has been used in Equation 1:

$$S_s(q) = 1 + \frac{A_{s\_mic}^{av}(q)^2[S_{PY}(q,R_{PY},f_{PY})-1]}{F_{s\_mic}(q)} \qquad 7.8$$

Herein the form factor of the average radial scattering length density distribution of micelles is used as $A_{s\_mic}^{av}(q) = N_s[\beta_s A_s(q, R_s) + \beta_c A_c(q)]$ and $S_{PY}(q, R_{PY}, f_{PY})$ is a hard-sphere interaction structure factor based on the Percus-Yevick approximation,[5] where R_{PY} is the interaction radius and f_{PY} is the hard-sphere volume fraction. A polydispersity for one parameter (R_s) is assumed for the micelle model which is described by a Gaussian distribution. Thus, the polydispersity function in Equation 1 can be replaced as:

$$\Psi(r_1) = \frac{1}{\sqrt{2\pi\sigma_{R_S}^2}} exp\left(-\frac{(r_1-R_s)^2}{2\sigma_{R_S}^2}\right) \qquad 7.9$$

Where σ_{R_S} is the standard deviation for R_s. In accordance with Equation 2, the number density per unit volume for the micelle model is expressed as:

$$N = \frac{\varphi}{\int_0^\infty V(r_1)\Psi(r_1)dr_1} \qquad 7.10$$

Where φ is the total volume fraction of copolymer in the spherical micelles and $V(r_1)$ is the total *volume* of copolymer in a spherical micelle $[V(r_1) = (V_s + V_c)N_s(r_1)]$.

Vesicle model

The vesicle form factor in Equation (1) is expressed as:[6]

$$F_{ves}(q) = N_v^2\beta_m^2A_m^2(q) + N_v\beta_{vc}^2F_c(q, R_g) + N_v(N_v - 1)\beta_{vc}^2A_{vc}^2(q) + 2N_v^2\beta_m\beta_{vc}A_m(q)A_{vc}(q) \qquad 7.11$$

The X-ray scattering length contrast for the membrane-forming block and the coronal stabiliser block is given by $\beta_m = V_m(\xi_m - \xi_{sol})$ and $\beta_{vc} = V_{vc}(\xi_{vc} - \xi_{sol})$, respectively, where ξ_m, ξ_{vc} and ξ_{sol} are the X-ray scattering length densities of the membrane-forming block, the coronal stabiliser block and the solvent. V_m and V_{vc} are the volumes of the membrane-forming block and the coronal stabiliser block, respectively. Using the molecular weights of each block and their respective mass densities, the individual block volumes can be calculated from $V = \frac{M_{n,pol}}{N_A\rho}$, where $M_{n,pol}$ corresponds to the number-average molecular weight of the block determined by ^{1}H NMR spectroscopy. The amplitude of the membrane self-term is:

$$A_m(q) = \frac{V_{out}\varphi(qR_{out}) - V_{in}\varphi(qR_{in})}{V_{out} - V_{in}} e^{\left(-\frac{q^2\sigma_{in}^2}{2}\right)} \qquad 7.12$$

where $R_{in} = R_m - \frac{1}{2}T_m$ is the inner radius of the membrane, $R_{out} = R_m + \frac{1}{2}T_m$ is the outer radius of the membrane, $V_{in} = \frac{4}{3}\pi R_{in}^3$, $V_{out} = \frac{4}{3}\pi R_{out}^3$. It should be noted that Equation 12 differs from that reported in the original work.[6] More specifically, the exponent term in Equation 12 represents a sigmoidal interface between the blocks, with a width σ_{in} accounting for a decaying scattering length density at the membrane surface. The numerical value of σ_{in} was fixed at 2.2. The mean vesicle aggregation number, N_v, is given by:

$$N_v = (1 - x_{sol})\frac{V_{out} - V_{in}}{V_m} \qquad 7.13$$

where x_{sol} is the solvent volume fraction within the vesicle membrane. A simpler expression for the corona self-term of the vesicle model than that used for the spherical micelle corona self-term was preferred because the contribution to the scattering intensity from the corona block is much less than that from the membrane block in this case. Assuming that there is no penetration of the solvophilic coronal blocks into the solvophobic membrane, the amplitude of the vesicle corona self-term is expressed as:

$$A_{vc}(q) = \Psi(qR_g)\frac{1}{2}\left[\frac{\sin\left[q(R_{out} + R_g)\right]}{q(R_{out} + R_g)} + \frac{sin[q(R_{in} - R_g)]}{q(R_{in} - R_g)}\right] \qquad 7.14$$

where the term outside the square brackets is the factor amplitude of the corona block copolymer chain such that:

$$\Psi(qR_g) = \frac{1 - exp^{(-qR_g)}}{(qR_g)^2} \qquad 7.15$$

The R_g value can be calculated from the total contour length of the stabiliser block, L, where L = $DP_{stabiliser} \times 0.255$ nm (since the projected contour length per monomer repeat unit is defined by two C-C bonds adopting an *all-trans* conformation, 0.255 nm) and the Kuhn length of 1.53 nm based on the known literature value for poly(methyl methacrylate) result in an approximate R_g of $(L \times 1.53/6)^{0.5}$.

For the vesicle model, it was assumed that two parameters are polydisperse: the overall radius of the vesicles and the membrane thickness (R_m and T_m, respectively). Each is assumed to have a Gaussian distribution, so the polydispersity function in Equation 1 can be expressed as:

$$\Psi(r_1, r_2) = \frac{1}{\sqrt{2\pi\sigma_{Rm}^2}} exp^{\left(-\frac{(r_1 - R_m)^2}{2\sigma_{Rm}^2}\right)} \frac{1}{\sqrt{2\pi\sigma_{Tm}^2}} exp^{\left(-\frac{(r_1 - T_m)^2}{2\sigma_{Tm}^2}\right)} \qquad 7.16$$

where σ_{Rm} and σ_{Tm} are the standard deviations for R_m and T_m, respectively. Following Equation 2, the number density per unit volume for the vesicle model is expressed as:

$$N = \frac{\varphi}{\int_0^\infty \int_0^\infty V(r_1, r_2)\Psi(r_1, r_2) dr_1 dr_2} \qquad 7.17$$

where φ is the total volume fraction of copolymer in the vesicles and $V(r_1, r_2)$ is the total volume of copolymers in a vesicle $[V(r_1, r_2) = (V_m + V_{vc})N_v(r_1, r_2)]$. Programming tools within the Irena SAS Igor Pro macros were used to implement the scattering models.[7]

Additionally, a Gaussian peak $\left(Aexp\left[-\left(\frac{q-q_{peak}}{width}\right)^2\right]\right)$ was added to the vesicle model in order to account for the subtle feature observed at q ~ 0.1 nm^{-1} for the 1.0 % w/w dispersions of $PNMEP_{28}$-$PLMA_{129}$ and $PNMEP_{28}$-$PLMA_{151}$ at 20 °C (Figure 3.11). Thus, the entire scattering pattern would be described as:

$$I(q) = \frac{d\Sigma}{d\Omega}(q) + Bq^{-p} + Aexp\left[-\left(\frac{q-q_{peak}}{width}\right)^2\right] \qquad 7.18$$

where the first term represents scattering from spherical micelles (Equations 1 and 2).

Model parameters

Scattering length densities:

ξ_{PLMA} = 8.81 × 10^{10} cm^{-2}

ξ_{PNMEP} = 11.6 × 10^{10} cm^{-2}

$\xi_{80:20\ ethanol\text{-}water}$ = 7.859 × 10^{10} cm^{-2}

ξ_{POAA} = 9.405 × 10^{10} cm^{-2}

ξ_{PDMAC} = 10.72 × 10^{10} cm^{-2}

$\xi_{n\text{-}Heptane}$ = 6.719 × 10^{10} cm^{-2}

ξ_{PSMA} = 9.237 × 10^{10} cm^{-2}

ξ_{PNAEP} = 11.46 × 10^{10} cm^{-2}

$\xi_{n\text{-}Dodecane}$ = 7.322 × 10^{10} cm^{-2}

Respective mass densities:

ρ_{PLMA} = 0.93 g cm^{-3}

ρ_{PNMEP} = 1.272 g cm^{-3}

ρ_{POAA} = 0.9959 g cm^{-3}

ρ_{PDMAC} = 1.16 g cm^{-3}

ρ_{PSMA} = 0.97 g cm^{-3}

ρ_{PNAEP} = 1.2625 g cm^{-3}

7.2 References

(1) Pedersen, J. S. Form Factors of Block Copolymer Micelles with Spherical, Ellipsoidal and Cylindrical Cores. *J. Appl. Crystallogr.* **2000**, *33*, 637–640.

(2) Pedersen, J. S.; Gerstenberg, M. C. The Structure of P85 Pluronic Block Copolymer Micelles Determined by Small-Angle Neutron Scattering. *Colloids Surfaces A*

Physicochem. Eng. Asp. **2003**, *213*, 175–187.

(3) Pedersen, J. S.; Svaneborg, C.; Almdal, K.; Hamley, I. W.; Young, R. N. A Small-Angle Neutron and x-Ray Contrast Variation Scattering Study of the Structure of Block Copolymer Micelles: Corona Shape and Excluded Volume Interactions. *Macromolecules* **2003**, *36*, 416–433.

(4) Pedersen, J. S. Structure Factors Effects in Small-Angle Scattering from Block Copolymer Micelles and Star Polymers. *J. Chem. Phys.* **2001**, *114*, 2839–2846.

(5) Kinning, D. J.; Thomas, E. L. Hard-Sphere Interactions between Spherical Domains in Diblock Copolymers. *Macromolecules* **1984**, *17*, 1712–1718.

(6) Bang, J.; Jain, S.; Li, Z.; Lodge, T. P.; Pedersen, J. S.; Kesselman, E.; Talmon, Y. Sphere, Cylinder, and Vesicle Nanoaggregates in Poly(Styrene-b-Isoprene) Diblock Copolymer Solutions. *Macromolecules* **2006**, *39*, 5583.

(7) Ilavsky, J.; Jemian, P. R. Irena : Tool Suite for Modeling and Analysis of Small-Angle Scattering. *J. Appl. Crystallogr.* **2009**, *42*, 347–353.